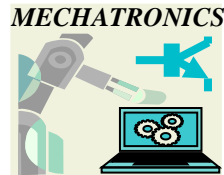University Politehnica Timişoara
Mechanical Engineering Fakulty
Department of Mechatronics

MECHATRONICS

HABILITATION THESIS

Contributions on Development of Mechanism Science with Applications in Robotics, Mechatronics and Mechanical Engineering

Erwin-Christian Lovasz

2015

Piaţa Victoriei nr. 2, RO 300006 - Timişoara, Tel: +40 256 403000, Fax: +40 256 403021, rector@rectorat.upt.ro, www.upt.ro

Table of contents

Acknowledgement

Because the thesis covers my past activities, it was the moment to remember a lot of people beginning since my childhood, my parents, friends, teachers, professors, collaborators who had an important contribution to my scientific development and achievements. I express my thanks to all my colleagues, friends, collaborators and co-authors from the Department and University, but also from the country and all over the world. Above all I find that my chance to meet and to work for a long time with Prof. Perju, Prof. Modler and Prof. Mesaroş-Anghel gave me the opportunity to enrich my knowledge and led to my academic evolution. They were models to me from both scientific and human standpoint. My membership in the professional organization IFToMM was also a very good opportunity to meet and to collaborate with recognised scientists and to enhance my research and teaching skills. My thanks are addressed to all of them, as they gave me impulse to work on this thesis. I believe that without their aid, my scientific achievements would not have existed.

But, first of all I would like express my gratitude to my family, my wife and my two brilliant daughters for staying close to me and understanding that my work needed dedication and a lot of time. I promise them that in better times I will try to be as I would like to be: a family father.

God blessed me to find the way and gave me the inspiration to finish this habilitation thesis that will be a milestone in my scientific and academic career. In the future I hope to have enough energy, opportunity, time and vision for self-improvement and continuing my academic path.

"Live for people and people will live for you"
Russian proverb

Abstract

The present habilitation thesis was structured in five sections: (I) Introduction, (II) Scientific achievements, (III) Academic and professional achievements, (IV) Career evolution and development plans and (V) References. The scientific, academic and professional achievements covered the period from 1998 to 2015.

Section (I) give an overview of the thesis content and shows the highlighted papers which were published by the author in ISI indexed Journals (2), Inspec indexed Journal (1), ISI indexed Conferences (2), Scopus indexed Conferences (2), Springer Link indexed Conference (2) and one awarded paper on 3rd Asian IFToMM Conference on Mechanism and Machine Science in Tian Jin.

The Section (II) described some of the scientific achievements within the author´s research directions and was organized in four chapters. Each chapter has a unitary structure usually including: *(a) State-of-art* on the research topic and research problem statement; *(b) Theoretical and/or experimental contributions* to the described problem, highlighting the aim, analytical background, numerical examples, applications or experimental results; (c) *Scientific contributions of the author*.

The first chapter "Scientific achievements regarding the design of the mechanisms using profiled wheels" shows the contributions on computing of the base circle radius and evaluating of the wear susceptibility of the cam mechanisms with translating or oscillating flat-face follower, and on the designing of different non-circular wheels of belt mechanisms for self-balancing applications.
The development of a unitary numerical method to compute the base circle radius was shown in the case of cam mechanisms with oscillating or translating flat-face follower using a base circle radius function. The method is based on the mathematical conditions to avoid the inflection or singularity points on the cam profile.
The second study in this chapter used the specific relative sliding as a characteristic parameter of the cam mechanism with oscillating or translating flat-face follower, in a unitary evaluation of cam mechanism's susceptibility to wear.
The using special type of belt mechanism structures were also studied and developed for self-balancing mechanisms. Some technical applications in the field of mechanical devices, measurement tools and robotic shown the computation algorithms in order to design the used non-circular wheels.

The second chapter "Scientific achievements regarding the design of complex mechanisms structures" laid out contributions in designing of geared linkages with non-circular gears and with linear actuation, respectively of 5-link belt mechanisms.
The study of geared linkages with non-circular gears presented the type synthesis, the approach for computing the centrodes and the transmission functions of non-circular gear pairs or centrode segments with nonlinear boundary conditions. The proposed general computation method allows the computing of ordinary non-circular gears pairs and planetary non-circular gear pairs.

Another special structure of the geared linkages with linear actuation was studied regarding the type synthesis, development the analytical analysis and dimensional synthesis method. An application using geared linkages with linear actuation was shown for designing and control of an active knee prosthesis.

The using of belt mechanism in mechatronic applications required the adjustment of the variable link lengths to the various movement tasks, which needs the increasing of the degree of freedom of the mechanisms and the using of circular wheel instead of a special profiled non-circular wheel. The computation of control functions mechanism was shown for different movement task and for a walking leg with 2 DoF.

The third chapter "Scientific achievements regarding of mechanism development for mechatronics, robotics and mechanical applications" presents some mechanism design and control applications for haptic exoskeleton used in space telerobotics, for a new class of planar parallel manipulators and for a fishing reel spool mechanisms.

The first application showed the developing strategy of a new lightweight, easy wearable and comfortable haptic arm exoskeleton for teleoperation with a robot having equivalent kinematic chain and with force-feedback. The chapter focuses on the specific design and control solutions for the elbow module of haptic arm exoskeleton, meant to enable force-feedback telemanipulation with redundant robotic arm (slave robot).

The development of the specific class of planar parallel manipulators using geared linkages with linear actuation was presented in the second application. The study focuses mainly on the kinematic analysis and the problem of singularities.

The third application developed a study of the existing or new mechanism solutions to provide axial movement of the spool with constant speed in a large range of the movement. The novel solution was finally manufactured, tested and patented.

The last chapter "Scientific achievements regarding the analysis of compliant mechanisms" shows the research of the compliant mechanisms, which use elastic connections, focused on the structural analysis of the compliant mechanisms with elastic connections, simulation and dynamic analysis of the compliant mechanisms with or without integrated piezo-actuators. The theoretical research reconsidered the definition of the kinematic joint, of the link and expressed a new formula for computing of mechanism's degree of freedom (mobility). Some alternative kinematic models of A-CM with active prismatic joints and rotational joints, having concentrated torsion rigidity and the ability to predict the actual motion of compliant mechanisms with integrated piezo-ceramic actuators were proposed and dynamic analyzed using Adams and Mathlab-Simulink.

The Section (III) of the habilitation thesis mentions the main achievements of the candidate within the last 17 years after defending the PhD thesis in co-advisorship between University Politehnica Timişoara and Technical University Dresden, defended on 27th of February 1998 at TU Dresden and on 03 of June 1998 at UP Timişoara. The teaching activities at the University Politehnica Timisoara comprised "Mechanism Science" and "Programming and Using of Computers", continuing with teaching on "Intensive Therapy Biomedical Devices", "Prosthesis", "Advanced Robotics", "Special Structure of Robots" and "Service Robotics". The teaching classes were held in German and Romanian language. The concentrated teaching classes at the TU Dresden, Szent István University in Gödölö and National Taiwan University of Science and Technology enriched the candidate the international teaching experience. A number of 6 books and course supports were published.

The research activities were developed in parallel with the teaching activities in the same research areas. The candidate leaded 5 research projects/grants as project coordinator or partner leader and was involved in 17 research projects at the UP Timişoara, TU Dresden and TU Ilmenau.

The publishing activity during this period as result of the research and development activities was very extensive, so I published 5 papers in ISI Journals, 11 papers in Scopus, Elsevier Science Direct and Inspec indexed Journals, 26 papers indexed ISI Conference, 27 Scopus, IEEE and Springer indexed conferences and other 69 papers without indexing in different national and international conferences and IFToMM World Congresses

The publishing activities were compleated with reviewing activities on main Journals and Conferences. From 2009 the candidate worked as member of the scientific committtee of the University Journal "Bulletin of the Transilvania University of Brasov" and from 2013 as editorial office secretary for the International Journal "Robotica & Management". In 2015 became Associate Editor by the Journal Advanced Robotics Systems.

The candidate was involved in three national and intenational profesional organization ARoTMM (Romanian Association of Mechanism and Machine Science) associated to the International Federation of Mechanism and Machine Science IFToMM (up 1991), SRR Romanian Society of Robotics (up 2000) and VDI -Verein Deutscher Ingenieure (up 1996). For two terms was elected as member in the IFToMM Permanent Commision for Constitution (2004-2011) and currently chaired the Technical Committee Linkages and Mechanical Controls. At the national level from 2005 worked as scientifical secretary of the national organization ARoTMM

Organized as chair or as co-chair several international Conferences and edited 5 books with the IFToMM Conference papers by Springer and Trans-Tech Publisher.

After the PhD defend received several post-doc and teaching fellowships in Germany (Humbold and Erasmus), Hungary (Pro Renovanda Cultura), Italy (Erasmus) and Taiwan.

To the academic and professional career was added a managerial activity as Head of the Mechatronics Department of the University Politehnica Timisoara for 2 periods, from 2008 up today.

The Section (IV) shows the career evolution and development plans organized in the following systematization: Key research directions, Objectives, Planned activities and Financial, human and infrastructure resources.

The Section (V) contains the references used in the section "Scientific achievements".

Rezumat

Teza de abilitare a fost structurată în cinci secţiuni: (I) Introducere, (II) Realizări ştiinţifice, (III) Realizări academice şi profesionale, (IV) Planul de evoluţie şi dezvoltare a carierei şi (V) Referinţe bibliografice. Realizările ştiinţifice, academice şi profesionale prezentate se referă la perioada 1998-2015.

Sectiunea (I) oferă o imagine a conţinutului tezei şi indică lucrările relevante publicate şi selecţionate de autor în reviste indexate în baza de date ISI-Web of Knowledge (2), reviste indexate în baza de date Inspec (1), conferinţe indexate în baza de date ISI-Web of Knowledge (2), conferinţe indexate în în baza de date Scopus (2), conferinţe indexate în baza de date Springer Link (2) şi o lucrare care a obţinut distincţia "Best Paper Award" la 3rd Asian IFToMM Conference on Mechanism and Machine Science în Tian Jin, China.

Sectiunea (II) descrie realizările ştiinţifice ale autorului în direcţia de cercetare ştiinţifică proprie şi este organizată în patru capitole. Fiecare capitol are o structură unitară care include în general: *a) Stadiul actual* al cercetărilor în tematica abordată; *(b) Contribuţii teoretice şi/sau experimentale* ale studiilor derulate, indicând obiectivul urmărit, fundamentarea teoretică, exemple numerice, aplicaţii şi/sau rezultate experimentale; (c) *Contribuţii ştiinţifice* proprii.

Primul capitol "Realizări ştiinţifice referitoare la sinteza mecanismelor utilizând roţi necirculare" expune contribuţiile la calculul razei de bază şi evaluarea uzurii mecanismelor cu camă cu tachet plan în mişcare de translaţie sau oscilaţie, respectiv sinteza diferitelor roţi necirculare ale mecanismelor cu elemente flexibile de lungime instantaneu variabilă utilizate în aplicaţii de auto-echilibrare.

Dezvoltarea unei metode unitare de calcul a razei de bază a fost abordată în cazul mecanismelor cu camă cu tachet plan în mişcare de translaţie sau oscilaţie utilizând o funcţie explicită dependentă de raza de bază. Metoda porneşte de la condiţia matematică de evitare a punctelor de inflexiune şi a punctelor singulare ale profilului camei.

Cel de al doilea studiu din cadrul acestui capitol utilizează alunecarea relativă specifică ca parametru caracteristic al mecanismului cu camă cu tachet plan în mişcare de translaţie sau oscilaţie pentru evaluarea unitară a uzurii camei şi a tachetului.

O serie de studii referitoare la utilizarea mecanismelor cu elemente flexibile de lungime instantaneu variabilă sunt prezentate în vederea auto-echilibrării unor structuri mecanice şi exemplificate în aplicaţii din domeniul echipamentelor mecanice, aparatelor de măsurare şi roboticii. Pentru aceste aplicaţii şunt prezentate algoritmii de calcul pentru sinteza roţilor necirculare.

Al doilea capitol "Realizări ştiinţifice referitoare la sinteza mecanismelor cu structuri complexe" descrie contribuţiile la sinteza mecanismelor cu bare şi roţi dinţate utilizând roţi necirculare sau având un element motor în mişcare de translaţie, respectiv a mecanismelor cu elemente flexibile cu lungime instantaneu variabilă având 5 elemente.

Studiul mecanismelor cu bare şi roţi dinţate necirculare prezintă analiza structurală, algoritmul de calcul al centroidelor roţilor dinţate necirculare şi a funcţiei de transmitere a unei treptei cu roţi

dinţate necirculare sau a segmentelor de centroidă având condiţii la limită nelineare impuse. Metoda de calcul generală permite calcularea treptei ordinare şi/sau planetare cu roţi dinţate necirculare.

O altă structură a mecanismelor cu bare şi roţi dinţate cu acţionare lineară a fost studiată din punctul de vedere al analizei structurale, dezvoltării metodei de calcul analitic pentru analiza şi sinteza dimensională. O aplicaţie utilizând mecanisme cu bare şi roţi dinţate a fost prezentată pentru proiectarea şi controlul unei proteze active de genunchi.

Utilizarea mecanismelor cu element flexibil de lungime instantaneu variabilă în aplicaţii mecatronice necesită modificarea corelată a lungimii unor elemente în funcţie de diferitele traiectorii de mişcare dorite, ceea ce implică creşterea gradului de mobilitate a mecanismului şi utilizarea unei roţi circulare în locul roţii necirculare special profilate. Studiul este exemplificat prin calculul funcţiilor de control a mecanismului cu elemente flexibile având 5 elemente pentru generarea diferitelor traiectorii de mişcare şi în cazul picioarelor unui robot mobil păşitor având gradul de mobilitate 2.

Al treilea capitol „Realizări ştiinţifice referitoare la dezvoltarea mecanismelor utilizate în aplicaţii mecatronice, robotice sau mecanice" prezintă proiectarea şi contolul unui exoschelet haptic utilizat în aplicaţii de telerobotica spaţială, a unei noi clase de manipulatoare paralele plane şi a unei mişcarii de translaţie uniforme a tamburului unei mulinete de pescuit.

Prima aplicaţie descrie strategia de dezvoltare a unui exoschelet haptic a membrului superior utilizând materiale cu densitate redusă, uşor de purtat şi confortabile, destinat teleoperării cu un robot având o structură antropomorfică echivalentă şi o reacţie de forţă (simţ). Capitolul este concentrat pe proiectarea şi controlul unor soluţii tehnice pentru modulul articulaţiei de cot (humero-cubito-radiale) a unui exoschelet haptic al membrului superior, menit să asigure o buclă de reacţie de forţă la telemanipularea cu un braţ robotic redundant (sclav).

Dezvoltarea unei noi clase specifice de manipulatoare paralele plane utilizând lanţuri cinematice cu bare şi roţi dinţate a făcut obiectul de studiu al celei de-a doua aplicaţii prezentate. Studiul a abordat în principal analiza cinematică şi problema singularităţilor.

Cea de-a treia aplicaţie prezintă studiul soluţiilor existente şi nou propuse pentru dezvoltarea unei soluţii optime a mecanismului care asigură o mişcare axială a tamburului unei mulinete cu viteză constantă într-un domeniu larg la mişcarea de avans respectiv revenire. Soluţia finală a fost manufacturată, testată şi patentată.

Ultimul capitol "Realizări ştiinţifice referitoare la analiza mecanismelor compliante" prezintă cercetări ale mecanismelor compliante, care utilizează conexiuni elastice, şi abordează analiza structurală, simularea şi analiza dinamică a mecanismelor compliante utilizând conexiuni elastice cusau fără piezo-actuatoare integrate. Cercetările teoretice reconsideră definiţile cuplelor cinematice, a elementelor şi propune o nouă formulă de calcul a gradului de mobilitate a mecanismelor compliante. Deasemenea sunt propuse o serie de modele cinematice echivalente pentru mecanismele compliante conţinând cuple de translaţie motoare şi cuple de rotaţie, care echivalză rigiditatea la torsiune şi permite o mişcare indentică cu cea a mecanismului compliant utilizând conexiuni elastice cu piezo-actuatoare integrate. Modelele au fost analizate dinamic utilizând programele Adams and Mathlab-Simulink.

Secţiunea (III) a tezei de abilitare prezintă realizările principale ale candidatului în ultimi 17 ani după susţinere tezei de doctorat în cotutelă între Universitatea Politehnica Timişoara şi Universitatea Tehnică Dresden, în data de 27 februarie 1998 la TU Dresden şi 03 iunie 1998 la UP Timişoara.

Activităţile de predare la Universitatea Politehnica Timisoara au cuprins cursurile de "Mecanisme" şi "Programarea şi utilizarea calculatoarelor", continuând cu cursurile "Aparate de terapie intensivă", "Proteze", "Robotică avansată", "Roboţi de construcţie avansată" şi "Roboţi de prestări servicii". Activităţile de predarea au fost susţinute în limba romană şi germană. Cursurile predate în module concentrate la TU Dresden, Szent István University in Gödölö şi National Taiwan University of Science and Technology au îmbogăţit experienţa internaţională a candidatului. Autorul a publicat 6 cărţi şi suporturi de curs.

Activităţile de cercetare au fost desfăşurate în paralel cu activităţile de predare în aceaşi arie tematică. Candidatul a coordonat 5 proiecte de cercetare obţinute prin competiţie naţională şi internaţională în calitatea de director sau responsabil de partener şi a fost implicat in calitate de membru al echipei de cercetare în 17 proiecte şi contracte de cercetare desfăşurate la UP Timişoara, TU Dresden şi TU Ilmenau.

Activitatea publicistică în perioada considerată ca rezultat al cercetărilor şi dezvoltărilor desfăşurate a fost foarte amplă, astfel a publicat 5 articole în reviste indexate în baza de date ISI-Web of Knowledge, 11 articole în reviste indexate în bazele de date Scopus, Elsevier Science Direct şi Inspec, 26 de lucrări în conferinţe indexate în baza de date ISI-Web of Knowledge, 27 de lucrări în conferinţe indexate în bazele de date Scopus, IEEE şi Springer şi alte 69 de lucrări neindexate în diferite conferinţe naţionale şi internationale respectiv Congrese mondiale IFToMM.

Activităile publicistice au fost completate de activităti de recenzare pentru reviste şi conferinţe majore. Din anul 2009 candidatul activează în calitate de membru al comitetului ştiinţific al Buletinului Universităţii „Transilvania" Braşov, iar din anul 2013 în calitate de secretar al biroului editorial al revistei internaţionale "Robotica & Management". In 2015 am fost solicitat să lucrez în calitate de editor asociat al revistei „Advanced Robotics Systems".

Candidatul este membru în trei asociaţii profesionale ARoTMM (Romanian Association of Mechanism and Machine Science) asociată la federaţia IFToMM (International Federation of Mechanism and Machine Science) începând din anul 1991, SRR (Romanian Society of Robotics) începând din anul 2000 şi VDI „Verein Deutscher Ingenieure" începând din anul 1996. A fost ales pentru două mandate succesive membru al Comisiei Permanente IFToMM pentru Constituţie (2004-2011) şi actualmente este preşedinte al Comitetului Tehnic IFToMM Linkages and Mechanical Controls. La nivel naţional din anul 2005 este secretarul ştiinţific al organizaţiei nationale ARoTMM.

A prezidat sau co-prezidat mai multe Conferinţe naţionale şi internaţionale şi a editat 5 cărţi cu lucrările unor conferinţe IFToMM publicate la editurile Springer şi Trans-Tech Publisher.

După susţinerea tezei de doctorat a obţinut mai multe burse post-doctorale şi de predare în Germania (Humbold şi Erasmus), Ungaria (Pro Renovanda Cultura), Italia (Erasmus) şi Taiwan.

Alături de cariera academică şi profesională a desfăşurat şi activităţi manageriale în calitate de Director al Departamentului de Mecatronică de la Universitatea Politehnica Timisoara timp de 2 mandate, începând din 2008 până în prezent.

Secţiunea (IV) prezintă planul de evoluţie şi dezvoltare a carierei sistematizat în următoarele subpuncte: Direcţii de cercetare prioritare, Obiective, Plan de activitate şi Resurse financiare, umane şi de infrastructură.

Secţiunea (V) conţine referinţele bibliografice utilizate în secţiunea "Realizări ştiinţifice".

I. Introduction

The habilitation thesis shows the main scientific achievements performed after defending the PhD thesis in co-advisory between the University Politehnica Timişoara and Technical University Dresden, 27.02.1998 in Dresden and 03.06.1998 in Timişoara.

The research activities and publications cover the specific topic of the scientific fields of mechanism science, robotics and mechatronics, respectively mechanical and biomechanical engineering.

The research and development achievements were systematized in four main thematic research areas and illustrated through 10 selected papers, presented below.

1. Design of the mechanisms using non-circular wheels

1.1. Lovasz E.-C., Perju D., Modler K.-H., Gruescu C.M., Maniu I., Zabava E.-S. - Numerical Iterative Method for Computing the Base Circle Radius of Cam Mechanisms with Translating Flat-Face Follower, New Trends in Mechanism and Machine Science Theory and Applications in Engineering, Springer Publisher, Series: Mechanisms and Machine Science, 7 (2012) 237-244.
1.2. Lovasz E.-C., Modler Karl-Heinz, Perju Dan, Mărgineanu Dan, Zăbavă Eugen - On the relative sliding at the cam mechanisms with the tangential/flat follower, Proceedings of X–th International Congress on the Theory of Machines and Mechanisms, Liberec, Cehien, (2008) 371-376.
1.3. Lovasz E.-C., Perju D., Dehelean N., Dehelean L.M., Maniu I., Moldovan C. - Self-Balanced Conco-Balancer Manipulator with Band Mechanism, Solid State Phenomena, 166-167 (2010) 259-265.

2. Design of complex mechanisms structures

2.1. Modler K.-H., Lovasz E.-C., Bähr G., Neumann R., Perju D., Perner M., Margineanu D. - General method for the synthesis of geared linkages with non-circular gears, Mechanism and Machine Theory, 44(4) (2009) 726-738.
2.2. Lovasz E.-C., Ciupe V, Modler K-H, Gruescu C.M., Hanke U, Maniu I, Mărgineanu D. - Experimental Design and Control Approach of an Active Knee Prosthesis with Geared Linkage, New Advances in Mechanisms, Transmissions and Applications, Proc. of 2nd MeTrApp Conference, Springer Publisher, Series: Mechanisms and Machine Science, 17 (2013) 149-156.
2.3. Lovasz E.-C., Pop C., Pop F., Dolga V.: Novel solution for leg motion with 5 link belt mechanism, International Journal of Advanced Mechanics and Engineering, 19(4) (2014) 699-708.

3. Mechanisms development for mechatronics, robotics and mechanical applications

3.1. E.-C. Lovasz, D. Mărgineanu, V. Ciupe, I. Maniu, C.M. Gruescu, S.D. Stan, E.S. Zăbavă, Design and Control Solutions for Haptic Elbow Exoskeleton Module Used in Space Telerobotics, Proceedings of 2014 IFToMM Asian Conference on Mechanism and Machine Science, July 9–10, 2014, Tianjin, China, RM3-3, online.

3.2. E.-C. Lovasz, S. Grigorescu, D. Margineanu, C.M. Gruescu, C. Pop, V. Ciupe, I. Maniu, Geared Linkages with Linear Actuation Used as Kinematic Chains of a Planar Parallel Manipulator, Proc. of 3rd MeTrApp Conference, Mechanisms, Transmissions and Applications, Series Mechanism and Machine Science, 31 (2015) 21-31.

3.3. Lovasz E.-C., Modler K.-H., Neumann R., Gruescu C.M., Perju D., Ciupe V., Maniu I.: Novel design solutions for fishing reel mechanisms, Chinese Journal of Mechanical Engineering 28(4) (2015) 726-736.

4. Design of compliant mechanisms structures

4.1. Lovasz E.-C., Perju D., Modler K.-H., Modler N., Gruescu C. M., Maniu I., Comşa A. - On the Structural Analysis of the Mechanisms with Elastic Connections, The 11th IFToMM International Symposium on Science of Mechanisms and Machines, Springer Publisher, Series: Mechanisms and Machine Science, 18 (2013) 59-67.

Mechanisms are components of the drive systems of machines, devices and apparatus successfully used for transmitting and transforming of the rotational/translation motion and system of forces system from drive to the driving element. The aim is to transform the continuous motion of the input element in an imposed mainly non-linear motion, on the output element.

The request of non-linear motion on the output element can be achieved using different mechanism structures, which should have a minimum number of elements and can be manufactured with low cost. These mechanisms should ensure energy-saving tasks and the required accuracy, have a good dynamic performance, meet the environmental requirements and offer easy adjustment options. In order to be used in robotic and mechatronic applications, they should have a very simple geometry of the elements and increased DoF and allow a simple mechanical control.

The research areas presented in this work focuses on the main subjects, namely:

- studies of mechanisms structures which used non-circular wheels;

- studies of complex mechanisms structures;

- studies of mechanisms structures used in robotics, mechatronics and mechanical applications;

- studies of compliant mechanisms structures.

The studies regarding the main research directions refers not only on the 10 representatives selected papers, but also about other published researches within the main thematic research areas.

For the coherence of the description of the research directions, the chapters structure usually include: *(a) State-of-art* on the research topic and research problem statement; *(b) Theoretical and/or experimental contributions* to the described problem, highlighting the aim, analytical background, examples, applications or experimental results; (c) *Scientific contributions of the author*.

The academic and professional achievements, the career evolution and development plans, respectively the used references complete the present habilitation thesis.

II. Scientific achievements

1. Scientific achievements regarding the design of the mechanisms using profiled wheels

The scientific achievements about the mechanisms, which use non-circular wheels/elements, were focused on following open or partial solved subjects:

- computing of the base circle radius of the cam mechanisms with translating and oscillating flat-face follower;
- evaluation of the wear susceptibility by the cam mechanisms with translating and oscillating flat-face follower;
- designing of different non-circular wheels of band mechanisms for achievement of force equilibrium in different applications.

1.1. Base circle radius of the cam mechanisms with translating and oscillating flat-face follower

1.1.1. State-of-art

In order to minimize the size of the cam mechanism with translating and oscillating flat-face follower it is necessary to design the minimum size of the cam, which implies the computing of the base circle radius. The already-developed graphic-analytical and analytical methods for the calculation of the base circle radius are mostly restricted for the cam mechanisms with translating or oscillating roller follower, respectively for cam mechanism with translating flat-face follower [18], [25], [50], [51], [87], [122]. A unitary method for geometrical and kinematic synthesis using the exact design of the cam-disk profile was presented by Antonescu in [155]. In [204] Moise proposed an optimization method for the determination of the minimum size of the cam mechanism with translating oblique flat-face follower using the curvature relationship. Wunderlich [24] proposed a method to compute the cam profile of the cam mechanism with oscillating flat-face follower based on its "support function" relating the distance from the centre to the profile tangent with its angle direction. Angeles [43] obtained the optimum parameters of the cam mechanism with oscillating flat-face follower through cam-disk area minimization. Yu [70] designed the cam mechanism with flat-face follower considering an optimized proper motion and the requirement to have a curvature radius of the cam profile greater than a minimum limit. Zayas [183], [168] described a procedure that allows the generation of figures of constant diameter which can be used as profiles of constant-diameter cams with circular arcs. A method using the equivalent four-bar linkage of a disk-cam mechanism was proposed by Long-Iong [91], which allows the computing of the curvature radius of the cam-disk profile.

1.1.2. Aim of the theoretical research

The bibliographical research shows that in the case of cam mechanisms with oscillating or translating flat-face follower give any unitary analytical or graphical algorithm. The aim of this research was to develop a unitary analytical or numerical method in order to compute the base circle radius in the case of cam mechanisms with oscillating or translating flat-face follower, which uses a base circle radius function and the mathematical conditions to avoid the inflection or singularity points on the cam profile. The analytical algorithms for the both cam mechanisms with flat face follower were presented by the author in [131], [192], [193], [215] and [216].

1.1.3. Theoretical contributions

1.1.3.1. Synthesis equation of the cam mechanism with translating flat-face follower

The synthesis equation, i.e. the cam profile equation can be found as envelope of the relative positions of the follower in respect with the cam considering the inversion movement method [18], [25], [50], [51], [87], [122]. The displacement function $s = s(\varphi)$, the eccentricity e and the base circle radius r_b are considered to be known. The eccentricity is considered positive if it is oriented along the positive direction of x-axis (Fig. 1.1.1).
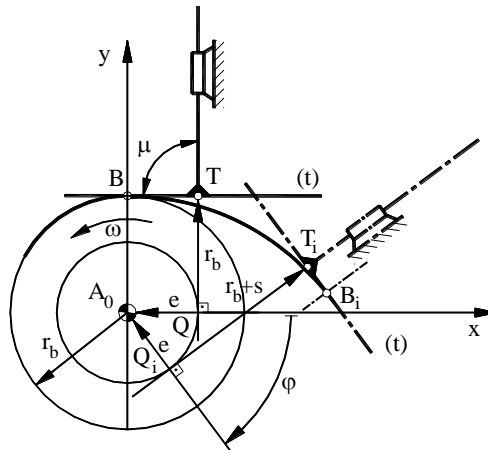
Fig. 1.1.1 Synthesis method of the cam mechanism with translating flat-face follower

In respect with the cam co-ordinate system, as shown in Figure 1.1.1, the parametric equations of the cam profile are:

$$x(\varphi) = [r_b + s(\varphi)] \cdot \sin\varphi + s'(\varphi) \cdot \cos\varphi , \quad y(\varphi) = [r_b + s(\varphi)] \cdot \cos\varphi - s'(\varphi) \cdot \sin\varphi , \tag{1.1.1}$$

with the current angle of the cam φ as parameter and $s'(\varphi) = ds/d\varphi$ the first derivative of the displacement function. It is important to notice that relationships (1.1.1) shows that the parametric equations of the cam profile are not influenced by the eccentricity e of the cam mechanism with flat-face follower.

1.1.3.2. Synthesis equation of the cam mechanism with oscillating flat-face follower

The cam profile equation used in synthesis can be calculated similarly with cam mechanism with translating flat-face follower in inverse movement.
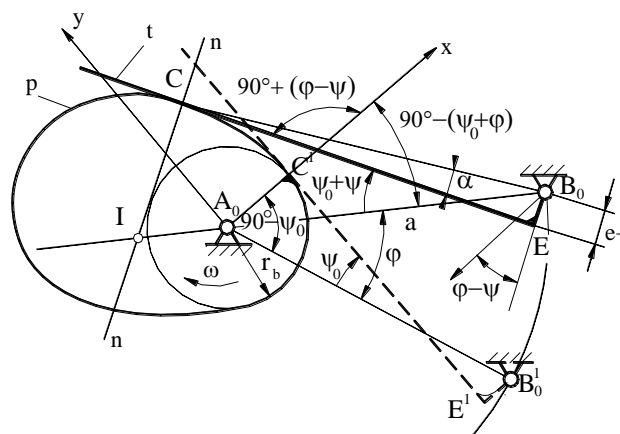
Fig. 1.1.2 Synthesis method of the cam mechanism with flat oscillating follower

The displacement function $\psi = \psi(\varphi)$, the follower arm offset e, the frame length a and the base circle radius r_b are known according to the technical application (Fig. 1.1.2). The initial flat-face follower angle in respect with the frame line $A_0B^1_0$ is:

$$\psi_0 = \arcsin((r_b + e)/a) \tag{1.1.2}$$

The parametric equation of the cam profile in respect with the cam co-ordinate system (Fig. 1.1.2), yields:

$$x(\varphi) = a \cdot \sin(\psi_0 + \varphi) - e \cdot \cos[\varphi - \psi(\varphi)] - \frac{a}{1 - \psi'(\varphi)} \cos[\psi_0 + \psi(\varphi)] \cdot \sin[\varphi - \psi(\varphi)],$$

$$y(\varphi) = -a \cdot \cos(\psi_0 + \varphi) - e \cdot \sin[\varphi - \psi(\varphi)] + \frac{a}{1 - \psi'(\varphi)} \cos[\psi_0 + \psi(\varphi)] \cdot \cos[\varphi - \psi(\varphi)], \tag{1.1.3}$$

with the current angle of the cam φ as parameter and $\psi'(\varphi) = d\psi/d\varphi$ the first derivative of the displacement function.

1.1.3.3. Numerical method for computing the base circle radius

The sizing of the base circle radius of the cam mechanism with translating or oscillating flat-face follower through a numerical method is based on the condition to avoid the cam profiles singularities:

$$\frac{dx(\varphi)}{d\varphi} \neq 0 \text{ and } \frac{dy(\varphi)}{d\varphi} \neq 0 \qquad (\forall) \varphi \in [0, 2\pi], \tag{1.1.4}$$

which means the derivatives of the parametric cam profile coordinates (1.1.3) should avoid being simultaneously zero.

A base circle radius function $f(\varphi, r_b)$ will be defined according to derivatives of the cam profile coordinates. The derivatives of the cam profile coordinates should ensure the conditions (1.1.4) if the general relationship:

$$r_b - f(\varphi, r_b) \neq 0, \quad (\forall) \varphi \in [0, 2\pi], \tag{1.1.5}$$

is satisfied.
The cam base circle radius, r_b, of cam mechanism with flat-face follower is compulsory to be strictly positive:

$$r_b > 0 \tag{1.1.6}$$

and the base circle radius function $f(\varphi, r_b)$ should be within the range $[\min\{f(\varphi, r_b)\}, \max\{f(\varphi, r_b)\}]$, where:

$$\min\{f(\varphi, r_b)\} < 0 \text{ and } \max\{f(\varphi, r_b)\} > 0. \tag{1.1.7}$$

To satisfy the conditions (1.1.5), (1.1.6) and (1.1.7), the cam base circle radius of the cam mechanism with flat-face follower results as:

$$r_b > \max\{f(\varphi, r_b); \varphi \in [0, 2\pi]\} \tag{1.1.8}$$

For computing the cam base circle radius out of the condition (1.1.8), a numerical iterative method is recommended to use.
In addition, the method assumes checking that the curvature radius is strictly positive in each point along the cam profile, which means [87]:

$$\rho(\varphi) = \frac{\sqrt{(x'(\varphi)^2 + y'(\varphi)^2)^3} \cdot \text{sgn}(\rho)}{x'(\varphi) \cdot y''(\varphi) - x''(\varphi) \cdot y'(\varphi)} > 0, \tag{1.1.9}$$

where:

$$sgn(\rho) = sgn\left(\frac{x(\varphi)\cdot y'(\varphi) - y(\varphi)\cdot x'(\varphi)}{x'(\varphi)\cdot y''(\varphi) - y'(\varphi)\cdot x''(\varphi)}\right) . \tag{1.1.10}$$

a) Case of cam mechanism with translating flat-face follower

The derivatives of the cam profile coordinates in case of cam mechanism with translating flat-face follower (1.1.1) are:

$$\frac{dx(\varphi)}{d\varphi} = [r_b + s(\varphi) + s''(\varphi)]\cdot\cos\varphi , \quad \frac{dy(\varphi)}{d\varphi} = -[r_b + s(\varphi) + s''(\varphi)]\cdot\sin\varphi , \tag{1.1.11}$$

where $s''(\varphi) = d^2 s / d\varphi^2$ is the second derivative of the displacement function.
The base circle radius function will be defined according to relationships (1.1.11):

$$f(\varphi, r_b) = -s(\varphi) - s''(\varphi) . \tag{1.1.12}$$

With the substitution of (1.1.1), (1.1.11) in (1.1.9) one gets the relationship of the curvature radius of the cam mechanism with translating flat-face follower:

$$\rho(\varphi) = \left|r_b + s(\varphi) + s''(\varphi)\right|\cdot sgn\left(\frac{r_b + s(\varphi)}{r_b + s(\varphi) + s''(\varphi)}\right) \tag{1.1.13}$$

where:

$$x'' = \frac{d^2 x(\varphi)}{d\varphi^2} = -[r_b + s(\varphi)]\cdot\sin\varphi + s'(\varphi)\cdot\cos\varphi - s''(\varphi)\cdot\sin\varphi + s'''(\varphi)\cdot\cos\varphi ,$$

$$y'' = \frac{d^2 y(\varphi)}{d\varphi^2} = -[r_b + s(\varphi)]\cos\varphi - s'(\varphi)\cdot\sin\varphi - s''(\varphi)\cdot\cos\varphi - s'''(\varphi)\cdot\sin\varphi . \tag{1.1.14}$$

The relationships (1.1.8) and (1.1.13) were expected and they are similar with the relationship obtained using the graphic-analytical method [18], [25], [50], [51], [87], [122].

a) Case of cam mechanism with oscillating flat-face follower

The derivatives of the cam profile coordinates in case of cam mechanism with oscillating flat-face follower (1.1.3) can be written in the form:

$$\frac{dx(\varphi)}{d\varphi} = A_1(\varphi)\cos\psi_0 + B_1(\varphi)\sin\psi_0 + C_1(\varphi) ,$$

$$\frac{dy(\varphi)}{d\varphi} = A_2(\varphi)\cos\psi_0 + B_2(\varphi)\sin\psi_0 + C_2(\varphi) , \tag{1.1.15}$$

where:

$$A_1(\varphi) = a\cdot\cos\varphi - a\cdot\cos[\varphi-\psi(\varphi)]\cdot\cos\psi(\varphi) + \frac{a\cdot\psi'(\varphi)}{1-\psi'(\varphi)}\cdot\sin[\varphi-\psi(\varphi)]\sin\psi(\varphi) -$$

$$- \frac{a\cdot\psi''(\varphi)}{(1-\psi'(\varphi))^2}\sin[\varphi-\psi(\varphi)]\cos\psi(\varphi),$$

$$B_1(\varphi) = -a\cdot\sin\varphi + a\cdot\cos[\varphi-\psi(\varphi)]\cdot\sin\psi(\varphi) + \frac{a\cdot\psi'(\varphi)}{1-\psi'(\varphi)}\cdot\sin[\varphi-\psi(\varphi)]\cos\psi(\varphi) + \tag{1.1.16}$$

$$+ \frac{a\cdot\psi''(\varphi)}{(1-\psi'(\varphi))^2}\sin[\varphi-\psi(\varphi)]\sin\psi(\varphi),$$

$$C_1(\varphi) = e\cdot(1-\psi'(\varphi))\cdot\sin(\varphi-\psi(\varphi)),$$

$$A_2(\varphi) = a \cdot \sin\varphi - a \cdot \sin[\varphi - \psi(\varphi)] \cdot \cos\psi(\varphi) - \frac{a \cdot \psi'(\varphi)}{1 - \psi'(\varphi)} \cdot \cos[\varphi - \psi(\varphi)] \sin\psi(\varphi) +$$

$$+ \frac{a \cdot \psi''(\varphi)}{(1 - \psi'(\varphi))^2} \cos[\varphi - \psi(\varphi)] \cos\psi(\varphi),$$

$$B_2(\varphi) = -a \cdot \cos\varphi + a \cdot \sin[\varphi - \psi(\varphi)] \cdot \sin\psi(\varphi) - \frac{a \cdot \psi'(\varphi)}{1 - \psi'(\varphi)} \cdot \cos[\varphi - \psi(\varphi)] \cos\psi(\varphi) - \qquad (1.1.17)$$

$$- \frac{a \cdot \psi''(\varphi)}{(1 - \psi'(\varphi))^2} \cos[\varphi - \psi(\varphi)] \sin\psi(\varphi),$$

$$C_2(\varphi) = -e \cdot (1 - \psi'(\varphi)) \cdot \cos(\varphi - \psi(\varphi)),$$

A base circle radius function will be defined according to the relationships (1.1.7) and (1.1.2):

$$f(\varphi, r_b) = -e + a \cdot \frac{2 \cdot \mathrm{tg}(\psi_0(\varphi)/2)}{1 + \mathrm{tg}^2(\psi_0(\varphi)/2)} . \qquad (1.1.18)$$

With the substitution of (1.1.2), (1.1.15) and the second derivatives of (1.1.2) in (1.1.9) follows a complicated relationship for computing the curvature radius of the cam mechanism with oscillating flat-face follower.

1.1.4.   Numerical examples

Through some numerical example will be solved the proposed method with chosen geometrical and kinematic values for the cam mechanism with translating or oscillating flat-face follower. In the examples for the rise and return sequences, the polynomial 3-4-5 motion curves are chosen.

a)   Case of cam mechanism with translating flat-face follower

In the Tab. 1.1.1 are given the geometrical and kinematical parameters of the cam mechanism with translating follower and of the imposed displacement diagram.

Tab. 1.1.1 Geometrical and kinematical parameters

inferior dwell 1	$\varphi_1 = 30°$	return	$\varphi_4 = 120°$
rise	$\varphi_2 = 120°$	inferior dwell 2	$\varphi_5 = 30°$
superior dwell	$\varphi_3 = 60°$	stroke	$h = 50\ mm$

In Fig. 1.1.3 and Fig. 1.1.4 is shown the variation of the derivatives (1.1.11), denoted $x'(\varphi)$ and $y'(\varphi)$, the base circle radius function $f(\varphi, r_b)$ and the curvature $\rho(\varphi)$ for two chosen values of the base circle radius, $r_b = 10\ mm$ and $r_b = 19.6\ mm$.

Fig. 1.1.3 shows that if both derivatives (1.1.11) do not obey the condition (1.1.4), the base circle radius function intersects the line corresponding to $r_b = 10\ mm$ for the same value of the cam rotation angle φ and the curvature radius will be null (does not obey the condition (1.1.9)). For this value of the base circle radius the cam profile singularities occur (Fig. 1.1.5.a).

In Fig. 1.1.4 is presented the case with both derivatives (1.1.11) different from zero and with the base circle radius function, which does not intersect the line corresponding for the chosen base circle, $r_b = 19.6\ mm$. The numerical solution of the associated equation to the relationship (1.1.5) is $r_b = 19.588\ mm$. The curvature radius of the cam profile obeys the condition (1.1.9) to be strictly positive. For this value of the base circle radius the cam profile avoids singularities (Fig. 1.1.5.b).

Fig. 1.1.3 Cam profile singularities by means of first derivative of the parametric equations (a), base circle radius function (b) and curvature (c) for r_b=10 mm

Fig. 1.1.4 Cam profile singularities by means of first derivative of the parametric equations (a), base circle radius function (b) and curvature (c) for r_b=19.6 mm
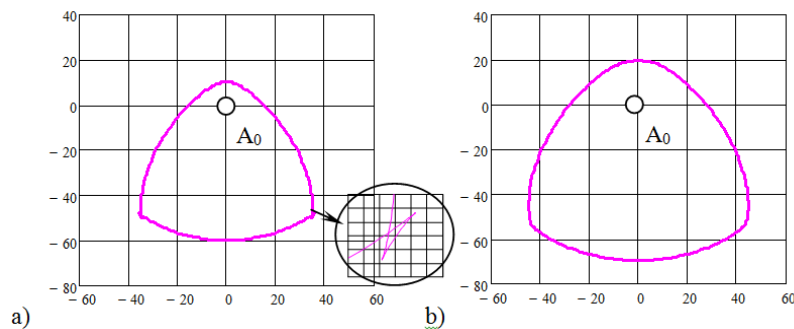
Fig. 1.1.5 Cam profile of the cam mechanism with flat-face translating follower with the base circle radius r_b=10 mm (a) and r_b=19.6 mm (b)

a)   Case of cam mechanism with oscillating flat-face follower

Tab. 1.1.2 shows the chosen geometrical and kinematical parameters of the cam mechanism with oscillating follower and of the imposed motion design.

In Fig. 1.1.6 and Fig. 1.1.7 are shown the variations of the first derivatives $x'(\varphi)$ and $y'(\varphi)$ and the base circle radius function $f(\varphi, r_b)$ for two chosen values of the base circle radius $r_b = 15\,mm$ and $r_b = 27\,mm$. Fig. 1.1.6 shows that for the two intersection points between the chosen value for the

base circle radius and the base circle radius function both first derivatives are simultaneous null. In this case, which does not satisfy the condition (1.1.4) the cam profile contains singularity points (Fig. 1.1.8.a). The base circle radius function does not intersect the value of the given base circle radius $r_b = 27\,mm$ and the consequence is the cam profile without singularities (Fig. 1.1.8.b). The numerical solution of the associated equation to relationship (1.1.5) is $r_b = 26.705\,mm$.

Tab. 1.1.2 Geometrical and kinematical parameters

inferior dwell 1	$\varphi_1 = 30°$	inferior dwell 2	$\varphi_5 = 30°$
rise	$\varphi_2 = 120°$	angular stroke	$\psi_{max} = 15°$
superior dwell	$\varphi_3 = 60°$	frame length	$a = 100\,mm$
return	$\varphi_4 = 120°$	follower arm offset	$e = 0\,mm$
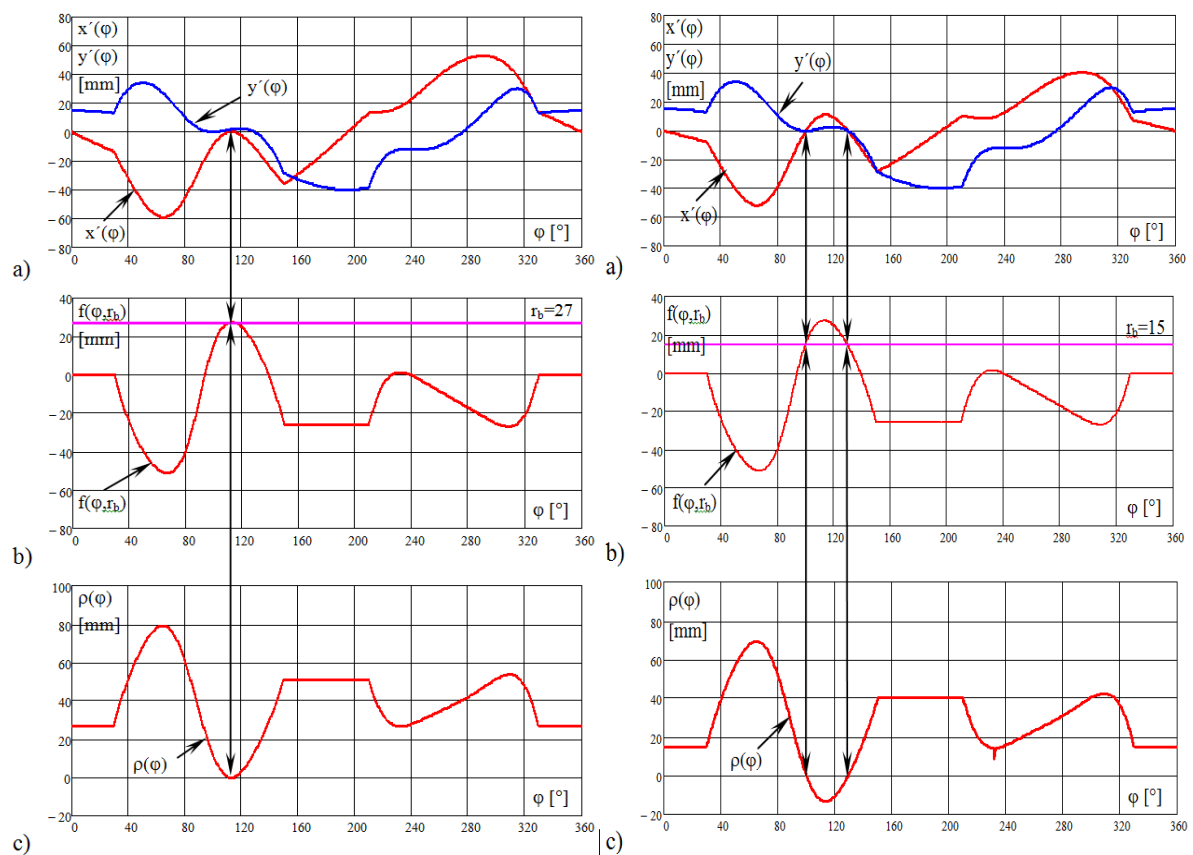
Fig. 1.1.6 Cam profile singularities by means of first derivative of the parametric equations (a), base circle radius function (b) and curvature (c) for r_b=15 mm
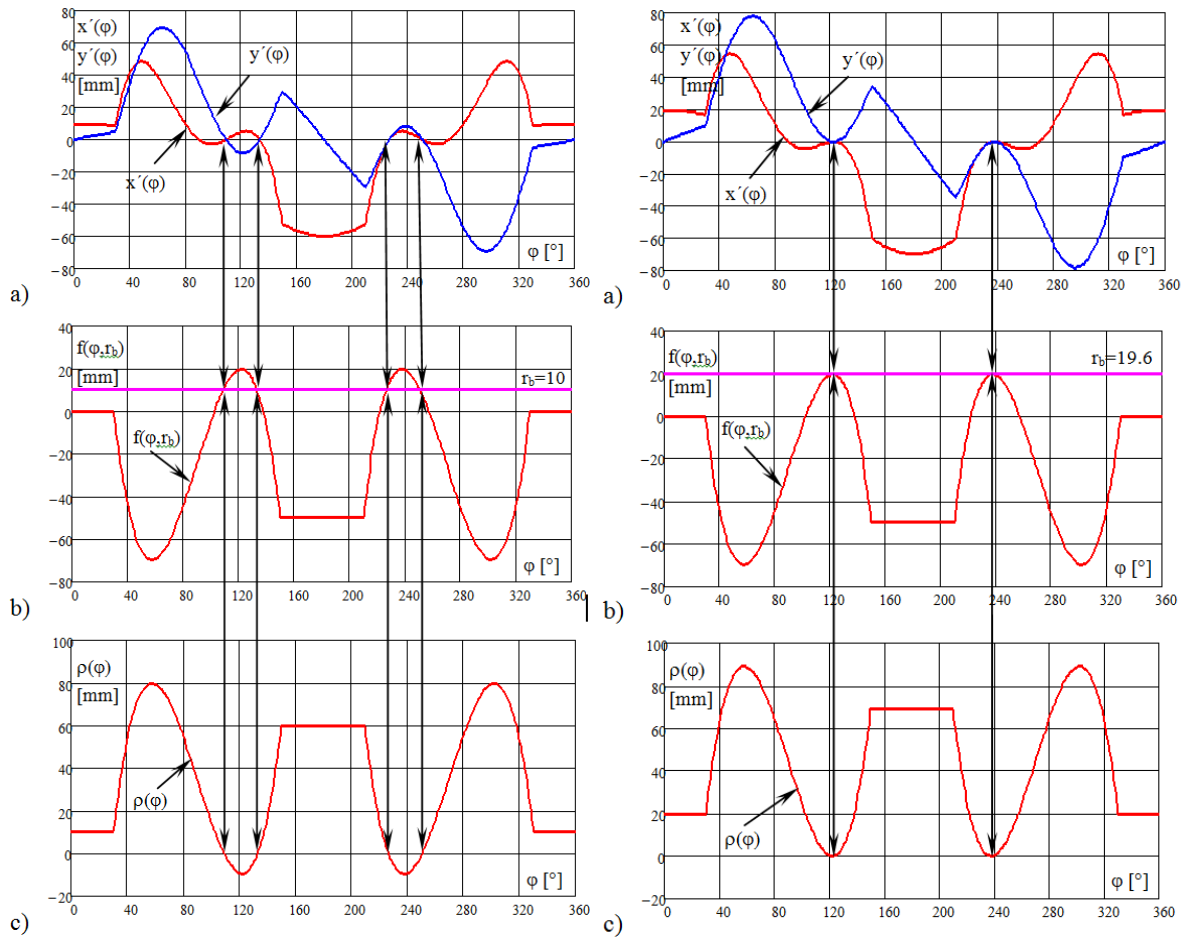
Fig. 1.1.7 Cam profile singularities by means of first derivative of the parametric equations (a), base circle radius function (b) and curvature (c) for r_b=27 mm
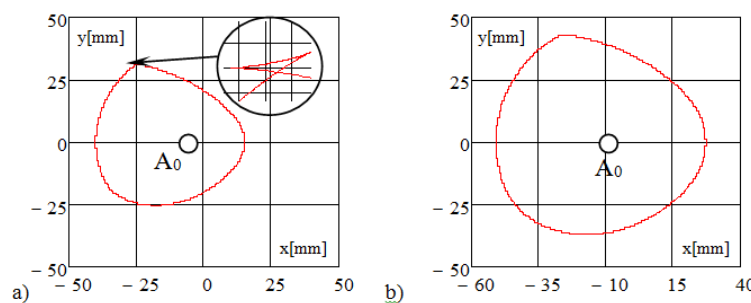
Fig. 1.1.8 Cam profile of the cam mechanism with flat-face oscillating follower with the base circle radius r_b=15 mm (a) and r_b=27 mm (b)

1.1.5. Scientific contributions

The proposed method allows the establishing of cam's base circle radius of the cam mechanism with translating and oscillating flat-face follower, in order to avoid the cam's profile singularities through a numerical method. This numerical iterative method is appropriate for specialized computer programs for the design of cam mechanism, in order to avoid random choosing of the base circle radius, which depends on the experience and skills of the designer or to avoid the use of the graphical-analytical method, which does not match with automatic computing.

The proposed numerical method allows a unitary approach for the computation of the cam base circle radius of the cam mechanism with translating flat-face follower and for the cam mechanism with oscillating flat-face follower.

For the chosen example problem, the graphical representation of the base circle radius function is presented as well in correspondence with the first derivatives of the cam profile coordinates and the cam curvature radius. The example problem confirms the theoretical hypothesis of the numerical method conceived to avoid the profile singularities through defining the base circle radius function and imposing the base circle radius bigger than the maximum value of the base circle radius function.

1.2. Evaluation of the wear susceptibility for cam mechanisms with flat-face follower

1.2.1. State-of-art

From tribology point of view, cam mechanisms imply a Hertzian frictional contact, in which the relative movement of the mating surfaces is rolling and/or sliding. Wear, as a gradual removal of material resulted at contacting surfaces in relative motion, affects both cam and follower.

There are four types of wear, which prevail, according to the specific parameters of an application:

- Abrasive wear – hard asperities from the materials in contact or third party material cause ridges, wedges, and cuttings of the surfaces or imbed into the surfaces
- Adhesive wear – the roughness picks of the mating surfaces weld, fracture and transfer material from one surface to another
- Fatigue wear – long time cyclic loading results into plasticization, subsurface cracks, delamination, fretting or pitting of surfaces
- Corrosion wear – new and undesired particles result from chemical/electrochemical reactions between the materials and lubricant and/or environmental chemical elements, enhanced by local heating processes [32].

Surfaces usually wear because of two or more processes simultaneously. Analytical general wear rate equations are very complicated and not suitable for practical use. [68] There are numerous attempts to describe mathematically the above processes and phenomena in wear models [32], which develop interdisciplinary knowledge including general mechanics, material science, chemistry, hydraulics and a thorough mechanics of contact [148]. A well-known model, which provides a simple relationship for the surface wear rate, in adhesive/abrasive wear, is Archard's model [13].

Cam mechanisms are extensively employed in engineering but do not have an extensive literature of their own from tribologic point of view. Most studies focus on automotive valve train, where a large number of factors are involved (cyclic loading, elasto-hydro-dynamic lubrication, high temperature, sliding and rolling friction etc.) [98].

Modern literature on cam mechanisms wear is dedicated to generation of wear models, considering variable cam material, technology and operation factors [232], [209], on purpose of knowing the size and distribution of wear, at various geometric parameters and working conditions [146].

FEM analysis is widely used to model and simulate the wear of cam, follower or both and to emphasize the contact pressure variation, as it is one the most important causes of wear development [66]. FEM analysis provides a skilful tool as it allows the study of different models, with variable parameters and establishing the influence of materials pair, cam position, lubrication conditions, hardness of surfaces on wear rate [212]. The same method was used in [143] to predict the wear considering that the wear rate of cam followers in a valve train system is mainly a function of contact stress between the cam and the follower, sliding velocity, coefficient of friction and hydrodynamic film thickness between the two surfaces.

Most advanced researches try to unify mechanism science and tribology, so that a large range of aspects to be reflected in the design algorithms. Such an interdisciplinary design is proposed in [229], combining mechanism and tribology criteria (minimum base radius and minimum contact stress), very important in tough condition of load and environment, such as applications in agriculture. Complex simulation of the wear process, described in [208], was designed to find maximum contact stress conditions in combined approach, from both tribology and mechanism (kinematics and dynamics) point of view. Most useful results of research come out from modelling and/or laboratory testing [114]. Practical evaluation of wear is reported by measuring roughness parameters before and after a camshaft running by means of a 3D/2D mapping [233]. The measurement of worn cam allowed the recovery of the original profile of the cam using the velocity transfer function of the follower, through a method presented in [172].

Some studies focus on contact dynamics. Different numerical models are used to compare contact forces and wear of different cam profiles [164]. Other researches pursue the optimization of the

surface properties from wear standpoint by applying proper surface treatment [145] or surface coatings [234]. Tribology tests, communicated in [234], were conducted on the traditional rig "reciprocating ball-on-disk", which provided information on wear behaviour under easy and safe control on load, sliding velocity, temperature, lubrication regime and surface properties.

Software development started to emerge in cam mechanisms combined design, mechanical and tribological. Authors of [211] implemented a program to control the cam-follower interface force, so that acceleration/deceleration effects in wear rate may be reduced. To minimize the maximum value of wear rate proportional factor, a genetic algorithm was applied on a general polynomial function TES in order to minimize surface fatigue and wear, as proposed in [195]. In [171] is given a suggestion on adjusting forward and backward acceleration, on purpose of having acceleration under control, as it is responsible of wear and "follower jump" effects.

1.2.2. Aim of the theoretical research

Taking into account the short presentation above, one may conclude that research results communicated in the literature did not yet lead to design algorithms, which satisfy both mechanical and tribological conditions. Most contributions refer to the camshaft of automotive, which are manufactured on large scale today. Thus, the researches regard especially the roller-follower. The references to the flat-face follower are scarce, and hence the subject is open to research.

The literature treats the cam mechanism by the model of rolling-sliding friction contact. For the specific case of flat-face follower, the amount of sliding is more important than for the roller follower. This is why the following study proposes the specific relative sliding as a characteristic parameter of the cam mechanism with flat-face follower, in the evaluation of cam mechanism's susceptibility to wear.

The specific relative sliding is defined as the ratio between sliding route and the sliding length of each of the two bodies/elements (s. Fig. 1.2.1)
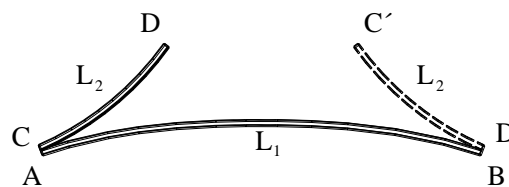
Fig. 1.2.1. The relative displacement of two elements with sliding and rolling of their relative movement

The absolute value of sliding route is equal with the length's difference $\left|L_1 - L_2\right|$, and the specific relative sliding are:

$$\sigma_1 = \frac{L_1 - L_2}{L_1} = 1 - \frac{L_2}{L_1}, \qquad \sigma_2 = \frac{L_2 - L_1}{L_2} = 1 - \frac{L_1}{L_2}. \tag{1.2.1}$$

Supposing the two bodies are made of the same material and have the same surface quality, it is obvious that the wear of the shortest body will be greater than the longest one: $\sigma_2 > \sigma_1$.

In such a way, the wear's susceptibility of a superior kinematic pair can be analyzed, particularly in the cam mechanisms with flat follower.

The evaluation of the wear susceptibility in the case of cam mechanism was published by the author in two papers [160] and [161].

1.2.3. Theoretical contributions

In the following paragraphs are developed the analytical calculus of the sliding lengths on the cam ΔL_C and follower ΔL_F in the case of the cam mechanism with translating and oscillating flat-face

follower. The computation of the sliding lengths ΔL_C and ΔL_F allow the computation of the specific relative sliding and the predicting of the wear susceptibility.

1.2.3.1. Specific relative sliding on a cam mechanism with translating flat-face follower

a)   Analytical computing method

Considering the cam mechanism with translating tangential follower in the initial (dotted line) and in a current position, like in Fig. 1.2.2, the relationship of the velocities in the contact point C can be expressed. The follower's velocity in a current position C can be expressed thus:

$$\overline{V_{C_2}} = \overline{V_{C_1}} + \overline{V_{C_2 C_1}}$$

(1.2.2)

where:

$$\overline{V_{C_1}} = \overline{\omega} \times \overline{r}$$

(1.2.3)

is the velocity of the contact point belongs to cam $\overline{V_C}$, and $\overline{V_{C_2 C_1}}$ is relative velocity between follower and cam in the considered position.
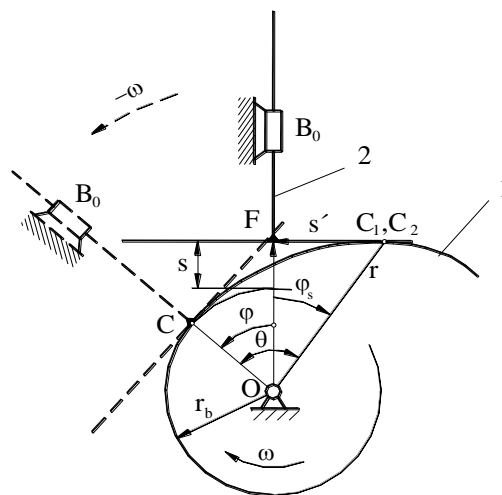
Fig. 1.2.2 Cam mechanism with centric translating flat-face follower

By dividing the relationship (1.2.2) with cam's angular velocity (ω), and representing it rotated with 90° it is obtained:

$$\overline{C_2 F} = \overline{C_1 O} + \overline{OF}$$

(1.2.4)

where:

$$C_2 F = \frac{V_F}{\omega} = \frac{ds/dt}{d\varphi/dt} = \frac{ds}{d\varphi} = s'$$

$$OF = r_b + s$$

(1.2.5)

s being current position of the follower, and r_b – base circle radius of the cam.

As can be seen in Fig. 1.2.2, the angular position of the contact point's vector OC in respect with the initial position (0) it differs of the cam's rotating angle φ with the quantity (supplementary angle):

$$\varphi_s = \text{arctg}\frac{s'}{r_b + s} \quad ,$$

(1.2.6)

resulting from the triangle COF.

The sliding length of cam arch between the two positions can be deduced from the mixed-linear triangle $COC_{1,2}$

$$dL_C = \sqrt{dr^2 + (r \cdot d\theta)^2} \; , \tag{1.2.7}$$

$$r = \sqrt{(r_b + s)^2 + s'^2} \; , \tag{1.2.8}$$

$$\frac{dr}{d\varphi} = \frac{s' \cdot (r_b + s + s'')}{\sqrt{(r_b + s)^2 + s'^2}} \tag{1.2.9}$$

$$d\theta = d\varphi + d\varphi_s \tag{1.2.10}$$

φ_s is given by the relationship (1.2.6), from which it is obtained:

$$\frac{d\varphi_s}{d\varphi} = \frac{s'' \cdot (r_b + s) - s'^2}{(r_b + s)^2 + s'^2} \tag{1.2.11}$$

With this value, from the relationship (1.2.10) it is obtained:

$$\frac{d\theta}{d\varphi} = \frac{(r_b + s)(r_b + s + s'')}{(r_b + s)^2 + s'^2} \tag{1.2.12}$$

and:

$$r \cdot d\theta = \frac{(r_b + s)(r_b + s + s'')}{\sqrt{(r_b + s)^2 + s'^2}} \cdot d\varphi \tag{1.2.13}$$

The relationship (1.2.7) with (1.2.9) and (1.2.13) becomes:

$$dL_C = (r_b + s + s'') \cdot d\varphi \tag{1.2.14}$$

The elementary sliding length on the follower, according with Fig. 1.2.2 ($L_F = FC_{1,2} = s'$), will be:

$$dL_F = \left| s'' \cdot d\varphi \right| \tag{1.2.15}$$

According to the relationships (1.2.1) of specific relative sliding is obtained:

$$\sigma_C = \frac{dL_C - dL_F}{dL_C} = 1 - \frac{s''}{r_b + s + s''} = \frac{r_b + s}{r_b + s + s''} \; , \qquad \sigma_F = \frac{dL_F - dL_C}{dL_F} = -\frac{r_b + s}{\left| s'' \right|} \; . \tag{1.2.16}$$

a)   Numerical computing method

Considering the cam mechanism with translating tangential follower in the initial position (doted line) and in two incremental successive current positions, like in Fig. 1.2.3, can be expressed the relationship of the velocities in the contact point C_i. In a current position (i), taking into account the contact point C_i, the follower's velocity can be expressed thus:

The sliding length of cam's arch between two successive incremental positions (i, i+1) can be deduced from the mixed-linear triangle $C_iC'_iC_{i+1}$

$$C_iC_{i+1} = \Delta L_{C_{i,i+1}} = \sqrt{(\Delta r_{i,i+1})^2 + (r_i \cdot \Delta\theta_{i,i+1})^2} \tag{1.2.17}$$

with:

$$\Delta r_{i,i+1} = r_{i+1} - r_i \tag{1.2.18}$$

$$r_i = \sqrt{(r_b + s_i)^2 + (s_i')^2} \; , \; r_{i+1} = \sqrt{(r_b + s_{i+1})^2 + (s_{i+1}')^2} \tag{1.2.18'}$$

and:

$$\Delta\theta_{i,i+1} = \left(\varphi_{i+1} + \varphi_{i+1}^s\right) - \left(\varphi_i + \varphi_i^s\right) = \Delta\varphi + \left(\varphi_{i+1}^s - \varphi_i^s\right) = \Delta\varphi + \Delta\varphi_{i,i+1}^s \tag{1.2.19}$$
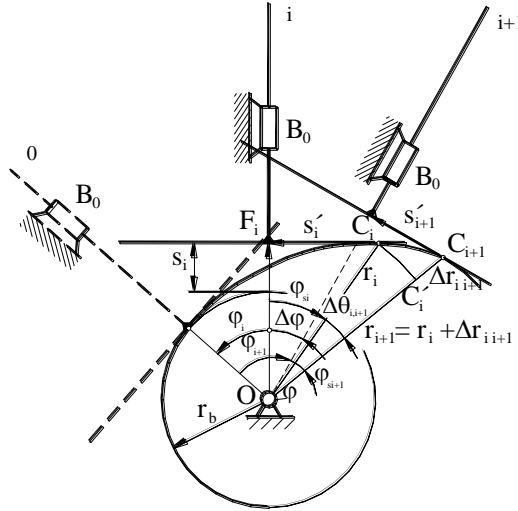
Fig. 1.2.3.Numerical evaluation of the sliding routes on cam and follower

$\Delta\varphi$ is the admitted increment of the impute angle φ .

$$\varphi_i^s = \arctan\frac{s_i'}{r_b + s_i}, \qquad \varphi_{i+1}^s = \arctan\frac{s_{i+1}'}{r_b + s_{i+1}} \tag{1.2.20}$$

The sliding length on the follower, for the same incremental positions, it is:

$$\Delta L_{F_{i,i+1}} = \left| s_{i+1}' - s_i' \right| \tag{1.2.21}$$

With these values, the specific relative sliding, for the considered interval (i, j), will be:

$$\sigma_{C_{i,j+1}} = \frac{\Delta L_{C_{i,j+1}} - \Delta L_{F_{i,j+1}}}{\Delta L_{C_{i,j+1}}} = 1 - \frac{\Delta L_{F_{i,j+1}}}{\Delta L_{C_{i,j+1}}}, \qquad \sigma_{F_{i,j+1}} = \frac{\Delta L_{F_{i,j+1}} - \Delta L_{C_{i,j+1}}}{\Delta L_{F_{i,j+1}}} = 1 - \frac{\Delta L_{C_{i,j+1}}}{\Delta L_{F_{i,j+1}}} . \tag{1.2.22}$$

1.2.3.2. Specific relative sliding on a cam mechanism with oscillating flat-face follower

a) Analytical computing method

In Fig. 1.2.4 the cam mechanism with oscillating flat-face follower is represented in the initial/starting position (for active stroke) $OB_0E_0C_0$ and in a current one: OBEC
The similarly relationship (1.2.4) in the case of cam mechanism with oscillating flat-face follower is:

$$\overline{C_2A} = \overline{C_1O} + \overline{OA}, \tag{1.2.23}$$

where:

$$C_2A = \frac{v_{C_2}}{\omega} = \frac{\omega_F \cdot BC}{\omega} = \frac{\frac{d\psi}{dt} \cdot BC}{\frac{d\varphi}{dt}} = \frac{d\psi}{dt} \cdot l_2 = l_2 \cdot \psi', \tag{1.2.24}$$

ω and ω_F being the angular velocities of cam and follower, respectively,

$$C_1O = r \tag{1.2.25}$$

is the current cam's radius of contact point, and
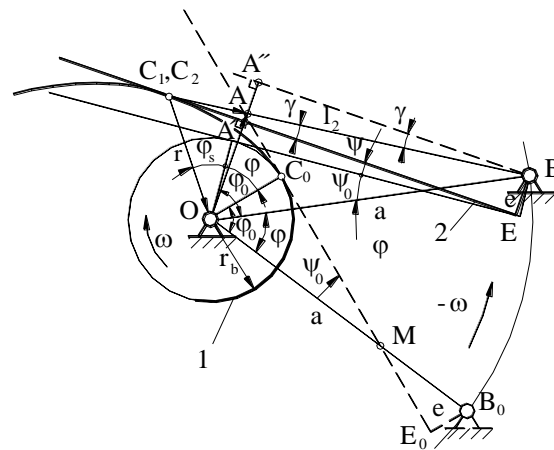
Fig. 1.2.4 Cam mechanism with eccentric oscillating flat-face follower

$$OA = \frac{v_{C_2 C_1}}{\omega} \ .$$ (1.2.26)

The position of follower's contact point C_2 in respect with oscillating center B can be expressed thus:

$$l_2 = C_2 B = C_2 A + AB$$ (1.2.27)

with:

$$AB = \frac{A''B}{\cos\gamma} \ ,$$ (1.2.28)

where:

$$A''B = a \cdot \cos(\psi_0 + \psi) \ ,$$ (1.2.29)

$$\gamma = \arcsin\frac{e}{l_2} \ .$$ (1.2.29')

With these values the relationship (1.2.28) becomes:

$$AB = \frac{l_2 \cdot a \cdot \cos(\psi_0 + \psi)}{\sqrt{l_2^2 - e^2}} \ .$$ (1.2.30)

From relationship (1.2.27), taking into account the relationships (1.2.24) and (1.2.30), it results:

$$l_2 = \frac{1}{1 - \psi'} \sqrt{a^2 \cdot \cos^2(\psi_0 + \psi) + e^2 \cdot (1 - \psi')^2}$$ (1.2.31)

The current cam's radius of the contact point can be calculated from the BOC triangle:

$$r = \sqrt{l_2^2 + a^2 - 2 l_2 a \cdot \cos(\psi_0 + \psi - \gamma)}$$ (1.2.32)

Taking into account the relationships (1.2.11) and (1.2.9') it is obtained:

$$r = \sqrt{e^2 + a^2 - 2 \cdot ea \cdot \cos(\psi_0 + \psi) - \frac{1 - 2 \cdot \psi'}{(1 - \psi')^2} \cdot a^2 \cdot \cos^2(\psi_0 + \psi)}$$ (3.33)

The starting values of the input and output angles respectively, can be calculated from the initial configuration of the cam mechanism: $OC_0E_0B_0$, i.e.

$$\frac{e}{r_b} = \frac{B_0 M}{a - B_0 M} \Rightarrow B_0 M = a \cdot \frac{e}{e + r_b}$$ (1.2.34)

and

$$OM = a - B_0M = a \cdot \frac{r_b}{e + r_b} \tag{1.2.35}$$

from which:

$$\sin\psi_0 = \cos\varphi_0 = \frac{r_b}{OM} = \frac{e + r_b}{a} \tag{1.2.36}$$

$$\psi_0 = \arcsin\frac{e + r_b}{a} \tag{1.2.36'}$$

$$\varphi_0 = \arccos\frac{e + r_b}{a} \tag{1.2.36''}$$

r_b being the base circle radius of the cam.

The angular position of the contact point's radius (r) in respect with the initial position differs of the cam's rotating angle (φ) with a supplementary angle (φ_s) which can be calculated by means sinus theorem in the triangle COB i.e.:

$$\frac{\sin(\varphi_0 + \varphi_S)}{l_2} = \frac{\sin(\psi_0 + \psi - \gamma)}{r} \tag{1.2.37}$$

from which follows:

$$\varphi_S = \arcsin\left(\frac{l_2}{r}\sin(\psi_0 + \psi - \gamma)\right) - \arccos\frac{e + r_b}{a} \tag{1.2.38}$$

The relationship (1.2.33) together with (1.2.38) and (1.2.36'') represents the polar equation of the cam's profile.

b)   Numerical computing method

The sliding length of cam's arch between two successive incremental positions can be calculated from the mixed-linear triangle $C_iC'_iC_{i+1}$ as in Fig. 1.2.5 with the relationships (1.2.17)-(1.2.19):
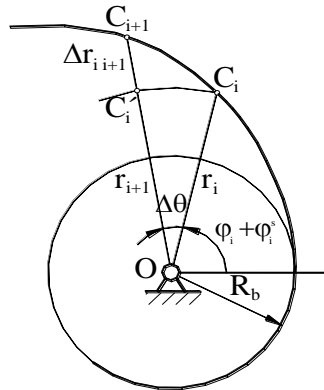
Fig. 1.2.5 Evaluation of incremental sliding length on the cam

The sliding length on the follower, for the same incremental positionsis:

$$\Delta L_{F_{i,i+1}} = \left| l_2^{i+1}\psi'_{i+1}\cos\gamma_{i+1} - l_2^i\psi'_i\cos\gamma_i \right| \tag{1.2.39}$$

with l_2 and γ from relationships (1.2.31) and (1.2.29') respectively.

The specific relative sliding for two successive incremental positions for cam and follower will be computed according to the relationships (1.2.22).With an angular increment $\Delta\varphi$ up to 1° a convenient result can be obtained in order identify the critic position of specific relative sliding for cam's profile and for follower, as well.

1.2.4. Numerical examples

1.2.4.1. Specific relative sliding on a cam mechanism with translating flat-face follower and circular eccentric disc cam

The following example considers as cam a circular eccentric disc cam and the follower as translating flat-face follower. From Fig. 1.2.6 results the transmission function of the cam mechanism as:

$$s = \varepsilon - \varepsilon \cdot \cos\varphi = \varepsilon \cdot (1 - \cos\varphi), \qquad (1.2.40)$$

By choosing $\varepsilon = r_b = h/2$, the transmissions functions of 0-order, first-order and second-order respectively becomes:

$$s = \frac{h}{2} \cdot (1 - \cos\varphi), \quad s' = \frac{h}{2} \cdot \sin\varphi, \quad s'' = \frac{h}{2} \cdot \cos\varphi. \qquad (1.2.41)$$
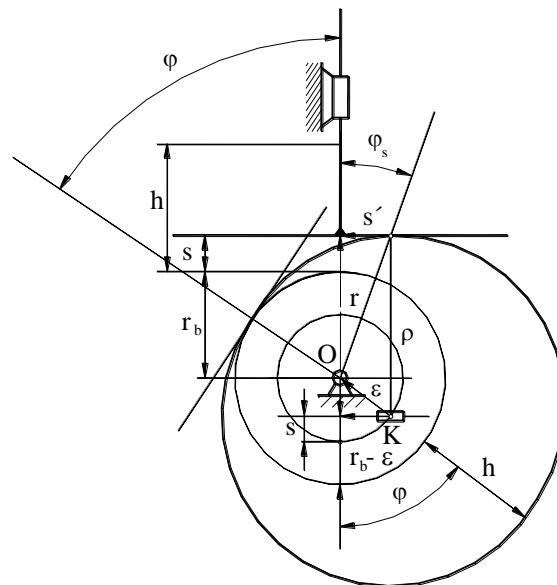
Fig. 1.2.6 Cam mechanism with translating flat-face follower and circular eccentric disc cam

By applying the incremental procedure with $\Delta\varphi = 10°$, the specific relative sliding for cam (σ_C) and follower (σ_F) respectively, have been obtained like in Tab. 1.2.1 and Fig. 1.2.7, for active stroke. Similarly the variation like in Fig. 1.2.4 was obtained for the same cam mechanism by means of infinitesimally approach.
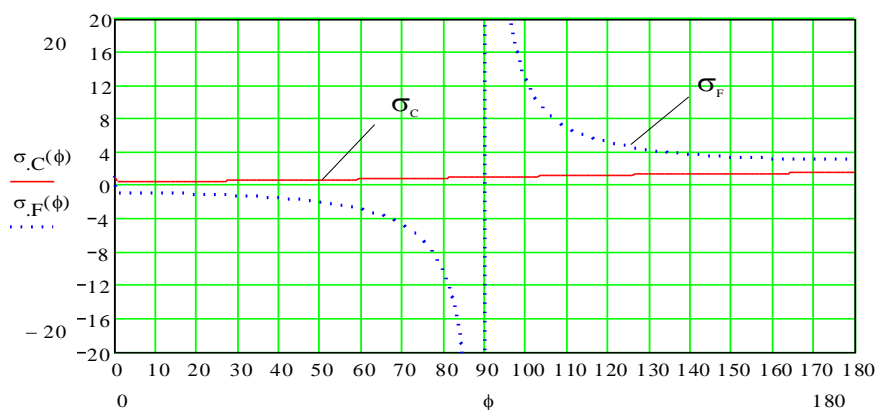
Fig. 1.2.7. The variation of specific relative sliding by incremental procedureand by means of analytical approach

The circular-eccentric disc cam was chosen as example in order to verify the proposed procedure, by comparing the total sum of incremental sliding lengths on the cam with the obvious value $\pi\rho$, were $\rho = h$ (see Fig. 1.2.6 and Tab. 1.2.1):

$$\sum_{i=0}^{n-1} \Delta L_{C_{i,i+1}} \cong \pi \cdot h, \qquad n = 18, \tag{1.2.42}$$

and also:

$$\sum_{i=0}^{n-1} \theta_{i,i+1} \cong \pi . \tag{1.2.43}$$

Tab. 1.2.1 Specific relative sliding for cam and follower for active stroke

interval	0-1	1-2	2-3	3-4	4-5	5-6	6-7	7-8	8-9	9-10	10-11	11-12	12-13	13-14	14-15	15-16	16-17	17-18
$\varphi°$	0-10	10-20	20-30	30-40	40-50	50-60	60-70	70-80	80-90	90-100	100-110	110-120	120-130	130-140	140-150	150-160	160-170	170-180
$\Delta\theta$	0.34	0.33	0.29	0.25	0.21	0.19	0.17	0.15	0.14	0.13	0.12	0.12	0.12	0.12	0.12	0.12	0.11	0.11
$\dfrac{\Delta L_C}{h}$	0.17	0.18	0.18	0.18	0.18	0.18	0.18	0.18	0.18	0.18	0.17	0.17	0.17	0.17	0.17	0.17	0.17	0.17
$\dfrac{\Delta L_F}{h}$	$8.607 \cdot 10^{-2}$	$8.226 \cdot 10^{-2}$	$7.595 \cdot 10^{-2}$	$6.734 \cdot 10^{-2}$	$5.667 \cdot 10^{-2}$	$4.429 \cdot 10^{-2}$	$3.056 \cdot 10^{-2}$	$1.59 \cdot 10^{-2}$	$7.615 \cdot 10^{-2}$	$-1.44 \cdot 10^{-2}$	$-2.913 \cdot 10^{-2}$	$-4.297 \cdot 10^{-2}$	$-5.551 \cdot 10^{-2}$	$-6.636 \cdot 10^{-2}$	$-7..519 \cdot 10^{-2}$	$-8.174 \cdot 10^{-2}$	$-8.580 \cdot 10^{-2}$	$-8.726 \cdot 10^{-2}$
σ_C	0.500	0.508	0.531	0.567	0.616	0.677	0.747	0.825	0.909	0.996	1.082	1.167	1.246	1.318	1.380	1.430	1.468	1.491
σ_F	-1	-1.033	-1.131	-1.309	-1.604	-2.093	-2.956	-4.731	-10.009	-228.82	13.148	7.005	5.069	4.149	3.634	3.324	3.137	3.035

1.2.4.2. Specific relative sliding on a cam mechanism with centric oscillating flat-face follower and polynomial 3-4-5 disc cam

The numerical example shows the critical values of specific relative sliding in the case of cam mechanism with centric oscillating flat-face follower. The considered transmission function for the cam mechanism is a polynomial 3-4-5:

$$\psi = \frac{\psi_{max}}{\varphi_1^3} \left(10 \cdot \varphi^3 - 15 \cdot \frac{\varphi^4}{\varphi_1} + 6 \cdot \frac{\varphi^4}{\varphi_1^2} \right), \tag{1.2.44}$$
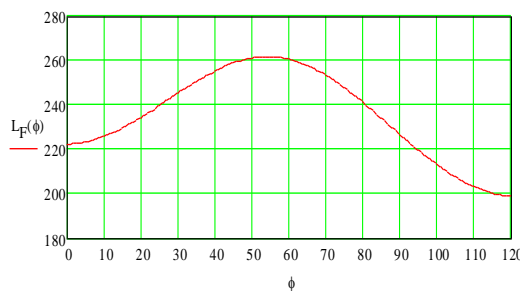
Fig. 1.2.8 The current position of the contact point belong to the follower C_2

with the active stroke characteristic angle $\varphi_1 = 2\pi/3$, the maximum stroke $\psi_{max} = 12°$, the frame length $a = 240mm$ and the base circle radius $r_b = 90mm$.

In Fig. 1.2.8 the current position of the contact point belong to the follower C_2 in respect with the oscillating center B (I_2), for the active stroke of the mechanism, is presented.

The current radius of the contact point belong to the cam (r), in respect with its angular position φ is shown in Fig. 1.2.9, and corresponding position of it in respect with the angular origin θ is shown in Fig. 1.2.10. By eliminating the independent variable φ between the two functions the polar equation of cam's profile $r(\theta)$ it results.
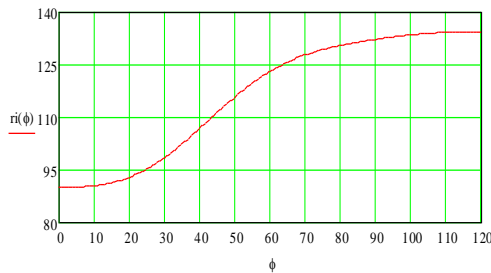
Fig. 1.2.9. The current radius (r) of the contact point belong to the cam
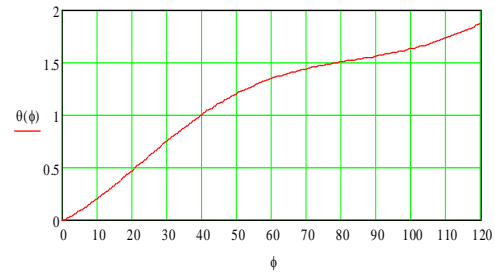
Fig. 1.2.10. The corresponding position of the current radius of the contact point in between the angular origin θ

The variation of the sliding length on the cam in respect with its angular position (φ) is presented in Fig. 1.2.11, and corresponding specific relative sliding for cam and follower, respectively, in Fig. 1.2.12. For all the above representations the admitted increment was $\Delta\varphi = 1°$. As can be seen the critical values of specific relative sliding for follower are at the beginning and at the end of the active stroke, as well as for the position with maximum value of the follower's angular velocity.
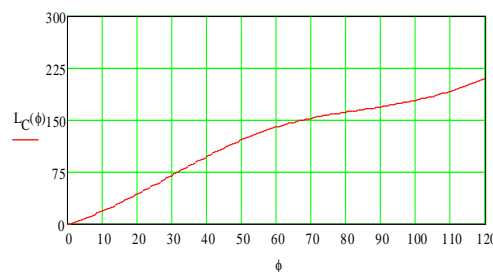
Fig. 1.2.11. The variation of the sliding length on the cam in respect with its angular position (φ)

The mentioned positions correspond with the maximum of wear and tear for cam and follower. For the cam no critical specific relative sliding exist for this case.
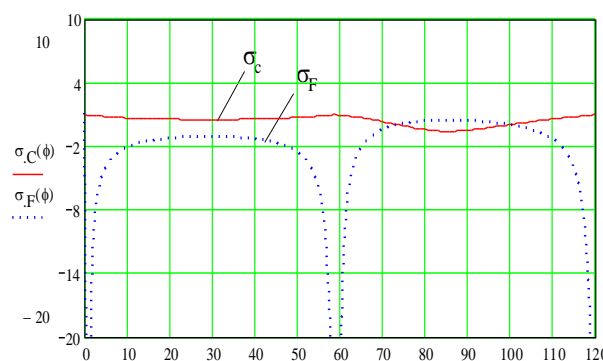
Fig. 1.2.12. Specific relative sliding for considered example problem

1.2.5. Scientific contributions

The proposed approach, the wear's critical portions on cam's profile and flat follower respectively, can be identified for any imposed or selected transmission function, taking also into account the force's regime.

For the cam mechanism with translating flat-face follower the critical zones for wear are around the centre cam projection on tangential follower and at the corresponding position to the maximum value of transmission function 1-order (s'_{max}) for each of the active or passive strokes. The wear's intensity is proportional with the specific relative sliding for cam and flat follower.

In the studied case of cam mechanism with oscillating flat-face follower the critical values of specific relative sliding for follower are at the position with maximum value of the follower's transmission function of first-order, as well as at the beginning and the end of the active stroke. This position corresponds to reversing relative velocity on the follower.

1.3. Special belt mechanisms used as self-balancing mechanisms

1.3.1. State-of-art

The technical literature shows many solutions for self-balancing of the manipulators and mechanisms. These solutions were developed for statically or dynamically conditions using counterweight, springs, belt mechanisms and actuators. Baradat et al in [157] systematized the balancing solutions for robotic systems by means of balancing using counterweights, springs, pneumatic or hydraulic cylinders, electromagnetic device, etc.

In [133] was given for reducing the vibrations a solution for dynamic balancing through inertial forces and moments optimisation. The dynamic balancing was formulated as an optimisation problem considering the balancing of the shaking forces accomplished through analytically balancing constraints. The objective function based on the sensitivity analysis of shaking moment in respect to the kinematic parameters of the links was used in order to minimise the shaking moment. The dynamic balancing of four, five, and six-bar linkages with prismatic pairs was presented by Feng in [47] by using a combination of mass redistribution and the addition of two inertial counterweights. The inertial counterweights were ordinary geared trains or planetary-gear trains. A complete balancing of planar linkages was developed by Ye and Smith in [60] as an equivalence method, which considered the effects of inertial moments and forces of a link by an equivalent simple links. The complete shaking forces and moments balancing of spatial mechanisms was presented in [154] using the methods of multibody dynamics.

Kazerooni in [45] treated a statically balanced method without using the gravity forces (without any counterweights) and choosing of smaller actuators and amplifiers. In [93] Wang and Gosselin studied static balanced manipulators with revolute actuators by using counterweights or springs. A hybrid methodology for balancing of spatial manipulator, that combines balancing using counterweights, springs and auxiliary parallelograms is presented by Agrawal and Fattah in [118]. Belt mechanism used for static force balancing of mechanisms was treated by Hain in [9] and Perju in [69]. In [69] Perju present an application of gear boxes with variable load for testing or running by using special types of belt mechanism with a spring.

Streit and Shin in [57] provided a mathematical algorithm for comparing the complexity of equilibration methodologies. For a few topologies of 3-DOF planar parallel mechanisms has been developed the dynamic analysis using counterweights or springs or a combination of both by Laliberte et al [90], in order to illustrate the behaviour of static balancing and to characterise of each of the mechanism topologies presented here. Static balancing can be used successfully in several mechatronic systems, including manual devices, flight simulators, robotic manipulators, and others, reducing substantial the actuator torques and power.

1.3.2. Aim of the theoretical research

After the presentation of the state-of-art in the field of the self-balancing mechanisms, one may conclude that the self-balancing methods using special type of belt mechanisms can be used in many technical applications in the field of mechanical devices, measurement tools, robotics, etc.
Based on the experience of the author in his PhD. study of the belt mechanism some applications of the special type of belt mechanism using a spring were published by the author in the papers [126], [144] and [194].

1.3.3. Theoretical contributions

In the following paragraphs are presented some applications of the special belt mechanism using a spring for achieving static force equilibrium of a loading platform and in a constant pressure chamber respectively self-balancing of a measurement tool and a manipulator.

1.3.3.1. Principle of force equilibrium

The special type of belt mechanism illustrated in the Fig. 1.3.1. can use for achieving the force equilibrium an elastic force F_e by considering a spring (a) or a gravitational force W by considering a counterweight (b). The main forces F, which have to be equilibrated, are usually of gravitational type.
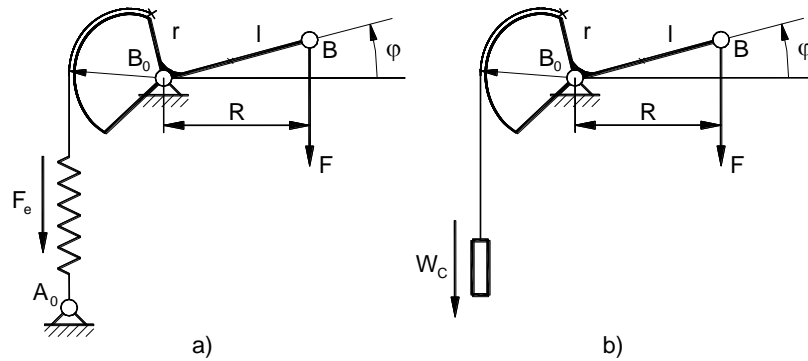
Fig. 1.3.1. Belt mechanism with a spring used for static force equilibrium

In both cases the equilibrium equation is of moment type. If a counterweight is used, the equilibrating mechanism has to ensure its displacement, in horizontal plane, so that the total moment it vanishes. That means the counterweight moves in horizontal plane opposite and proportional with the projection of the centre of gravity of the equilibrated element/mechanism in the same plane. If the centre of gravity of the equilibrated element it moves only vertical (like at an elevator), then the counterweight will move also vertically only, i.e. at constant arm.

In this case the equilibrium moment's equation it has the form:

$$F \cdot R = Q \cdot r,$$ (1.3.1)

where: F is the force or weight to be equilibrated,

Q - the weight of the counterweight W_C,

R and r - the arms of the two forces (variable or constant).

The second solution is to use an elastic force, given by a spring, for equilibration. In this case in the equation (1.3.1) Q means the elastic force of the spring F_e. The elastic force is usually a linear variable force of the form:

$$F_e = F_{e0} + k \cdot s,$$ (1.3.2)

where: F_{e0} is the pretension elastic force of the spring

k - the spring's elasticity constant

s - the spring's deflection/elongation.

The synthesis problem consists in finding the equation of a noncircular wheel $r = r(\varphi)$ for a corresponding selected spring so that the equilibrium should be done. This kind of equilibrating mechanisms belongs to the class of, so-called, belt mechanisms or centroid mechanisms.

1.3.3.2. Self-balancing of a measurement head

The simplest equilibrating mechanism is the self-balancing of a body in vertical movement for its entirely working range [126], as is the case of vertical displacement of the measuring head of a co-ordinate measuring apparatus (Fig. 1.3.2).

In this case the equilibrium equation (1.3.1) becomes:

$$W \cdot R_0 = (F_{e0} + k \cdot s) \cdot r.$$ (1.3.3)

With the clearance condition $r \leq R_0$ ($r_{max} = R_0$) the pretension elastic force will be:

$$F_{e0} = W.$$ (1.3.4)
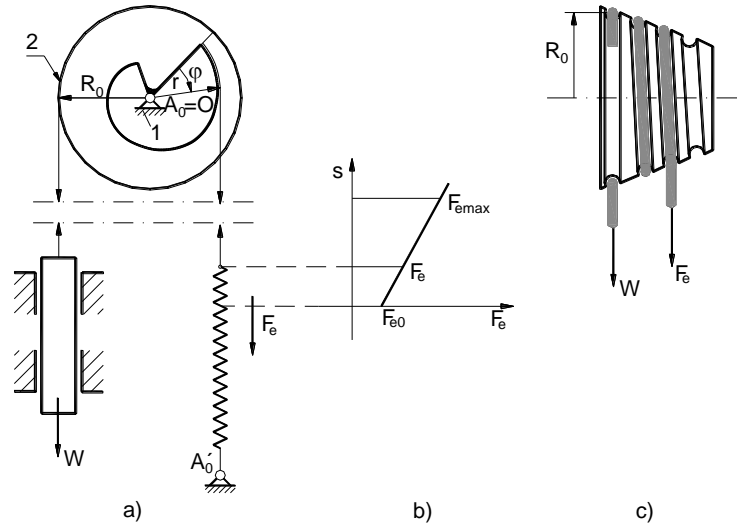
Fig. 1.3.2. Self-balanced measuring head of a co-ordinate measuring apparatus

If the stroke H of the equilibrated element is not very large, the maximum angle of the pulley assembly φ_{max} can be up to 2π radians. In this case

$$R_0 = H/\varphi_{max} = H/2\pi.$$ (1.3.5)

For a long stroke, but a reasonable clearance, the noncircular wheel of the pulley assembly is made as a conical helix (see Fig. 1.3.2c) allowing more than one turn.
With the constant value of the left hand side term of equation (1.3.3),

$$W \cdot R_0 = C$$ (1.3.6)

and the wrapping condition:

$$r \cdot d\varphi = ds,$$ (1.3.7)

the equation (1.3.3) becomes:

$$C \cdot d\varphi = (F_{e0} + k \cdot s) \cdot ds.$$ (1.3.8)

Integrating this equation one obtains:

$$k \cdot s^2 + 2 \cdot F_{e0} \cdot s - 2 \cdot C \cdot \varphi = 0,$$ (1.3.9)

from which, the current arc of the noncircular wheel it results:

$$s = \frac{1}{k}(\sqrt{F_{e0}^2 + 2Ck \cdot \varphi} - F_{e0}).$$ (1.3.9′)

The equation of the profile of noncircular wheel, in polar co-ordinate, is obtained by derivation of the equation (1.3.9) according to (1.3.7) i.e.:

$$r = \frac{ds}{d\varphi} = \frac{C}{\sqrt{F_{e0}^2 + 2Ck \cdot \varphi}}.$$ (1.3.10)

In the extreme position the equilibrium equation is:

$$r_{min} \cdot F_{emax} = r_{max} \cdot F_{emin} = C; \qquad F_{emin} = F_{e0},$$ (1.3.11)

with the boundary conditions: $r_{max} = r|_{\varphi=0} \leq R_0$, $r_{min} = r|_{\varphi=\varphi_{max}}$.
For $\varphi_{max} = 2\pi$,

$$r_{min} = \frac{C}{\sqrt{F_{e0}^2 + 4\pi Ck}}.$$ (1.3.12)

With these values, from equation (1.3.9) it results:

$$k^2 \cdot s_{max}^2 + 2F_{e0}k \cdot s_{max} - 4\pi kR_0 F_{e0} = 0.$$ (1.3.13)

Admitting one of the two variable (s_{max} or k) the second can be found from equation (1.3.13) or equation (1.3.9).

Numerical example

By considering the characteristic values for self-balancing measurement head are given in Tab. 1.3.1,

Tab. 1.3.1. Characteristic values for self-balancing measurement head

Nr.	Characteristic dimension	Notation	Value
1	Weight of measurement head	W	100 N
2	Pretension force of the spring	$F_{e0} = F_{min}$	100 N
3	Radius of the circular wheel	R_0	50 mm
4	Spring's elasticity constant	k	2 N/mm
5	Maximum rotation angle	φ_{max}	360°

the stroke H of the equilibrated element and the maximum elongation of the spring can be calculated:

$$H = 2\pi R_0 = 314\,mm, \qquad s_{max} = \frac{1}{k}(\sqrt{F_{e0}^2 + 4\pi Ck} - F_{e0}) = 134.12\,mm.$$

In Fig. 1.3.3 the variation of the spring's elongation in respect with current angle φ of pulley assembly are presented, and in the Fig. 1.3.4 the radius of noncircular profile is represented in polar coordinate; i.e. the actual profile of the noncircular wheel.
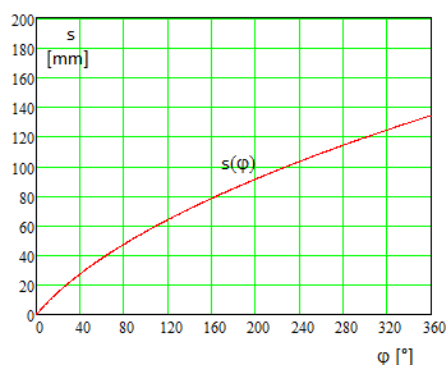
Fig. 1.3.3. The spring elongation $s=s(\varphi)$ Fig. 1.3.4. The profile of noncircular wheel $r=r(\varphi)$
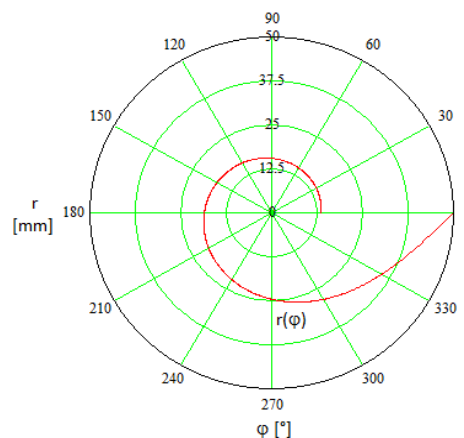
1.3.3.3. Force equilibrium in a constant pressure chamber

In some technical applications, a constant pressure of a gas is necessary to be maintained in a chamber with variable volume. This is the case of biogas reservoir, or the equipment for gas meters' calibration [144]. Usually the pressure-tight (packing) is made using a bell and a vessel with a liquid. The gas pressure under bell depends on the weight of it and of the immersion dipping of the bell's wall. In order to have a constant gas pressure, the apparent bell's weight has to be constant. That means the Archimedean force has to be compensated. The compensatory mechanisms can used a band mechanism with massless wire and an noncircular wheel or a simple pulley mechanism with circular wheel and a heavy wire/chain. In the following is presented the first type of compensatory mechanism. In Fig. 1.3.5 a constant pressure chamber, using a bell and a vessel with liquid seal/packing, is presented. The value of pressure inside the bell is:

$$p = \rho \cdot g \cdot y,$$ (1.3.14)
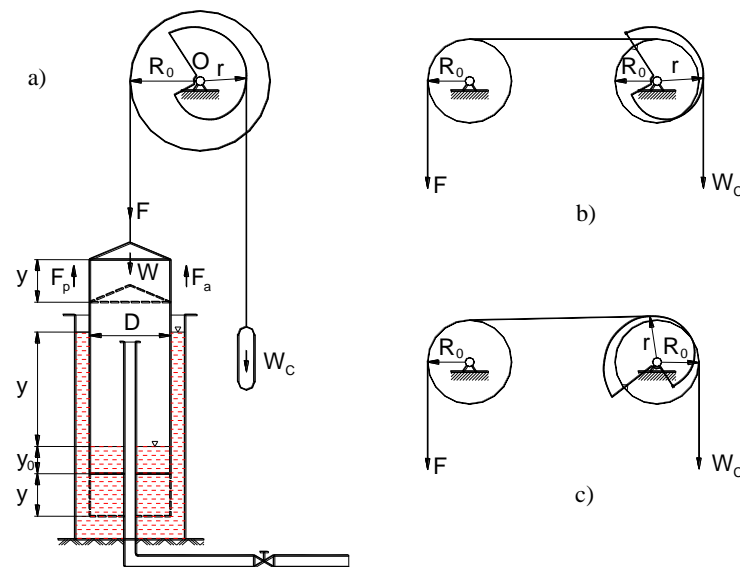
Fig. 1.3.5. Compensatory band mechanism of the Archimedean effect

where ρ is the liquid density and g – local gravitational acceleration.
The apparent weight of the bell is:

$$F = W - F_p - F_a,\tag{1.3.15}$$

where: W is the bell's weight,

$$F_p = p \cdot \pi \cdot D^2 / 4\tag{1.3.16}$$

is the acting force due to the pressure inside the bell,

$$F_a = A_i \cdot \rho \cdot g \cdot (y_0 + y)\tag{1.3.17}$$

is the Archimedean (accessional) force due to the bell's immersion into the liquid with $(y_0 + y)$ dipping, y_0 being the initial immersion dipping,

$$A_i = \pi \cdot D_m \cdot b = \pi \cdot (D + b) \cdot b\tag{1.3.18}$$

is the ring shaped transversal aria of the bell's wall of thickness b.
The equilibrium condition of the two coupled wheels of the compensatory mechanism with massless wire (Fig. 1.3.5.a), has the form (1.3.1).
The correlation between the vertical displacement of the bell and the rotation angle of the two wheels is given by the obvious relationship:

$$y = R_0 \cdot \varphi.\tag{1.3.19}$$

With these values, from the equilibrium condition, the equation of the noncircular wheel's profile, in polar coordinate, results, in the form:

$$r = R_0 \cdot \frac{F}{G_c} = R_0 \cdot \frac{W - F_p - A_i \cdot \rho \cdot g \cdot (y_0 + R_0\varphi)}{W_c} = R_0(k_1 + k_0 \cdot \varphi),\tag{1.3.20}$$

i.e. an Archimedean spiral.
Obviously, the equation (1.3.20) has to satisfy the condition $r \geq 0$, even for maximum bell's displacement (y_{max}) i.e.:

$$W - F_p - A_i \cdot \rho \cdot g \cdot (y_0 + y_{max}) \geq 0.\tag{1.3.21}$$

Accepting:

$$W - F_p - A_i \cdot \rho \cdot g \cdot y_0 = W_c,\tag{1.3.22}$$

the condition (1.3.21) becomes:

$$W_c \geq A_i \cdot \rho \cdot g \cdot y_{max} \left(= A_i \cdot \rho \cdot g \cdot R_0 \cdot \varphi_{max}\right),$$ (1.3.23)

and the equation (1.3.20) will have the form:

$$r = R_0 \cdot \left[1 - \frac{A_i \cdot \rho \cdot g \cdot R_0}{W_c} \cdot \varphi\right].$$ (1.3.24)

For a large diameter D of the bell, a solution like in Fig. 1.3.5.a is not a practical one. In this case, some arrangements like in Fig. 1.3.5.b or Fig. 1.3.5.c should be used. The solution represented in Fig. 1.3.5c has the advantage that the counterweight moves on a vertical line. In this case the counterweight may be guided, in a tube for example, in order to prevent its oscillation.

Numerical example

By considering a bell having the characteristic values given in Tab. 1.3.2,

Tab. 1.3.2. Characteristic values for self-balancing of a constant pressure chamber

Nr.	Characteristic dimension	Notation	Value
1	Bell diameter	D	0.5 m
2	Thickness of the bell	b	5 mm
3	Density of the packing liquid	ρ	$0.88 \cdot 10^3$ kg/m^3
4	Gas volume	V	0.2 m^3
5	Radius of the circular wheel	R_0	0.3 m

the bell's stoke y_{max} can be computed from the bell volume relationship as $y_{max} \cong 1.02\,\text{m}$. The profile's equation (1.3.24) of the noncircular wheel can be written simplified as:

$$r = R_0(1 - k\varphi).$$ (1.3.25)
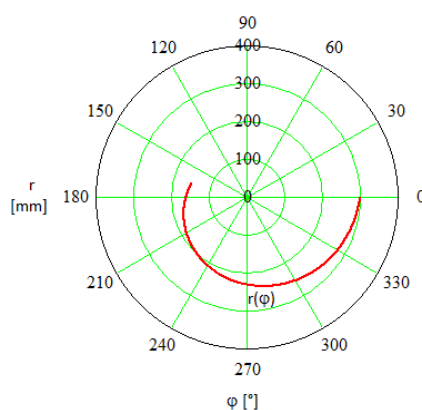
Fig. 1.3.6. The profiled wheel for compensatory belt mechanism

Choosing the value for the radius of the circular bell (s. Tab. 1.3.1), the maximum rotating angle of the two wheels will be:

$$\varphi_{max} = y_{max}/R_0 = 1,02/0,3 = 3,4\,\text{rad} = 194,9^0$$

Admitting the boundary conditions for the noncircular wheel $r_{max} = R_0$ for $\varphi = 0$ and $r_{min} = 0.5 \cdot R_0$, the equation (1.3.25) becomes:

$$r = 300 \cdot (1 - 0,147 \cdot \varphi)\quad[\text{mm}]$$ (1.3.26)

where φ increasing in clockwise direction.

In Fig. 1.3.6 the profile of the noncircular wheel is presented.

1.3.3.4. Force equilibrium of a mechanism of bistable type

The mechanisms´ synthesis problem of bistable type is more complicated as the previous case. As example problem is taken into account the mechanism of a loading ledge/platform. The platform

has to be in equilibrium in a certain position only, which is the median angular position φ_m between the angular positions φ_{min} and φ_{max}. Above this position on the platform it acts an ascension force and under it a symmetrical, equal and opposite force. At the ends of stroke these forces have to have prescribed absolute values (F_m). An existing solution for this kind of mechanism is a cam-follower one, with the follower as driving element (Fig. 1.3.7.a), with its specific disadvantages.
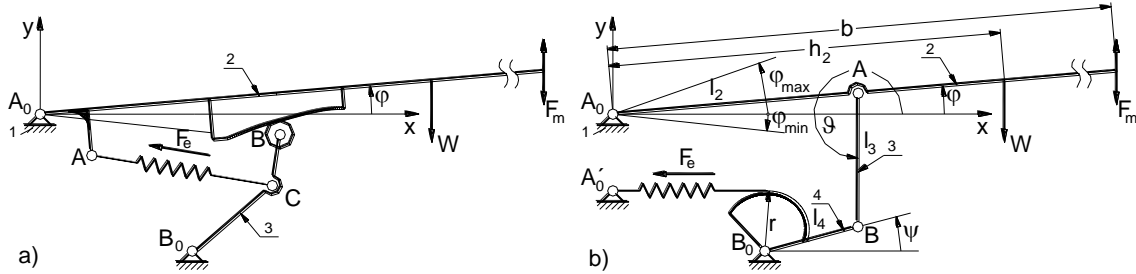
Fig. 1.3.7. Two solutions for a loading ledge mechanism

In [126] was propose a four-bar mechanism actuated by means of a spring and a noncircular wheel (a band mechanism – Fig. 1.3.7.b) in order to accomplish the imposed conditions. In order to compute the kinematic parameters of the four bar mechanism is considered the closed loop equation:

$$l_2 \cdot e^{i\cdot\varphi} + l_3 \cdot e^{i\cdot\vartheta(\varphi)} - l_4 \cdot e^{i\cdot\psi(\varphi)} - (x_{B_0} + i \cdot y_{B_0}) = 0 . \tag{1.3.27}$$

and its complex conjugate, the current position of links 3 and 4 respectively, in function of the independent variable φ, it results in the forms:

$$\psi(\varphi) = 2 \cdot \arctan \frac{B_1(\varphi) + \sqrt{A_1^2(\varphi) + B_1^2(\varphi) - C_1^2(\varphi)}}{A_1(\varphi) - C_1(\varphi)} , \tag{1.3.28}$$

$$\vartheta(\varphi) = 2\pi + 2 \cdot \arctan \frac{B_2(\varphi) - \sqrt{A_2^2(\varphi) + B_2^2(\varphi) - C_2^2(\varphi)}}{A_2(\varphi) - C_2(\varphi)} , \tag{1.3.29}$$

where:

$$A_1(\varphi) = 2l_4(x_{B_0} - l_2 \cdot \cos\varphi), \quad B_1(\varphi) = 2l_4(y_{B_0} - l_2 \sin\varphi),$$
$$C_1(\varphi) = (x_{B_0}^2 + y_{B_0}^2) + l_2^2 - l_3^2 + l_4^2 - 2l_2(x_{B_0} \cos\varphi + y_{B_0} \sin\varphi), \tag{1.3.30}$$

$$A_2(\varphi) = 2l_3(-x_{B_0} + l_2 \cdot \cos\varphi), \quad B_2(\varphi) = 2l_3(-y_{B_0} + l_2 \sin\varphi),$$
$$C_2(\varphi) = (x_{B_0}^2 + y_{B_0}^2) + l_2^2 + l_3^2 - l_4^2 - 2l_2(x_{B_0} \cos\varphi + y_{B_0} \sin\varphi). \tag{1.3.31}$$

The reacting force in the joint B is on BA direction and has the value:

$$R_B(\varphi) = W \frac{-h_2 \cdot \cos\varphi}{l_2 \cdot \sin(\vartheta(\varphi) - \varphi)} . \tag{1.3.32}$$

The moment in respect with joint B_0 of this force is:

$$M_1(\varphi) = R_B(\varphi) \cdot l_4 \cdot \sin(\vartheta(\varphi) - \psi(\varphi)) . \tag{1.3.33}$$

The variation of manipulating force F_m in the working span of the platform is accepted in the form:

$$F_m(\varphi) = \begin{cases} -F_m + 2\lambda F_m(1 - \cos(\pi \frac{\varphi - \varphi_{min}}{2\lambda\Delta\varphi})) & \varphi \in (\varphi_{min}, \varphi_{min} + \lambda\Delta\varphi) \quad ; \quad \lambda = 12/25 \\ -F_m + 2F_m[\lambda + (1-\lambda)\cos(\pi(\frac{1}{2} + \frac{(\varphi - \varphi_{min}) - \lambda\Delta\varphi}{2(1-\lambda)\Delta\varphi}))] & \varphi \in (\varphi_{min} + \lambda\Delta\varphi, \varphi_{max}) \end{cases} \tag{1.3.34}$$

which gives a supplementary moment on driving link:

$$M_2(\varphi) = F_m(\varphi) \cdot \frac{-b \cdot \cos\varphi}{l_2 \cdot \sin(\vartheta(\varphi) - \varphi)} \cdot l_4 \cdot \sin(\vartheta(\varphi) - \psi(\varphi)) . \tag{1.3.35}$$

The total moment acting on this link becomes:

$$M(\varphi) = M_1(\varphi) + M_2(\varphi) . \tag{1.3.36}$$

This moment have to be equilibrated by the moment of the elastic force of the spring i.e.:

$$M(\varphi) = (F_{e0} + k \cdot s) \cdot r . \tag{1.3.37}$$

With the wrapping condition (1.3.7) for driving link, this equation can be written in the form:

$$M(\varphi) \frac{d\psi}{d\varphi} d\varphi = (F_{e0} + k \cdot s) \cdot ds . \tag{1.3.38}$$

where:

$$\frac{d\psi}{d\varphi} = \psi'(\varphi) = \frac{l_2 \cdot (-x_{B_0} \sin\varphi + y_{B_0} \cos\varphi + l_4 \sin(\psi(\varphi) - \varphi))}{l_4 \cdot (-x_{B_0} \sin\psi(\varphi) + y_{B_0} \cos\psi(\varphi) + l_2 \sin(\psi(\varphi) - \varphi))} . \tag{1.3.39}$$

By integrating equation (1.3.38) it is obtained:

$$s(\varphi) = \frac{1}{k}(\sqrt{F_{e0}^2 + 2kM_{int}} - F_{e0}) . \tag{1.3.40}$$

The equation of the profiled driving element, in polar co-ordinate, results as derivate of relationship (1.3.40):

$$r = \frac{ds}{d\psi} = \frac{1}{\psi'(\varphi)} \frac{ds}{d\varphi} = \frac{M'_{int}}{\psi'(\varphi)} \frac{1}{\sqrt{F_{e0}^2 + 2kM_{int}}} , \tag{1.3.41}$$

where:

$$M'_{int} = M(\varphi) \cdot \psi'(\varphi) . \tag{1.3.42}$$

Numerical example

For the loading ledge mechanism are considered the characteristic values in Tab. 1.3.3.

Tab. 1.3.3. Characteristic values for the loading ledge mechanism

Nr.	Characteristic dimension	Notation	Value
1	Weight of the loading ledge	W	5.800 N
2	Manipulating force	F_m	200 N
3	Minimum angular position	φ_{min}	-5°
4	Maximum angular position	φ_{max}	20°
5	Median angular position	φ_m	7,5°
6	Weight position on the loading ledge	h_2	1.050 mm
7	Manipulating force position on the loading ledge	$l_m = b$	2.100 mm
8	Length of the link 2	l_2	600 mm
9	Length of the link 3	l_3	340 mm
10	Length of the link 4	l_4	300 mm
11	Coordinate of the joint B	x_{B_0} y_{B_0}	300 mm, 300 mm

The geometrical parameters of the four bar mechanism were chosen as in Tab. 1.3.3 to be fulfilled the following conditions:
-   because the working angular span is relatively small (25°), it is favorable to amplify the rotation angle by means of the four-bar mechanism;
-   it has been done approximately of two times, with the input and output links parallel to each other in the median position of the platform.

The reacting force in the joint B and his corresponding moment in respect with joint B_0 are represented in Fig. 1.3.8.

In order to integrate the equation (1.3.38) the left hand function is approximated with a polynomial one in the form:

$$M(\varphi)\frac{d\psi}{d\varphi} = 2342164366 \cdot \varphi^3 - 1172153875 \cdot \varphi^2 - 188445402 \cdot \varphi + 642539455 . \quad (1.3.43)$$

The profiled element is presented in Fig 1.3.9.a, and the computed manipulating force (F_m) with this profile is presented in Fig. 1.3.9.b. As can be seen in Fig. 1.3.9.b, the error due to the function approximation for the manipulating force is less than 2%.

a)   b)
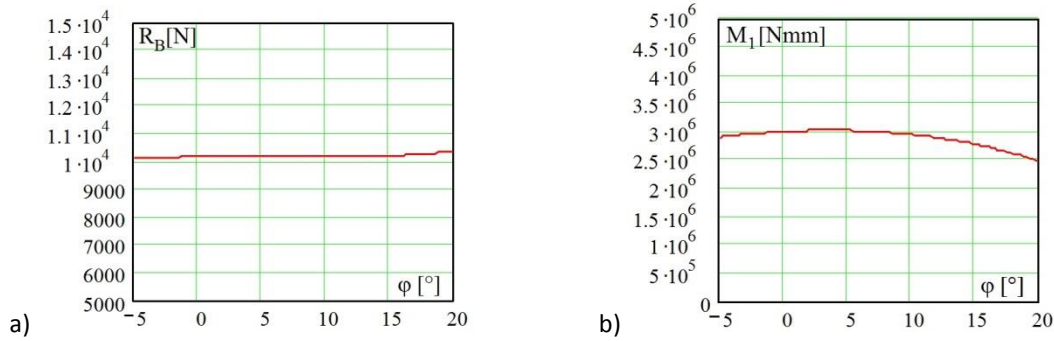
Fig. 1.3.8. The reacting forces (a) and its moment (b) on driving link

a)   b)
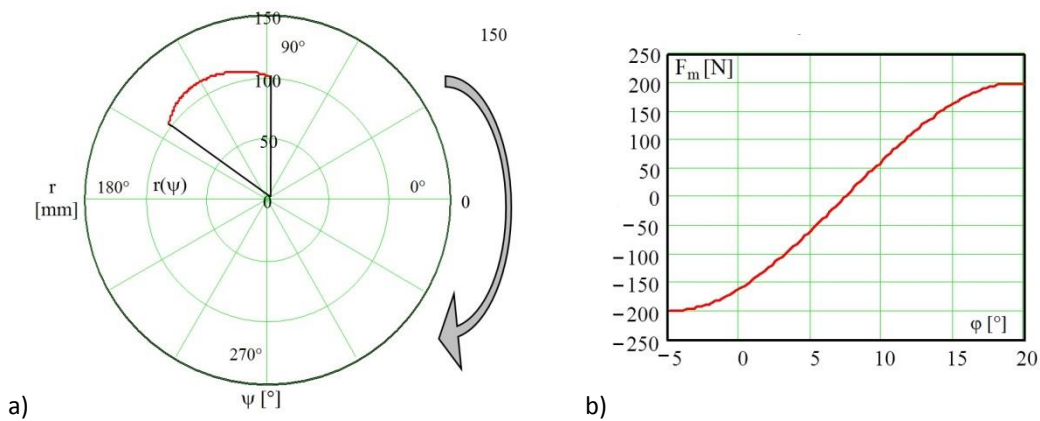
Fig. 1.3.9. The synthesized profile (a) and the resulting manipulating force (b)

In all the cases the influence of the transmission's angle variation at the noncircular wheel was neglected, because this variation is less than ±15°, which implied an error under 3.5%.

1.3.3.5. Force equilibrium by self-balancing Conco-Balancer manipulator

The Conco-Balancer is a pneumatic manipulator [250], which are used to handling a widely variety of different jobs, as example to handling products in logistic departments or to support devices in an industrial process, with a large versatility. In order to be easy manipulated by an operator the manipulator must be self-balanced. Through the gravitational self-balancing (weight W_C) will be compensate the different position of the load in the workspace (Fig. 1.3.10). The operator is functioning as a guide in the control system. The characteristic point – manipulator´s hook of element (7) is loaded with the handling weight W. The operator increase the pressure in the pneumatic cylinder (4) until the handling weight W is compensated (balanced) through the pneumatic force F_p. The balancing weight W_C helps to the previous compensation.

The pneumatic valve system permits the operator to set the clearing of pneumatically cylinder in order to modify the position of the characteristic point in the workspace. The statically balancing through the pneumatic cylinder is reduced by a setting height only for a certain position. For

repositioning of the characteristic point in the workspace the operator must act with his own muscular force. The Conco-Balancer manipulator kinematic schema is presented in the Fig. 1.3.10. The most known technical solution for self-balancing with counterweight, springs and actuators can be substituted through a band mechanism. The non-circular profile of the band mechanism permits the variation of the compensated moment, generated through a variable balancing force F_e, in order to be easy manipulated the load by the operator. In order to reducing the operator´s effort in [194] is presented a solution with a band mechanism of type RRRB with a circular wheel. The span of the band is realized with a spring. In this solution one end of the spring is jointed with the element 2 and the other wrap on one non-circular wheel.
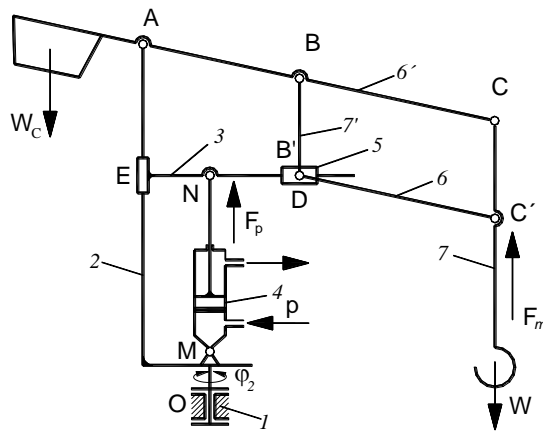
Fig. 1.3.10. Kinematic schema of Conco-Balancer

The new proposed solution (see Fig. 1.3.11) used also a band mechanism, but in this case the non-circular wheel is jointly with element (6´). This solution for self-balancing simplified the construction of the manipulator and conserved the advantage, that the load will be easy manipulated in the workspace.
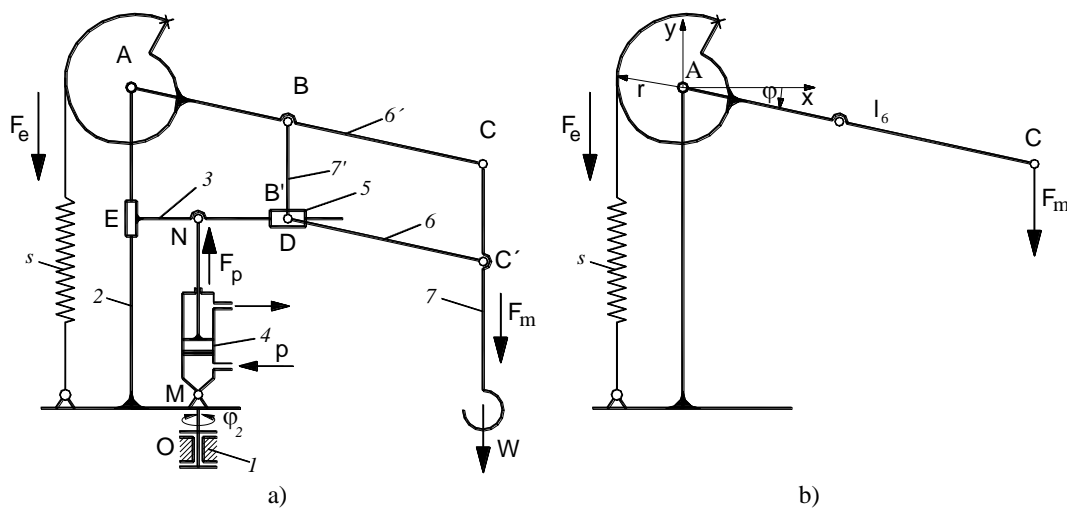
Fig. 1.3.11. Kinematic schema of the Conco-Balancer with self-balancing band mechanism

The manipulator is statically balanced by a setting height in a certain position only, which is the median position $\varphi_m = (\varphi_p + \varphi_n)/2$ (see Fig. 1.3.11.b). Around this position on the manipulator´s arm acts the variable moments given by the spring´s force F_e and the prescribed force of the operator F_m. The manipulator is self-balanced when the moment's equilibrium equation (1.3.1) is satisfied:

$$F_m \cdot l_6 \cdot \cos\varphi = F_e \cdot r , \qquad\qquad\qquad (1.3.44)$$

where: l_6 - the length of the manipulator arm (element 6´).

In (1.3.44) the own weight of the manipulators elements are neglected and the elastic force of the spring is a linear variable one of the form (1.3.2).

The syntheses of the self-balancing band mechanism involve the determination of the equation of a non-circular wheel $r = r(\varphi)$ for a chosen spring in order to fulfil the moment´s equilibrium relationship (1.3.44). The equilibrium equation (1.3.44) with (1.3.2) becomes:

$$F_m \cdot l_6 \cdot \cos\varphi = (F_{e0} - k \cdot s) \cdot r \,. \tag{1.3.45}$$

With the wrapping condition (1.3.7) the Equation (1.3.35) becomes:

$$F_m \cdot l_6 \cdot \cos\varphi \cdot d\varphi = (F_{e0} - k \cdot s) \cdot ds \,. \tag{1.3.46}$$

Through the integration of the differential equation (1.3.46) it obtains:

$$k \cdot s^2 - 2 \cdot F_{e0} \cdot s - 2 \cdot F_m \cdot l_6 \cdot \sin\varphi = 0 \,, \tag{1.3.47}$$

from which, the current arc of the non-circular wheel it results:

$$s = \frac{1}{k}(\sqrt{F_{e0}^2 + 2F_m \cdot l_6 \cdot k \cdot \sin\varphi} + F_{e0}) \,. \tag{1.3.48}$$

By derivation of the current arc of the non-circular wheel (1.3.48) in respect to the rotation angle φ is obtained the equation in polar co-ordinate of the non-circular wheel profile, i.e.:

$$r = \frac{ds}{d\varphi} = \frac{F_m \cdot l_6 \cdot \cos\varphi}{\sqrt{F_{e0}^2 + 2F_m \cdot l_6 \cdot k \cdot \sin\varphi}} \,. \tag{1.3.49}$$

Considering the median position on the horizontal direction, i.e. $\varphi_{min} = -\varphi_{max}$, than the equilibrium condition in the extreme position is:

$$r_n \cdot F_{emax} = r_p \cdot F_{emin} = C,, \tag{1.3.50}$$

with:

$$F_{emin} = F_{e0} \,, \tag{1.3.51}$$

$$C = F_m \cdot l_6 \cdot \cos\varphi_{max} \,, \tag{1.3.52}$$

$$r_n = r\big|_{\varphi=\varphi_{min}} \,, \qquad r_p = r\big|_{\varphi=\varphi_{max}} \,. \tag{1.3.53}$$

Admitting one of the two variable: wrapping length s_{max} or spring´s elastic constant k, the second can be found from the differential equation (1.3.46) for $\varphi \in (-\varphi_{min}, \varphi_{max})$ and $s \in (0, s_{max})$:

$$k \cdot s_{max}^2 + 2F_{e0} \cdot s_{max} - 2F_m \cdot l_6 \cdot (\sin\varphi_{max} + \sin\varphi_{min}) = 0 \,. \tag{1.3.54}$$

Numerical example

For the Conco-Balancer manipulator with self-balancing band mechanism are considered the characteristic values given in Tab. 1.3.4.

Tab. 1.3.4. Characteristic values for the Conco-Balancer manipulator

Nr.	Characteristic dimension	Notation	Value
1	Weight to be manipulated	W	1.500 N
2	Manipulating force	F_m	50 N
3	Pretension elastic force of the spring	F_{e0}	100 N
4	Spring's elasticity constant	k	20 N/m
5	Minimum angular position	φ_{min}	-60°
6	Maximum angular position	φ_{max}	60°
7	Median angular position	φ_m	0°
8	Length of the link 6	l_6	1.200 mm

The manipulating force of the operator is established as constant in the angular range $\varphi \in (-\varphi_{min}, \varphi_{max})$ (s. Fig. 1.3.12.a) and the resulting moment $M(\varphi)$ given from the manipulating force F_m is represented in Fig. 1.3.12.b.
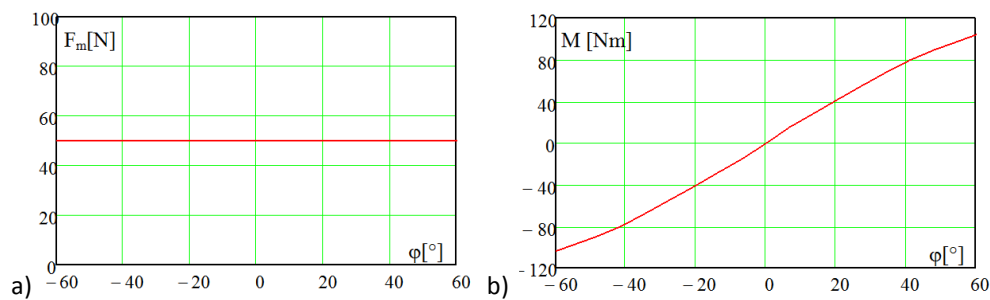
Fig.1.3.12 Manipulating force of the operator $F_m=F_m(\varphi)$ (a) and his resulting moment $M=M(\varphi)$ (b)

Fig. 1.3.13.a shows the variation of the spring's elongation in respect with current angle φ of the manipulator arm and Fig. 1.3.13.b the non-circular profile represented in polar coordinate $r = r(\varphi)$.
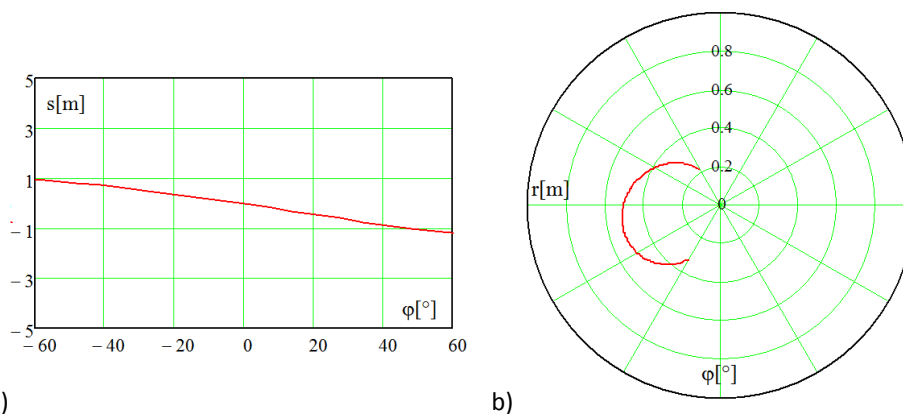
Fig. 1.3.13 The variation of the spring's elongation (a) and the profile of the non-circular wheel (b)

1.3.4. Scientific contributions

The research shows some synthesis application of the belt mechanisms using named also band mechanisms, which represents the main research of the author.

The equilibrating mechanisms based on elastic forces acting at variable arms can be used successfully in order to reduce the total weight, clearance needed and the cost.

In the theoretical considerations the friction forces have been neglected and the solutions represent the first approximation only. Generally, in such cases the friction forces extend the equilibrium's range, so that these forces have a favourable influence in the presented applications.

The examples using belt mechanisms have shown solution for self-balancing of measuring head of a co-ordinate measuring apparatus, the compensation of the Archimedean effect, static equilibrium of a loading ledge/platform and the self-balancing of a Conco-balancer manipulator.

All examples show explicitly the theoretical background for the moment compensation by means of belt mechanisms having a profiled non-circular wheel and are followed with a corresponding numerical example.

2. Scientific achievements regarding the design of complex mechanisms structures

The scientific achievements about the well-known geared linkages were focused on following open unsolved subjects:

- synthesis of the geared linkages with non-circular gears;
- analysis and synthesis of the geared linkages with linear actuation;
- analysis and synthesis of path generating 5-link belt mechanisms.

2.1 Synthesis of the geared linkages with non-circular gears

2.1.1. State-of-art

Geared linkages structurally contain a linkage and one or more gear pairs parallel connected to it. This type of geared linkages is suitable to generate a large swinging angle motion (e.g. windscreen wiper transmissions), a pilgrim-step motion [48], [31], a step motion, a dwell motion and a motion with approximately constant transmission ratio in defined ranges. The kinematic characteristics (transmission functions) are already realized by four-bar linkage with a parallel connected circular gear pair (Fig. 2.1.1a).

The issue to generate a dwell or a constant transmission ratio in a defined range implies to have the higher derivatives of the transmission function zero. This task cannot be satisfied with 5-links geared linkages with classical circular gear pairs, but that can be possible by using a non-circular gear pair (Fig. 2.1.1b).
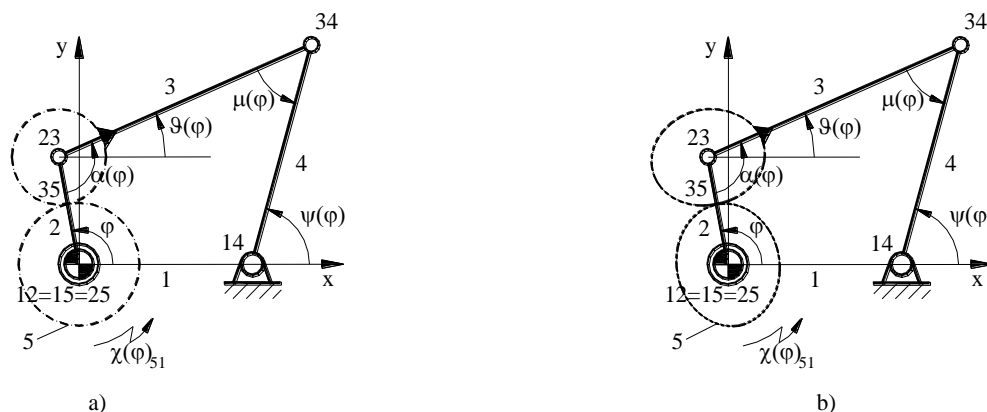
Fig. 2.1.1. 5-links geared linkages
a) with circular gear pair   b) with non-circular gear pair

In [46], [121] the non-circular gears generation employing the enveloping method using tools similar to the circular gears generation was presented. This method fulfils the rolling condition without sliding. A mathematical model of the non-circular gears manufactured with rack cutter is proposed in [65] and with shaper in [76], based on the inverse movement relation and on the motion equation. A computerized method to generate elliptical gear tooth profile by means of shaper cutters is proposed in [106]. The proposed non-circular gears applications would be: reducing torque and speed fluctuations in rotating shaft [72]; actively balancing shaking moments and torque

fluctuations in planar linkages [49], [116]; maximising the human output during low speed pedalling on the power drive mechanism for the high performance bicycle by planetary gear train [141] or by band or tape drives [52]; steering mechanism [55]; modulation of the blood flow in external circulations machines - generating a function with quick forward stroke corresponding to the systolic phase and slow return stroke corresponding to the diastolic phase - through a slider-crank linkage driven by non-circular gears [153], [132]; kinematic optimization of ball-screw transmission in order to reduce the peak acceleration of the screw – through a serial connected non-circular gear with a ball-screw transmission [142]; variable speed ratio belt transmissions [105], a.o. The authors dealt with a particular case of the considered geared linkages in [151].

Non-circular geared linkages find their industrial applications where purely mechanical device is desirable to obtain required motion with robust operation, e.g. automatic equipment in printing presses, textile industry, packaging machines and windscreen wiper transmissions.

2.1.2. Aim of the theoretical research

This study shows the type synthesis of the 5-links geared linkage with non-circular gears, the approach for computing the centrodes and the transmission functions of non-circular gear pairs or centrode segments (similar to the circle arcs) with nonlinear boundary conditions [178]. These centrodes are the pitch curves of the non-circular gears. The tooth geometry may be done as it shown in [105], [96], [8]. The equations for computing of the centrodes are generally represented, so that also centrodes for linear actuators also can be computed. Elliptical gears and other non-circular gears (arbitrary transmission ratio) come in sight as particular cases. The general computation method allows the computing of non-circular gears pairs and planetary non-circular gear pairs.

2.1.3. Theoretical contributions

2.1.3.1. Type synthesis of the 5-links geared linkage

The considered class of mechanisms consists of a four-bar linkage and a parallel connected gear pair, whose input link is linked on the frame joints. One gear (or rack) is rigidly connected to the coupler and the second is jointed in the frame. All the structure of the 5-links geared linkages are systematically represented in Fig. 2.1.2 [31].
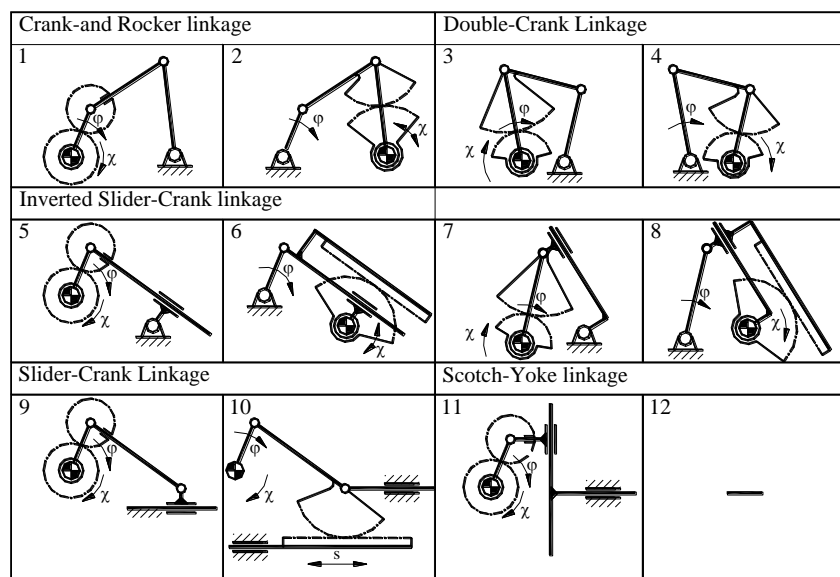

Fig. 2.1.2. Systematization of 5-links geared linkages

The output gear (in frame jointed gear) should be out of technological reasons a pivot-mounted either in the input instantaneous centre 12 or 14 of the basic linkage. Therefore, the motion of the output link is an overlay of the coupler rotation angle (translation stroke) relative to the crank and the crank rotation angle (rocker rotation angle) relative to the fixed link.

2.1.3.2. General synthesis method for five-links geared linkages

a)   General computation model

The general computational model described unitary the different structures of the 5-links geared-linkages. By considering the inverse motion, the coupler-steered either complete rotating or swinging gear pair motion is equivalent to a periodic and non-constant I/O motion (input/output) of links 3 and gear (element) 5 about instantaneous centre 23 and 25, respectively. Then, link 2 becomes the frame, which is rigidly connected to the reference system (Fig. 2.1.3b). The x-axis of the reference system passes through evermore the instantaneous centre 35, which is the contact point of the centrodes of this equivalent motion.
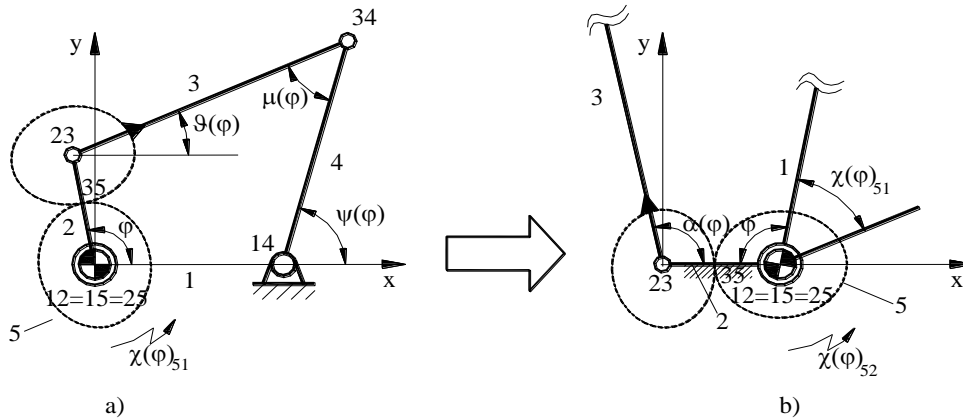

Fig. 2.1.3. Computation model of the five-links geared linkage
a) geared linkage with non-circular gear pair
b) gear mechanism with non-circular gear pair and non-linear input motion

In Fig. 2.1.3a is shown the general computation model for the geared linkages with rotating output gear on the crank. The transmission functions for the synthesis of the centrodes are the relative rotation angles or linear strokes of the link 3 (coupler) and the gear 5 (output element) in respect to the crank or the rocker. By choosing the crank as reference system (Fig. 2.1.3b) results a gear pair, whose input motion is given by the coupler motion. The input motion is a non-linear motion used for designing the non-circular gears.

b)   Determination of the centrodes

Let consider the motion of link 3 and gear 5 in the x, y-reference system shown in Fig. 2.1.3b. The input and output angles of the elements in the reference system are given by the transmission functions $\alpha = \alpha(\varphi)$ ($\alpha = \pi - \varphi + \vartheta$) and $\chi_{52} = \chi_{52}(\varphi)$, respectively (see Fig. 2.1.3 and 2.1.4). In Fig. 2.1.4 and in the following equations from (2.1.1) to (2.1.9), a generalized notation is used. Any point of element 3 is denoted by a complex number X_1 in the plane Σ_1. Any point of element 5 is denoted by a complex number X_2 in the plane Σ_2. The instantaneous poles 23 and 25 are generalized by designations M_1 and M_2, respectively. In order to provide also a translation in direction M_1-M_2 into our calculation, we assume that the function (2.1.4) is used in the instantaneous pole-distance

relation (2.1.3). The centrodes of the motion of plane Σ_2 with respect to plane Σ_1 is determined by the following relationships expressed by complex numbers:

$$X_0 = M_1 + X_1 \cdot e^{i \cdot (\alpha(\varphi) - \alpha(0))} \tag{2.1.1}$$

$$X_0 = M_2 + X_2 \cdot e^{i \cdot (\chi_{52}(\varphi) - \chi_{52}(0))} \tag{2.1.2}$$

$$M_1 + A = M_2 \tag{2.1.3}$$

where:

$$A = a_x(\varphi) + i \cdot a_y(\varphi) . \tag{2.1.4}$$

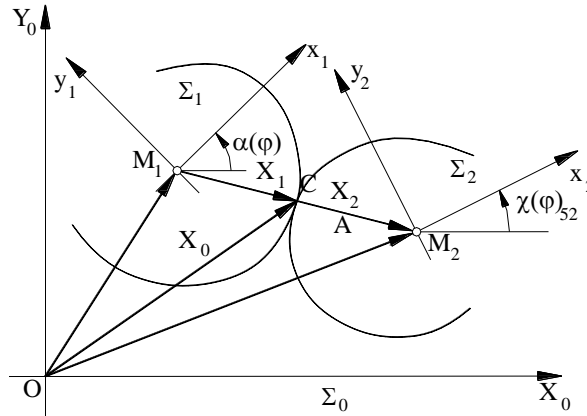

Fig. 2.1.4. Computation model of the centrodes

The planes Σ_1 and Σ_2 fulfil a one-parameter-motion parametrized by φ. By the Aronhold-Kennedy theorem [127], it follows:

$$(\chi'_{52}(\varphi) - \alpha'(\varphi)) \cdot X_0 = \chi'_{52}(\varphi) \cdot M_2 - \alpha'(\varphi) \cdot M_1 - i \cdot (M_2 - M_1) . \tag{2.1.5}$$

The derivative of equation (2.1.3) yields

$$M'_2 - M'_1 = A' . \tag{2.1.3'}$$

Using this in (2.1.5) and eliminating M_1 and M_2, from the relationships (2.1.1) and (2.1.2) the paths of the instantaneous centre C in plane Σ_1 and Σ_2, respectively are obtained in the form:

$$X_1 = (X_0 - M_1)e^{-i(\alpha(\varphi) - \alpha(0))} = \left[\frac{1}{\chi'_{52}(\varphi) - \alpha'(\varphi)} \left(\chi'_{52}(\varphi) \cdot A - i \cdot A' \right) \right] e^{-i(\alpha(\varphi) - \alpha(0))}, \tag{2.1.6}$$

$$X_2 = (X_0 - M_2)e^{-i(\chi_{52}(\varphi) - \chi_{52}(0))} = \left[\frac{1}{\chi'_{52}(\varphi) - \alpha'(\varphi)} \left(\alpha'(\varphi) \cdot A - i \cdot A' \right) \right] e^{-i(\chi_{52}(\varphi) - \chi_{52}(0))}. \tag{2.1.7}$$

The curves $X_1 = X_1(\varphi)$ and $X_2 = X_2(\varphi)$ are the centrodes of non-circular gears which accomplished the desired motion.

Particular cases:

1) If $M_1 = 0$, A=const., $\alpha = \alpha(\varphi)$, and $\chi_{52} = \chi_{52}(\varphi)$, then both the planes Σ_1 and Σ_2 rotate around M_1 and M_2, respectively. The parametric representations of the centrodes (2.1.6) and (2.1.7) become:

$$X_1 = \left(\frac{\chi'_{52}(\varphi)}{\chi'_{52}(\varphi) - \alpha'(\varphi)} \right) \cdot A \cdot e^{-i(\alpha(\varphi) - \alpha(0))} , \tag{2.1.8}$$

$$X_2 = \left(\frac{\alpha'(\varphi)}{\chi'_{52}(\varphi) - \alpha'(\varphi)} \right) \cdot A \cdot e^{-i(\chi_{52}(\varphi) - \chi_{52}(0))} . \tag{2.1.9}$$

2) If $M_1 = 0$, $A(\varphi) = a_x(\varphi) + i \cdot a_y(\varphi)$, and $\chi'_{52}(\varphi) = 0$, then the input plane rotates around M_1 and the output plane fulfils a given non-linear translation. The parametric representations of the centrodes (2.1.6) and (2.1.7), in this case, will be:

$$X_1 = -\left(\frac{1}{i \cdot \alpha'(\varphi)} \right) \cdot A' \cdot e^{-i(\alpha(\varphi) - \alpha(0))} , \tag{2.1.10}$$

$$X_2 = -\left[A + \left(\frac{1}{i \cdot \alpha'(\varphi)} \right) \cdot A' \right] , \tag{2.1.11}$$

describing a gear segment and a rack, respectively.

3) If $M_1 = 0$, $A'(\varphi) \neq 0$, and $\alpha'(\varphi) = 0$, then the input plane is fixed in the reference plane, and the output plane fulfils arbitrary rotations and translations. The parametric representations of the centrodes (6) and (7) become:

$$X_1 = \left[A + \left(\frac{1}{i \cdot \chi'_{52}(\varphi)} \right) \cdot A' \right] , \tag{2.1.12}$$

$$X_2 = \left[\left(\frac{1}{i \cdot \chi'_{52}(\varphi)} \right) \cdot A' \right] \cdot e^{-i(\chi_{52}(\varphi) - \chi_{52}(0))} , \tag{2.1.13}$$

4) The case $\chi'_{52}(\varphi) - \alpha'(\varphi) = 0$ means that the radius of each centrode becomes infinitely.

4.1) If the planes rotate in opposite direction, the transmission ratio $\chi'_{52}(\varphi) / \alpha'(\varphi)$ is negative, which correspond to external-external contacting centrodes.

4.2) If the planes rotate in the same sense, then the transmission ratio $\chi'_{52}(\varphi) / \alpha'(\varphi)$ is positive which correspond to internal-external contacting centrodes.

c)   Boundary conditions for non-circular gears

For the synthesis of non-circular gears, Litvin [46] states the condition for closed centrodes: The gear ratio function must be periodic, and its period T is related to the periods T_1 and T_2 of revolutions of the gears as follows:

$$T = \frac{T_1}{n_2} = \frac{T_2}{n_1} \tag{2.1.14}$$

where n_1 and n_2 are integer numbers. In [121], it is shown that the condition can be satisfied by a specific centre distance, if one of the gear centrodes is already given as a closed curve and also the transmission function. In this approach, it is assumed that the input and output angle functions of a variable φ are expressed by kinematical parameters in the following way

$$\alpha(\varphi) = N \cdot \varphi + A \cdot \sin(\Omega \cdot \varphi) , \tag{2.1.15}$$

$$\chi_{52}(\varphi) = n \cdot \varphi + a \cdot \sin(\omega \cdot \varphi) , \tag{2.1.16}$$

where:

N, n : average angular transmission ratio,

A, a : maximum angular amplitude,

Ω, ω : angular frequency of input link and output element, respectively.

In the case $0 \le \varphi \le 2\pi$, this approach satisfies the condition for closed centrodes for all kinematical parameters N, n, A, a, Ω and ω, because the gear transmission function $\chi'_{52}(\varphi)/\alpha'(\varphi)$ is periodic with period 2π and the input and output angles satisfy $\alpha(2\pi) = N \cdot 2\pi$ and $\chi_{53}(2\pi) = n \cdot 2\pi$.

However, with arbitrary input and output angular functions, the resulting centrodes may intersect itself. The condition for a non-intersecting simply closed centrode $c(\varphi)$ is that the rotation index

$$I = \frac{1}{2\pi} \int_{\varphi=0}^{2\pi} \kappa(\varphi) \cdot \|\dot{c}(\varphi)\| \cdot d\varphi \qquad (2.1.17)$$

has to be equal to ± 1. Here, $\kappa(\varphi)$ designates the curvature of $c(\varphi)$, so that the condition becomes:

$$\frac{1}{2\pi} \int_{\varphi=0}^{2\pi} \left(\frac{x'(\varphi) \cdot y''(\varphi) - x''(\varphi) \cdot y'(\varphi)}{x'(\varphi)^2 + y'(\varphi)^2} \right) \cdot d\varphi = \pm 1 . \qquad (2.1.18)$$

The sign in (2.1.18) depends on the rotation direction along the curve. The representation of a centrode using the model (2.1.15) and (2.1.16) is already very complicated. Therefore, the condition (2.1.18) cannot be evaluated in general. For specific numerical values in (2.1.15) and (2.1.16), the relationship (2.1.18) leads to an integral of the form:

$$\int R[\sin(\varphi), \cos(\varphi)] d\varphi = \pm 1 . \qquad (2.1.19)$$

which is known to be always solvable. However, the solution of (2.1.19) is obtained by transformation of the integrand into a rational function followed by decomposition into partial fractions. The roots of polynomial functions must be determined, which serve as coefficients of certain solution functions. Because the polynomial functions are usually at least of eighths order, a general solution is not possible in the considered way.

A series of calculations with the model (2.1.15), (2.1.16) showed, by means of graphical representations, that non-intersecting simply closed centrodes always satisfied the conditions

$$\Omega = K \cdot N \cdot n \text{ and } \omega = k \cdot N \cdot n \qquad (2.1.20)$$

where K and k are integer numbers. However, the calculation of many examples showed also that the conditions (2.1.20) are not sufficient. It is therefore an open problem to prove that (2.1.20) is a necessary condition for the non-intersection of simply closed centrodes.

2.1.3.3. Synthesis of the centrodes of the non-circular gear pair

For a selected geared linkage structure as in Fig. 2.1.2, the non-circular gear pair is designed to realize a target transmission function $f_{51} = f_{51}(\varphi)$ The dimensions of the basic linkage will be given and the corresponding angle or stroke functions in relation to the geometrical input parameter $f_{21}(\varphi) = \varphi$ will be determined in the form

$$f_{31} = f_{31}(\varphi) \text{ and } f_{41} = f_{41}(\varphi) \qquad (2.1.21)$$

Due to the inverse motion analysis (see Fig. 2.1.5), the computation model needs the consideration of further functions:
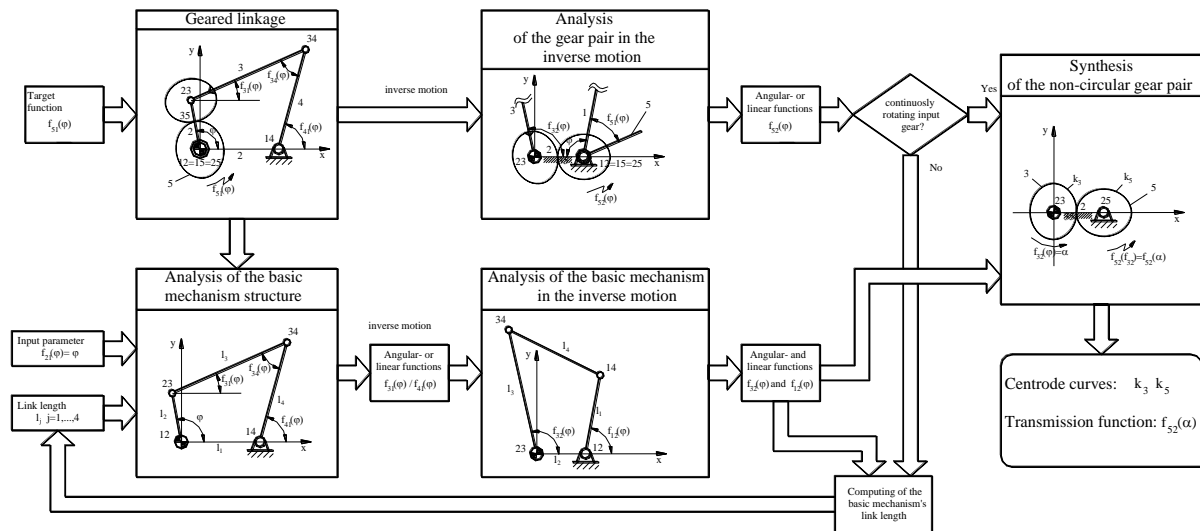
Fig. 2.1.5 Block diagram of the synthesis procedure

Due to the inverse motion analysis (see Fig. 2.1.5), the computation model needs the consideration of further functions:

$$f_{ij} = f_{ij}(\varphi) \text{ and } f_{ik} = f_{ik}(\varphi), \qquad i, j, k = 1,...,4 \ (i \neq j \neq k). \tag{2.1.22}$$

For the non-circular gear pair the target transmission function is:

$$f_{5i} = f_{5i}(\varphi) \tag{2.1.23}$$

If the input gear swings, there are two values φ_1, $i = 1, 2$ with

$$f'_{23}(\varphi_i) = 0. \tag{2.1.24}$$

In these positions the maximum or the minimum of the function $f_{23}(\varphi_i)$ arises.

By the synthesis of a non-linear transmission with a gear sector or rack, the elimination of the parameter φ is necessary. With this procedure the transmission characteristic of the centrode pair is computable, if at least one of the available transmissions function $f_{ij} = f_{ij}(\varphi)$ or $f_{5i} = f_{5i}(\varphi)$ is bijective, for instance

$$F : f_{23} = f_{23}(\varphi) \Rightarrow F^{-1} : \varphi = \varphi(f_{23}), \qquad f_{52} = f_{52}(\varphi), \ f_{52} = f_{52}[\varphi(f_{23})] = f_{52}(f_{23}) \tag{2.1.25}$$

The resulting transmission function of the non-circular gear pair allows the application of the gears also in other transmission structures.

2.1.4.   Numerical example

2.1.4.1. Geared linkage with constant transmission ratio in a given range

In this example, a constant transmission ratio is to be achieved by a geared crank-rocker with a non-circular gear pair (Fig. 2.1.1.b and Fig. 2.1.6). The output gear 5 is jointed at the frame point 12. Therefore, the target transmission function of the output element 5 is given by a suitable spline function:

$$\chi_{51} = \chi_{51}(\varphi), \qquad \chi'_{51} = \chi'_{51}(\varphi), \tag{2.1.26}$$
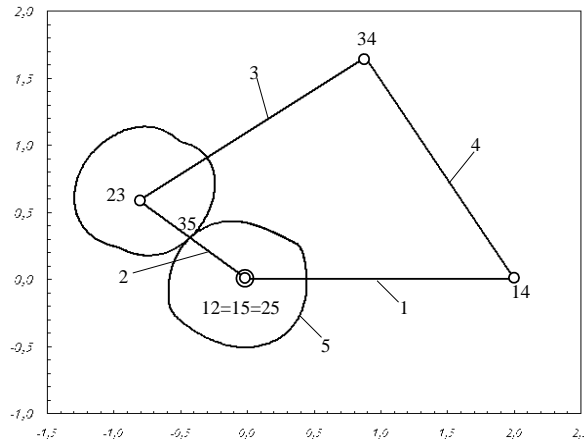
Fig. 2.1.6. Crank-rocker linkage and non-circular gear pair. Numerical example

with an average transmission ratio $\chi'_{52} = 1$ in the range $1.26 \le \varphi \le 5.03$. The derivatives of second and higher order are zero (Fig. 2.1.7a).
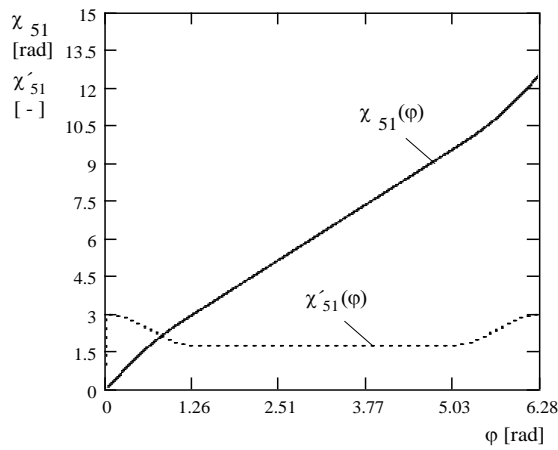
a) Transmission function of the geared linkage
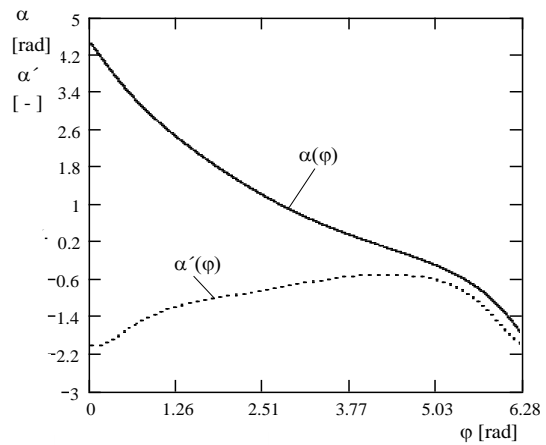
b) Angular function of the coupler in respect to the crank (in the inverse motion)
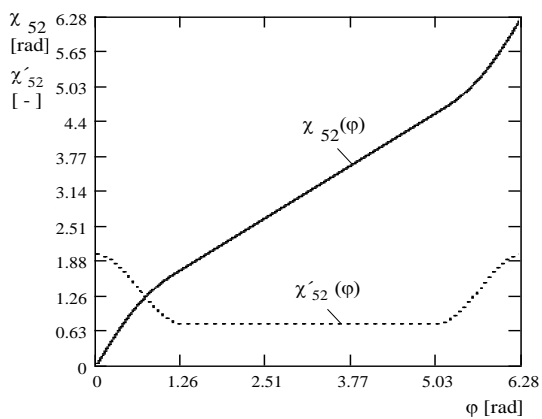
c) Transmission ratio of the output gear in the inverse motion
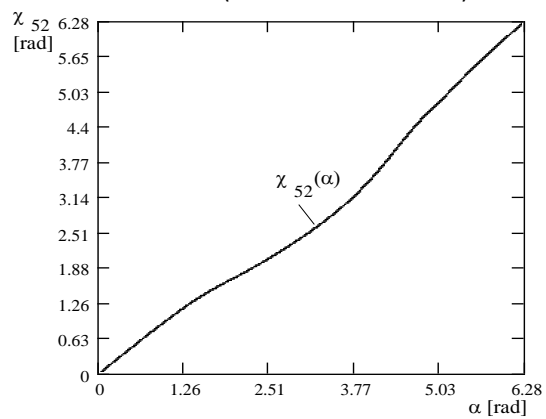
d) The 0-order transmission function of the non-circular gear pair

Fig. 2.1.7. Crank-rocker linkage with non-circular gear pair. Characteristic functions.

The crank rocker as basic mechanism has the dimensions $l_1 = l_3 = l_4 = 2$ and $l_2 = 1$. From the vector equation of the closed loop of the four bar linkage [48], the implicit transmission equation of this mechanism is obtained:

$$F(\varphi, \vartheta(\varphi)) = 0 = l_1^2 + l_2^2 + l_3^2 - l_4^2 - 2l_1l_2\cos\varphi - 2l_1l_3\cos\vartheta(\varphi) + 2l_2l_3\cos(\varphi - \vartheta(\varphi)) \quad (2.1.27)$$

It follows the desired 0-order transmission function (geometrical function):

$$\vartheta(\varphi) = 2\cdot\arctan\left(\frac{b(\varphi) - \sqrt{a^2(\varphi) + b^2(\varphi) - c^2(\varphi)}}{a(\varphi) - c(\varphi)}\right) \quad (2.1.28)$$

where

$$a(\varphi) = 2l_3(l_2\cos\varphi - l_1), \quad b(\varphi) = 2l_2l_3\sin\varphi, \quad c(\varphi) = l_1^2 + l_2^2 + l_3^2 - l_4^2 - 2l_1l_2\cos\varphi \quad (2.1.29)$$

The relationship of the coupler rotation angle in respect to the crank is:

$$\alpha(\varphi) = \vartheta(\varphi) - \varphi + \pi. \quad (2.1.30)$$

By differentiation it results:

$$\alpha'(\varphi) = \vartheta'(\varphi) - 1. \quad (2.1.31)$$

where by differentiation of the relationship (2.1.27) is obtained:

$$\vartheta'(\varphi) = \frac{l_2l_3\sin(\varphi - \vartheta(\varphi)) - l_1l_2\sin\varphi}{l_2l_3\sin(\varphi - \vartheta(\varphi)) + l_1l_3\sin\vartheta(\varphi)}. \quad (2.1.32)$$

All the functions used for the computation of the centrodes and the centrodes in the initial position are shown in Fig. 2.1.7.

The transmission function of the output gears in the inverse motion is

$$\chi_{52}(\varphi) = \chi_{51}(\varphi) - \varphi, \quad (2.1.33)$$

which is depicted in Fig. 2.1.7c.

The computation of the 0-order transmission equation of the geared linkages follows by the substitution of the relationship (2.1.30) in (2.1.27) in the form:

$$F_0(\varphi, \alpha) = 0 = l_1^2 + l_2^2 + l_3^2 - l_4^2 - 2l_1l_2\cos(\varphi) - 2l_1l_3\cos(\alpha + \varphi - \pi) + 2l_2l_3\cos(\pi - \alpha). \quad (2.1.34)$$

The inverse transmission function follows by reformulation:

$$\varphi(\alpha) = 2\cdot\arctan\left(\frac{b(\alpha) - \sqrt{a^2(\alpha) + b^2(\alpha) - c^2(\alpha)}}{a(\alpha) - c(\alpha)}\right), \quad (2.1.35)$$

where

$$a(\alpha) = 2l_1(l_3\cos\alpha - l_2), \quad b(\alpha) = -2l_1l_3\sin\alpha, \quad c(\alpha) = l_1^2 + l_2^2 + l_3^2 - l_4^2 - 2l_2l_3\cos\alpha. \quad (2.1.36)$$

The equation (2.1.35) describes the angular function of crank 1 with respect to frame 2 in the inverse motion, where the angle α is the new parameter and the angle φ will be eliminated.

In order to obtain the correct inverse function, the initial position of the coupler with respect to the crank is

$$\alpha(0) = \alpha(\varphi = 0). \quad (2.1.37)$$

Using the parameterized function

$$\alpha(t) = \alpha(0) - 2 \cdot \pi \cdot t, \quad t \in R, 0 \leq t \leq 1, \tag{2.1.38}$$

and replacing relationship (2.1.35) in (2.1.33), the transmission function of the non-circular gear pair (Fig. 2.1.7d) can be written in the form

$$\chi_{52}(t) = \chi_{52}(\phi(\alpha(t))) \quad . \tag{2.1.39}$$

The synthesis method presented here is a generally valid method for mechanism structures, which contain non-circular gears.

2.1.4.2. Generation of pilgrim-step motions with constant transmission ratio

This example shows the synthesis of a geared linkage with an inverted slider-crank mechanism (Fig. 2.1.8), which realizes a long pilgrim-step with constant transmission ratio (pilgrim-step motion). The centrodes of the non-circular gears are non-circular segments (s. Fig. 2.1.8). The output element 5 is the jointed in the frame point 12. Because the coupler gear realizes a swinging motion, the start angle ϕ_1 and the end angle ϕ_2 in the range with pilgrim-step motion are prescribed by

$$\phi_1 = 0.2 \cdot 2\pi \quad \text{to} \quad \phi_2 = 0.9 \cdot 2\pi. \tag{2.1.40}$$
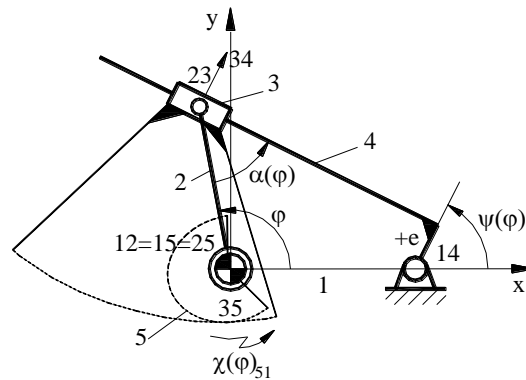
Fig. 2.1.8. Kinematical scheme of the inverted slider-crank linkage
with non-circular gear segments

For the extreme values of the angle between crank and slider ($\alpha(\phi) = \pi/2 - \phi$; $\alpha'(\phi) = -1$) the following geometrical condition holds [150]:

$$0 = l_2^2 \cos^2(\phi) - 2l_1 l_2 \cos(\phi) + l_1^2 - e^2. \tag{2.1.41}$$

Using the boundary conditions (2.1.40) yield an equations system, with the solutions for the frame length and the eccentricity of the inverted slider-crank linkage:

$$\begin{aligned} l_1 &= 0.5 \cdot l_2 \cdot (\cos(0.2 \cdot 2\pi) + \cos(0.9 \cdot 2\pi)) \approx 0.559 \cdot l_2, \\ e &= 0.5 \cdot l_2 \cdot (\cos(0.2 \cdot 2\pi) - \cos(0.9 \cdot 2\pi)) = -0.25 \cdot l_2. \end{aligned} \tag{2.1.42}$$

For this inverted slider crank with the computed lengths (2.1.42) the first derivative of the angle of rotation $\alpha(\phi)$ is zero at the reverse points (2.1.40). In the range $I : \phi_1 \leq \phi \leq \phi_2$ the transmission ratio χ'_{51} of the output element can be arbitrarily chosen, supposed that suitable centrodes are obtained ($\chi' - \alpha' \neq 0$). For the pilgrim-step motion the relationship:

$$\chi'_{51} = \chi'_{52} + 1 \leq 0 \tag{2.1.43}$$

has to be satisfied, hence

$$\chi'_{52} < -1. \tag{2.1.44}$$

Furthermore, at reverse points the following boundary conditions hold:

$$\chi'_{52}(\varphi_1) = \chi'_{52}(\varphi_2) = 0. \tag{2.1.45}$$

Regarding these conditions (2.1.44) and (2.1.45), a spline function $\chi_{52}(\varphi)$ can be designed (Fig. 2.1.9c). The functions $\alpha(\varphi)$ and $\alpha'(\varphi)$ (Fig. 2.1.9.b) are obtained by the implicit 0-order transmission equation of the inverted slider-crank:

$$0 = l_2 \sin(\alpha) - l_1 \sin(\varphi + \alpha) - e. \tag{2.1.46}$$

The 0-order transmission function is:

$$\alpha(\varphi) = 2 \cdot \arctan\left(\frac{q(\varphi) - \sqrt{p(\varphi)^2 + q(\varphi)^2 - r(\varphi)^2}}{p(\varphi) - r(\varphi)}\right), \tag{2.1.47}$$

where

$$p(\varphi) = -l_1 \sin\varphi, \quad q(\varphi) = l_2 - l_1 \cos\varphi, \quad r(\varphi) = -e. \tag{2.1.48}$$

The first order angular function is:

$$\alpha'(\varphi) = \frac{l_1 \cos(\varphi + \alpha(\varphi))}{l_2 \cos\alpha(\varphi) - l_1 \cos(\varphi + \alpha(\varphi))}. \tag{2.1.49}$$
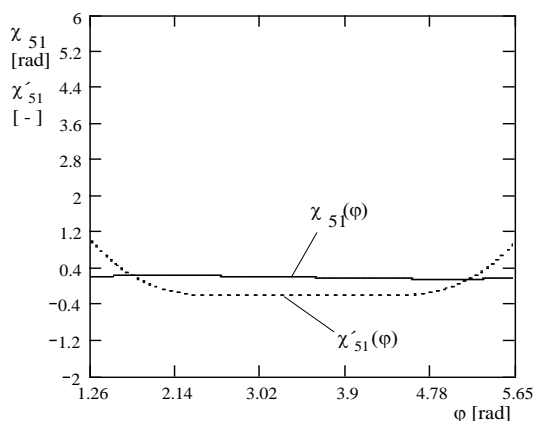
a) Transmission function of the geared linkage
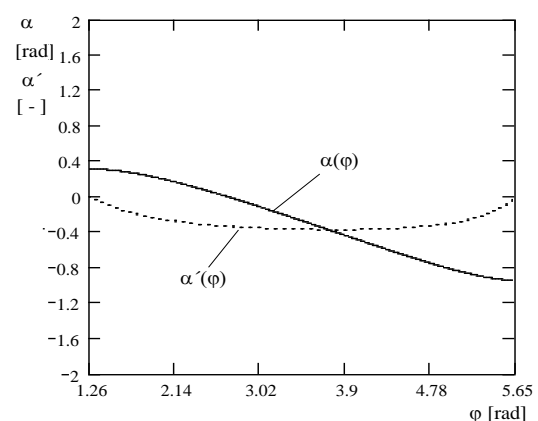
b) Angular function of the slider in respect to the crank in the range I (in the inverse motion)
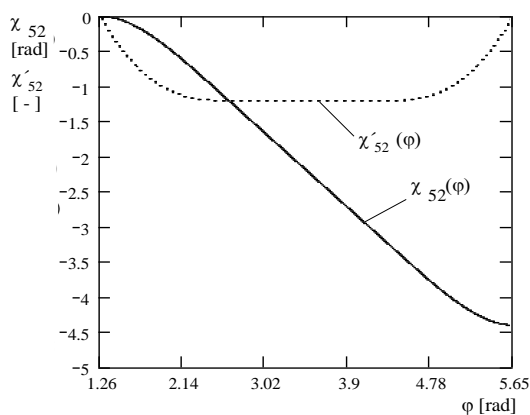
c) Target function and transmission ratio of the output gear in the range I in the inverse motion
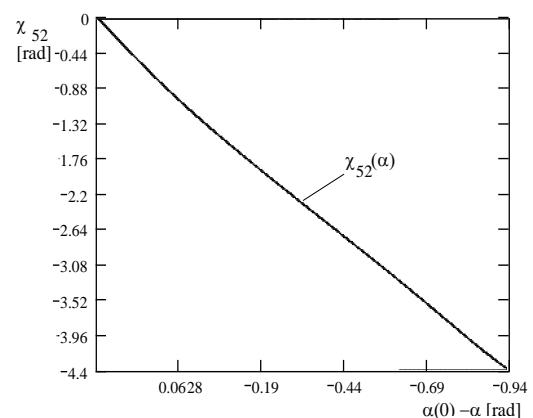
d) The 0 order transmission function of the non-circular gear pair in the range I

Fig. 2.1.9. Inverted slider-crank linkage with non-circular gear segments. Characteristic functions.

Because the angular function $\alpha(\varphi)$ is not bijective, there is no unique spline function for the target transmission function of the output element in the range $0 \le \varphi \le 2\pi$. Nevertheless, we obtain two different centrodes for the range I and its conjugate $\bar{I}$. The both centrodes must be analysed regarding the transmission behaviour in the corresponding range.

Using the relationships (2.1.8) and (2.1.9) the centrodes of the non-circular gear pair consist of two non-circular segments are computed. These synthesized centrodes as well as the inverted slider crank are shown in Fig. 2.1.10 in the position $\varphi = 216°$.

Fig 2.1.10. Inverted slider-crank linkage with
non-circular gear segments. Numerical example

In the following the 0-order transmission function of the non-circular gear pair is discussed in terms of an evenly progressing input-angle function. In addition, by φ_1 and $\alpha_1 = \alpha(\varphi_1)$ the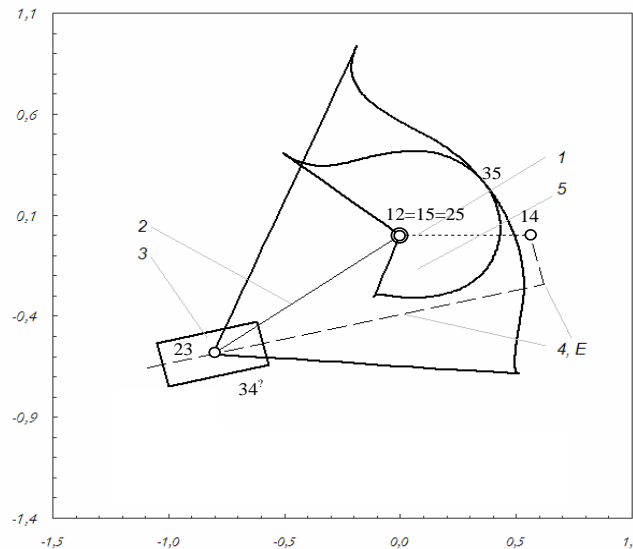 maximum point and the maximum value is denoted. Analogously, φ_2 and $\alpha_2 = \alpha(\varphi_2)$ designate the minimum point and value of the function $\alpha(\varphi)$. Let consider the corresponding inverse function $\varphi = \varphi(\alpha)$ defined in the interval $W : \alpha_2 \le \alpha \le \alpha_1$. Thus it can be supposed that the transmission function of the non-circular gear pair is a function $\chi_{52}(\alpha)$, where the input-gear rotates mathematically positive when the angle α runs from the angle α_1 to the angle α_2. This process is described by the function

$$\alpha(t) = (\alpha_2 - \alpha_1) \cdot t + \alpha_1, \qquad\qquad 0 \le t \le 1. \qquad\qquad (2.1.50)$$

The inverse function $\varphi = \varphi(\alpha)$ is determined by (2.1.35) using the equation (2.1.46). Hence, the coefficients of the relationship (2.1.35) are

$$a(\alpha) = -l_1 \sin\alpha, \quad b(\alpha) = -l_1 \cos\alpha, \quad c(\alpha) = l_2 \sin\alpha - e \qquad\qquad (2.1.51)$$

By using the relationships (2.1.52), (2.1.36) and (2.1.53) the transmission function $\chi_{52}(\alpha)$ of the non-circular segments can be computed and it is graphically represented in Fig. 2.1.9.d. For the computation of the transmission function of the entire gear-pair mechanism, the initial position of the mechanism must be considered. Furthermore, for each angular function value $\alpha(\varphi)$ has to be assigned an appropriate parameter value t.

For the analysis of the transmission characteristic of the geared linkage, it is sufficient to use the value range W of the function $\alpha(\varphi)$ directly as definition range for the inverse function $\varphi(\alpha)$. The

target function of the geared linkage can be obtained by the relationships (2.1.39), (2.1.35) and (2.1.51):

$$\chi_{51}(\varphi) = \varphi + \chi_{52}(\varphi(\alpha)) \, . \tag{2.1.52}$$

The target function is shown in Fig. 2.1.9.a.

2.1.5. Scientific contributions

A method, which can be adapted in very simple way to technological requirements for five-links geared linkages, has been developed. The general synthesis method consists of three parts: change of the reference system (inverse motion analysis), description of the mechanism as non-linearly steered non-circular gear pair, and finally an inverse transformation into the initial coordinate system.

A generally valid procedure for the computation of the 0-order transmission function of centrodes has been developed, which is realized by non-linear defaults. This also allows a renewed solution of known problems such as elliptical gear-transmissions, non-circular gears forming connected mechanisms or congruent non-circular gears with symmetrical 0-order transmission functions. The method allows the computation of simple centrodes of a gear pairs and of gear pairs in complex transmission structures which are connected parallel or serially.

For the computation of the transmission function by the help of proposed method, the explicit knowledge of the centrodes is not necessary. The centrodes are defined by 0-order and first order transmission functions of the mechanism.

Three numerical examples were presented in this chapter. It was computed a geared linkage with constant transmission ratio in a given interval. Secondly, an inverted slider-crank mechanism with constant transmission ratio during a pilgrim-step was shown. For specific applications the centrodes of non-circular gears should fit the requirements of the enveloping process applied for generation of non-circular gears and the area of parameters of the linkage applied for function generation should be chosen free of singularities.

2.2 Analysis and synthesis of the geared linkages with linear actuation

2.2.1. State-of-art

Linear actuators are frequently used in mechatronics systems for generating a translation input movement. The mechanisms using linear actuators should contain a minimum number of elements in order to obtain a robust and low cost product. This condition is satisfied by using a direct linear actuation, a slider-crank, an inverted slider crank, a double slider, but also in the case of geared five-bar linkages with linear actuation. The geared linkages with rotating input motion was studied in many researches, considering two structure types of geared linkages with serial and parallel connected gear train.

The geared linkages with serial connected gear train were studied beginning with Reuleaux [16] for some applications as sewing, stamping, steering and straight-line generators mechanisms. Freudenstein and Primerose studied in [14] the kinematical motion behaviour of the coupler point. Roth and Freudenstein [17] proposed a numerical synthesis method of the geared five-bar linkage for path generating tasks and Oleksa and Tesar [15] for the function generating tasks. The studies of this type of mechanisms were continued by Mundo et al. [163], [179] using non-circular gear train to connect the two links jointed in the frame and Parlaktas et. al. [196] developed a novel analysis method considering the expressions for the transmission angle.

The geared linkages with parallel connected gear train were studied by Neumann [29] as step mechanism with non-uniform continuous motion with high transmission ratio, with high swing angle [36] respectively with instantaneous dwell or pilgrim step [37], [39] and Hain [38]. Horani [28] and Rankers [41] developed analysis and synthesis methods for geared linkages with oscillating motion. Luck and Modler [48] and Volmer [31] presented the analysis and synthesis of the geared linkages.

Only a few theoretical and experimental researches consider the geared five-bar linkages with parallel connected geared train and linear actuation. Gnasa in [88] and [100] studied linkages and more link geared linkages with linear hydraulic actuation to be used as acting mechanism between the manipulator links.

2.2.2. Aim of the theoretical research

The aim of the theoretical research is to perform the type synthesis, to develop an analytical analysis method and to propose a dimensional synthesis method for the geared linkages with linear actuation and parallel connected gear train. As linear actuators can be used pneumatic or hydraulic cylinders, linear electric motors, or screw type actuators. In [110] and [124] were presented the unitary developed analysis and synthesis methods for the geared linkages with linear actuation. An application of the geared linkages with linear actuation shows the development of the design and a control approach of active knee prosthesis. The novel solution for the knee prosthesis using geared linkages and linear actuation was presented in [176], [197] and [224].

2.2.3. Type synthesis of the geared linkage with linear actuation

The type synthesis follows to find out the possible kinematic chains and the mechanism structures of the geared linkages with linear actuator. The basic equation for a mechanism with a constrained motion, according to Alt, is:

$$2 \cdot \left(e_1 + e_2/2\right) - 3 \cdot n + 3 + F = 0 \ . \tag{2.2.1}$$

were: e_1 - is the number of kinematic pairs with $f = 1$ degree of freedom,

e_2 - the number of kinematic pairs with $f = 2$ degree of freedom,

n - the number of links and

F - the degree of freedom of the mechanism.

In the case of geared linkages the mechanism contains at least one kinematic pair with the degree of freedom $f = 2$ i.e. $e_2 = 1$. Considering the mechanism degree of freedom $F = 1$, from the equation (1) follows the correlation between n and e_1, in the form:

$$n = (2 \cdot e_1 + 5)/3 .$$ (2.2.2)

Integer solution for n can be obtained for:

$$e_1 = 2 + 3 \cdot k \qquad (k = 0,1,...) .$$ (2.2.3)

Fig. 2.2.1 Kinematic chains of the geared linkages with linear actuators

The first integer solution follows for $e_1 = 2$ and the resulted structure is a geared planetary mechanisms. The solution for the geared linkages chain with minimal structure follows is $e_1 = n = 5$. The chain must contain an prismatic kinematic pair, which is the drive kinematic pair. The number of closed loops for the planar kinematic chain is to be computed with the relationship:

$$N = \sum_{i=1}^{2} e_i - n + 1 \qquad\qquad (2.2.4)$$

The number of contours for the geared linkages with linear displacement actuator is $N = 2$, where the degree of freedom for each loop must be positive:

$$F_j = 3 \cdot (n-1) - 2 \cdot e_1 - e_2 > 0. \qquad\qquad (2.2.5)$$

The numbers of the elements of different ranks satisfy the diophantine equations system:

$$n = n_2 + n_3 + n_4 + n_5,$$
$$2 \cdot \sum_{i=1}^{2} e_i = 2 \cdot n_2 + 3 \cdot n_3 + 4 \cdot n_4 + 5 \cdot n_5. \qquad\qquad (2.2.6)$$

The elements n_4 and n_5 are useless, so that the equations' system (2.2.6) becomes:

$$\begin{cases} n_2 + n_3 = 5 \\ 2n_2 + 3n_3 = 12 \end{cases} \qquad\qquad (2.2.7)$$

having the solutions $n_2 = 3$ and $n_3 = 2$.

Fig. 2.2.1 shows the 11 possible kinematic chains obtained under the upper structural condition, but only 6 kinematic chains fulfil the conditions (2.2.5) and the gear contact condition (s. Fig. 2.2.2).
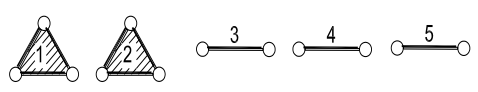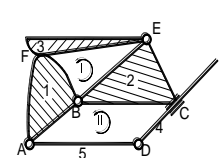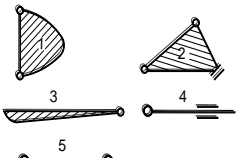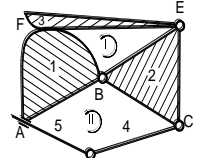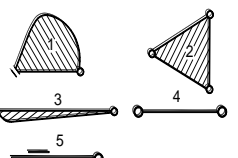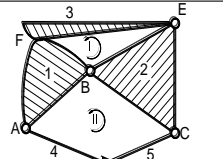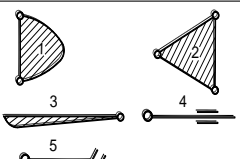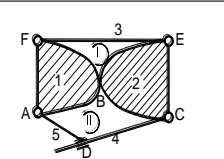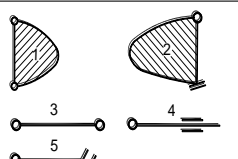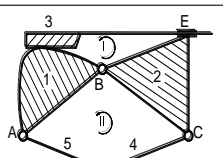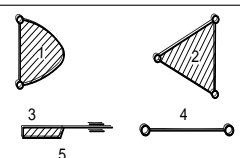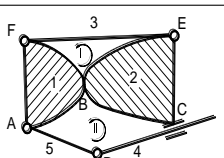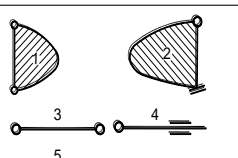
Fig. 2.2.2 Useful kinematic chains of the geared linkages with linear actuators

Using the Reuleaux method to develop the 6 kinematic chains and the criteria's:
- the drive is of slider type,
- the mechanism should not be consist of basically mechanisms in serial order,
- all the links must be included in the motion transmission,

then 4 structure of geared linkages mechanisms remain to be considered.
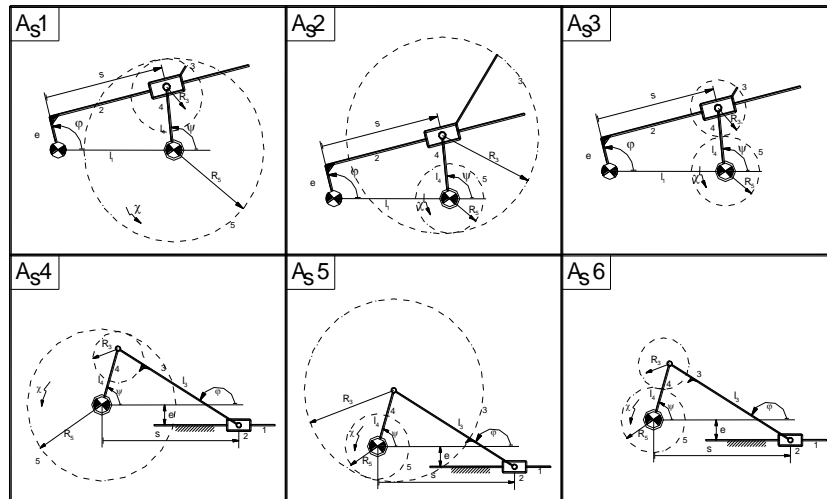
Fig. 2.2.3 Planetary geared linkages of type $A_s i$
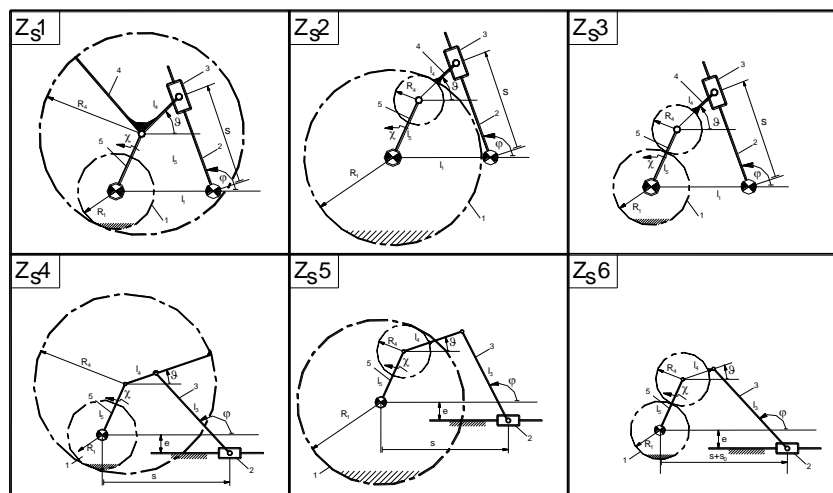
Fig. 2.2.4 Cycloidal geared linkages of type $Z_s i$

These will be classified and noted as:
- Planetary geared linkages, type Asi (Fig. 2.2.3),
- Cycloidal geared linkages, type Zsi (Fig. 2.2.4).

2.2.4. Kinematic analysis of the geared linkages with linear actuation

The kinematic analysis of planetary geared linkage with linear displacement actuator considers the mechanism consist of two basic structures: a 4-bar linkages and a planetary gear train (s. Fig. 2.2.5).
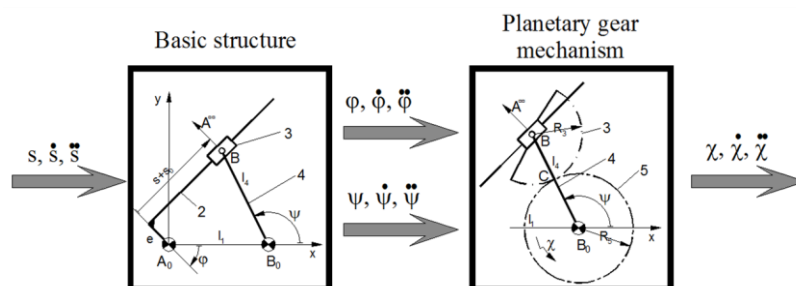
Fig. 2.2.5 Kinematic analysis of the geared linkages with linear actuation

The transmission functions $\varphi(s)$ and $\psi(s)$ of the 4-bar linkages depend on the input parameter, the stoke s, can be determined by considering the closure loop vector equation.

The transmission function of the geared linkages is obtained in form:

$$\chi(s) = (1-\rho)\cdot\psi(s) + \rho\cdot\varphi(s),$$ (2.2.8)

where: $\chi(s)$ - output parameter – transmission function of geared linkage,

$\rho = \pm r_3/r_5$ - gear ratio,

$\varphi(s)$, $\psi(s)$ - transmission functions of the 4-bar linkage.

The first order transmission function $\chi'(s)$ and the second order transmission function $\chi''(s)$ can be computed in form:

$$\chi'(s) = (1-\rho)\cdot\psi'(s) + \rho\cdot\varphi'(s),$$ (2.2.9)

$$\chi''(s) = (1-\rho)\cdot\psi''(s) + \rho\cdot\varphi''(s).$$ (2.2.10)

The angular velocity and acceleration result from the first and second derivative of the transmission function in respect with the time t:

$$\dot{\chi}(t) = \chi'(s)\cdot\dot{s}(t),$$ (2.2.11)

$$\ddot{\chi}(t) = \chi''(s)\cdot\dot{s}(t)^2 + \chi'(s)\cdot\ddot{s}(t),$$ (2.2.12)

where: $\dot{s} = \dot{s}(t)$, $\ddot{s} = \ddot{s}(t)$ are the input linear velocity and acceleration respectively, which computed from dynamical analysis.

2.2.4.1. Geared linkages with inverted slider-crank as basic structure

The geared linkages mechanism types A_s1-A_s3 contain an inverted slider-crank as basic structure and a planetary gear train with the satellite gear rigid connected to the slider (Fig. 2.2.6). The vector closed loop equation of the basic mechanism, in complex number, has the form:

$$(e - i(s_0 + s))\cdot e^{i\cdot\varphi} = l_1 + l_4\cdot e^{i\cdot\psi}.$$ (2.2.13)
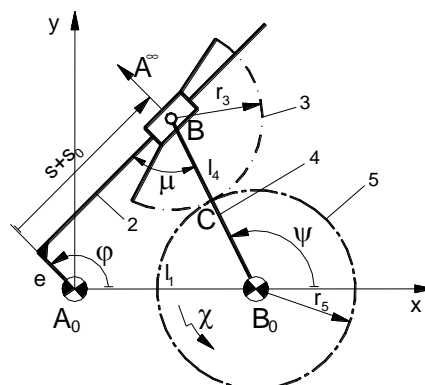
Fig. 2.2.6 Geared linkage with inverted slider-crank as basic structure

The transmission functions of the basic structure $\varphi(s)$ and $\psi(s)$ follow from the complex number relationship (2.2.13) depending on the input parameter s:

$$\varphi(s) = 2\arctan\left(\left(B(s)\pm\sqrt{A(s)^2 + B(s)^2 - C(s)^2}\right)\Big/(A(s) - C(s))\right)$$ (2.2.14)

where:

$$A(s) = 2 \cdot l_1 \cdot e, \quad B(s) = 2 \cdot l_1 \cdot (s_0 + s), \quad C(s) = -l_1^2 - e^2 - (s_0 + s)^2 + l_4^2. \tag{2.2.15}$$

and:

$$\psi(s) = \arccos\big((e^2 + (s_0 + s) - l_1^2 - l_4^2)/2l_1 l_4\big). \tag{2.2.16}$$

The first and second transmission function of the $\varphi(s)$, in respect with the input parameter s, are:

$$\varphi'(s) = \frac{l_1 \sin \varphi(s) - (s_0 + s)}{l_1\big(e \cdot \sin \varphi(s) - (s_0 + s)\cos \varphi(s)\big)}, \tag{2.2.17}$$

$$\varphi''(s) = \frac{2l_1 \cos \varphi(s) \cdot \varphi(s)' - l_1\big(e \cdot \cos \varphi(s) + (s_0 + s)\sin \varphi(s)\big)\varphi(s)'^2 - 1}{l_1\big(e \cdot \sin \varphi(s) - (s_0 + s)\cos \varphi(s)\big)}. \tag{2.2.18}$$

The first and second transmission function of the $\psi(s)$, in respect with the input parameter s, are:

$$\psi'(s) = -(s_0 + s)/(l_1 l_4 \sin \psi(s)), \tag{2.2.19}$$

$$\psi''(s) = -\big(1 + l_1 l_4 \cos \psi(s) \cdot \psi(s)'^2\big)/(l_1 l_4 \sin \psi(s)). \tag{2.2.20}$$

The transmission functions of different orders of the geared linkages, can be computed taking into account the relationships (2.2.14), (2.2.15), (2.2.17) and (2.2.18), respectively (2.2.16), (2.2.19) and (2.2.20).

2.2.4.2. Geared linkages with slider-crank as basic structure

The geared linkages mechanism types A_s4-A_s6 used as basic structure a slider-crank and a planetary gear train with the satellite gear rigid connected to the coupler (Fig. 2.2.7). The complex number equation of the basic mechanism vector closed loop follows:

$$(e + i(s_0 + s)) + i \cdot l_3 \cdot e^{i \cdot \varphi} = i \cdot l_4 \cdot e^{i \cdot \psi}. \tag{2.2.21}$$

The transmission functions of the basic structure $\varphi(s)$ can be computed with the relationship (2.2.14), where:

$$A(s) = 2 \cdot l_3 \cdot (s_0 + s), \quad B(s) = -2 \cdot l_3 \cdot e, \quad C(s) = e^2 + (s_0 + s)^2 + l_3^2 - l_4^2. \tag{2.2.22}$$

and the transmission function $\psi(s)$:

$$\psi(s) = \arcsin\big((l_3 \sin \varphi - e)/l_4\big). \tag{2.2.23}$$
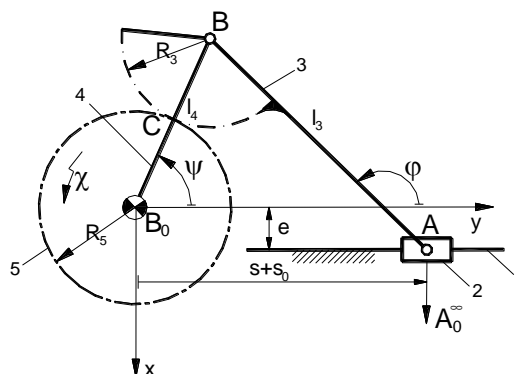
Fig. 2.2.7 Geared linkage with slider-crank as basic structure

The first and second transmission function of the $\varphi(s)$ and $\psi(s)$, in respect with the parameter s, follows:

$$\varphi'(s) = \frac{l_3 \cos\varphi + (s_0 + s)}{l_3((s_0 + s) \cdot \sin\varphi + e \cdot \cos\varphi)},$$ (2.2.24)

$$\varphi''(s) = \frac{1 - 2l_3 \sin\varphi \cdot \varphi' + l_3(e \cdot \sin\varphi + (s_0 + s)\cos\varphi)\varphi'^2}{l_3((s_0 + s) \cdot \sin\varphi + e \cdot \cos\varphi)},$$ (2.2.25)

$$\psi'(s) = -l_3 \cos\varphi \cdot \varphi' / (l_4 \cos\psi),$$ (2.2.26)

$$\psi''(s) = -\left(l_3 \sin\varphi \cdot \varphi'^2 - l_3 \cdot \cos\varphi \cdot \varphi'' - l_4 \sin\psi \cdot \psi'^2\right)/(l_4 \sin\psi).$$ (2.2.27)

2.2.5.   Quality parameters of the geared linkages with linear actuation

The geared linkages with linear displacement actuator reproduce an approximately linear dependence between the input and output movement for a very large swivel angle range, i.e. an approximate constant first order transmission function or transmission ratio.

This function described a flat-point function [61], see Fig. 2.2.8. The mathematical conditions to become a flat-point function are:

$$\chi'' = 0, \quad \chi''' = 0, \quad \chi'''' = 0.$$ (2.2.28)
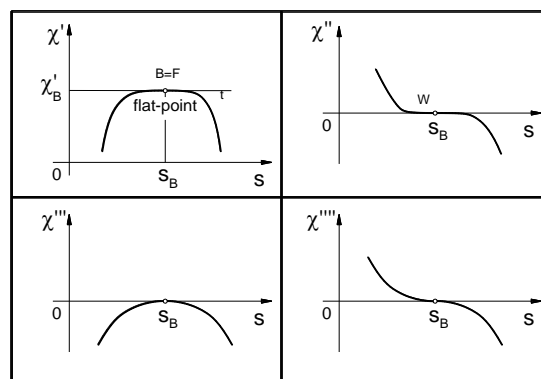
Fig. 2.2.8 Flat-point first order geometrical function

The conditions (2.2.28) lead to an equations system, which cannot be solved with analytical methods. An alternative method to realize the dimensional synthesis of the geared linkages using the condition (2.2.28) is provided by the optimum synthesis.

To assess the approximately linear dependence between the input and output parameters is recommended to study the behaviour of first order transmission function of the geared linkages. For this purpose should be defined the following parameters (s. Fig. 2.2.9):
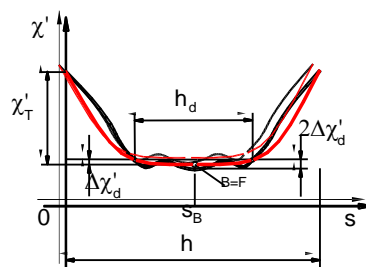
Fig. 2.2.9 Dwell quality parameters

- dwell length $\qquad$ h_d, $\qquad$ (2.2.29)

- relative dwell length $\qquad$ $Rd = \dfrac{h_d}{h} 100\%$, $\qquad$ (2.2.30)

- dwell clearance $\qquad$ $\Delta\chi'_d$ $\qquad$ (2.2.31)

- relative dwell deviation $\qquad$ $Rdd = \dfrac{\Delta\chi'_d}{\chi'_T} 100\%$ $\qquad$ (2.2.32)

where: h - the stroke of the linear actuator

χ'_F - the maximum value of the transmission function 1-st order.

2.2.6.   Optimum synthesis of the geared linkages

The input parameters for the optimum synthesis problem are: the desired function, the selected structure of the geared linkages (Fig. 2.2.3), the given stroke h and the gear ratio ρ.
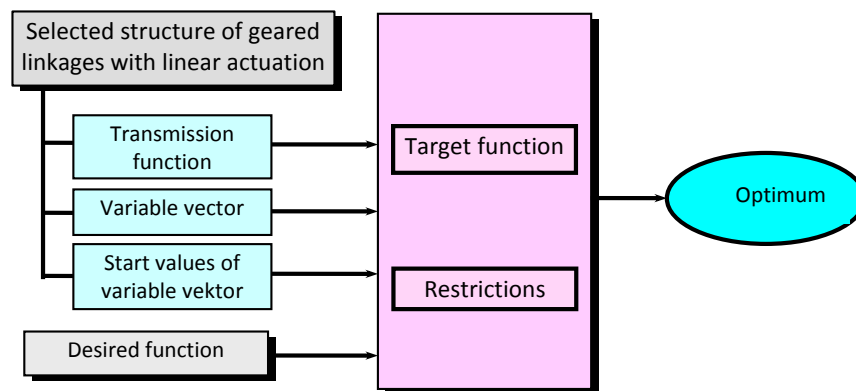
Fig. 2.2.10 Optimum synthesis strategy of the geared linkages with linear actuation

The first order transmission function (s. Fig. 2.2.10) will be determined for the selected structure of geared linkages $\chi'(s)$. As vector of the variable will be considered:

$$\mathbf{x} = (\lambda_2, \lambda_3, \lambda_4)^T,$$ (2.2.33)

where the unitary (no-dimensional) variables are:

$$\lambda_2 = l_2/l_1, \quad \lambda_3 = l_3/l_1, \quad \lambda_4 = l_4/l_1.$$ (2.2.34)

The desired transmission function 1-st order of the geared linkage mechanism with linear actuator will be chosen as constant, what means a constant ratio:

$$\chi'_{desire} = \frac{\chi_{max}}{h} = ct.$$ (2.2.35)

where: χ_{max} - maximal swivel angle of output gear.

The target function defined as the deviation between the transmission function 1-st order and the desired transmission function 1-st order is to be minimized, in order to realize a motion with approximately constant ratio. The target function is:

$$F(\mathbf{x}) = \int_o^{s_H/l_1} |\chi'(s, \lambda_2, \lambda_3, \lambda_4) - \chi_{max}/h| \, ds := Min.$$ (2.2.36)

The restrictions are given as boundary geometrical and transmission angle of the base mechanism condition:

$$g_k(\mathbf{x}) = g_k(\lambda_2, \lambda_3, \lambda_4) \geq b_k \qquad\qquad (2.2.37)$$

The start values of the variables vector:

$$\mathbf{x}^{(0)} = \left(\lambda_2{}^{(0)}, \lambda_3{}^{(0)}, \lambda_4{}^{(0)}\right)^{\mathsf{T}} \qquad\qquad (2.2.38)$$

will be convenient chosen. Generally, the local optimum values give the optimum values for the links length.

2.2.7. Numerical examples

The example problem shows the synthesis and analysis of a geared linkage with inverted slider-crank as basic structure for performing a large oscillating angle with approximately constant transmission ratio and a favourable transmission angle of the basic linkage.

2.2.7.1. Synthesis of the geared linkages with inverted slider-crank as basic structure

The input parameters for the optimal synthesis of the geared linkage with inverted slider-crank as basic structure are given in the Tab. 2.2.1.

Tab. 2.2.1. Input parameters for the optimal synthesis

Nr.	Parameter	Value
1	Gear ratio	$\rho = 0.5$
2	Minimum transmission angle	$\mu_{min}° = 30°$
3	Maximum unitary stroke	$h/l_1 = 0.4$

In the case of the considered geared linkage structure the unitary variables are λ_2 and λ_4 and the restrictions are given like secondary condition as inequation. The secondary conditions in our example described the start and end of the geometrical conditions:

$$(\lambda_4 - 1)^2 - \lambda_2^2 - (s_0/l_1)^2 < 0, \qquad\qquad (2.2.39)$$

$$-(\lambda_4 + 1)^2 + \lambda_2^2 + ((s_0 + s_H)/l_1)^2 < 0 . \qquad\qquad (2.2.40)$$

The condition for a convenient transmission angle $\mu > \mu_{min}$ at the start position will be used to determine the start unitary displacement s_0/l_1:
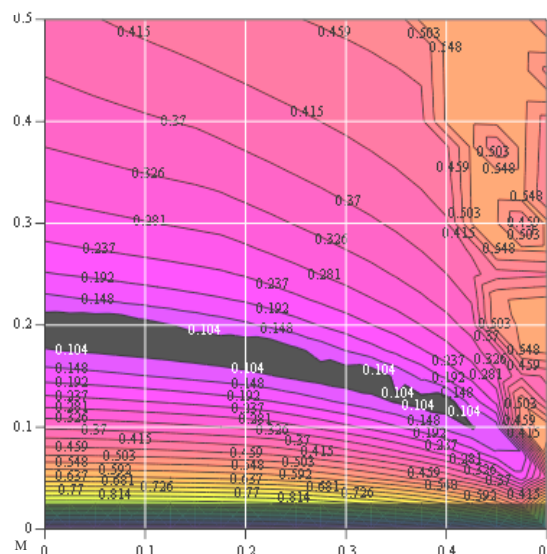
Fig. 2.2.11 Optimum synthesis strategy of the geared linkages with linear actuation

$$\left(\frac{s_0}{l_1}\right) = -\lambda_4 \sin\mu_{min} + \sqrt{1 - (\lambda_2 - \lambda_4 \cos\mu_{min})^2} \ , \tag{2.2.41}$$

One local minimum value for the unitary variables results from the contour line diagram (s. Fig. 2.2.11). There are $\lambda_2 = 0.08$ and $\lambda_4 = 0.2$.

The links length will be $l_2 = 8\,mm$ and $l_4 = 20\,mm$ by setting the frame length of $l_1 = 100\,mm$.

2.2.7.2. Analysis of the geared linkages with inverted slider-crank as basic structure

The analysis of the geared linkages confirm the initial considerations to reproduce an approximately linear dependence between the input and output movement for a very large swivel angle range and implicit an approximately constant transmission ratio in the considered range (s. Fig. 2.2.12). Also, it shows that the mechanism allows a maximum oscillating angle of $\chi_{max}° \cong 173°$ for a start position $s_0 = 81\,mm$ and a stroke $h = 33.2\,mm$. The oscillating angle will be limited to 120° symmetrical in respect to the flat point (Fig. 2.2.12), in order to minimize the deviation of the first derivative of the transmission function in respect to the constant value of the transmission ratio.
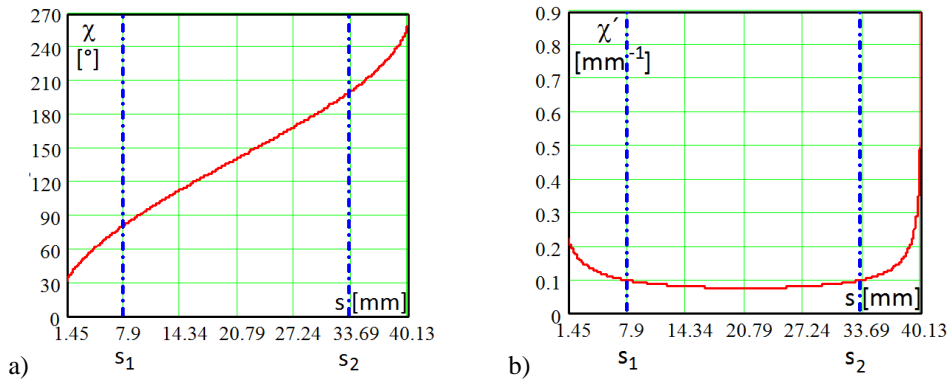
Fig. 2.2.12 The transmission function (a) and the first order transmission function (b) of the geared linkage

The new displacements s_1 and s_2 are determined with the conditions:

$$\chi(s_2)° - \chi(s_1)° = 120° \tag{2.2.42}$$

$$\chi'(s_2) = \chi'(s_1) \tag{2.2.43}$$

The new displacements in our example are s_1=7.58 mm and s_2=33.34 mm, that means, for the geared linkages, the initial stroke and the stroke will be changed to s_0=88.58 mm and h=25.76 mm, respectively.

The quality parameters for characterising the behaviour of the transmission function of the geared linkages are:

- dwell length $h_d = 25.76\,mm$,

- relative dwell length $Rd = \dfrac{h_d}{h} 100\% = 77.5\%$,   (2.2.30)

- dwell clearance $\Delta\chi'_d \cong 0.011\,rad/mm$,   (2.2.31)

- relative dwell deviation $Rdd = \dfrac{\Delta\chi'_d}{\chi'_T} 100\% = 5.4\%$.   (2.2.32)

2.2.8. Design and control of active knee prosthesis with geared linkage

The development in the field of knee prostheses pursues a biological static and dynamic behaviour of the lower human limb, a uniform distribution of the body weight both on the prosthetic limb and the healthy limb, ensuring the walking stability and identical movement for both limbs. All these requirements improve the life quality and the work capacity of the amputees.

In order to insure the walking stability, usually a large series of mechanical, pneumatic and hydraulic solutions is used for the knee prosthesis. These prostheses are designed either as passive or active systems. The mechanical solutions can use a simple and least expensive cinematic joint with dampening system or poly-centric (physiological) hinge [53].
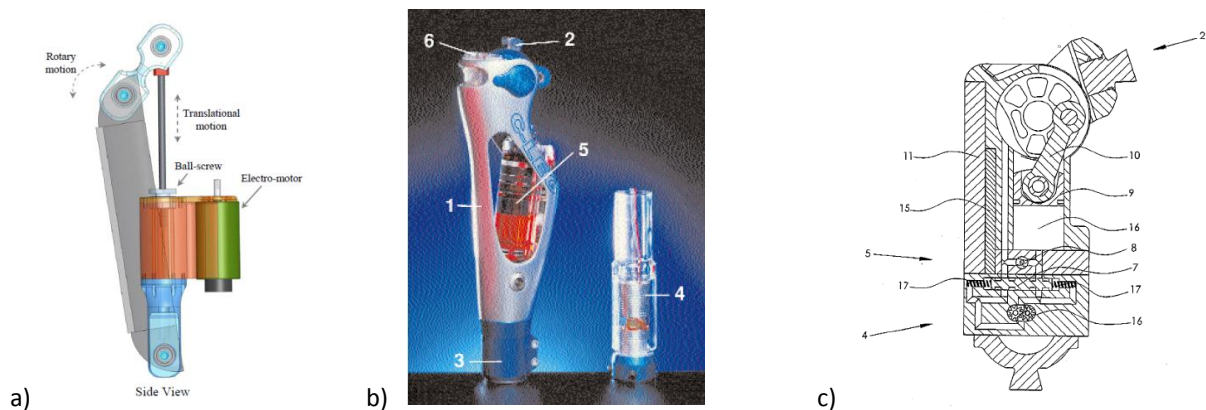
Fig. 2.2.13. Design solutions for the knee prosthesis

a) with active prosthetic knee   b) with trans-femoral amputees C-Leg   c) with own hydraulic acting system

In [153] the purposed design of the active prosthetic knee (APK) is an inverted slider crank, using a screwball system accompanied by a high-speed brushed servomotor to provide one degree of freedom and the full necessary torque at the knee joint (s. Fig. 2.2.13.a). In [78] a prosthetic system for trans-femoral amputees C-Leg is described. It is based on a hydraulic knee joint with electronic control of both swing and stance phase (s. Fig. 2.2.13.b). The required resistance for flexion or extension of the knee is calculated and then provided by a hydraulic unit equipped with electronic servo valves. The design and evaluation of knee joint controllers, used for controlled driving of the knee actuator is presented in [166]. The paper work [83] develops a knee-ankle-foot orthesis with a joint unit that controls knee movements using a microcomputer. By means of using sensors the gait phase is optimized [99]. A new technique for dynamic damping control is presented in [147] based on natural humanoid walk for above knee prosthesis which exploits biologically inspired central pattern generator (CPG).

Gramnaes in [136] propose a design of active and passive knee prosthesis system, using a slider crank mechanism with its own hydraulic acting system (s. Fig. 2.2.13.c). This prosthesis allows the blocking of the knee joint in the extended limb position through the geometry of the piston and crank.

The human knee joint allows a rotation motion with an angle of 130°. As presented in the state-of-art, the active prostheses with 1 DOF uses an inverted slider-crank (Fig. 2.2.13.a,b or 2.2.14.a,b) or a slider crank (Fig. 2.2.13.c). These mechanisms with hydraulic or pneumatic actuation used a double acting cylinder (Fig. 2.2.14.c) assembled in parallel with a throttle [1] or a ball-screw reducer and an electromotor as rotational actuator. Such mechanisms provide a non-linear transmission function and allow a limited rotation angle between the thigh and the leg.
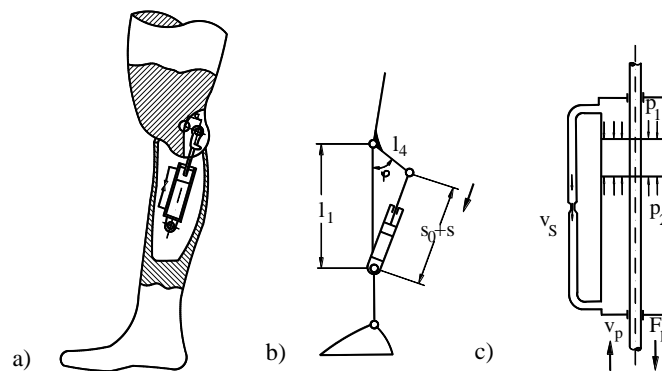
Fig. 2.2.14. Knee joint prosthesis (a). Kinematic schema of the inverted slider-crank (b).
Hydraulic or pneumatic double acting cylinder (c)

The disadvantages of the inverted slider-crank can be avoided by using a geared linkage with a linear actuation. The geared linkage contains an inverted slider-crank as basic structure connected in parallel with a gear train. The input parameter is the stroke s of the slider and the output parameter is the rotation angle of the output gear χ. Therefore, the analysis and synthesis of the geared linkage with linear actuation, used as driving mechanism was developed in the previous capitol. In order to obtain an approximately constant transmission ratio for a large rotation angle, an optimization synthesis was previous recommended.

The imposed parameters for the optimization problem are the gear ratio, $\rho = 0.62$, the minimal transmission angle $\mu_{min}° = 10°$, needed to limit the rotation angle, and the maximum unitary stroke $h/l_1 = 0.08$. Through the optimization synthesis results one local minimum value for the non-dimensional links lengths from the contour line diagram for $\lambda_2 = 0$ and $\lambda_4 = 0.9$. Thus, the links lengths are $l_2 = 0\,mm$ and $l_4 = 36\,mm$ for the frame length of $l_1 = 400\,mm$. This mechanism allows a maximum rotation angle of $\chi_{max}° \cong 144°$ for a start position $s_0 = 364\,mm$ and a stroke $h = 36\,mm$. The rotation angle is limited to 120° (Fig. 2.2.15) with the displacements $s_1 = 0.5\,mm$ and $s_2 = 32\,mm$, which means that for the knee-joint, the start position and the stroke are $s_0 = 364.5\,mm$ and $h = 396\,mm$, respectively.
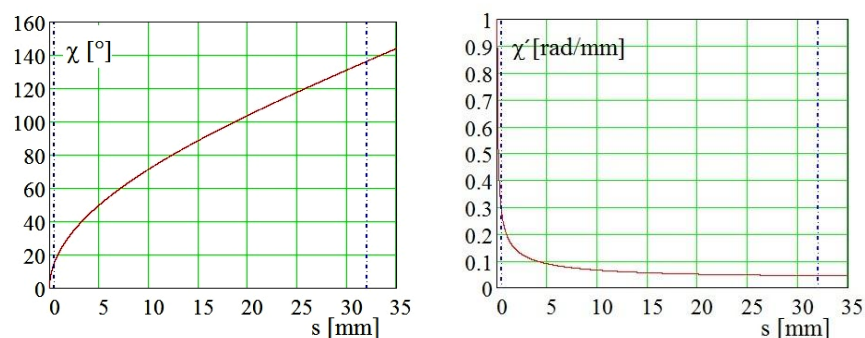
Fig. 2.2.15. Transmission function and instantaneous transmission ratio of the geared linkage with inverted slider-crank used for the knee joint

The developed CAD model of the proposed geared linkage with the assembly of the actuator used for a knee prosthesis is shown in Fig. 2.2.16.a,b [197], [224]. A double acting cylinder was chosen to drive the prosthesis in order to fulfill the requirement of stability by stepping.
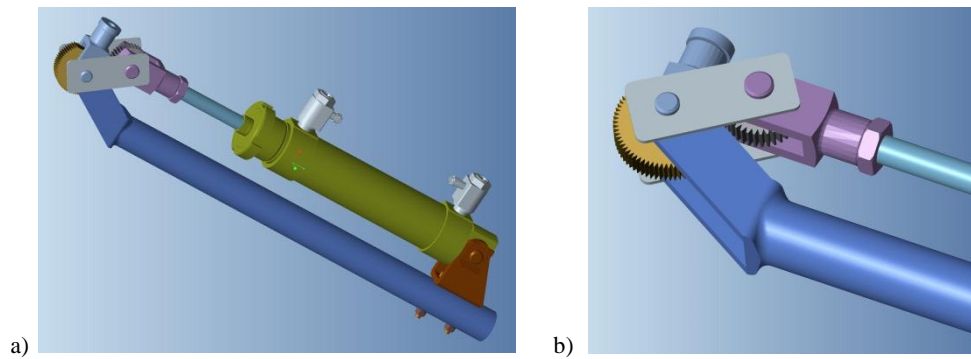
<center>a)   b)</center>
<center>Fig. 2.2.16. CAD model of the knee joint prosthesis</center>

The manufactured active prosthesis as a demonstrative model (s. Fig. 2.2.17) was developed with myoelectric sensors for controlling the valves and monitoring the velocity of the parts on different loads. In order to mimic the human gait in the best way it is necessary to control the braking action based on adjustment of throttles. The different levels of screwing the throttles on both ends of the cylinder lead to different braking actions on each end of the cylinder.

The control functions of the prosthesis are performed by an electro-pneumatic and an electronic module. The two different modules used different power sources; compressed air (reservoir) and electricity (battery).

For the control of the prosthesis (Fig. 2.2.18) are used a set of 2x3 myoelectric sensors attached to the wearer's muscles, one set of 3 sensors for extension and the other set of 3 sensors for flexion. The very weak electrical signals collected by the sensors are amplified using two amplifier stages and then sent as a higher voltage analog signal to the ADC. In turn, the electronic unit monitors the converted values for the two signal channels and decides if the extension or flexion of the prosthesis is required. Based on the signal values of the sensors, 3 levels of the speed values of the prosthesis can be selected.
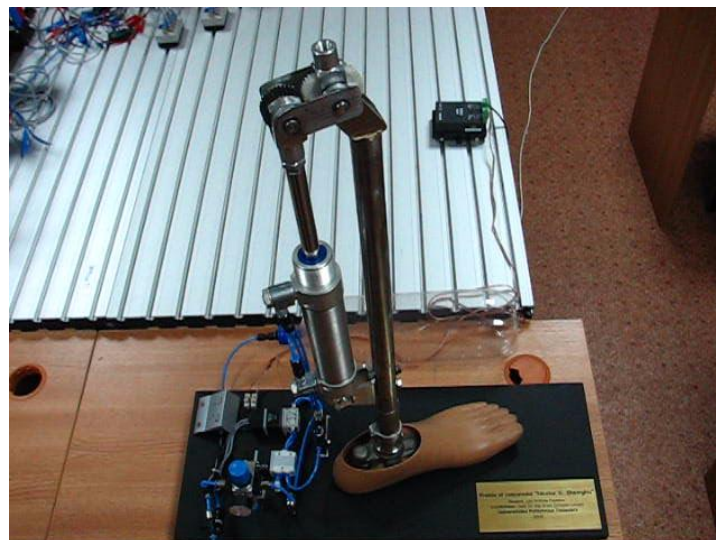
<center>Fig. 2.2.17 Active knee prosthesis demonstrative model</center>

The interface between the low power ECU and the high power electro-valves is achieved with a relay board. The board comprises 4 relays: 2 for feed power to the corresponding valves for extending or retracting the pneumatic cylinder and 2 for providing the power to the throttled valves, which control the air flow in the cylinder and implicit the velocity of the prosthesis movement.
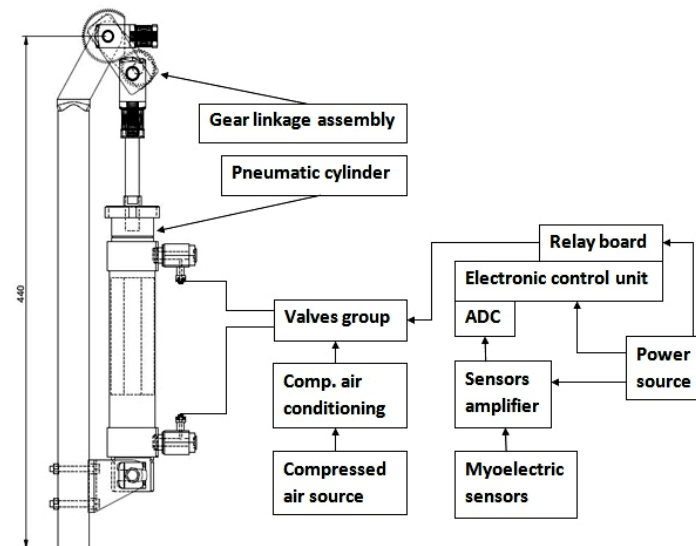
Fig. 2.2.18 Active knee prosthesis control device

The pneumatics consists of the cylinder, the electro-valves group, the compressed air conditioning group (filtering, pressure limiting, 3-way valve for refill) and the air reservoir. The developed force is controlled individually by the pressure inside each chamber of the cylinder so that the prosthesis can be adjusted according to the application. The pneumatic circuit also involves two electrically piloted check valves that restrict the air evacuation form the cylinder when there is no command to move it. In this state, the prosthesis behaves like having a slightly damped elastic element that provides the wearer with a level of compliance.

The working pressure of the system is 0.4 MPa and the pressure limit inside the pneumatic circuit is 1.0 MPa. Using high pressure air reservoir (~2.0 MPa) which increases the autonomy, it is necessary to be used an intermediate pressure regulator. Since the air consumption of the demonstrative model is approximated to 1.10 nl/min, another extended autonomy of the prosthesis can be provided by wearing a small and silent compressor, but with the disadvantage of increasing the total weight caused by the compressor and additional batteries weight.

2.2.9. Scientific contributions

The structural synthesis identified the 4 useful mechanism structures of the geared linkages and classified them in two types: planetary geared linkages (Asi) and cycloidal geared linkages (Zsi).

The kinematic analysis of the geared linkages with linear displacement actuator of first type shows the capability to perform a very large oscillating angle with approximately constant ratio and a favourable transmission angle of the basic structure in defined motion range of the input element.

The proposed optimum synthesis method allows the computation of an optimal links length for the geared linkages taking into account the constructive and kinematic constrains.

The behaviour of the geared linkages recommends this class of mechanism to be used in mechanic and mechatronic applications with large oscillating angle.

The proposed drive mechanism with geared linkage is an original solution for the knee prosthesis, which was designed and manufactured in the laboratories of the Politehnica University of Timisoara.

The prosthesis implements a geared linkage in order to mimic the movement of the human knee during the flexure/extension and to improve the similar design solutions using inverted slider crank or slider crank as driving mechanism for the knee joint movement.

The optimal dimensioning of the links was performed on the criterion of getting natural values of movement extension and to block in the start position the upper and lower limbs by walking.

The prosthesis is original in regard of the used mechanism which allows a large rotation angle with favourable transmission angle of the basic structure, small weight at simple and sturdy construction. The approximately linear transmission function permits an easier control of the movement in the considered range.

The electro-pneumatic system actuates and controls the mechanical knee joint´s movement. The extension of the rotation and its forward/backward sense is controlled by means of a set of 2x3 myoelectric sensors and an electronic unit.

2.3. Analysis and synthesis of path generating 5-link belt mechanisms

2.3.1. State-of-art

Belt mechanisms using links with variable length are suitable to generate non-linear transmission functions or to describe special paths. The variable length link consists of a belt as a flexible and inextensible element enveloped or developed on at least one non-circular/circular wheel. Belt mechanism reproduces theoretically any transmission function (between input-output parameters), with a theoretically absolute accuracy in a defined range of the input parameters.

K. Hain began with the study of the belt mechanisms as periodical mechanisms [7]. The study was continued by Dizioglu in [10] with an analytical dynamic analysis of belt mechanisms used in weaving looms. In [11] K. Hain deals with the grapho-analytical synthesis of the belt mechanism with four elements. R. Bayer, by means of using the Euler relationships, presents in [12] a grapho-analytical analysis method for computing the kinematic parameters of the belt mechanism. Perju in [40] shows an analytical synthesis based on the relationship between the evolute and involute and exemplified the use of one type of a belt mechanism in the linearization of a centrifugal tachometer scale. The development of the computation capacities allowed the development of analytical methods for analysis and synthesis of belt mechanisms. Thus, an analytical method using the tangent condition between the belt and non-circular wheel(s) and the preservation of the total length of the belt (free and enveloped length) is presented by Luck, Modler and Wadewitz in [56], [75] and [73]. Perju, Modler and Lovasz in [73], [74] [80] and [81] present a general analytical method using the relationship between the evolute and involute considering the inverse movement. The analytical methods were developed for path generating [56], [75] and [81] and function generating [73], [74], [80] and [81] belt mechanisms respectively.

Perju and Moldovan in [205] and [218] developed analysis methods for belt mechanisms with circular wheels centric or eccentric jointed. Ebert modelled the belt mechanisms and then computed the dynamic behaviour [200].

2.3.2. Aim of the theoretical research

For using belt mechanism in mechatronic systems is necessary to adjust the variable link lengths to the various movement tasks. This requirement is possible by increasing the degree of freedom of the mechanisms and by using of circular wheel instead of a special profiled non-circular wheel. Theoretically, any movement task can be generated by using of controlled actuator´s movement. A mechatronic application shows the applicability of this new type of 5-link belt mechanism [239], [242] as a walking leg mechanism.

2.3.3. Theoretical contributions

The 5-link belt mechanisms are planar mechanisms, which contain a centrode kinematic pair, accomplished by enveloping or developing of a belt on a profiled or circular wheel. The belt is considered flexible, inextensible and permanently tensile loaded, in order to be assimilated to instantaneous rigid links.

2.3.3.1. Structural synthesis of 5-link belt mechanisms

For the structural synthesis of the 5-link belt mechanism are considered the centrode, the revolute and/or the prismatic kinematic pairs with one degree of freedom $f=1$.

The constrained motion condition is:

$$2 \cdot e_1 - 3 \cdot n + 3 + F = 0,$$

(2.3.1)

where: e_1 - the number of the kinematic pairs with *f=1*,

n - the number of elements.

The constrained motion condition is fulfilled for $e_1 = 5$, $n = 5$ and the degree of freedom (DOF) F=2, i.e. the driving movements (inputs) must be correlated and controlled according with the imposed kinematic task. The systematic development of the 5-link belt mechanism structure is based on the 4 possible kinematic chains and the Reuleaux method, which choose an element of the kinematic chain as frame and other two elements as driving and driven elements. The structural synthesis of the 5-link belt mechanism structures is shown in Fig. 2.3.1, where R means revolute kinematic pair, P – prismatic kinematic pair and C- centrode kinematic pair. The notation of the developed structures comprises the sequence of the joints abbreviation and the frame element of the chain in brackets.

Fig. 2.3.1 Structural synthesis of the 5-link belt mechanisms

The selection of the useful structures of 5-link belt mechanisms needs some boundary conditions:
-    all driving elements should be jointed to the frame
-    one of them should be the circular wheel.

2.3.3.2. Kinematic analysis of the path generating 5-link belt mechanisms

The structure of 5-link belt mechanism of type RRRCR(e) is recommended to be used as path generating mechanism considering the profiled wheel as circular wheel and the frame length equal to zero (s. Fig. 3.3.2). The simple manufacturing of the circular wheel allows a continuous adjustment of the enveloped belt length and recommends this structure to be use in mechatronic applications. The permanent tensile load of the belt can be realized by means of a compression spring between the 2 rigid links or a belt or by manufacturing of the links from composite material with axial rigidity. The rotating driving elements are accepted to be the link 2 and the circular wheel 5.

The task of the 5-link belt mechanism is the exact tracing of a given curve:

$$K = x(t) + i \cdot y(t),$$ (2.3.2)

with the parameter $t \in [0,1]$.

Based on the kinematic schema in Fig. 2.3.2, the same coupler point K can be expressed through the relationship written in complex numbers:

$$K = l_2 \cdot e^{i \cdot \varphi(t)} + l_5 \cdot e^{i(\alpha + \vartheta(t))}.$$ (2.3.3)
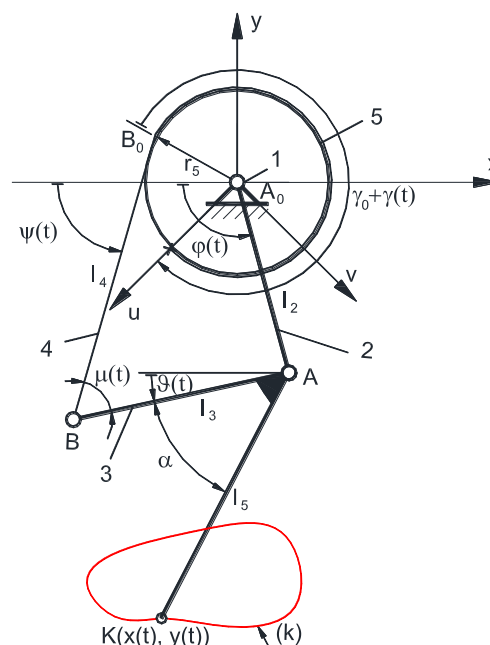
Fig. 2.3.2 Kinematic schema of the 5-link belt mechanisms

From the equations (2.3.2) and (2.3.3) and eliminating the exponent $\alpha + \vartheta(t)$ results:

$$\varphi(t) = 2 \cdot \arctan \frac{B(t) \pm \sqrt{A^2(t) + B^2(t) - C^2(t)}}{A(t) - C(t)},$$ (2.3.4)

where:

$$A(t) = 2 \cdot l_2 \cdot x(t) \qquad B(t) = 2 \cdot l_2 \cdot y(t) \qquad C(t) = l_5^2 - x^2(t) - y^2(t) - l_2^2.$$ (2.3.5)

In an analog procedure the positional angle of the coupler (3) results:

$$\vartheta(t) = \varphi(t) - \alpha + \arccos\left(\frac{x^2(t) + y^2(t) - l_2^2 - l_5^2}{2 \cdot l_2 \cdot l_5} \right).$$ (2.3.6)

Further is presented the calculus of the drive angle $\theta(t)$ of the wheel and the calculus of the wheel angle $\gamma(t)$ in the mobile system of the wheel and belt angle $\gamma(t)$ in the frame system:

$$\theta(t) = \psi(t) - \gamma(t),$$
(2.3.7)

where:

$$\gamma(t) = \frac{l - \sqrt{l_2^2 + l_3^2 - r_5^2 + 2 \cdot l_2 \cdot l_3 \cos(\varphi(t) - \vartheta(t))}}{r_5} - \gamma_0,$$
(2.3.8)

$$\psi(t) = 2\arctan\frac{r_5 \mp \sqrt{r_5^2 + l_4(t)^2 - (l_2\cos\varphi(t) + l_3\cos\vartheta(t))^2}}{l_4(t) + l_2\cos\varphi(t) + l_3\cos\vartheta(t)}.$$
(2.3.9)

$$l_4(t) = l - [\gamma_0 + \gamma(t)] \cdot r_5,$$
(2.3.10)

with: l - the total length of the belt, r_5 - the radius of the circular wheel and γ_0 the initial enveloped belt angle for t = 0.

According with the relationships (2.3.4) and (2.3.7) for computing the parameterized drive angles $\varphi(t)$ and $\theta(t)$ can be generated different imposed curves (2.3.2) with the 5-link belt mechanism. The ranges of the movement tasks depend on the workspace of the coupler point K.

2.3.3.3. Synthesis of the path generating 5-link belt mechanisms

The synthesis of the path generating 5-link belt mechanisms should consider the boundary conditions of the imposed tracing curve (2.3.1). The path should belong to the workspace of the coupler point. The workspace of the coupler points $(x_K(t), y_K(t))$ is defined as a concentric range between the boundary circles:

$$l_2 - l_5 < \sqrt{x_K(t)^2 + y_K(t)^2} < l_2 + l_5.$$
(2.3.11)

The links l_2 and l_4 follows from (2.3.11) as:

$$l_2 = \frac{\min(\sqrt{x_K(t)^2 + y_K(t)^2}) + \max(\sqrt{x_K(t)^2 + y_K(t)^2})}{2},$$
$$l_5 = \frac{\max(\sqrt{x_K(t)^2 + y_K(t)^2}) - \min(\sqrt{x_K(t)^2 + y_K(t)^2})}{2}.$$
(2.3.11)

In order to avoid the singularities, it is necessary to have the transmission angle always positive and $\mu(t) > \mu_{min}$, where:

$$\mu(t) = \psi(t) - \vartheta(t),$$
(2.3.12)

By considering the relationships of the joint B of the belt mechanism described with two polygonal loops in the fixed axes system xA_0y:

$$B = l_2 \cdot e^{i \cdot \varphi(t)} + l_3 \cdot e^{i \cdot \vartheta(t)},$$
(2.3.13)

$$B = (l_4(t) - i \cdot r_5) \cdot e^{i \cdot \psi(t)}$$
(2.3.14)

and using the relationships (2.3.12) with $\mu(t) > \mu_{min}$, (2.3.4) - (2.3.10) follows the links length l_3, by accepting the radius of the circular wheel r_5.

2.3.4.   Numerical examples

The examples shows the generations of circle, straight line and special paths. The special path represent an application of the 5-link belt mechanism as a walking leg mechanism to generate a similar path as the known Jensen leg.

2.3.4.1. Generating of different paths with a 5-link belt mechanism

The example problems consider a the belt mechanism RRRCR(e), which should generate different circular paths and a straight line path. In both cases, their equations is expressed in parametric form recommended for control of the actuators.

The circular path is defined through the equations:

$$x(t) = a_0 + R \cdot \cos 2\pi \cdot (t_0 + t) \quad , \quad y(t) = b_0 + R \cdot \sin 2\pi \cdot (t_0 + t) , \tag{2.3.15}$$

and straight line path through the equations:

$$x(t) = a_1 + (a_2 - a_1) \cdot t , \quad y(t) = b_1 + (b_2 - b_1) \cdot t , \tag{2.3.16}$$

with the parameter $t \in [0,1]$ and the initial parameter of the path t_0 computed according with the initial drive angle ($t_0 \rightarrow \varphi_{min}$). The path geometrical parameters are given in the Tab. 2.3.1.

Tab. 2.3.1. Path's geometrical parameters

Circle 1	$a_0 = 0\,mm$	$b_0 = 55\,mm$	$R = 15\,mm$	
Circle 2	$a_0 = 0\,mm$	$b_0 = 55\,mm$	$R = 24\,mm$	
Straight line	$a_1 = 30\,mm$	$a_2 = -30\,mm$	$b_1 = 30\,mm$	$b_2 = 60\,mm$

The given and synthetized geometrical parameters of the belt mechanism RRRCR(e) are shown in Tab. 2.3.2.

Tab. 2.3.2. Geometrical parameters of the belt mechanisms

Frame length	$l_1 = 0\,mm$	Coupler length	$l_3 = 70\,mm$	Belt length	$l = 256.8\,mm$
Crank length	$l_2 = 50\,mm$	Coupler length	$l_5 = 30\,mm$	Wheel radius	$r_5 = 30\,mm$
		Coupler angle	$\alpha° = 120°$		

In Fig. 2.3.3, Fig. 2.3.4 and Fig. 2.3.5 are shown the 5-link belt mechanisms in two extreme positions with the corresponding drive angles $\varphi(t)$ and $\theta(t)$, the transmission angle $\mu(t)$ and the belt angle $\psi(t)$ in the reference system for three different movement tasks.
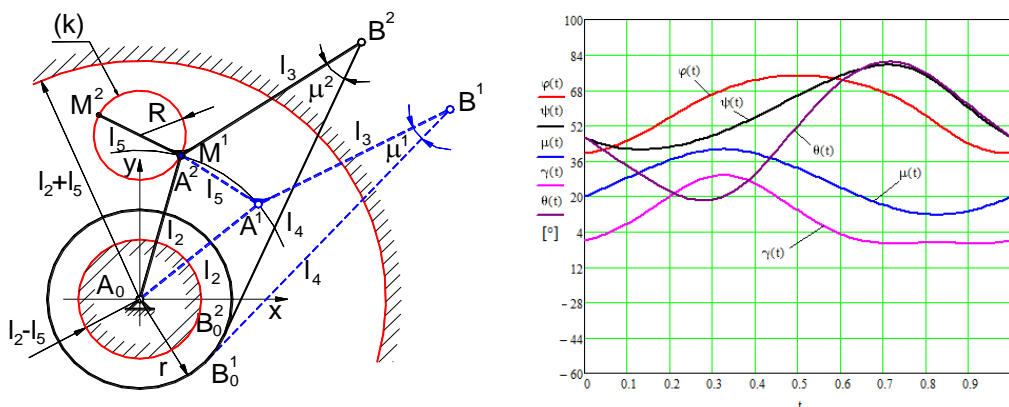
Fig. 2.3.3 Examples of 5-link belt mechanism for generating of a circular path (circle 1)
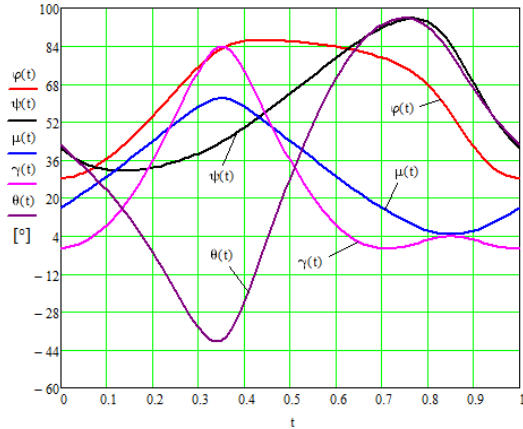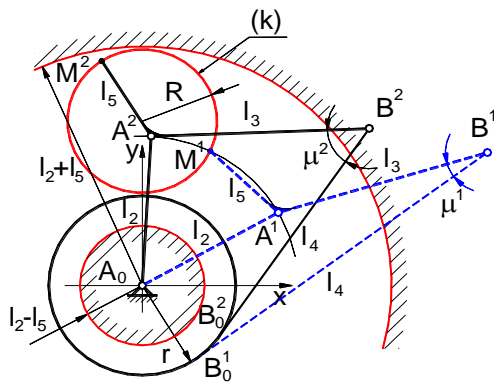
Fig. 2.3.4. Examples of 5-link belt mechanism for generating of a circular path (circle 2)
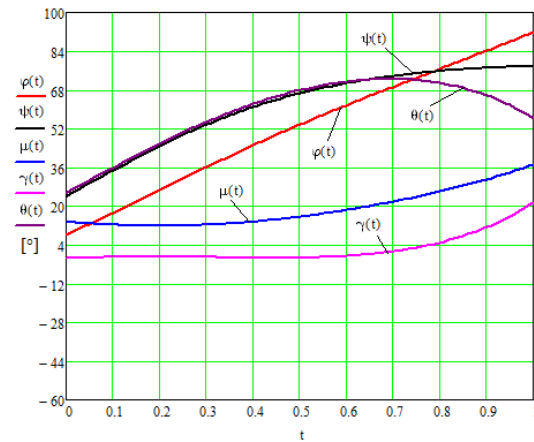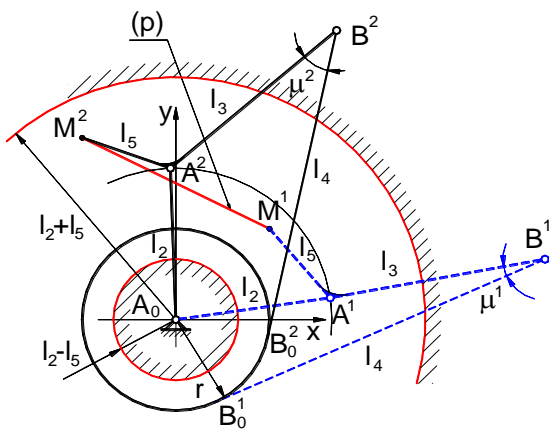
Fig. 2.3.5 Examples of 5-link belt mechanism for generating of a circular path (straight line)

2.3.4.2. Generating of the Jensen leg path with a 5-link belt mechanism

For computing the Jansen leg path is necessary to perform the geometrical analysis. This analysis implies to determinate of the angular positions of each mechanism´s elements and the coordinates of the coupler point M.

From structural point of view the mechanism is composed by eight bars connected through revolute joints and has assigned a single degree of freedom. The three main closed loops of linkages are A_0AB_0B (first four bar linkage), A_0AEB_0 (second four bar linkage) and final B_0CDE (five bar linkage). The crank accomplishes a complete rotation ($\varphi \in [0, 2\pi]$) while the end point M describes the trajectory presented in Fig. 2.3.6.

The equation of the closed loops used for the kinematic analysis were developed using the complex number method:

$$l_2 \cdot e^{i \cdot \varphi} + l_3 \cdot e^{i \cdot \vartheta_1(\varphi)} = (x_{B_0} + i \cdot y_{B_0}) + l_3 \cdot e^{i \cdot \psi_1(\varphi)},$$

$$l_2 \cdot e^{i \cdot \varphi} + l_5 \cdot e^{i \cdot \vartheta_2(\varphi)} = (x_{B_0} + i \cdot y_{B_0}) + l_6 \cdot e^{i \cdot \psi_1(\varphi)} \qquad . \qquad\qquad (2.3.17)$$

$$l_{41} \cdot e^{i \cdot (\alpha_0 + \psi_1(\varphi))} + l_7 \cdot e^{i \cdot \gamma(\varphi)} = l_6 \cdot e^{i \cdot \psi_2(\varphi)} + l_8 \cdot e^{i \cdot \delta(\varphi)}$$

where x_{B_0}, y_{B_0} are known coordinates.

By separating of the terms in each of the equations (2.3.17) and through multiplication with their complex conjugate relationships result equations. By solving of this equations follows the $\psi_1(\varphi)$,

$\psi_2(\varphi)$, $\delta(\varphi)$. The parametric coordinates of the point M are described through the following relations:

$$x_M + i \cdot y_M = x_{B_0} + i \cdot y_{B_0} + l_6 \cdot e^{i \cdot \psi_2(\varphi)} + l_{81} \cdot e^{i \cdot (\delta(\varphi) + \beta_0)} \tag{2.3.18}$$

$$x_M(\varphi) = x_{B_0} + l_6 \cdot \cos \psi_2(\varphi) + l_{81} \cdot \cos(\delta(\varphi) + \beta_0)$$
$$y_M(\varphi) = y_{B_0} + l_6 \cdot \sin \psi_2(\varphi) + l_{81} \cdot \sin(\delta(\varphi) + \beta_0) \tag{2.3.19}$$
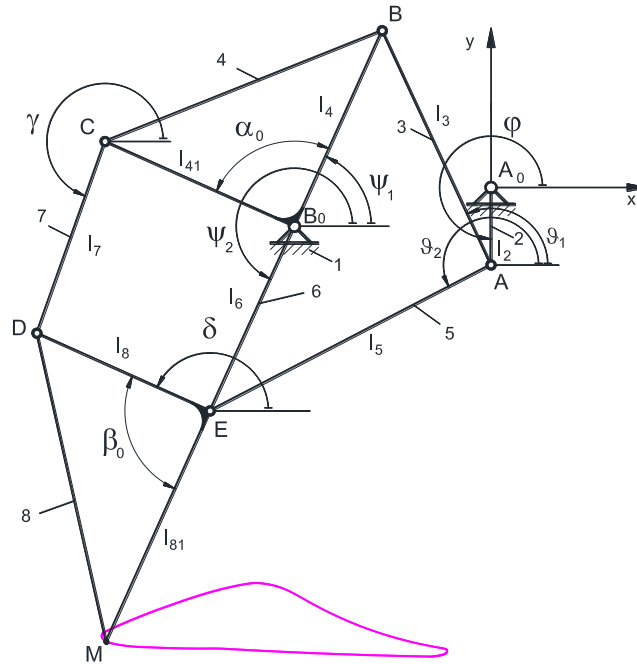
Fig. 2.3.6. Jansen leg mechanism

Based on input data characterized by the link lengths in mm (l_2 =15, l_3 = 50, l_4=41.5, l_{41}=40.1, l_5=61.9, l_6=39.3, l_7=39.4, l_8=36.7, l_{81}=49, α_0=90°, β_0=90°), the coordinates for A_0 (x_{A0}=0, y_{A0}=0), B_0 (x_{B0}=-38, y_{B0}=-7.5) the coordinates of the end point M were calculated. The trajectory shape described by the leg mechanism is shown in Fig. 2.3.7.
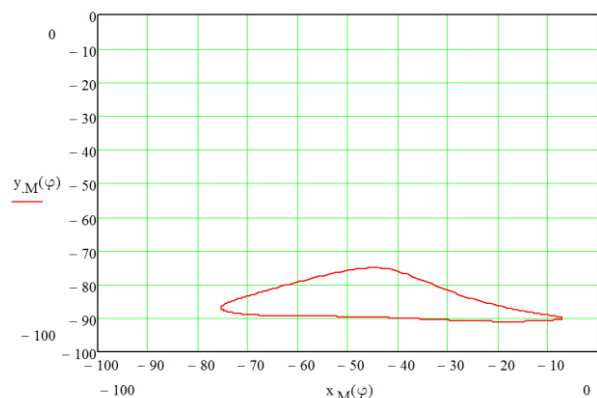
Fig. 2.3.7. View of Jansen leg mechanism's trajectory

The interpolation of the Jansen leg mechanism path divided into seven sub-curves lead to dependency of parameter $t \in [0,1]$ instead of the drive angle φ. For each sub-curve an interpolation function is applied based on a second order spline. This method is chosen in order to have a unitary form for each polynomial expression corresponding to the sub-curve and to avoid the global forms

of interpolation that usually do not converge. The new parametric equations obtained, will be further used for generating of modified trajectories different from the initial one considered an increasing of the step height. The parametric equations for the curve are expressed depending of the parameter *t* as in:

$$x_{M,i}(t) = x_i + m_{x,i} \cdot (t - t_i) + a_{x,i} \cdot (t - t_i)^2, \quad y_{M,i}(t) = y_i + m_{y,i} \cdot (t - t_i) + a_{y,i} \cdot (t - t_i)^2 \quad (2.3.20)$$

$$m_{x,i+1} = m_{x,i} + 2 \cdot a_{x,i} \cdot (t_{i+1} - t_i), \quad m_{y,i+1} = m_{y,i} + 2 \cdot a_{y,i} \cdot (t_{i+1} - t_i) \quad (2.3.21)$$

$$a_{x,i} = \frac{x_{i+1} - x_i}{(t_{i+1} - t_i)^2} - \frac{m_{x,i}}{(t_{i+1} - t_i)}, \quad a_{y,i} = \frac{y_{i+1} - y_i}{(t_{i+1} - t_i)^2} - \frac{m_{y,i}}{(t_{i+1} - t_i)} \quad (2.3.22)$$

where i represents the interpolation range, $m_{x,i}$ $m_{y,i}$ are the slope of the segment curve and the second order coefficients $a_{x,i}$ $a_{y,i}$. The interpolation values and input geometrical data used in the example for the 5-link belt mechanism are presented in Tab. 2.3.3 and Tab. 2.3.4.

Tab. 2.3.3. Interpolation values for the Jansen leg trajectory

m_{x1}	103.487			m_{y1}	-7.874			
i	1	2	3	4	5	6	7	8
t_i	0	0.389	0.553	0.639	0.764	0.833	0.958	1
x_i	-74.363	-26.179	-7.636	-10.581	-39.419	-59.112	-75.319	-74.363
y_i	-87.965	-90.811	-90.395	-85.984	-46.329	-45.890	-86.849	-87.965

Tab. 2.3.4. Input geometric data of the 5-link belt mechanisms

Frame length	$l_1 = 0\,mm$	Coupler length	$l_3 = 10\,mm$	Belt length	$l = 650\,mm$	Coupler angle	$\alpha° = 135°$
Crank length	$l_2 = 55\,mm$	Coupler length	$l_5 = 50\,mm$	Wheel radius	$r_5 = 20\,mm$		

a)   b)
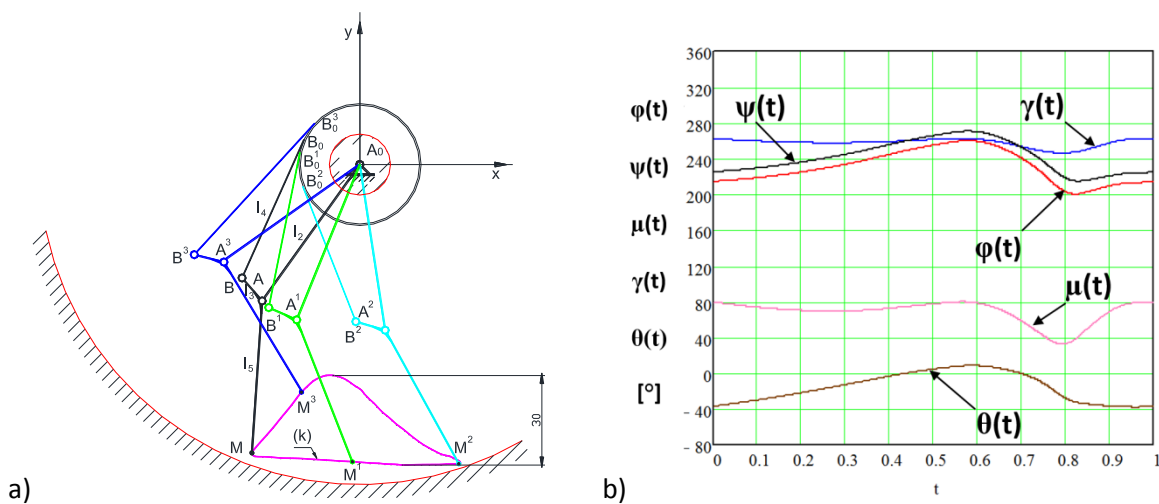
Fig. 2.3.8. a) The 5-link belt mechanism generating a trajectory with h = 30 mm;
b) The drive angles $\varphi(t)$, $\theta(t)$, belt angles $\psi(t)$, wheel angle $\gamma(t)$ and transmission angles $\mu(t)$

After introducing and computing the mathematical relations for the 5-link belt mechanism with the chosen parameters in different positions corresponding to the control points from the given curve it is obtained the following drive angles $\theta(t)$, $\varphi(t)$, wheel angle $\gamma(t)$, belt angles $\psi(t)$ and transmission

angles $\mu(t)$ presented in Fig. 2.3.8, Fig. 2.3.9 and Fig. 2.3.10. This operations were done for three different paths with various heights (h = 30, 42, 55 mm).
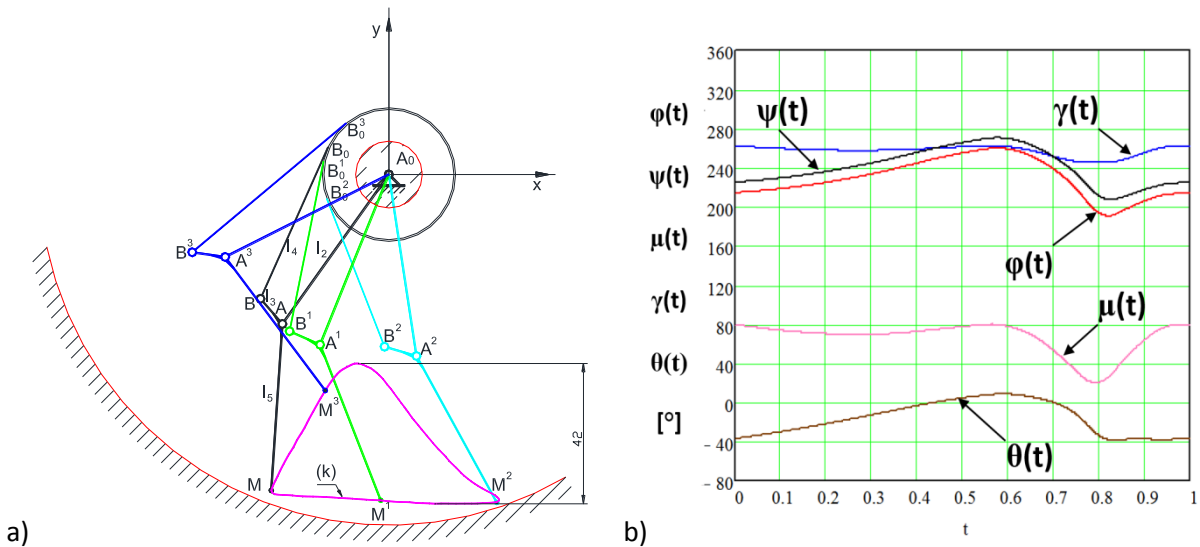
Fig. 2.3.9. a) The 5 link belt mechanism generating a trajectory with h = 42 mm;
b) The drive angles $\varphi(t)$, $\theta(t)$, belt angles $\psi(t)$, wheel angle $\gamma(t)$ and transmission angles $\mu(t)$
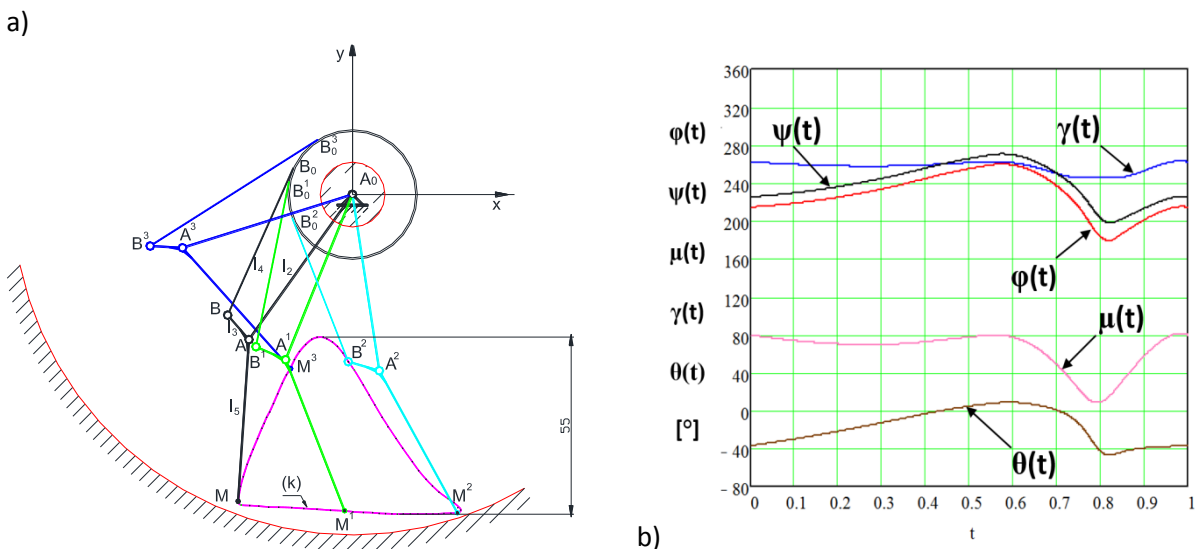
Fig. 2.3.9. The 5 link belt mechanism generating a trajectory with h = 55 mm;
b) The drive angles $\varphi(t)$, $\theta(t)$, belt angles $\psi(t)$, wheel angle $\gamma(t)$ and transmission angles $\mu(t)$

2.3.5. Scientific contributions

The 5-link belt mechanism is a special type of planar belt mechanism with two degrees of freedom, which achieves any movement task precisely in a defined range, through using a belt as a flexible and inextensible element and at least one particular profiled wheel as circular wheel.

The examples computed by using MathCAD shown that the control of the both actuators allow to generate theoretically any paths in the wheel´s plane.

The size of the 5-link belt mechanism is smaller and workspace is larger in comparison with the similar 5-bar linkage, having the same link lengths.

This characteristic recommends the 5-link belt mechanism for use in mechatronic applications, such as kinematic chains of mobile robots, planar manipulators, etc.

The second example of a walking leg mechanism shows that 5-link belt mechanism reproduced properly the Jansen characteristic point path and the control functions for the driving elements can be easily implemented. The controlled rotation angles do not have jumps in their variation towards the parameter t. Weil the transmission angle only positive values has, the singularities throughout the entire control range are avoided.

Through the control of the actuators the mechanism structure using 5-link belt mechanism can be adapted to follow both the Jansen trajectory and similar trajectories with different step heights. So, through this way can be improved the step height in order to avoid different obstacles.

3. Scientific achievements regarding of mechanism development for mechatronics, robotics and mechanical applications

The scientific achievements in the field of mechatronics, robotics and mechanics performed the mechanism development for specific applications. These studies were focused on improvement or new development of the existing solutions. The following applications will be presented:

- design and control solutions for haptic elbow exoskeleton module used in space telerobotics;
- design, control and simulation of a planar parallel manipulator using geared linkages as kinematic chains;
- design solutions for fishing reel spool mechanisms.

3.1. Design and control solutions for haptic exoskeleton used in space telerobotics

3.1.1.   State-of-art

Robotics science developed on various directions, depending on the application area: industrial robots [210], medical robots [225], [226], mobile robots [86], service robots [108], [101] etc. One of the newest facilities implemented in robots' use is the haptic feedback. This application implies the use of special devices and also of exoskeletons.

Exoskeletons were firstly developed for rehabilitation of persons with limb injuries. A large number of patents propose kinematic, design and control of such exoskeletons. For instance, Joutras et al. [89] patented a complex equipment including an exoskeleton, which comprises of almost all joints of human body (shoulder, elbow, wrist, knee, foot joint and neck). The equipment is conceived for rehabilitation by movements of body segments, which are controlled in amplitude and resistant loading. The whole system is designed for static functioning, as the patient sits in a special wheel-chair. Dariush [186] focused on getting a method of controlling an exoskeleton actuator. He developed a theoretical approach to compute the equivalent joint torque for compensation of gravity and external forces, using anthropometric and exoskeleton parameters and external forces.

Perry and Rosen [165] propose a 7-DOF exoskeleton arm with sEMG neural activation. The solution claims a better human-machine interface, which works at the neuro-muscular level, thus reducing the effects of electro-mechanical delay. Patoglu [217] designed an entire exoskeleton, focusing on 3-DOF self-aligning joint elements. Schena [228] proposes the electro-active polymer actuators as devices to provide haptic sensations, emphasizing the better efficiency and lower costs of this technology. The subject started to be treated previously by Bar-Cohen [119].

New force rendering approach with variable feedback gain is proposed by Farkhatdinov et al. in [111], where haptic feedback improves the quality of mobile robot teleoperation by smoothing the trajectory. Caldwell and Tsagarakis [120] constructed and tested a 7-DOF prototype upper arm training and rehabilitation exoskeleton, weighing less than 2 kg due to the use of pneumatic muscle actuators as power source (s. Fig. 3.1.1.a).

Principle considerations and discussions on the potential tasks and limitations of haptic devices make the subject of various works within the last two decades [187], [112], [59], [219]. Recently, most European researches are developed within the frame of ESA projects. The results of these

projects are communicated in papers such as [191], [203], [211], whose authors bring together the expertise of most European countries. Letier et al. [191], [203] focus on the opportunity of developing an upper limb exoskeleton. This is a 7-DOF haptic control chain, for haptic teleoperation of slave robots (s. Fig. 3.2.1.b). The conclusion of the research work is that haptic exoskeletons for outer space teleoperation is still at the level of research developments, because of problems regarding global ergonomics (weight, fixations) and robustness (hardware and software).

a)   b)
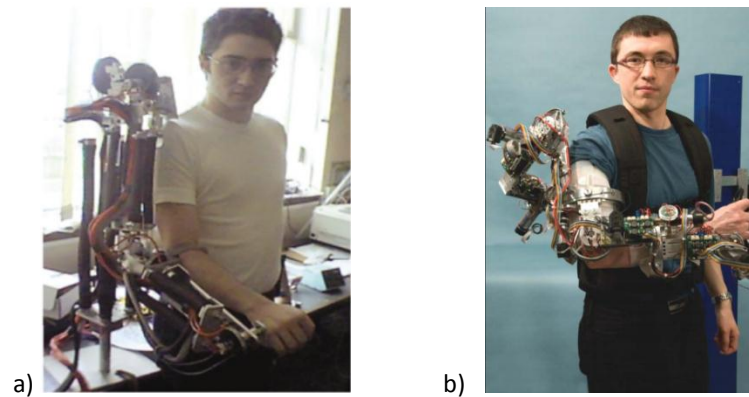
Fig. 3.1.1. Design solutions for the haptic arm exoskeleton
a) 7-DOF prototype upper arm training and rehabilitation exoskeleton
b) 7-DOF haptic arm exoskeleton for teleoperation of slave robots

Gancet et al. [211] introduce the MINDWALKER project, where EEG based kinematic control is a central concept. The project proposes new technologies, such as EEG dry cap, new VR based tools with visual feedback, EEG-BNCI (Brain Neural Computer Interfaces) control. A lower limb exoskeleton structure was developed on medical purposes, but there is prospect for implementation in space applications.

3.1.2. Aim of the theoretical research

The conclusion which results by searching technical literature is that structure, kinematics and control of exoskeletons exist in different variants. However, space applications require specific development or even new technologies.

The aim of the research is the developing of a new lightweight, easy wearable and comfortable haptic arm exoskeleton for teleoperation with a robot having equivalent kinematic chain and with force-feedback. The presentation focuses on the specific design and control solutions for the elbow module of haptic arm exoskeleton, meant to enable force-feedback telemanipulation with redundant robotic arm (slave robot). The design solutions for haptic elbow exoskeleton were presented by the author in [240], [241] and [244].

3.1.3. Theoretical contributions

3.1.3.1. Introduction

In space extravehicular activities is necessary to maintain, to adjust or to assembly some devices. In order to perform these activities safe for the human operator in spacecraft, it is compulsory to use an extravehicular robot haptic controlled by an exoskeleton arm attached to the operator arm. The haptic force feedback on the arm exoskeleton allows avoiding damages by excessive forces given by the extravehicular robot. The haptic arm exoskeleton should have 2-DOF on the shoulder, 1-DOF on elbow and 2-DOF on wrist, that control the corresponding robot joints as indicated in Figure 3.1.2.

The modular concept was used by developing the haptic device, in order to simplify the testing and control procedures and to allow different configurations adapted to perform tasks and to the structure of the controlled robotic chain.
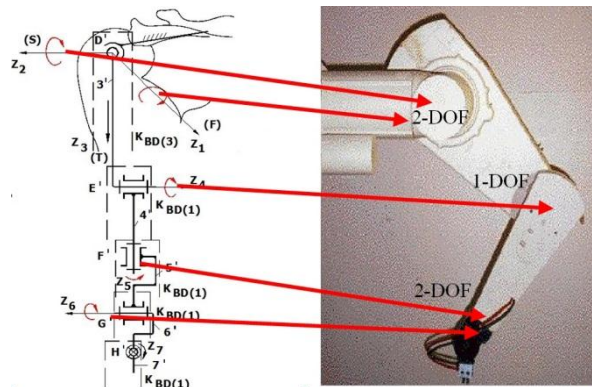
Fig. 3.1.2. Correspondence between the haptic control of the arm exoskeleton and the robot´s joints

Fig. 3.1.3 details the haptic control strategy of the arm exoskeleton modules. In order to transmit the angular movement of the human arm, the exoskeleton must be able to acquire it with an angular sensor/transducer, to convert it in a signal and to control remotely the robotic arm movement. For the force feedback will be used a force sensor/transducer, which transmits remotely back to the exoskeleton and implicitly to the human arm the reaction force. It is important that the motion control of the robotic arm and the force feedback to the human arm should be reversible (to allow direct and back drive).
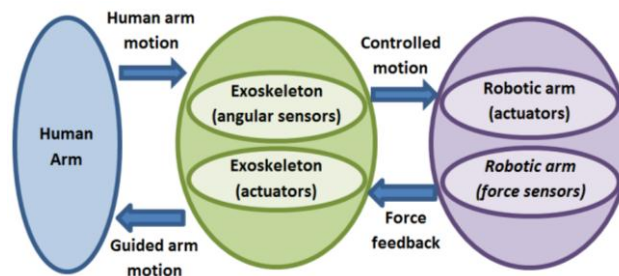
Fig. 3.1.3 Haptic exoskeleton control scheme

The chapter focuses on the development of the haptic elbow exoskeleton module. The design solutions for achieving the mechanical feedback can use controlled mechanism structures or direct actuators. The input parameters for designing the haptic elbow exoskeleton module are given in the Tab. 3.1.1.

Tab. 3.1.1 Input parameters for the optimal synthesis

Nr.	Parameter	Value
1	Maximal rotation angle of the elbow	$\chi = 110°$
2	Maximal reaction load on the operator's hand	$F = 25\,N$
3	Forearm length	$l_f = 400\,mm$
4	Equivalent haptic reaction moment	$M_R = 10\,Nm$

3.1.3.2. Analysis and choice of angular sensors useable for the elbow module

In the first step of the haptic motion control strategy is required acquisition of the angular parameter of the elbow exoskeleton joint rotation. The acquisition methods of the angular parameter and corresponding sensors/transducers or devices are gathered in Table 3.1.2.

Tab. 3.1.2 Angular acquisition methods and devices

No	Method	Sensors/Transducers	Image
1	Electro-magnetic	Potentiometer, Encoder	
2	Optic	CCD camera	
3	Magnetic	Digital magnetic compass	
4	Inertial-magnetic	3-axes angular rate gyroscopes	

The electromagnetic method uses a potentiometer or an encoder in the elbow joint of the exoskeleton module. The accuracy is high, but needs to be connected directly to the elbow joint.

The optical method is a non-contact method, which uses CCD cameras for capturing the markers glued on the elbow exoskeleton braces. The captured frames with the successive positions of the markers are analyzed and with an implemented algorithm the angular parameters are computed.

The system for acquiring the angular information based on magnetic sensors with 3 axes uses magnetic method which computes the 3D orientation of the elbow module braces referring to the earth magnetic axes. This system has not a high accuracy, but the information from the magnetic sensors is easy to be acquired and computed.

The inertial-magnetic method acquire the movement of the exoskeleton using inertial sensors (accelerometers or gyroscopes) combined recently with magnetic sensors, based on the MEMS (Micro Electro-Mechanical Sensors) technology. The using in space application is not recommended.

For the developed elbow exoskeleton module a rotational potentiometer was chosen for the angle acquirement as angular sensor/transducer connected with the two braces of the module as shown in Figure 3.1.4.
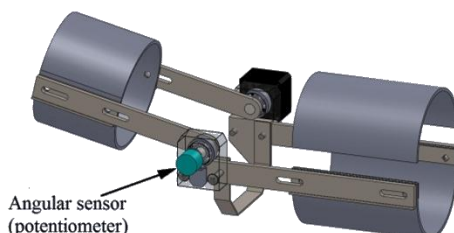
Fig. 3.1.4. Design solution for the angular sensor

The rotational potentiometer has a linear dependence to electrical resistance, provides an absolute angular position for initialization and calibration without influence of parasites and detects the direction of rotation. Although it allows a wide variation of the voltages power supply, it uses a reduced number of supply wires, has reduced mass and size and requires easy maintenance.

3.1.3.3. Analysis and choice of actuators/devices useable for the haptic force feedback on the elbow module

The second step of the strategy is the analysis and choice of the actuators able to generate the force feedback according to the required moment on the robotic arm joints. The moment in the robotic arm joints can be acquired through calibration of the current in the corresponding robot actuators or using torque sensors. The potential useful actuators for generating the force feedback are synthetized in the Table 3.1.3.

The servomotor is easy to actuate, but it supplies a limited torque at small size and needs to impose the backdrive without additional control. The supply voltage is in range of 8-14 V, depending on the maximal torque and rotation speed. The angular possition signal is a step signal with variable width (500..1500 ms), which is directly provided by the microcontroller of the control board.

The double acting pneumatic cylinder is powered with variable pressure, proportional to the force signal received from the robotic arm joint. The control of the pressure is performed by means of two proportional pressure regulators. They convert an analog voltage supply in the range 0-10 V signal to proportional pressure values between 0-10 bar. The pneumatic acting system contains a pressure source (compressor and tank), a compressed air preparation unit (filtering and regulation of pressure), two proportional pressure regulators, which provide air pressure for the double acting cylinder, so that it can generate the required force on forward or return stroke.

Tab. 3.1.3 Actuators/devices useable for the haptic force feedback

No	Type of actuator	Image
1	DC Servomotor	
2	Double acting pneumatic cylinder	
3	DC Linear stepper motor	
4	DC Electromagnetic brake	
5	DC Vibrations motor	
6	DC Mio-stimulator	

The linear stepper actuator uses a bipolar stepper motor, rotating a nut for driving the lead screw. The control is performed by an Ardumoto board receiving direction and steps number signal from the main controller.

A suitable solution to generate a force feedback proportional with the torque on the robotic arm joint is given by the use of electromagnetic brakes. They have the advantage of a small size and free forward/return motion of the elbow joint, but its characteristic is nonlinear dependency of the torque to the command signal.

The vibrations motor has a proportional dependency between the simulated force and the variable frecquecy of the pulses applied to the motor. The voltage supply of the vibration motor is limited to 5 V with a voltage regulator and the activation signal is delivered by the Arduino microcontroller board.

A very simple mechanical solution assumes the use of miostimulation electrodes pair sets. The miostimulators are placed on antagonist muscles on the upper limb.

The choice of the favourable actuator type depends on the design of the elbow arm exoskeleton module.

3.1.3.4. Mechanical design solutions for the haptic elbow exoskeleton module

The above study on the angular sensor/transducer and the actuators/devices usable for the haptic elbow exoskeleton module allows the developing of some mechanical design solutions.

a. Mechanical design of a haptic elbow module with direct actuation

This mechanical design uses a servomotor mounted directly on the exoskeleton elbow joint. On the opposite side of the connection plates is mounted the potentiometer.

a)   b)
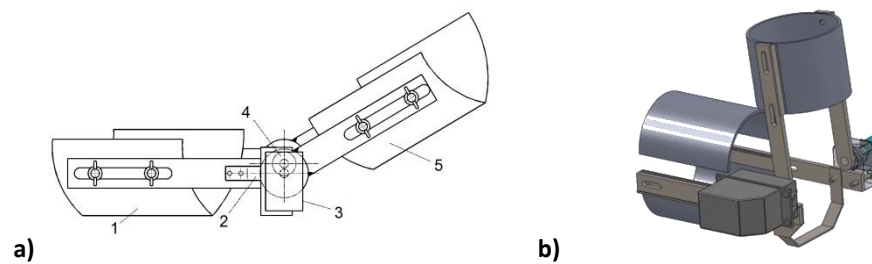
Fig. 3.1.5. Schema (a) and design (b) of a haptic elbow arm exoskeleton module with servomotor

Fig. 3.1.5 show the scheme (a) and design (b) of the elbow exoskeleton module. The module contains two adjustable braces (1) and (5) mounted of the elbow exoskeleton jointed plates. The braces are fixed on the arm and forearm. The angular movement of the exoskeleton module is acquired with the potentiometer (4) and the force feedback is provided by the DC servomotor (3), fixed by the connection piece (2) on arm brace (1). The shaft end of the servomotor is jointed on the forearm brace (5). In order to receive the imposed equivalent haptic reaction moment of 10 Nm, it is necessary to choose an adequate servomotor. Because of the low power provided by electro-motors, a higher mass and larger size motor is required, as shown in Fig. 3.1.5.b.

b. Mechanical design of a haptic elbow module with double acting pneumatic cylinder

The elbow exoskeleton module which uses a linear actuator, as double acting pneumatic cylinder needs to convert the linear movement of the piston in a rotational movement of the module joint with 110°. The geared linkages with linear actuation are able to reproduce an approximately linear transmission function for a very large rotation angle (s. § 2.2). This design of the elbow exoskeleton module allows an easy control of the haptic force feedback through acting pressure in the cylinder. The scheme (a) and design (b) of the elbow exoskeleton module actuated with the geared linkage and pneumatic cylinder are shown in Fig. 3.1.6.

a)   b)
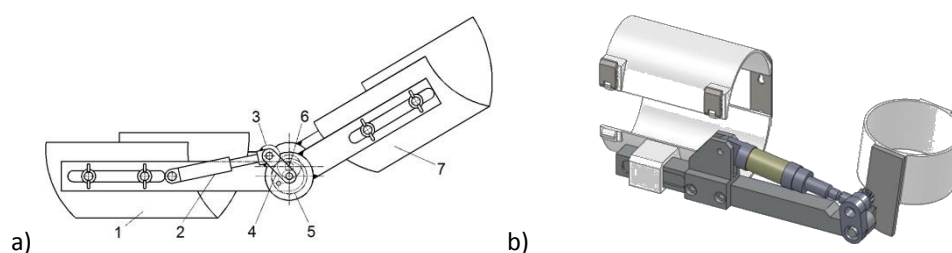
Fig. 3.1.6. Schema (a) and design (b) of a haptic elbow arm exoskeleton module using geared linkage with double acting pneumatic cylinder

The back end of the cylinder is connected to the arm brace plate (1) through a revolute joint and actuates as an active slider. The output gear (5) is fixed on the forearm brace plate. The design solution similarly uses a potentiometer as angular sensor (4).

Through the optimization synthesis (s. § 2.2) for geared linkage with the pneumatic cylinder stoke of 23 mm and the frame distance A_0B_0 = 120 mm, results the length of the rocker B_0B = 20 mm and an initial length of the cylinder A_0B = 111 mm. The transmission function (a) and instantaneous transmission ratio (b) of the geared linkage with inverted slider-crank used for elbow module are shown in Fig. 3.1.7.

a)   b)
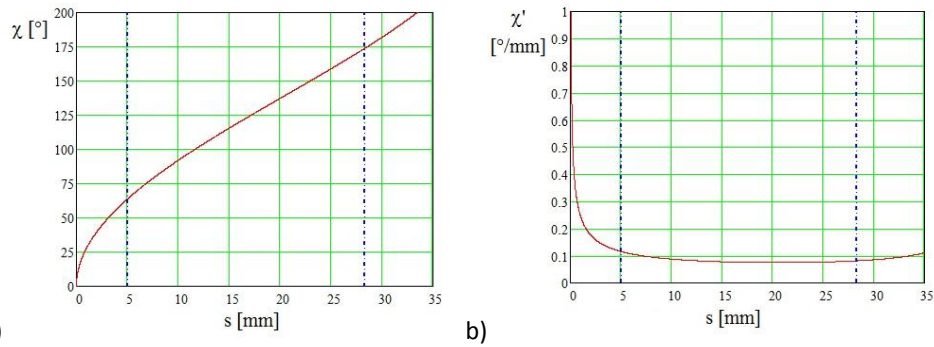
Fig.3.1.7. Transmission function (a) and instantaneous ratio (b) of the geared linkage and pneumatic cylinder

This solution is slim due to the small diameter of the pneumatic cylinder needed to obtain the haptic force response in the elbow joint, allows direct and back drive and offers compliance for the module. But, for space activities use it is not recommended because the air preparation inserts oil in the compressed air, which affects the space craft environment.

   c.   Mechanical design of a haptic elbow module with linear stepper motor

By using a stepper motor with screw nut as linear actuator of the geared linkages the design is bulky because of the higher motor size. The force feedback is controlled by electrical signals and the direct drive is influenced by the friction in the lead thread.

a)   b)
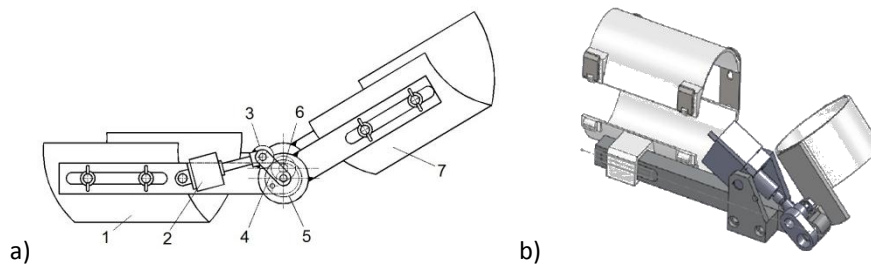
Fig. 3.1.8 Schema (a) and design (b) of a haptic elbow arm exoskeleton module using geared linkage with linear stepper motor

The design solution is similar with the previous one. The stepper motor is fixed by its front plate on an oscillating yoke. Therefore the frame distance of the geared linkage is much smaller. Similarly, through optimization synthesis (s. § 2.2) for the stepper linear actuator with 23.3 mm stroke and a frame distance of $A_0B_0 = 80$ mm yield the length of the rocker $B_0B = 20$ mm and an initial length of the cylinder $A_0B = 72$ mm. The corresponding transmission function (a) and instantaneous transmission ratio (b) of the geared linkage with inverted slider-crank are very similar with the previous case and are shown in Fig. 3.1.9.

a)   b)
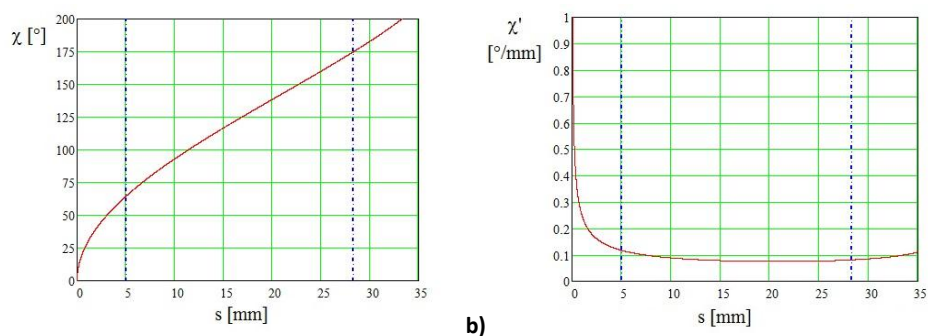
Fig.3.1.9. Transmission function (a) and instantaneous ratio (b) of the geared linkage and linear stepper motor

d.   Mechanical design of a haptic elbow module with wire or belt drive

The design solution using wires or belts allows the remote drive of the elbow joint by servomotors mounted behind the shoulder joint on the frame of the whole exoskeleton.

The wire or the belt (5) is wrapped around a driven pulley (6) mounted on the axle of the elbow joint and around the driving pulley (4) on the servomotor´s end shaft. Guiding rollers may be used (s. Fig. 2.3.10) to lead the wire to the remote driving unit. In this case the tension in the wire must be controlled by the driving torque. By using a belt drives, for each transmission segment is needed an own belt transmission (s. Fig. 2.3.11).

The design solution can use as angular sensor a potentiometer (7) mounted either on the elbow joint (s. Fig. 3.1.10) or on the driving pulley (4).
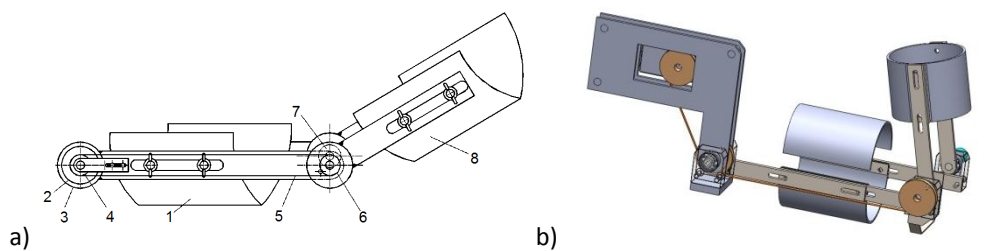
Fig. 3.1.10 Schema (a) and design (b) of a haptic elbow arm exoskeleton module with wire drive
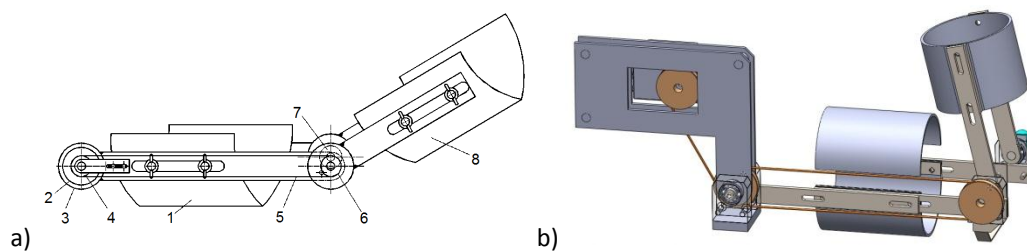
Fig. 3.1.11 Schema (a) and design (b) of a haptic elbow arm exoskeleton module with belt drive

e.   Mechanical design of a haptic elbow module with electromagnetic brake

In order to allow an easier direct haptic feedback it is recommended to use brakes mounted directly in the elbow joint (s. Fig. 3.1.12).
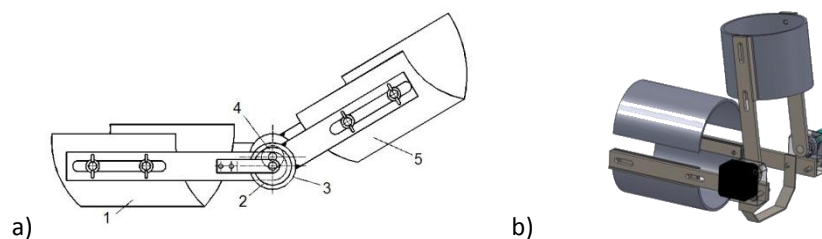
Fig. 3.1.12 Schema (a) and design (b) of a haptic elbow arm exoskeleton module with electromagnetic brake

The design solution is compact and by using of two brakes mounted on opposed sides of the elbow joint the equivalent haptic reaction moment may be doubled, approximately as required. The angular sensor as potentiometer (4) is also mounted on the elbow joint. This solution does not perform back drive, i.e. if the robotic arm is forced by external load to move against the command direction the brakes will block the joint. This situation does not occur usually in space applications due to the zero gravity conditions.

f.   Mechanical design of a haptic elbow module using vibrations motors

The design of the elbow module is similar with the others using only an angular sensor in the elbow joint and has a vibration motor monted on the elbow module. This solution does not impose the position of the vibrator motors on the elbow module, but the calibration effort, the neccesity of user training and his disconfort must be highlighted.

g.   Mechanical design of a haptic elbow module using mio-stimulators

Simmilarlly, this elbow module uses only an angular sensor in the elbow joint and has some set pairs of mio-stimulators monted on the human arm. The solution is very simple, but has the same disadvantages with the previous one.

3.1.3.5. Experimental design of the elbow exoskeleton module

The above studies on the angular sensor/transducer and the actuators/devices usable for the haptic elbow exoskeleton module allow the developing of some mechanical design solutions.

The numerous elbow module solutions described above were compared through multi-criteria analysis, taking into account their size and mass, the maximal haptic reaction, the haptic sensitivity threshold, the possibility for back drive, energetic efficiency, compliance, ergonomics, training duration for operators, complexity and costs.

In Fig. 3.1.13, a synthetic image of the selection process is shown, highlighting the main solutions for gathering data from the exoskeleton, kinematics, actuation and haptic feedback.
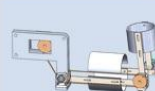
Fig. 3.1.13 Comparative studies of the proposed solution

The most convenient solution is found to be the elbow exoskeleton module with electromagnetic brake. A prototype for this design solution was manufactured (s. Fig. 3.1.14)

The elbow module prototype consists of a two pieces arm brace strapped on operator's arm and a forearm brace in one piece guided on the forearm and allowing the subsequent motions of the hand: flexion-extension and pronation-supination. On both braces, guides and rods are mounted on both sides, allowing length adjustment. The elbow joint is composed of PMMA bearing housings fixed on the arm rods, deep grove ball bearings and axles fixed on the forearm rods. The structural rigidity is improved by a rib under the elbow between the arm rods.

Fig. 3.1.14. The elbow module without angular sensor and brakes

The design with two brakes on each side of the elbow joint (s. Fig. 3.1.15) doubles the haptic feedback with no need of synchronization (as if two servomotors would have been used). The brake housing mounted on the arm rod supports the ball bearings, making the design more compact. The angular sensor is mounted on the outer side of the brace and its shaft end is coupled to the axle.

Fig. 3.1.15. The elbow module with two brakes and angular sensor

The forearm brace is fitted with a handle to allow hand operation. The brake is powered by 24 V power supply. The braking torque is proportional to the voltage applied through an H-bridge (Ardumoto).

In order correlate the information transmitted or received by the controller to the real movement and force exerted, some angular and force measurements were be made. An imagistic method was used to obtaining the rotation angles of the device, by taking subsequent pictures of the assembly in different positions and then importing those pictures into a CAD program and measuring the angular position between two well-marked elements on the exoskeleton. Force measurements were conducted by reading a dynamometer while applying different percentages of power and different voltages to the brakes. Fig. 3.1.16 shows the dependency of the measured angles as function of reported unit values (impulses) and Fig. 3.1.17 the dependency of the force feedback in respect to the command voltage.
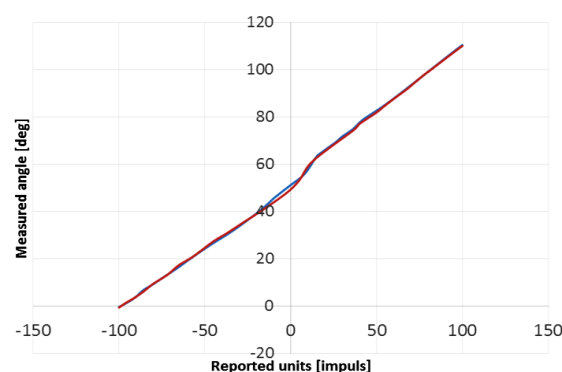
Fig. 3.1.16. Units reported as a function of angular position
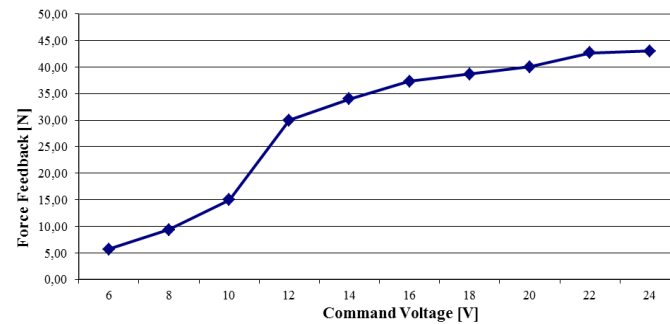
Fig. 3.1.17. Force feedback as function of command voltage applied

3.1.3.6. Control strategy of the elbow exoskeleton module

The program control module runs in parallel two independent code branches, so that the reception and transmission of information about joint position is separated (both in structure and the timing) of the force generating reaction.

The program structure is similar for all the technical solutions proposed and it is represented in the flow chart of Fig. 3.1.18. The force generation control blocks are highlighted and the chosen solution will be implemented.
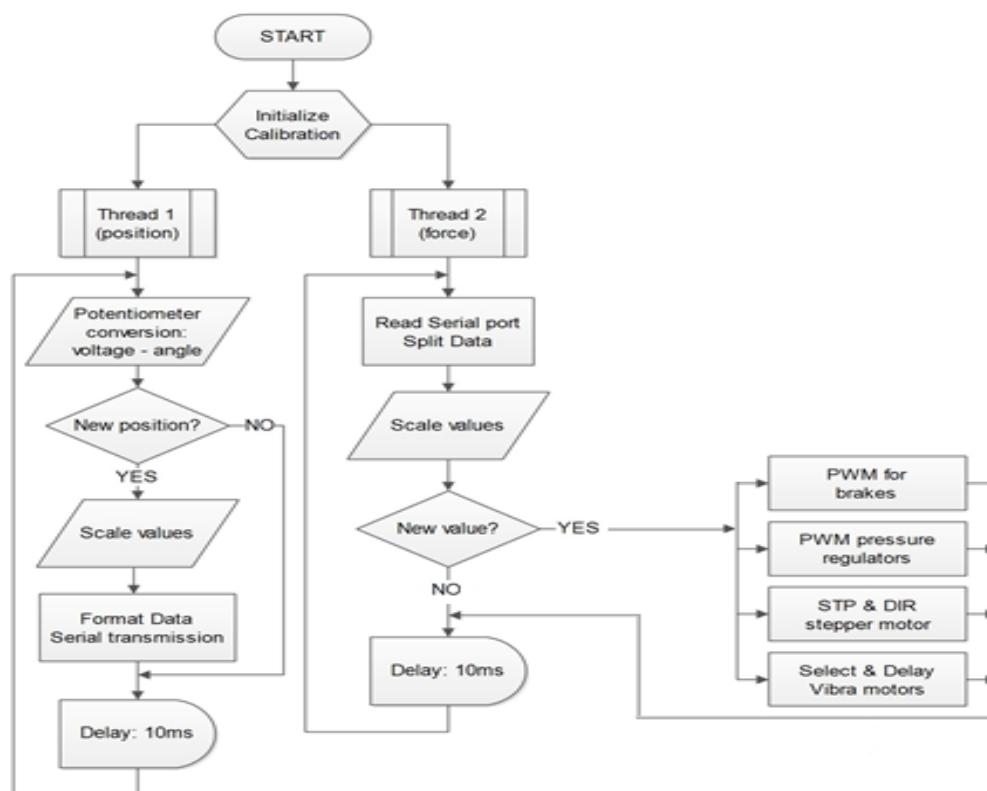
Fig. 3.1.18. Control program flow chart

The program starts with a common routine for initialization and calibration, which verifies that the communication is working, checks the limit positions of the potentiometer (the operator will run several full flexion – extension movements) and also checks the operation of the haptic force generator by operating it with an average force value.

The first branch (Thread 1) reads the position value of the potentiometer and converts this analog input voltage into a discrete numerical value (average of 3 readings every 2 ms). If this value differs

by more than 10 units (equivalent to 3 degrees), previously read value is scaled in the range (0-120) degrees, formatted in a string of alphanumeric characters and transmitted on the serial port. After that, the branch becomes dormant until the passing of the 10 ms - constant time base - measured from the beginning of the branch routine. After this period, the process is repeated.

The second branch (thread 2) still operates with a time base of 10 ms and serves to produce the electric signal needed to generate the reaction haptic force.

The routine begins with reading the serial port and when information is available (sent by slave robot controller) it is separated from the suffix / prefix to extract the value of the moment /force to be generated. That value is then scaled within the applicable range for the chosen technical solution and then compared to the previous torque/force. If they differ by more than 0.3 Nm / 3 N, the value is converted, as appropriate, in duty cycle for PWM signals (two solutions), number of steps and direction for a stepper motor, or motor ID and time interval for vibrating motors. Next, the signal that is applied to the output pins of the control board. Like in the first branch, this one is also latent until the passage of 10 ms, and at the end of this time the routine is repeated.

3.1.4. Scientific contributions

The study presents the design and control strategy for the elbow module of arm exoskeletons meant to work in outer space. Starting from the general control scheme of the haptic exoskeleton are analyzed the sensors able to acquire the angular human elbow movement and the actuators for achieving the haptic feedback. Several solutions were designed for the mechanical structure of the elbow module. The elbow module may be actuated by rotation and linear actuators, depending on the mechanical structure on which they are attached to.

The proposed mechanical solutions include the use of servomotors directly or through wire or belt drives connected on the elbow joint, pneumatic and stepper linear actuators used in geared linkages and direct connected brakes on elbow joint. Also, mechanical solutions using vibrator motor or mio-stimulator are shown. Theses design solutions are compared using a multi criteria algorithm with several conditions as: size and mass, maximal haptic reaction, haptic sensitivity threshold, back drive, energetic efficiency, compliance, ergonomics, training duration for operators, complexity and costs.

As optimal design solution for the elbow exoskeleton module it is selected the module with brakes and angular potentiometer. This solution was manufactured and tested for the force feedback given by voltage steps applied on the brake, comparable with the haptic feedback from the robotic arm.

The next steps in development of the exoskeleton are calibration of the feedback direct from the robotic arm and the development of the next modules: wrist module with 2-DOF (flexion-extension and pronation-supination) and shoulder module with 2-DOF (adduction-abduction and forth and back projection).

3.2. Design, control and simulation of a new class of planar parallel manipulators

3.2.1. State-of-art

Parallel manipulators due to their major advantages became a stand-alone branch of robotics science. There was a continuous and valuable gain of knowledge during the last decades, which now allow thorough analysis and practical creation. Nowadays, parallel manipulators science enriches with new structures fit to dedicated tasks.

The large number of possible architectures inspired approaches in generalization or classification by Ibarreche et al. [223] and Hernandez et al. [237].

The PhD thesis of Zlatanov D. [44] investigates a general class of mechanism configurations with non-redundant or redundant mechanisms with arbitrary kinematic chains, usually referred to as kinematic singularities. Mathematical tools, such as singularity criteria and identification methods, were developed for the study of the singularity. Kotlarski et al. demonstrates in [175] the efficiency of kinematic redundancy through adding a prismatic actuator on the base platform used to increase the useable workspace of planar parallel mechanisms and exemplified on 3(P)RRR and 3(P)RPR structures. The same author in [214] considers the kinematic redundant schemes of four known structures, the 3<u>R</u>RR, the 3R<u>P</u>R, the 6U<u>P</u>S, and the 6<u>R</u>US. A theoretical and experimental study of the kinematic geometry of general 3-RPR planar parallel robots with SCARA-type motions having base joints actuated and largely overlooked was made by Briot in [156] resulting a large singularity-free workspace.

A study of workspace and singularity characteristics is developed in [189] by Huang et al. for 3-RRR, and 3-RPR planar parallel manipulators regarding the influence of various geometric parameters such as pivot locations, link lengths, and size of end-effector. Results are shown a composite ratio of the available workspace to the density of singularity within that workspace. Another study by Huang in [202] in the design optimization for 2-DoF planar parallel robots is presented in order to maximize two key performance characteristics of workspace and dexterity. Bonev in his PhD thesis [107] demonstrate the incontestable effectiveness of geometric methods to the design and analysis of planar and spatial parallel mechanisms. Several new designs are identified, having few or any singularities at all and numerous advantages of Tilt & Torsion angles representation are shown.

a)   b)
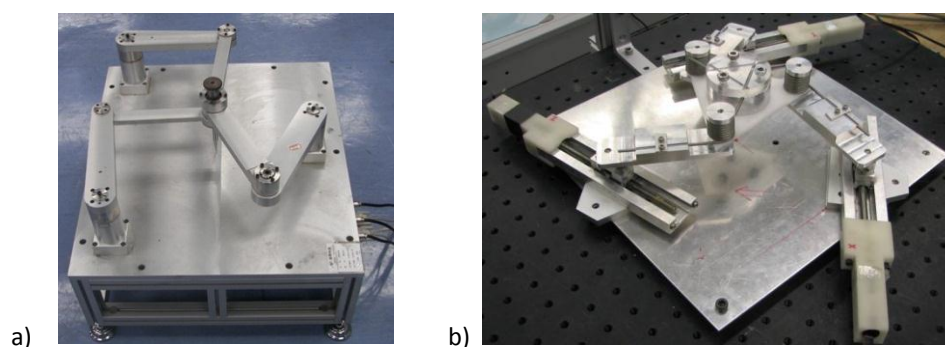
Fig. 3.2.1. Design solutions for planar parallel manipulators
a) 3-<u>R</u>RR manipulator   b) 2-<u>P</u>RR manipulator

Williams describes in [92] the design, construction and real-time closed-loop feedback control of a planar 3-DoF in parallel-actuated manipulator using three pneumatic cylinders. In [213] Joubair et al. a calibration method developed to improve the absolute accuracy of a 3-DoF planar parallel robot. Singh in [243] studied the dynamic model and control of a novel 3-DoF planar parallel robotic motion platform in the presence of parameter uncertainties, payload variations, frictional effects and

external disturbances. Simulations with a typical trajectory were presented and compared with traditional controllers (PID) controller and computed torque controller. Wei in [220] investigates algorithms for designing inexpensive planar parallel robots with prescribed backlash-free workspace (s. Fig. 3.2.1.b).

Chablat et al. in [135] present a recursive model for the kinematics of a 3-PRP planar parallel manipulators and using several matrix equations offer iterative expressions and graphs for the displacements, velocities and accelerations of three prismatic actuators. Other study of Chablat in [170] about the kinematic geometry of a 3-RPR planar parallel robot with actuated base joints and congruent equilateral base and mobile platform focused on computing of the singularity loci and studied the geometrical degeneracies of the direct kinematic model considering the global behavior at all singularities. An improved method based on geometrical solver to obtain the guaranteed singularity-free workspace of planar parallel manipulators was developed by Kotlarski in [174] without calculating the inconvenient interval form of the Jacobian's determinant. Now the interval-based approach error sources, like manufacturing tolerances, can be considered (s. Fig. 3.2.1.a).

The singularity problem and the workspace characterization of 3-DoF manipulators were treated by Buium et al. in [230], [231]. Duca et al. in [235] and [236] introduce the transmission indices for structural groups of dyad type as connecting chains between the fixed and mobile platform and classified their singularities.

Pisla in [181] presented and simulated several aspects of the kinematics and design for two variants of reconfigurable parallel robots. The structural design of an innovative parallel robot with six degrees of freedom is studied by Plitea in [227] and its proposed configurations with five, four, three and two degrees of freedom. The kinematic analysis and the workspace representations of all presented configurations of the parallel robot are presented.

The book of Merlet [139] shows the specific problematic of parallel robots regarding the structural synthesis and architecture, the direct and inverse kinematic, kinematic analysis, singularities, workspace, static and dynamic analysis, calibration and design.

3.2.2.   Aim of the theoretical research

The presentation contributes to the development of the specific class of planar parallel manipulators using geared linkages with linear actuation. It describes a new kinematic connection chain and focuses mainly on the kinematic analysis and the problem of singularities [245] and [248]. A mechatronic application of this new class of parallel manipulator in the food industry was published in [246].

3.2.3.   Theoretical contributions

The state-of-art shows that the parallel manipulators used as connection chains between the fixed and mobile platform by three second order Assur groups that have zero DoF. Usually in the case of non-redundant configurations are used 3 connection chains equilateral positioned in relation with the mobile platform. These configurations used a limited number of elements, but have some disadvantages regarding the singularities and the generated workspace.

3.2.3.1. Structural analysis of the parallel manipulator 3-R(RPRGR)RR

Many studies illustrated that geared linkages with linear actuation allow a large rotation angle with proper transmission angle for the output element and an approximately linear transmission function

in a large range (approximately constant transmission ratio) [124], [224]. This property recommends our mechanism to be used as part of the kinematic chain for the parallel manipulators and it is expected that this structure avoids the first type singularities in a wider range. This mechanism type is very compact; the self-locking condition is fulfilled by using a screw-nut for converting the movement and also for ensuring a high transmission ratio without gear box. Additionally, while the geared linkages, as actuation chains, are jointed with the frame; it is expected that the dynamic behaviour does not worsen. Fig. 3.2.1 shows the kinematic schema of the novel planar parallel manipulator using geared linkages with linear actuation.
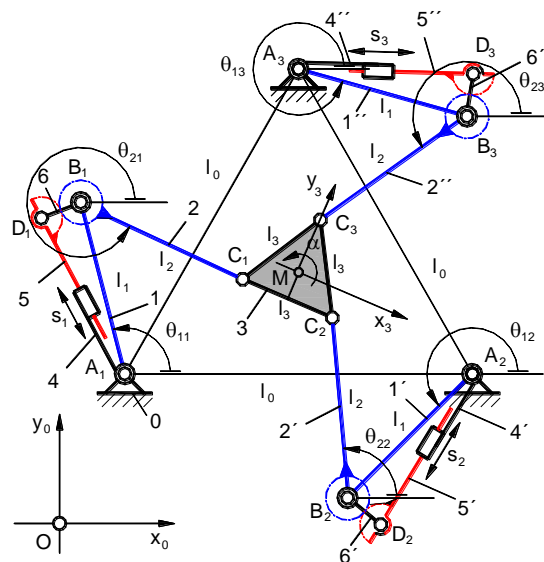
Fig. 3.2.2. Kinematic schema of the planar parallel manipulator 3-R(RPRGR)RR

The proposed notation of this type of manipulator chain should be 3-R(RPRGR)RR, where R – revolute joint, P – prismatic joint and G - gear pair. In brackets ( ) is indicated the parallel connected actuating kinematic chain and underlined (ex. P) the active joint. The considered geared linkage chains use 3 linear actuators $n_{act} = 3$, which actuate the output elements 2, 2′ and 2″ connected to the mobile platform. The number of the elements of each kinematic chain of the planar parallel manipulator increases to 5 elements $n_{chain} = 5$. The proposed planar parallel manipulator allows 3 DOF for the mobile platform (3): 2 translations along the Ox_0 and Oy_0 axis, and the rotation around the Oz axis, which means the mobility of the whole structure is computed with the relationship:

$$M = 3 \cdot (n-1) - 2 \cdot e_1 - e_2 = 3 \cdot (17-1) - 2 \cdot 21 - 3 = 3, \tag{3.2.1}$$

where: n is the number of the elements,

e_1 - number of kinematic pair with $f=1$,

e_2 - number of kinematic pair with $f=2$.

Considering the relationship (3.2.1), the mechanism structure of the planar parallel manipulator follows a constrained motion expressed through the condition:

$$M = n_{act}. \tag{3.2.2}$$

3.2.3.2. Kinematic analysis of the parallel manipulator 3-R(RPRGR)RR

The planar parallel manipulator 3-R(RPRGR)RR ensures 3 DOF for the mobile platform (3): 2 translations along the reference axis Ox_0 and Oy_0 and 1 rotation around the reference axis Oz_0.

Using the simplified computing model, illustrated in Fig. 3.2.3, the direct and invers positional kinematic approach of the planar parallel manipulator is presented.
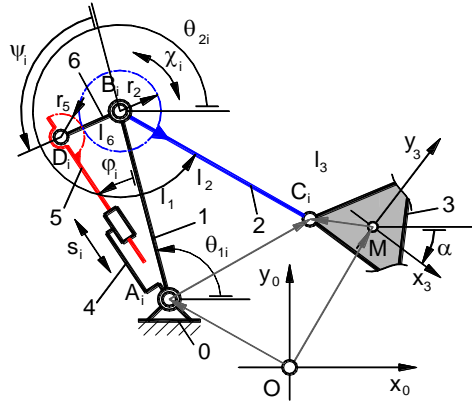
Fig. 3.2.3. Simplified computing model for the kinematic analysis

According to Fig. 3.2.3 the Chasles vector equation [23], is:

$$\overrightarrow{OA_i} + \overrightarrow{A_iC_i} = \overrightarrow{OM} + \underline{R} \cdot \overrightarrow{MC_i^{(3)}}, \quad i = \overline{1,3}.$$ (3.2.3)

Equation (3.2.3) developed in matrix form becomes:

$$\begin{bmatrix} x_{A_i} \\ y_{A_i} \end{bmatrix} + \begin{bmatrix} l_1 \cos\theta_{1i} + l_2 \cos\theta_{2i}(s_i) \\ l_1 \sin\theta_{1i} + l_2 \sin\theta_{2i}(s_i) \end{bmatrix} = \begin{bmatrix} x_M \\ y_M \end{bmatrix} + \begin{bmatrix} \cos\alpha & -\sin\alpha \\ \sin\alpha & \cos\alpha \end{bmatrix} \cdot \begin{bmatrix} x_{C_i}^{(3)} \\ y_{C_i}^{(3)} \end{bmatrix}, \quad i = \overline{1,3},$$ (3.2.4)

a. Direct positional kinematics

The direct kinematics approach of the planar parallel manipulator 3-R(RPRGR)RR consists in computing the coordinates of the characteristic point (TCP) on the mobile platform (x_M, y_M) and its orientation with the angle α. This is accomplished by knowing the actuating parameters s_i, the geometry of the frame and mobile platform – equilateral triangle with the sides length l_0 and l_3 respectively, the coordinates of the joints belonging to the fixed frame platform (x_{A_i}, y_{A_i}), the link lengths of the chain l_1, l_2, l_6 and the gear ratio ρ.

For the parallel connected geared linkage the output angle $\chi_i(s_i)$ can be computed (s. 2.2.8), as its transmission function [124], [224]:

$$\chi_i(s_i) = (1-\rho) \cdot \psi_i(s_i) + \rho \cdot \phi_i(s_i),$$ (3.2.5)

where

$$\rho = \pm r_5 / r_2,$$ (3.2.6)

$$\phi_i(s_i) = \arccos \frac{l_6^2 - l_1^2 - (s_0 + s_i)^2}{2 \cdot l_1 \cdot (s_0 + s_i)},$$ (3.2.7)

and

$$\psi_i(s_i) = \arccos \frac{(s_0 + s_i)^2 - l_1^2 - l_6^2}{2 \cdot l_1 \cdot l_6}.$$ (3.2.8)

Considering $\Delta\chi_i$ constant values imposed by the planar parallel manipulator designing conditions results the generalized coordinates.

$$\theta_{2i}(s_i) = \chi_i(s_i) + \Delta\chi_i.$$ (3.2.9)

Using the matrix equation (3.2.4) reference system OX0Y0 to the joints Ci of the mobile platform:

$$\begin{bmatrix} x_M \\ y_M \end{bmatrix} = \begin{bmatrix} x_{A_i} \\ y_{A_i} \end{bmatrix} + \begin{bmatrix} l_1\cos\theta_{1i} + l_2\cos\theta_{2i}(s_i) \\ l_1\sin\theta_{1i} + l_2\sin\theta_{2i}(s_i) \end{bmatrix} - \begin{bmatrix} \cos\alpha & -\sin\alpha \\ \sin\alpha & \cos\alpha \end{bmatrix} \cdot \begin{bmatrix} x_{C_i}^{(3)} \\ y_{C_i}^{(3)} \end{bmatrix}$$ (3.2.10)

with $i = \overline{1,3}$, where:

$$x_{C_i}^{(3)} = l_3\cos(\frac{\pi}{2} + i\frac{\pi}{3}), \quad y_{C_i}^{(3)} = l_3\sin(\frac{\pi}{2} + i\frac{\pi}{3}).$$ (3.2.11)

Because the coordinates of the characteristic point M of the mobile platform must be the same for all three vector equations $i = \overline{1,3}$ the following equation system can be set up:

$$\begin{cases} x_M = x_{A_i} + l_1\cos\theta_{1i} + l_2\cos\theta_{2i}(s_i) - x_{C_i}^{(3)}\cos\alpha + y_{C_i}^{(3)}\sin\alpha \\ y_M = y_{A_i} + l_1\sin\theta_{1i} + l_2\sin\theta_{2i}(s_i) - y_{C_i}^{(3)}\cos\alpha - y_{C_i}^{(3)}\sin\alpha \end{cases} \quad i = \overline{1,3}.$$ (3.2.12)

By solving the equation system (3.2.12) follows the coordinates of the characteristic point (x_M, y_M) and the orientation angle α of the mobile platform (3), as well as the three generalized coordinates θ_{1i}, $i = \overline{1,3}$ in frame jointed links (3, 3′, 3″).

b. Inverse positional kinematics

The inverse positional kinematic approach of the planar parallel manipulator allows computing the actuators parameter s_i by knowing the parametric coordinates of the characteristic point ($x_M(t)$, $y_M(t)$) and the orientation angle $\alpha(t)$ of the mobile platform, with $t \in [0,1]$, the geometry of the frame and mobile platform through the side lengths of the equilateral triangles l_0 and l_3 respectively, the coordinates of the frame joints (x_{A_i}, y_{A_i}), the link lengths of the chain l_1, l_2, l_6 and the gear ratio ρ.

The matrix equation (3.2.4) in the case of the inverse positional kinematic is rewritten in the parametric form:

$$\begin{bmatrix} l_1\cos\theta_{1i}(t) + l_2\cos\theta_{2i}(t) \\ l_1\sin\theta_{1i}(t) + l_2\sin\theta_{2i}(t) \end{bmatrix} = \begin{bmatrix} x_M(t) \\ y_M(t) \end{bmatrix} - \begin{bmatrix} x_{A_i} \\ y_{A_i} \end{bmatrix} + \begin{bmatrix} \cos\alpha(t) & -\sin\alpha(t) \\ \sin\alpha(t) & \cos\alpha(t) \end{bmatrix} \cdot \begin{bmatrix} x_{C_i}^{(3)} \\ y_{C_i}^{(3)} \end{bmatrix} \quad i = \overline{1,3},$$ (3.2.13)

From the equation (3.2.13) follows the generalized coordinates θ_{1i} and θ_{2i}, $i = \overline{1,3}$ of the planar parallel manipulator in the form:

$$\theta_{1i}(t) = 2 \cdot \arctan\frac{Q_{1i}(t) \mp \sqrt{P_{1i}^2(t) + Q_{1i}^2(t) - R_{1i}^2(t)}}{P_{1i}(t) - R_{1i}(t)},$$ (3.2.14)

where:

$$P_{1i}(t) = 2 \cdot l_1 \cdot (x_M(t) + x_{C_i}^{(3)} \cdot \cos\alpha(t) - y_{C_i}^{(3)} \cdot \sin\alpha(t) - x_{A_i}),$$

$$Q_{1i}(t) = 2 \cdot l_1 \cdot (y_M(t) + x_{C_i}^{(3)} \cdot \sin\alpha(t) + y_{C_i}^{(3)} \cdot \cos\alpha(t) - y_{A_i}),$$

$$R_{1i}(t) = l_2^2 - l_1^2 - (x_M(t) + x_{C_i}^{(3)} \cdot \cos\alpha(t) - y_{C_i}^{(3)} \cdot \sin\alpha(t) - x_{A_i})^2 -$$

$$- (y_M(t) + x_{C_i}^{(3)} \cdot \sin\alpha(t) + y_{C_i}^{(3)} \cdot \cos\alpha(t) - y_{A_i})^2.$$ (3.2.15)

and

$$\theta_{2i}(t) = 2\arctan\frac{Q_{2i}(t) \mp \sqrt{P_{2i}^2(t) + Q_{2i}^2(t) - R_{2i}^2(t)}}{P_{2i}(t) - R_{2i}(t)} \ , \tag{3.2.16}$$

where:

$$P_{2i}(t) = 2 \cdot l_2 \cdot (x_M(t) + x_{C_i}^{(3)} \cdot \cos\alpha(t) - y_{C_i}^{(3)} \cdot \sin\alpha(t) - x_{A_i}) ,$$

$$Q_{2i}(t) = 2 \cdot l_2 \cdot (y_M(t) + x_{C_i}^{(3)} \cdot \sin\alpha(t) + y_{C_i}^{(3)} \cdot \cos\alpha(t) - y_{A_i}) ,$$

$$R_{2i}(t) = l_1^2 - l_2^2 - (x_M(t) + x_{C_i}^{(3)} \cdot \cos\alpha(t) - y_{C_i}^{(3)} \cdot \sin\alpha(t) - x_{A_i})^2 - \tag{3.2.17}$$

$$- (y_M(t) + x_{C_i}^{(3)} \cdot \sin\alpha(t) + y_{C_i}^{(3)} \cdot \cos\alpha(t) - y_{A_i})^2 .$$

As shown the parametric generalized coordinates $\theta_{1i}(t)$ and $\theta_{2i}(t)$ are functions which depend on the imposed parametric coordinates of the characteristic point $x_M(t)$, $y_M(t)$ and the orientation angle $\alpha(t)$ of the mobile platform:

In order to compute the actuation/drive parameters s_i it is necessary to solve the invers transmission function of the geared linkage with linear actuation. By using the designing conditions of the planar parallel manipulator obtained from the equation (7) the calculus of rotation angle of the output link (2) – the gear of the geared linkage is:

$$\chi_i(t) = \theta_{2i}(t) - \Delta\chi_i . \quad i = \overline{1,3} , \tag{3.2.18}$$

The inverse transmission function based on the equation (3.2.5) can be computed on numerical way from the equation:

$$\psi_i(t) + \rho \cdot (\varphi_i(t) - \psi_i(t)) - \chi_i(t) = 0 . \tag{3.2.19}$$

Based on the conclusions from [27] and [28] that the geared linkages with linear actuation shows an approximately linear transmission function and by knowing its geometrical parameters it can be interpolated an inverse transmission function as an 3rd order polynomial Lagrange function with very high precision:

$$s_i(\chi_i) = \sum_{k=1}^{4}\left((s_i)_k \cdot \prod_{\substack{j=1 \\ j \neq k}}^{4} \frac{(\chi_i) - (\chi_i)_j}{(\chi_i)_k - (\chi_i)_j} \right) . \tag{3.2.20}$$

3.2.3.3. Singularities of the parallel manipulator 3-R(RPRGR)RR

Taking into account the vector equation in matrix form (3.2.4), by separating the sub matrix containing terms θ_{1i} and eliminating the θ_{1i}, $i = \overline{1,3}$, reaching the expression:

$$l_1^2 = \left(x_M + x_{C_i}^{(3)}\cos\alpha - y_{C_i}^{(3)}\sin\alpha - x_{A_i} - l_2\cos\theta_{2i}(\chi_i(s_i))\right)^2 + $$

$$+ \left(y_M + x_{C_i}^{(3)}\sin\alpha + y_{C_i}^{(3)}\cos\alpha - y_{A_i} - l_2\sin\theta_{2i}(\chi_i(s_i))\right)^2 . \tag{3.2.21}$$

By considering the equation (3.2.21) as an implicit function $F_i(x_M, y_M, \alpha)$, where:

$$F_i(x_M, y_M, \alpha) = \left(x_M + x_{C_i}^{(3)}\cos\alpha - y_{C_i}^{(3)}\sin\alpha - x_{A_i} - l_2\cos\theta_{2i}(\chi_i(s_i))\right)^2 + $$

$$+ \left(y_M + x_{C_i}^{(3)}\sin\alpha + y_{C_i}^{(3)}\cos\alpha - y_{A_i} - l_2\sin\theta_{2i}(s_i)\right)^2 - l_1^2 = 0 \tag{3.2.22}$$

and $\theta_{2i}(\chi_i(s_i))$ depending on $\chi_i(s_i)$, i=1,2,3 is determined by the drive stroke s_i.

The three dimensional functions $F_i(x_M, y_M, \alpha)$ are functions of driven elements 2, 2' and 2'', expressed by $\chi_i(s_i)$, so it can be simplified written:

$$F_i(X, Q) = 0, \qquad (3.2.23)$$

with: $X = [s_1, s_2, s_3]$ and $Q = [x_M, y_M, \alpha]$.

The function (3.2.23) differentiation with respect to time is leading to the known relation:

$$J_s \cdot \dot{X} + J_q \cdot \dot{Q} = 0, \qquad (3.2.24)$$

where J_s and J_q are Jacobian matrices that show the parallel manipulator´s singularities of first type and second type, respectively.

a. Singularities of first type

The first type singularities express the cases in which the actuation of the drive elements does not move the mobile platform. The computation of this type of singularity implies to satisfy the condition to have the Jacobian matrix determinant J_s equal to zero [139]:

$$\det(J_s) = \det\begin{bmatrix} \dfrac{\partial F_1(X,Q)}{\partial s_1} & \dfrac{\partial F_1(X,Q)}{\partial s_2} & \dfrac{\partial F_1(X,Q)}{\partial s_3} \\ \dfrac{\partial F_2(X,Q)}{\partial s_1} & \dfrac{\partial F_2(X,Q)}{\partial s_2} & \dfrac{\partial F_2(X,Q)}{\partial s_3} \\ \dfrac{\partial F_3(X,Q)}{\partial s_1} & \dfrac{\partial F_3(X,Q)}{\partial s_2} & \dfrac{\partial F_3(X,Q)}{\partial s_3} \end{bmatrix} = 0, \qquad (3.2.25)$$

where:

$$\frac{\partial F_i(X,Q)}{\partial s_i} = 2l_2 \{[x_M + x_{C_i}^{(3)}\cos\alpha - y_{C_i}^{(3)}\sin\alpha - x_{A_i} - l_2\cos\theta_{2i}(\chi_i(s_i))]\sin\theta_{2i}(\chi_i(s_i)) +$$
$$- [y_M + x_{C_i}^{(3)}\sin\alpha + y_{C_i}^{(3)}\cos\alpha - y_{A_i} - l_2\sin\theta_{2i}(\chi_i(s_i))]\cos\theta_{2i}(\chi_i(s_i))\} \cdot \chi_i'(s_i), \qquad (3.2.26)$$

$$\frac{\partial F_i(X,Q)}{\partial s_j} = 0, \quad i \neq j, \quad i = \overline{1,3}, \quad j = \overline{1,3}. \qquad (3.2.27)$$

The substitution of (3.2.26) and (3.2.27) in the Jacobian matrix determinant lead to the equation for computing the singularities of first type:

$$0 = \frac{\partial F_1(X,Q)}{\partial s_1} \cdot \frac{\partial F_2(X,Q)}{\partial s_2} \cdot \frac{\partial F_3(X,Q)}{\partial s_3}. \qquad (3.2.28)$$

Because the similarity of the partial derivative terms in (3.2.28), if any term is zero, than the equation is satisfied and the study of avoiding the singularities of first type can be reduced on study of one partial derivative term of one actuating kinematic chain:

$$0 = \frac{\partial F_i(X,Q)}{\partial s_i}, \quad i = \overline{1,3}. \qquad (3.2.29)$$

b. Singularities of second type

The second type singularities correspond to the positions when non-actuated drives allow an infinitesimal motion of the mobile platform inside the workspace. These can be determined when the Jacobian matrix determinant J_q is zero. In addition J_q depicts the parallel manipulator´s workspace boundaries [139], [230].

$$\det(J_q) = \det \begin{bmatrix} \dfrac{\partial F_1(X,Q)}{\partial x_M} & \dfrac{\partial F_1(X,Q)}{\partial y_M} & \dfrac{\partial F_1(X,Q)}{\partial \alpha} \\ \dfrac{\partial F_2(X,Q)}{\partial x_M} & \dfrac{\partial F_2(X,Q)}{\partial y_M} & \dfrac{\partial F_2(X,Q)}{\partial \alpha} \\ \dfrac{\partial F_3(X,Q)}{\partial x_M} & \dfrac{\partial F_3(X,Q)}{\partial y_M} & \dfrac{\partial F_3(X,Q)}{\partial \alpha} \end{bmatrix} = 0 \tag{3.2.30}$$

where:

$$\frac{\partial F_i(X,Q)}{\partial x_M} = 2 \cdot [x_M + x_{C_i}^{(3)} \cos\alpha - y_{C_i}^{(3)} \sin\alpha - x_{A_i} - l_2 \cos\theta_{2i}(\chi_i(s_i))], \tag{3.2.31}$$

$$\frac{\partial F_i(X,Q)}{\partial y_M} = 2 \cdot [y_M + x_{C_i}^{(3)} \sin\alpha + y_{C_i}^{(3)} \cos\alpha - y_{A_i} - l_2 \sin\theta_{2i}(\chi_i(s_i))], \tag{3.2.32}$$

$$\frac{\partial F_i(X,Q)}{\partial \alpha} = 2 \cdot \{[y_M + x_{C_i}^{(3)} \sin\alpha + y_{C_i}^{(3)} \cos\alpha - y_{A_i} - l_2 \sin\theta_{2i}(\chi_i(s_i))](x_{C_i}^{(3)} \cos\alpha - y_{C_i}^{(3)} \sin\alpha) - $$
$$- [x_M + x_{C_i}^{(3)} \cos\alpha - y_{C_i}^{(3)} \sin\alpha - x_{A_i} - l_2 \cos\theta_{2i}(\chi_i(s_i))](x_{C_i}^{(3)} \sin\alpha + y_{C_i}^{(3)} \cos\alpha)\} \tag{3.2.33}$$

The substitution of partial derivatives (3.2.31), (3.2.31) and (3.2.31) in the relationship (3.2.30) allows the computing of second type singularities. The singularities of second type use identical terms in the Jacobian matrix determinant J_q with the planar manipulator 3-RRR [230].

3.2.4. Numerical example

3.2.4.1. Singularities analysis for a parallel manipulator 3-R(RPRGR)RR

The first example accept the dimensions of the planar parallel manipulator 3-R(RPRGR)RR given in Table 3.2.1 and chosen in order to reduce the singularities of second order and to dimension the optimal link lengths of the geared linkages on the criterion of maximizing the angle of driven elements 2, 2', 2'' with favorable transmission angle ($\mu > 30°$) by the inverted slider-crank.

Tab. 3.2.1. Geometrical parameters of the planar 3-R(RPRGR)RR manipulator

Frame platform length (0)	$l_0 = 120\,\text{mm}$	Carrier length (6)	$l_6 = 10\,\text{mm}$
Mobile platform length (3)	$l_3 = 25\,\text{mm}$	Gear ratio	$\rho = 1.5$
Chain link length (1,1',1'')	$l_1 = 50\,\text{mm}$	Initial stroke	$s_0 = 42.5\,\text{mm}$
Chain link length (2,2',2'')	$l_2 = 50\,\text{mm}$	Stroke	$h = 15\,\text{mm}$
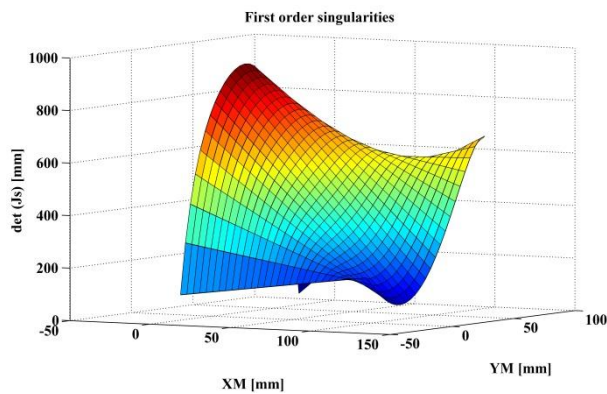
Fig. 3.2.4 Analysis of the singularities of first type for the planar 3-R(RPRGR)RR manipulator
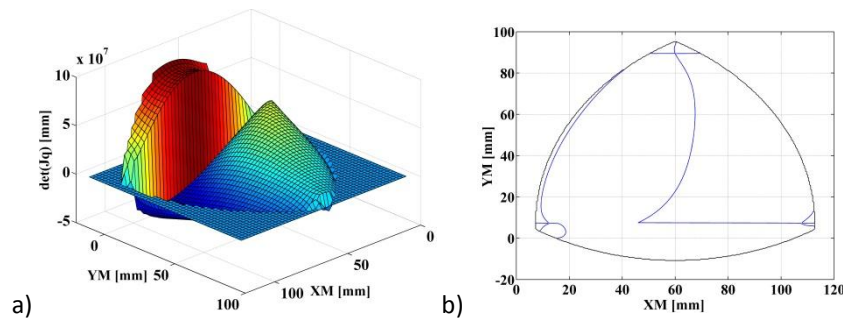
Fig. 3.2.5. Analysis of the singularities of second type for the planar 3-R(RPRGR)RR manipulator in 3D (a) and 2D (b) representation

Fig. 3.2.4 and Fig. 3.2.5 shows the singularities analysis by exploring the plane for the characteristic coordinates of the TC $x_M \in [0, 110]$ and $y_M \in [-10, 100]$, with a constant rotation angle of the mobile platform $\alpha = 30°$.

The absence of zero values for the partial derivatives (3.2.29) of each parallel connected actuating kinematic chain (Fig.3.2.4) shows that the 3-R(R$\underline{P}$RGR)RR structure avoids the singularities of first type in the considered (large) range.

Fig. 3.2.5 shows the second type singularities of the 3-R(R$\underline{P}$RGR)RR manipulator in the workspace, which does not depend on the geared linkage actuating chains. The results are identical with other studies about planar 3-R$\underline{R}$R manipulator [17].

3.2.4.2. Design of the a parallel manipulator 3-R(RPRGR)RR

The second example shows the design of a parallel manipulator 3-R(RPRGR)RR with real values using an linear actuator with the maximum stoke of 140 mm. The geometrical parameters of the parallel manipulator (s. Tab. 3.2.2) are chosen as previous in order to reduce the singularities and to achieve a large oscillating angle of the actuating elements 2, 2´ and 2´´.

Tab. 3.2.2. Geometric parameters of the parallel manipulator

Frame platform length (0)	$l_0 = 1039{,}23\,\text{mm}$	Carrier length (6)	$l_6 = 80.00\,\text{mm}$
Mobile platform length (3)	$l_3 = 294.44\,\text{mm}$	Gear ratio	$\rho = 2.6$
Chain link length (1,1´,1´´)	$l_1 = 512.00\,\text{mm}$	Initial stroke	$s_0 = 452.00\,\text{mm}$
Chain link length (2,2´,2´´)	$l_2 = 400.00\,\text{mm}$	Stroke	$h = 120\,\text{mm}$
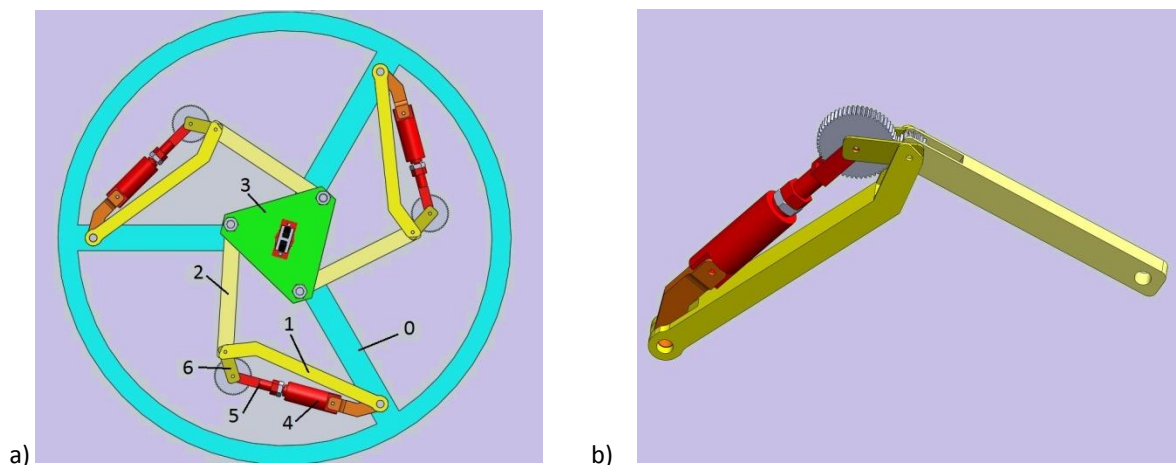
Fig. 3.2.6. Design of the planar parallel manipulator 3-R(RPRGR)RR

Fig. 3.2.6.a shows a bottom view of the planar parallel manipulator CAD design and Fig. 3.2.6.b a detail of the geared linkages with linear actuation.

3.2.4.3. Transmission function of the geared linkages as connecting chain

The transmission function of the geared linkage with linear actuation was computed using the relationships (3.2.5) - (3.2.8) and it is shown in Fig. 3.2.7.a. The linear actuator stroke was limited in the range $s = [20,140]$ mm in order to obtain a range with approximately constant transmission ratio. Through the limitation of the stroke, the oscillating angle is limited to $\Delta\chi_i = 360°$. The rotation motion of the output element for the forward stroke is orientated in clockwise direction.
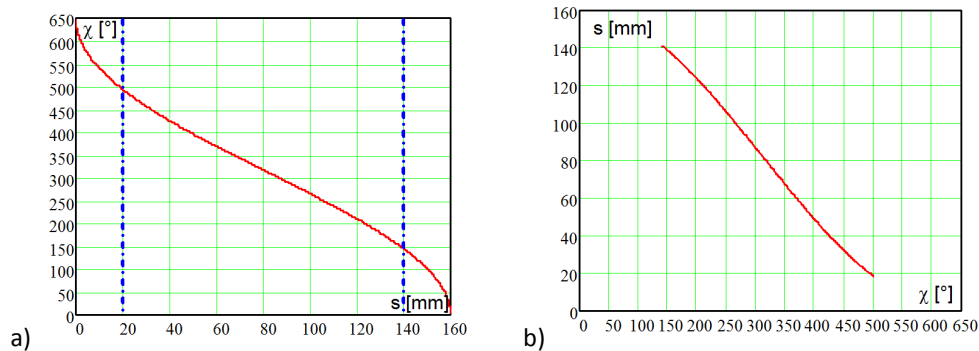
Fig. 3.2.7. Transmission function and Interpolated inverse transmission function of the geared linkage

Because the difficulties to solve on analytical way the inverse transmission function of the geared linkages it was computed an interpolation function based on the numerical values of the transmission function. The interpolated inverse transmission function in the mentioned range is shown in Fig. 3.2.7.b, where the interpolation nodes for the Lagrange function (3.2.20) were chosen as follow:

$$
\begin{aligned}
(s_i)_1 &= 20\,\text{mm} &\rightarrow\quad (\chi_i)_1 &= 493.5° \\
(s_i)_2 &= 40\,\text{mm} &\rightarrow\quad (\chi_i)_2 &= 425.2° \\
(s_i)_3 &= 120\,\text{mm} &\rightarrow\quad (\chi_i)_1 &= 210.3° \\
(s_i)_1 &= 140\,\text{mm} &\rightarrow\quad (\chi_i)_1 &= 144.9°
\end{aligned}
\tag{3.2.34}
$$

3.2.4.4. Kinematic analysis of the manipulator for translation along the x_0-axis

Considering the translation motion along the x_0-axis between the initial position (x_i, y_i) and the final position (x_f, y_f) is necessary to parameterize it in the form:

$$
x_M(t) = x_i + (x_f - x_i)\cdot t,\; y_M(t) = k,\; \alpha(t) = 0.
\tag{3.2.35}
$$

The considered values for the example of translation along the x-axis are given in Tab. 3.2.3.

Tab. 3.2.3 Motion parameters by translation along the x-axis

Initial coordinate on x-axis	$x_i = 100.00\,\text{mm}$
Initial coordinate on y-axis	$y_i = 300.00\,\text{mm}$
Initial orientation angle	$\alpha_i = 0.00\,°$
Final coordinate on x-axis	$x_f = 900.00\,\text{mm}$
Final coordinate on y-axis	$y_f = 300.00\,\text{mm}$
Final orientation angle	$\alpha_f = 0.00°$

In Fig. 3.2.8 are represented the variation of the generalized coordinates $\theta_{1i}(t)$ and $\theta_{2i}(t)$ of the chain links (1) and (2), the actuator strokes s_i and motion of the mobile platform between the initial and final positions.
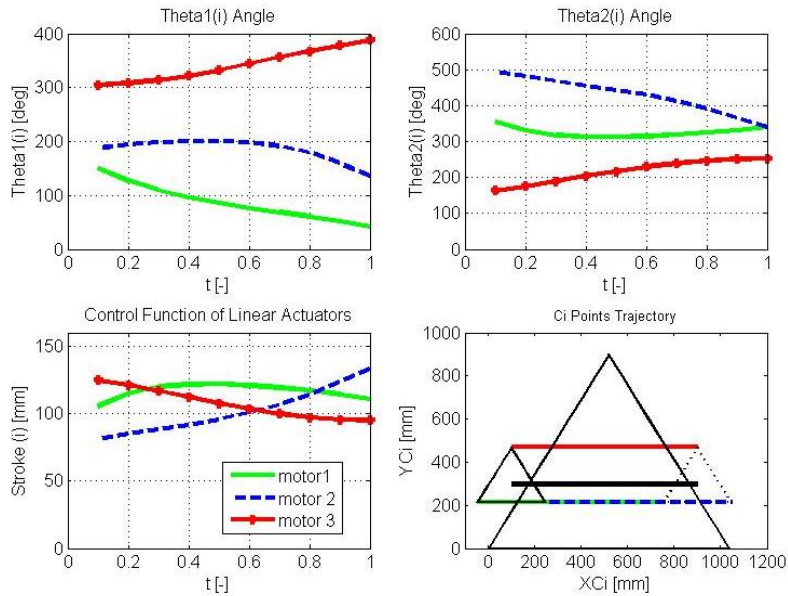
Fig. 3.2.8. Generalized coordinates of the connection chain links, strokes of the linear actuators and the motion of the parallel manipulator mobile platform, for the translation along the x-axis

The continuous line (green) shows the parameters of the chain - 1, the dashed line (blue) the parameters of the chain - 2 and the dotted line the parameters of the chain – 3.

3.2.4.5. Kinematic analysis of the manipulator for translation along the y_0-axis

The parameterization of the translation motion along the y_0-axis between the initial position (x_i, y_i) and the final position (x_f, y_f) follows in form:

$$x_M(t) = k, \ y_M(t) = y_i + (y_f - y_i) \cdot t, \ \alpha(t) = 0. \tag{3.2.36}$$
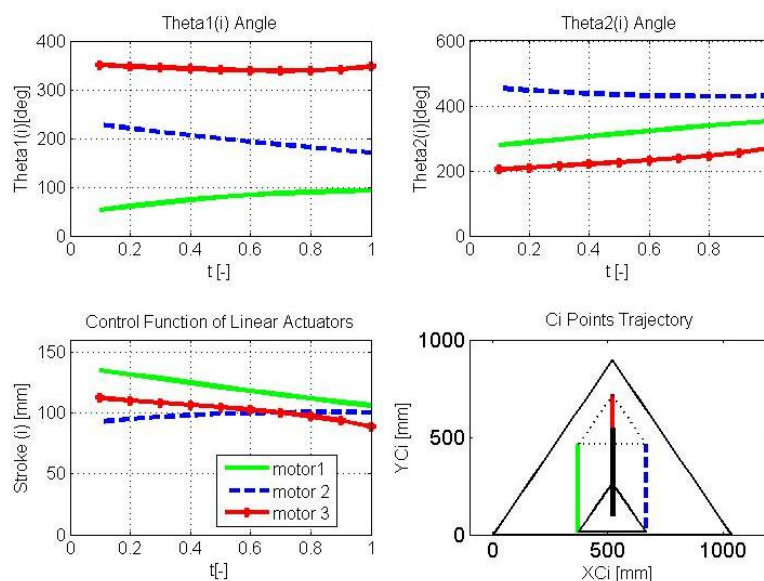
Fig. 3.2.9. Generalized coordinates of the connection chain links, strokes of the linear actuators and the motion of the parallel manipulator mobile platform, for the translation along the y-axis

The variation of the generalized coordinates $\theta_{1i}(t)$ and $\theta_{2i}(t)$ of the connection chain links (1) and (2), the strokes s_i of the linear actuators and the motion of the mobile platform between the initial and final positions along the y-axis are drawn in Fig. 3.2.9. The considered values for the example are given in Table 3.2.4.

Tab. 3.2.4 Motion parameters by translation along the y-axis

Initial coordinate on x-axis	$x_i = 519.50\,mm$
Initial coordinate on y-axis	$y_i = 100.00\,mm$
Initial orientation angle	$\alpha_i = 0.00\,°$
Final coordinate on x-axis	$x_f = 519.50\,mm$
Final coordinate on y-axis	$y_f = 600.00\,mm$
Final orientation angle	$\alpha_f = 0.00°$

3.2.4.6. Kinematic analysis of the manipulator for rotation around z-axis

The parameterization of the rotation around the z-axis in a given position $(x_i = x_f, y_i = y_f)$ from an initial orientation α_i to a final orientation α_i can be formulated as:

$$x_M(t) = p, \quad y_M(t) = q, \quad \alpha(t) = \alpha_i + (\alpha_f - \alpha_i) \cdot t. \tag{3.2.37}$$

Also the variations of the generalized coordinates $\theta_{1i}(t)$ and $\theta_{2i}(t)$, the strokes s_i of the linear actuators and the rotation of the mobile platform between the initial and final orientation around the z-axis are plotted in Fig. 3.2.10. The considered values for the example of rotation around z-axis are given in Table 3.2.5.
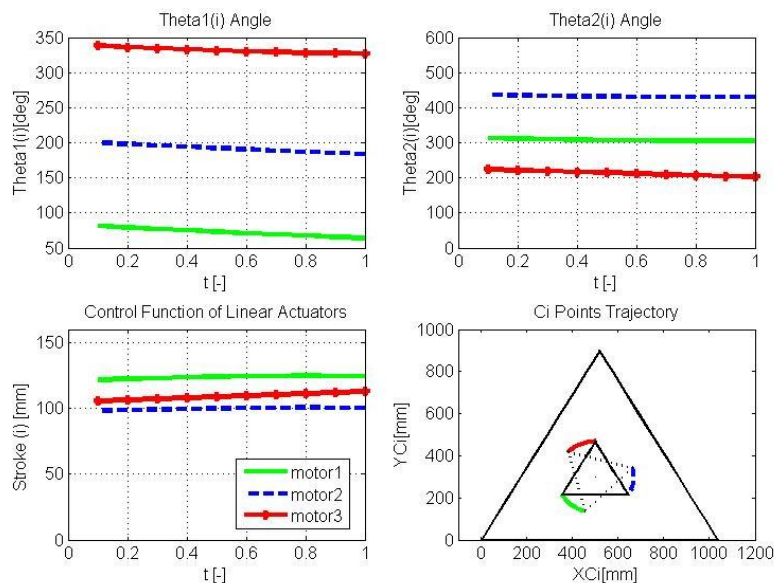
Fig. 3.2.10. Generalized coordinates of the connection chain links, strokes of the linear actuators and the motion of the mobile platform of the parallel manipulator for the rotation around z-axis

Tab. 3.2.5 Motion parameters by rotation around z-axis

Initial coordinate on x-axis	$x_i = 500.00\,mm$
Initial coordinate on y-axis	$y_i = 300.00\,mm$
Initial orientation angle	$\alpha_i = 0.00\,°$
Final coordinate on x-axis	$x_i = 500.00\,mm$
Final coordinate on y-axis	$y_i = 300.00\,mm$
Final orientation angle	$\alpha_f = 50.00°$

3.2.4.7. Kinematic analysis of the manipulator for combined motion in the reference system

Considering a combined motion in the reference system OX_0Y_0, it is necessary to parameterize the motion between the initial position (x_i, y_i) and the final position (x_f, y_f) considering a proportional orientation of the mobile platform along the movement in the form:

$$x_M(t) = x_i + (x_f - x_i) \cdot t,$$
$$y_M(t) = x_i + (x_f - x_i) \cdot t, \qquad\qquad (3.2.38)$$
$$\alpha(t) = \alpha_i + (\alpha_f - \alpha_i) \cdot t.$$

In the Fig. 3.2.11 are represented the variation of the generalized coordinates $\theta_{1i}(t)$ and $\theta_{2i}(t)$ of the chain links (1) and (2), the actuator strokes s_i and motion of the mobile platform between the initial and final positions. The considered values for the example of combined motion are given in the Tab.3.2.6.
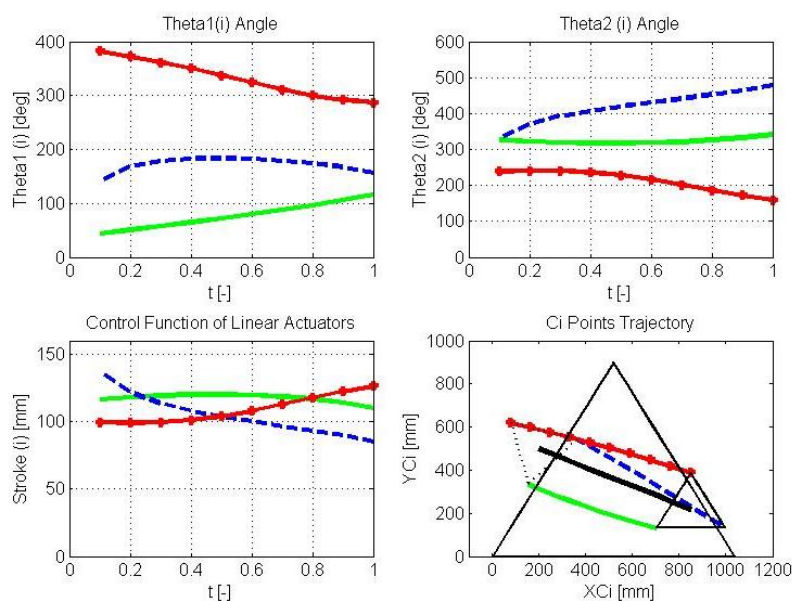
Fig. 3.2.11. Generalized coordinates of the connection chain links, strokes of the linear actuators and the motion of the mobile platform of the parallel manipulator for combined motion in the reference system

Tab.3.2.6. Motion parameters by combined motion in the reference system

Initial coordinate on x-axis	$x_i = 850.00\,\text{mm}$
Initial coordinate on y-axis	$y_i = 220.00\,\text{mm}$
Initial orientation angle	$\alpha_i = 0.00\,°$
Final coordinate on x-axis	$x_i = 200.00\,\text{mm}$
Final coordinate on y-axis	$y_i = 500.00\,\text{mm}$
Final orientation angle	$\alpha_f = 50.00°$

3.2.4.8. CAD simulation of the manipulator for combined motion in the reference system

The results of the computing MatLab program regarding the geometrical parameters of the parallel manipulator were validated with the simulation results of the CAD model previous presented. In the Fig. 3.2.12 are represented the mobile platform in the initial and final considered positions of combined motion.

The simulation results regarding the generalized coordinates $\theta_{1i}(t)$ and $\theta_{2i}(t)$ of the all chains for the links (1) and (2) are represented in Fig. 3.2.13.
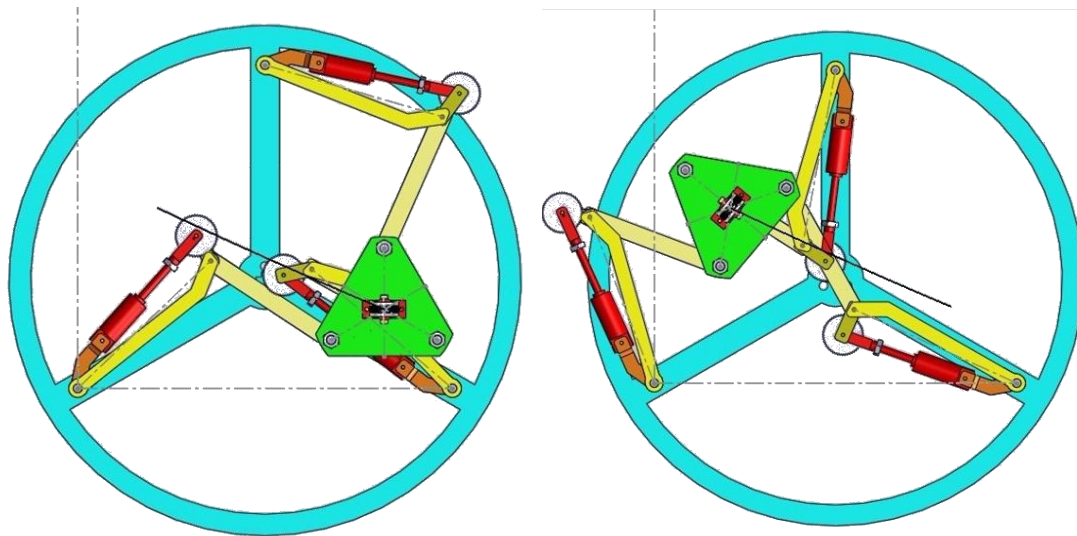
Fig. 3.2.12. CAD model of the parallel manipulator in the initial (a) and final (b) position

a)   b)
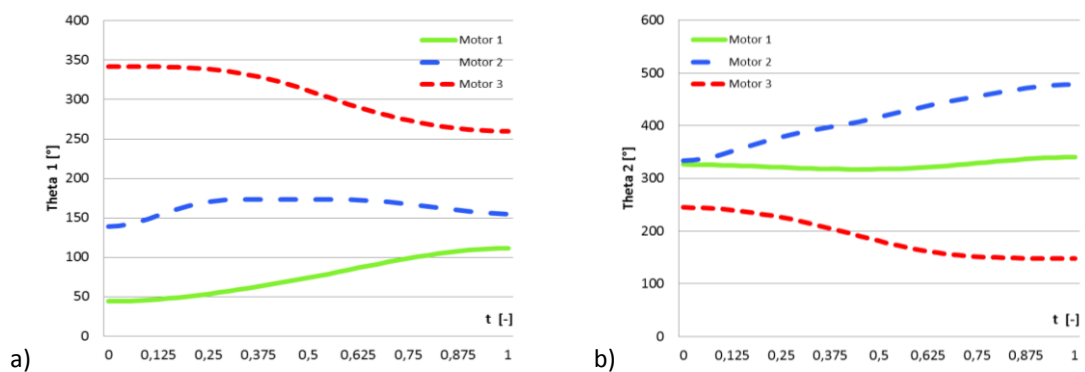
Fig. 3.2.13. Generalized coordinates $\theta_{1i}(t)$ and $\theta_{2i}(t)$ of the connection chain links (1) and (2), of the parallel manipulator mobile platform for the combined motion in the reference system

The simulation results regarding the strokes of the linear actuators of the planar parallel manipulator are plotted in Fig. 3.2.14.
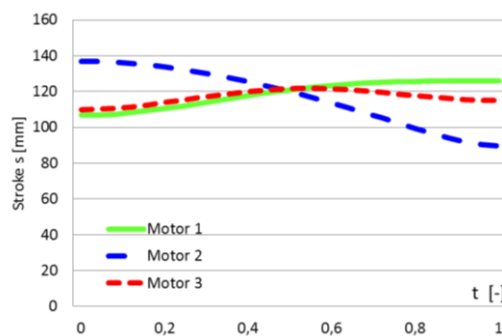
Fig. 3.2.14. The parallel manipulator strokes of the linear actuators $s_i(t)$ for the combined motion in the reference system

3.2.5. Scientific contributions

The research proposes an original solution of a planar parallel manipulator 3-R(RPRGR)RR, which uses a parallel connected geared linkage with linear actuation.

The kinematic chain implements geared linkages actuated with an electrical linear actuator beside binary elements and rotation joints. The extension of the rotation and its forward/backward sense is controlled by means of a geared linkage with inverted slider crank basic structure.

The analysis of the singularities of this manipulator shows that the geared linkages with linear actuation allow the avoiding of singularities of the first type by choosing of optimal initial stroke and working stroke.

Some major advantages of this novel type of planar parallel manipulator are indicated. So, the used mechanism allows a large rotation angle, is light weighted for a simple and sturdy construction. The linear transmission function can be achieved by means of a fairly simple and reliable system. The using of linear actuators with screw-nut fulfills the self-locking condition and ensures a high transmission ratio without needing a gear box.

The output data of the kinematic analysis program were compared and validated with the simulation results of a CAD model, increasing the reliability of the results. A special regard was focused on the singularity linkages position and on two possible solutions of chains position for the same Cartesian coordinates of characteristic point.

There were identified small differences between the control functions of linear motors, even if the angles values of the two links ($\theta_{1i}(t)$ and $\theta_{2i}(t)$) are the same in both models (CAD and mathematical computing with Matlab). This is due to the designing process of parallel manipulator elements and the initial position of the stroke in initial position.

3.3. Mechanical design solutions for fishing reel spool mechanisms

3.3.1. State-of-art

The companies which produce reels use different types of simple or complex mechanisms including gears, cams and linkages. There are solutions, which accept the continuous variation of the linear velocity and try to compensate the out coming drawbacks by an asymmetrical design of the spool. The mechanism associated to this concept is quite simple, consisting of two elliptical gears and a bevel gear, as conceived by Leroux in [21].

Most mechanisms used in fishing reel construction include gears (spur, bevel and/or elliptical) and a special scotch-yoke mechanism, to which a stud moves along a shaped guiding groove in the yoke. Such a solution was patented by Bancroft in patent [185]. Most designers provide a shape of the yoke groove roughly resembling with the letter „S", which is very important for the output transmission function. A quasi-linear transmission function was obtained by Jeong with the solution described in the patent [103]. Beside the irregular deviations from the linear shape of the transmission function, a major disadvantage of the solution is the abrupt endings of the motion curve, which means there are high acceleration and deceleration around the end points of the strokes. A slight improvement on transmission function shape was obtained at Okuma Fishing Tackle [125] by tilting the guide groove. A different original solution featuring specific design of the „S" guide slot were described by Baumgartner in [58]. In order to avoid the drawbacks of the solutions above, a solution with fixed spool and additional device to compensate line storage at the margins of the spool was proposed by Zanon in [71]. This concept assumes a complex mechanism, involving many parts.

On the market there are also reels with mechanisms based on cylindrical cams, as proposed by Sugahara in patent [207]. The long size of the cam and the accompanying extra-set of precise mechanical parts is a disadvantage, which is not compensated by a very good shape of the transmission function. In order to avoid end effects, Nilsen proposes in [104] a double speed fishing reel, producing a high speed operation and a low speed operation, respectively. The construction is very complex, including a very large number of mobile or fixed parts.

Some solutions proposed by Crawford and Ryall in [169], [64] are based on simple mechanisms of actuation and additional systems to control the dragging of the line. A mechanical system based on a finger lever was patented by Miller in [34], which guides the line. It is an additional assembly to the actuation system based on a bevel gear. Some reel mechanisms integrate assemblies [115], which provide supplemental information, such as the estimate weight of the fish.

3.3.2. Aim of the theoretical and experimental research

The aim of the theoretical and experimental research was to study the existing mechanical solutions or finding of new solution for the axial movement of the spool, in order to provide constant speed in a large range of the movement. The novel solution was also manufactured, tested and patented.
The theoretical and experimental results of the research were published by the author in the papers [140] and [247].

3.3.3. Theoretical and experimental contributions

Reels attached to fishing rods should perform the unwinding of the line when the bait, the weight and the hook are cast toward the water and the winding of the line onto the spool, when the line is

removed from the water. Ideally, the speed of the axial movement of the spool should be constant, in both directions, so that the line would wind and unwind uniformly by rotating of the line guide onto the spool. Large deviations to provide a constant speed of the axial movement of the spool cause two negative effects. When casting the line, the effect of clinging occurs and at removal of line and bulges form at both ends of the spool (Fig. 3.3.1). The bigger the spool is the more obvious the effects show. In practice, long lines are desirable for efficient fishing, so that the spool should be long and thick.

a)   b)
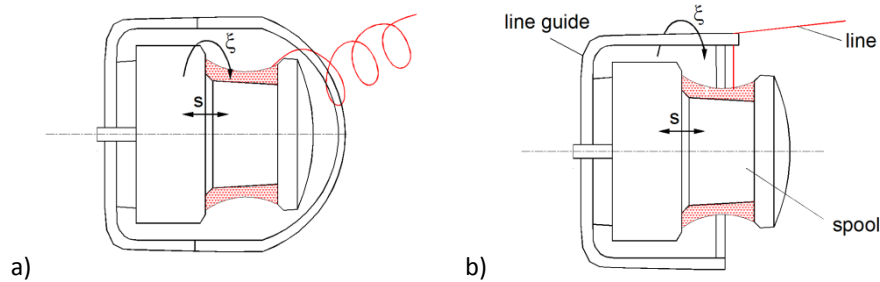
Fig. 3.3.1. Forming of bulges at both ends of the spool

From mechanism point of view, the crank rotated manually drives the mechanism, which must rotate and translate reversible the spool of the reel at constant speed. The movement of the spool is a long translation. Kinematical, it is necessary to transform a rotation with constant angular velocity into a reversible translation movement combined with a rotation movement. Along with the linear stroke, the rotation movement should follow with a constant transmission ratio.

Based on the previous description, the research was based on the following requirements for the fishing reel spool mechanism:

 - the input link of the reel spool mechanism is a crank, which rotates with constant angular velocity. The angle is denoted φ;
 - the output element is the spool, which moves reversibly along a linear direction with the stroke s;
 - the line guide is also rotated onto the spool, with correlated angular velocity to the crank´s one;
 - the desired transmission function generated by the reel spool mechanism should be a straight line - curve one.

The desired transmission function should contain four curved arches with imposed linear section and boundary conditions. Fig. 3.3.2 illustrates the desired transmission function of the spool for a complete input rotation of the crank.
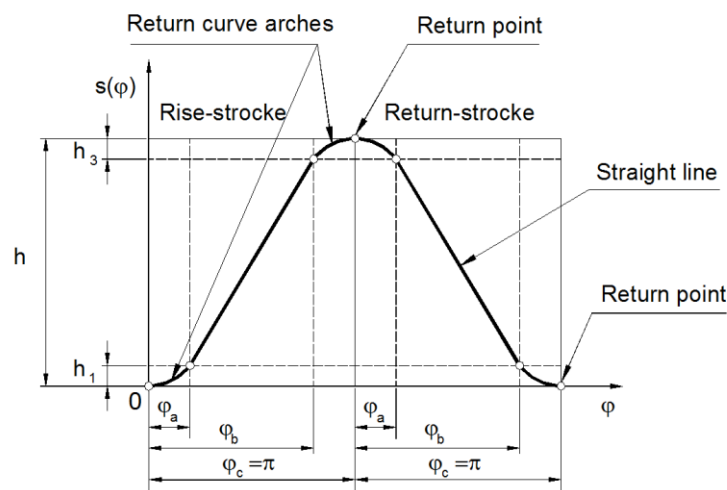
Fig. 3.3.2. The transmission function of the spool

The drawing emphasizes the four arches denoted φ_a, φ_c-φ_b and π+φ_a, π+φ_c-φ_b respectively, corresponding to the beginning of (un)winding along the stroke h_1 and the ending of (un)winding along the stroke h_3 of the spool. The transmission function of the spool is symmetrically shaped. The first half corresponds to the rise-stroke and half of the input rotation (φ_c=180°) and contains a middle linear segment and two curved arches.

The mathematical form of the transmission function of the spool movement is given in the following relationships [67]:

$$s(\varphi)=\begin{cases} h_1\left\{1-\cos\dfrac{\pi\cdot\varphi}{2\cdot\varphi_a}\right\}, & 0\leq\varphi<\varphi_a; \\[2mm] h_1+\dfrac{h-2h_1}{\pi-2\varphi_a}(\varphi-\varphi_a), & \varphi_a\leq\varphi<\varphi_b; \\[2mm] h-h_1\left\{1-\cos\dfrac{\pi\cdot(\varphi-\pi)}{2\varphi_a}\right\}, & \varphi_b\leq\varphi<\varphi_c; \\[2mm] h-h_1\left\{1-\cos\dfrac{\pi\cdot(\varphi-\pi)}{2\varphi_a}\right\}, & \pi\leq\varphi<\pi+\varphi_a; \\[2mm] h-h_1+\dfrac{2h_1-h}{\pi-2\varphi_a}(\varphi-\pi-\varphi_a), & \pi+\varphi_a\leq\varphi<\pi+\varphi_b; \\[2mm] h_1\left\{1-\cos\dfrac{\pi\cdot(\varphi-2\pi)}{2\cdot\varphi_a}\right\}, & \pi+\varphi_b\leq\varphi\leq\pi+\varphi_c; \end{cases}$$
(3.3.1)

with:

$$h_1=h_3=h\frac{2\cdot\varphi_a}{\pi^2-2\cdot(\pi-2)\varphi_a},$$
(3.3.2)

$$\varphi_a=\varphi_c-\varphi_b.$$
(3.3.3)

The return points refer to changing of sliding sense, which takes place twice during a complete input rotation. The criteria for selecting an optimal novel design solution for the fishing reel spool mechanism must contain the following analytical conditions [79]:

- the transmission function should have a minimal average deviation from the desired TF along the whole rotation of the crank:

$$\Delta s_a=\frac{\int_0^{2\pi}\left|s_a(\varphi)-s(\varphi)\right|d\varphi}{2\pi},$$
(3.3.4)

where: $s_a(\varphi)$ is the achieved the transmission function of the spool mechanism and $\Delta s(\varphi)=s_a(\varphi)-s(\varphi)$ - the current deviation of the transmission function;

- the curved arches of the transmission function s(φ) must be designed so that the jerk at the return points should be avoided;

$$s'(0)=0,\quad s'(\pi)=0,\quad s'(2\pi)=0;$$
(3.3.5)

- the mechanism is supposed to contain a minimum number of parts n;

$$n\rightarrow\min;$$
(3.3.6)

- the required workspace of the mechanism along the translation direction is limited. A compact construction is desirable, which is characterized by the relationships:

$$c_x=\dim x(\text{workspace})_{s\in[0,h]},\qquad c_y=\dim y(\text{workspace})_{s\in[0,h]}.$$
(3.3.7)

3.3.3.1. Mechanism solution for the fishing reel spool motion

The structural analysis provided a lot of solutions of mechanisms, which transform the rotation motion of the driving element into reciprocating motion of the driven element with a straight line – return curve arches function [35].
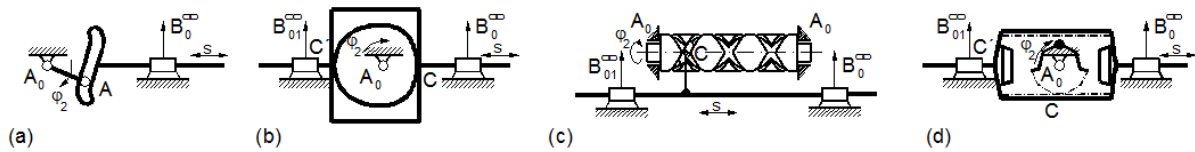
Fig. 3.3.3. Basic mechanism structures suitable for the spool mechanism
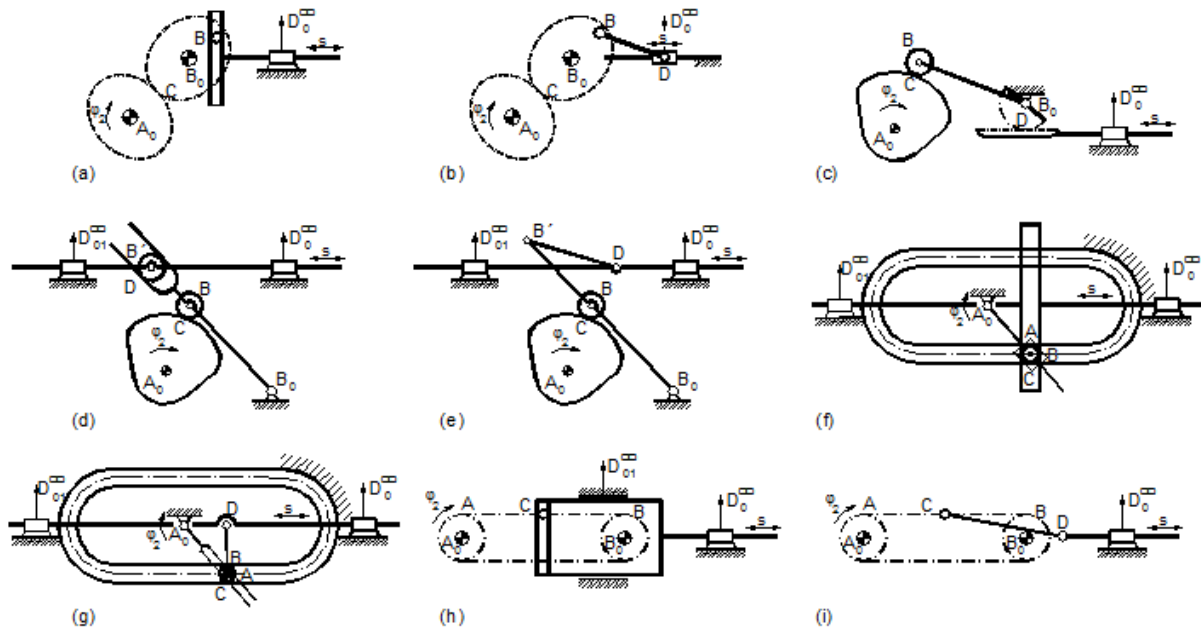
Fig. 3.3.4. Combined mechanism structures suitable for the spool mechanism

Fig. 3.3.3 and Fig. 3.3.4 shows a systematic overview of the mechanism structures, which are grouped into two large categories: basic and combined mechanisms.

The category of basic mechanisms contains:

(1) scotch-yoke with "S" profiled yoke (Fig. 3.3.4.a);

(2) cam mechanism with constant width and double flat faced follower (Fig. 3.3.4.b);

(3) cylindrical cam mechanism with translating follower (Fig. 3.3.4.c);

(4) gear mechanism with geared sector and double symmetrical rack (Fig. 3.3.4.d).

The category of combined mechanisms contains:

(1) noncircular gear mechanism in series with a scotch-yoke (Fig. 3.3.5.a);

(2) noncircular gears mechanism in series with a slider - crank (Fig. 3.3.5.b);

(3) cam mechanism with oscillating roller follower in series with a gear and
    rack sector pair (Fig. 3.3.5.c);

(4) cam mechanism with oscillating roller follower in series with an inverted
    slider - crank (Fig. 3.3.5.d);

(5) cam mechanism with oscillating roller follower in series with a slider - crank (Fig. 3.3.5.e);

(6) scotch-yoke with variable crank length (Fig. 3.3.5.f);

(7) slider-crank with variable crank length (Fig. 3.3.5.g);

(8) scotch-yoke driven by a belt mechanism (Fig. 3.3.5.h);

(9) slider-crank driven by a belt mechanism (Fig. 3.3.5.i).

3.3.3.2. Synthesis of some fishing reel spool mechanism

In order to find an optimal solution for the spool mechanism with the above described requirements the mechanisms' synthesis was achieved. The numerical input data for the synthesis of several mechanisms is given in Table 3.3.1.

Tab. 3.3.1. Input numerical data for the reel spool mechanism

Mechanism parameters	Values
Stroke	$h = 17 \, mm$
Reference center distance	$a = 20 \, mm$
Stud mounting radius	$r_{SB} = 8.5 \, mm$
Gear transmission ratio	$i_{01} = 3$
Up-stroke angle	$\varphi_c = 180°$
Return-stroke angle	$\varphi_c = 180° \, 180°$
Curved arches angle	$\varphi_a = 45°$

Between the fishing reel crank and the input gear of the spool mechanism, which transforms the rotation motion in a rectilinear translation, a gear train with the ratio i_{01} is connected:

$$i_{01} = d\varphi / d\varphi_2 \, .$$

(3.3.8)

Because the gear ratio has a constant value, the shape of the TF is identical with relationship given in (3.3.1), where the rotation angle is φ_2 and it belongs within the range $\varphi_2 \in [0, 2\pi]$.

a.   Scotch-yoke with "S" shaped yoke

The scotch-yoke with "S" shaped yoke (modified) is a usual solution for the spool mechanism [103], which allows the achievement of the transmission function approximately, over some ranges of the angle φ_2.
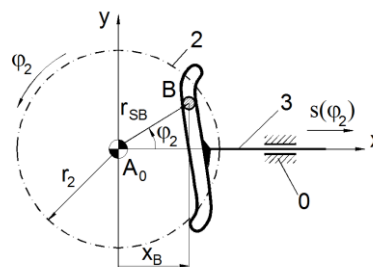
Fig. 3.3.5. Kinematic schema of the scotch-yoke with "S" shaped yoke

The equation for the synthesis of the scotch-yoke with "S" shaped yoke (s. Fig. 3.3.5) give the profile coordinates (u,v) of the "S" shaped yoke:

$$u(\varphi_2) = r_{SB} \cdot \cos\varphi_2 + s(\varphi_2) \, ,$$
$$v(\varphi_2) = r_{SB} \cdot \sin\varphi_2 \, .$$

(3.3.9)

The complete profile of the shaped yoke has a vertical elongate "∞" form, which have guiding problems for the stud because the crossed profiles. In praxis is used only a half of the resulted yoke shape profile. Fig. 3.3.6 shows the pitch curve of the theoretical "S" profile of the yoke over the ranges $\varphi_2 \in [\pi/2, \pi] \cup [3\pi/2, 2\pi]$ with r2 = 11 [mm] with a stud radius of r = 2 [mm].

The theoretical achieved transmission function with the spool mechanism with "S" shaped yoke, considering only a half of the resulted pitch curve reproduces approximately the desired

transmission function. The desired and computed transmission function respectively the deviation Δs to the desired transmission function are shown in Fig. 3.3.7.
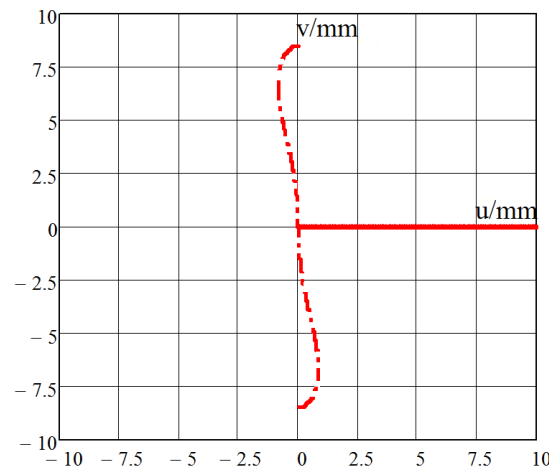
Fig. 3.3.6. Pitch curve of the scotch-yoke with "S" profiled yoke
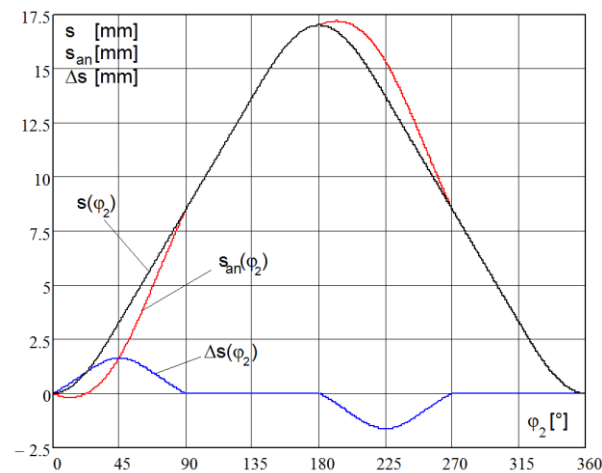
Fig. 3.3.7. Deviation of the transmission function of the scotch-yoke with "S" profiled yoke

The scotch-yoke with "S" shaped yoke is a simple and compact mechanism solution, but fulfills the imposed transmission function only approximately in some ranges.

    b.   Cam mechanism with constant width and double flat faced follower

The cam mechanism with constant width and double flat faced follower is represented in the kinematic schema in Fig. 3.3.8. This mechanism achieves the transmission function through a proper synthesis of the cam profile.
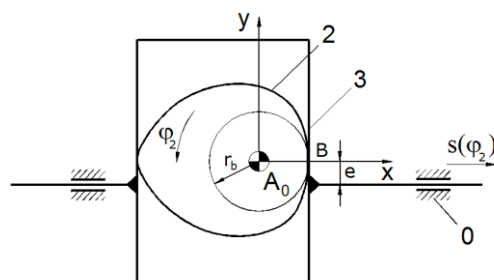
Fig. 3.3.8. Kinematic schema of the cam mechanism with constant width and double flat faced follower

Synthesis computations input data are: e = 0 [mm]; r_b = 3 [mm]. The cam profile of the cam mechanism with constant width and double flat faced follower is computed with the relationships [63], [50]:

$$x_B(\varphi_2) = [r_b + s(\varphi_2)]\sin\varphi_2 + s'(\varphi_2)\cos\varphi_2 ,$$
$$y_B(\varphi_2) = [r_b + s(\varphi_2)]\cos\varphi_2 + s'(\varphi_2)\sin\varphi_2 ,$$

(3.3.10)

with:

$$s'(\varphi_2) = \partial s(\varphi_2)/\partial\varphi_2 .$$

(3.3.11)

The resulting cam profile after the synthesis approach is shown in Fig. 3.3.9.
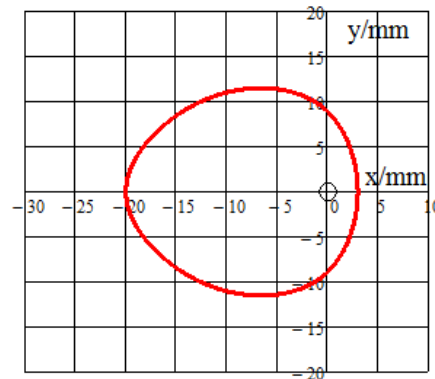
Fig. 3.3.9. Cam profile of the cam mechanism with constant width and double flat faced follower

The transmission function and its deviation Δs achieved with the spool mechanism using a cam mechanism with constant width and double flat faced follower is drawn in Fig. 3.3.10.
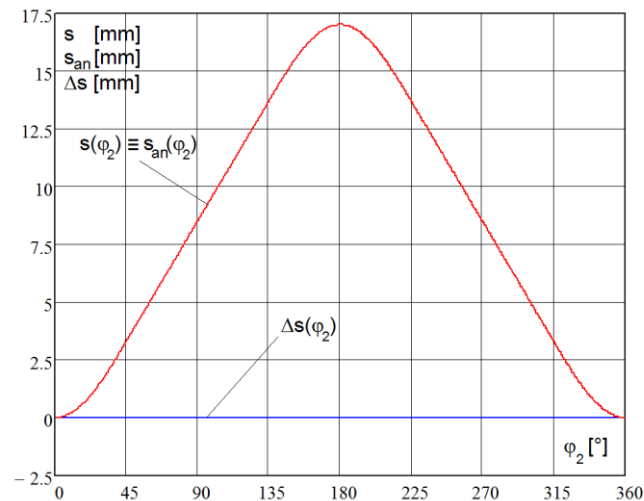
Fig. 3.3.10. Deviation of the transmission function of the cam mechanism
with constant width and double flat faced follower

In order to obtain a cam profile without singularities, the cam mechanism size is larger with the double of base circle radius r_b than the double stud mounting radius r_{SB} and thus the cam mechanism (Fig. 3.3.8) workspace is more than twice larger than the scotch-yoke mechanism (Fig. 3.3.5). It is possible to use also a cam mechanism with translating roller follower, but in this case the cam profile has a concave interval and the size of the cam needs to be slightly increased.

c. Gear mechanism with geared sector and double symmetrical rack

This mechanism structure uses a geared sector and double symmetrical racks. For the smooth return of the driven element a yoke is used. The stud is fixed with the driving geared sector 2 and moves

along an open grooved cam profile at both return points of the driven element 3 containing the grooved cam profile (Fig. 3.3.11).
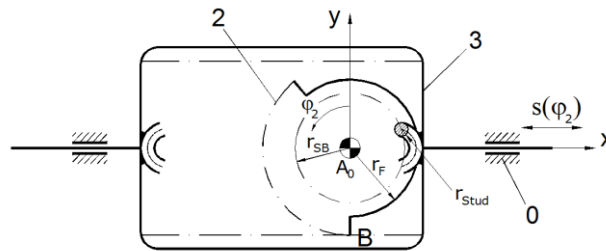
Fig. 3.3.11. Kinematic schema of the gear mechanism with geared sector and double symmetrical rack

To achieve the imposed stroke of the driven element the mounting radius of the stud was chosen r_{Stud}=0.5 [mm].
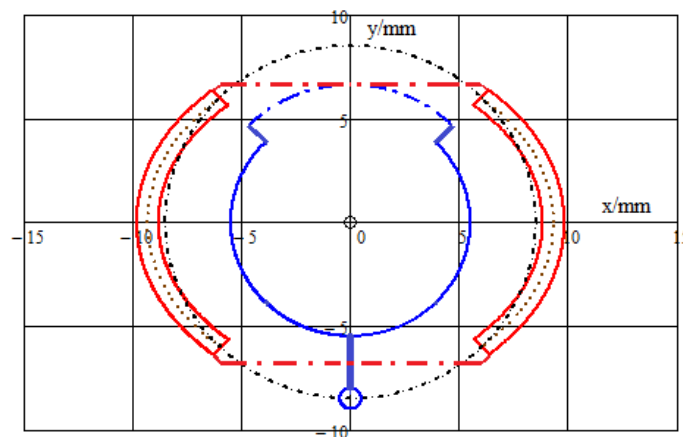
Fig. 3.3.12. Grooved cam profiles and geared sector with double simmetrically rack

The angular position of the stud is symmetrically opposite to the gear sector, as shown in Fig. 3.3.12. For synthesis of the return curve arches one uses the transmission function given by the relationship (3.3.1) over the return intervals. The transmission function of the gear mechanism with geared sector and double symmetrical rack looks identical with the previous mechanism (Fig. 3.3.10).

The gear mechanism with geared sector and double symmetrical rack is a compact mechanism solution, but uses grooved cam profiles at the beginning and the end of the return movement of the driven element to avoid the jerk [222], [238]. The manufacturing of the yoke with the double symmetrical rack and the open grooved cam profiles needs higher costs and special technological machines.

d.   Noncircular gear mechanism in series with a scotch-yoke

The mechanism with noncircular gears in series with a classical scotch-yoke transmits the nonlinear motion of the noncircular gear train by means of a stud, which is fixed into the output noncircular gear to a linear grooved yoke. Thus, the uniform rotation of the driving element 2 turns into a translation of the slider, obeying a transmission function $s(\varphi_2)$. The stud fixed on the noncircular gear 3 performs the nonlinear motion $\varphi_3(\varphi_2)$, depending on the variable transmission ratio of the noncircular gears [79], [85].

The synthesis of the mechanism represented in the kinematic schema in Fig. 3.3.13 is developed on the basis of the ratio between the sliding $s(\varphi_2)$ and the current position radius of the stud, r_{SB} given by the cosine of the angle $\varphi_3(\varphi_2)$, with the relationship:

$$\varphi_3(\varphi_2) = \arccos\left[\frac{s(\varphi_2)}{r_{SB}}\right]. \tag{3.3.12}$$
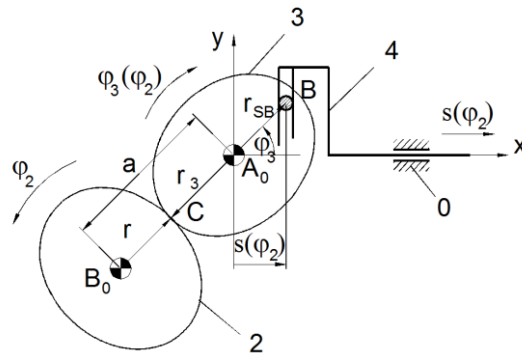
Fig. 3.3.13. Kinematic schema of the noncircular gears mechanism in series with a scotch-yoke

The rotation angle $\varphi_3(\varphi_2)$ depends on the variable transmission ratio of the noncircular gear. Accepting on constructive basis the reference center distance a follow relationships for computing the reference pitch curves radii of the noncircular gears r_2 and r_3, which use the center distance and transmission ratio relationships, in the form:

$$r_3(\varphi_2) = \frac{a}{1+\varphi_3'(\varphi_2)}, \qquad r_2(\varphi_2) = a - r_3(\varphi_2). \tag{3.3.14}$$
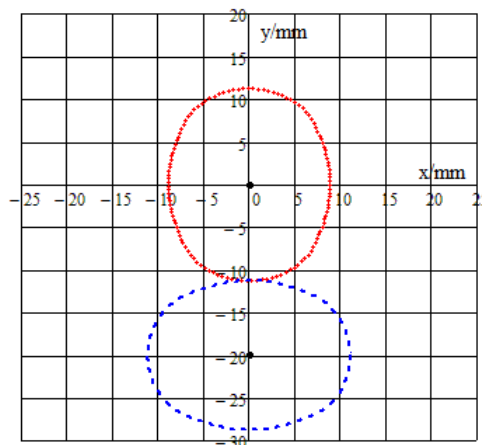
Fig. 3.3.14. Pitch curves of the noncircular gear mechanism in series with a scotch-yoke

The additional data used for the mechanism synthesis are the positions of the noncircular gears center axis: $A_0(0,0)$; $B_0(0,-20)$. The resulting profiles of the noncircular gears can be shown in Fig. 3.3.14. The achieved transmission function upon a full cycle is identical with the desired transmission function and is represented in Fig. 3.3.10.

This mechanism solution allows the achievement of the imposed transmission function, but increases the transversal dimension of the workspace of the mechanism (A_0y) and slightly dimension of the workspace along the translation direction (A_0x). Also a disadvantage is the use of an additional element.

e. Slider-crank with variable crank length

The mechanism uses as crank a slider which guides a double roller along the slider straight line and a fixed cam profile (s. Fig. 3.3.15). The design allows getting a variable crank length, where the variable

crank is the driving element [206]. Usually the cam is a grooved cam, which profile allows obtaining of the imposed transmission function (3.3.1). In order to compute the cam profile it is necessary to establish the synthesis equation. According to the vector equation written in complex numbers follows the variable crank length as:

$$l_2(\varphi_2)=[s_0-s(\varphi_2)]\cdot\cos\varphi_2-\sqrt{l_3^2-[s_0-s(\varphi_2)]^2\sin^2\varphi_2} \ . \qquad (3.3.15)$$

The pitch curve coordinates of the cam are:

$$x(\varphi_2) = l_2(\varphi_2)\cdot\cos\varphi_2 \ , \quad y(\varphi_2) = l_2(\varphi_2)\cdot\sin\varphi_2 \ . \qquad (3.3.16)$$
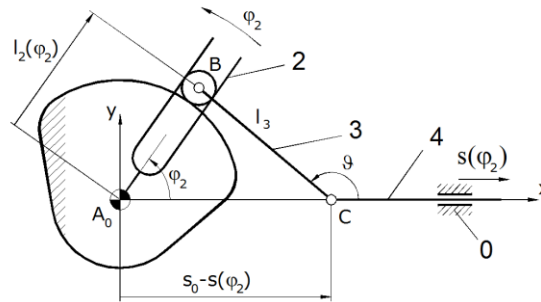
Fig. 3.3.15. Kinematic schema of the slider-crank with variable crank length

For the numerical example shown in Fig. 3.3.16 were chosen the initial stroke s_0=8.5 [mm], the coupler length l_3=6 [mm] and the roller radius r_R=2 [mm].
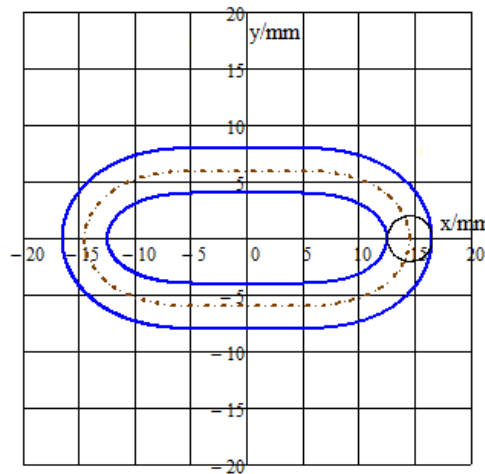
Fig. 3.3.16. Grooved cam profile of the slider-crank mechanism with variable crank length

The transmission function of the mechanism fulfills the desired transmission function and shows identical with the function depicted in Fig. 3.3.10.

The mechanism solution with variable crank length achieves the imposed transmission function, but the size of the mechanism is large and uses an additional element. It must be mentioned that the coupler and the slider must be largely tolerated in order to avoid the self-locking in the movement interval with constant transmission ratio, because they move together on overlapped direction.

   f.   Scotch-yoke driven by a belt mechanism

The combined mechanism uses a toothed belt mechanism to drive the scotch-yoke. A stud is fixed in the toothed belt and slides in the yoke. This mechanism achieves partially the requested transmission function, only within the interval with constant transmission ratio. The return curve

arches are generated by the rotation movement of the stud around the belt gears. The kinematic schema of the mechanism is given in Fig. 3.3.17.
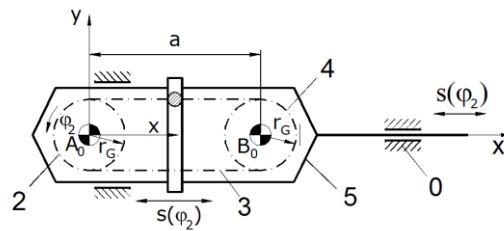
Fig. 3.3.17. Kinematic schema of the scotch-yoke driven by a belt mechanism

The synthesis of the mechanism for the imposed stroke and transmission function yields the belt gear radius r_G and the reference center distance a using the relationships:

$$r_G = h_1, \qquad a = h - 2 \cdot r_G .$$
(3.3.17)

For the numerical example, the driving belt mechanism is shown in Fig. 3.3.18, with the gear radius r_G =3.3 [mm] and the reference center distance a = 10.4 [mm].
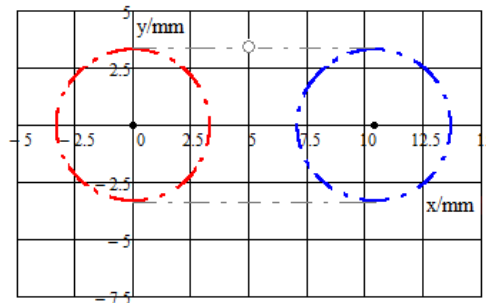
Fig. 3.3.18 Toothed belt mechanism of the scotch-yoke driven by a belt mechanism
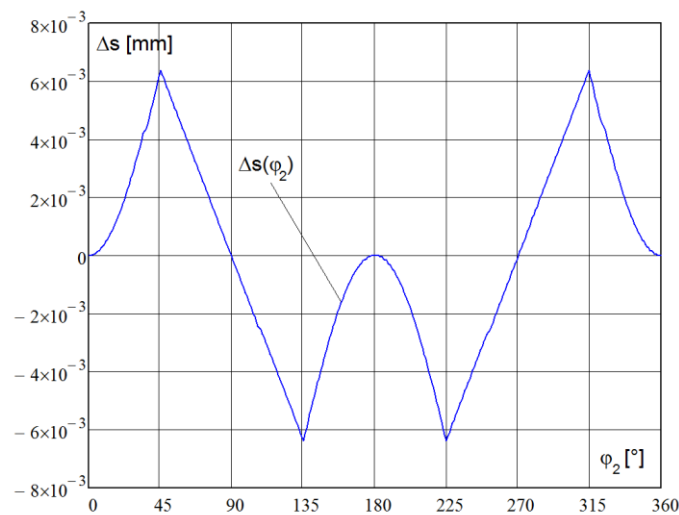
Fig. 3.3.19. Deviation of the transmission function of the cam mechanism with constant width and double flat faced follower

For the analysis of the scotch-yoke mechanism driven by a belt mechanism the archived transmission function is given by the relationships:
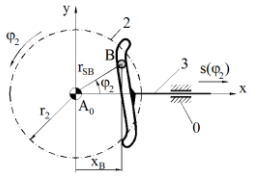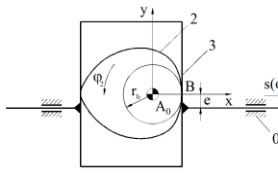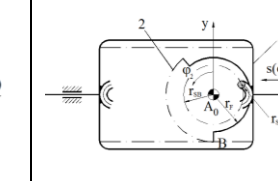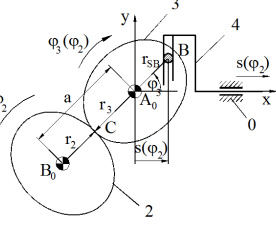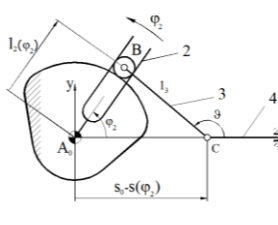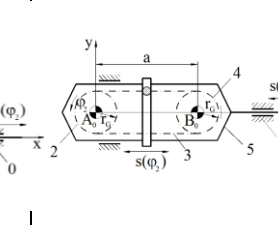
$$s(\varphi)=\begin{cases} r_G(1-\cos(2\varphi)); & 0\leq\varphi<\dfrac{\pi}{4}; \\[2mm] r_G+\dfrac{2(h-2r_G)}{\pi}(\varphi-\dfrac{\pi}{4}); & \dfrac{\pi}{4}\leq\varphi<3\dfrac{\pi}{4}; \\[2mm] h-r_G\left[1-\cos(2\varphi)\right]; & 3\dfrac{\pi}{4}\leq\varphi<5\dfrac{\pi}{4}; \\[2mm] h-r_G-\dfrac{2(h-2r_G)}{\pi}(\varphi-5\dfrac{\pi}{4}); & 5\dfrac{\pi}{4}\leq\varphi<7\dfrac{\pi}{4}; \\[2mm] r_G(1-\cos(2\varphi)); & 7\dfrac{\pi}{4}\leq\varphi<2\pi. \end{cases}$$

(3.3.18)

This mechanism achieves a transmission function alike the desired transmission function (3.3.1) and has a compact size, but uses additional elements. The deviation of the archived transmission function is shown in the Fig. 3.3.19.

3.3.3.3. Choice of the optimal design solution for the fishing reel spool mechanism

In order to find the optimal design solution the selecting criteria were computed and they are summarized in Tab. 3.3.2

Tab. 3.3.2. Summarized values of the selection criteria for the reel spool mechanism

Selection criteria			
$\Delta s_a\,/\,mm$	0.464	0	0
$s'(0), s'(\pi), s'(2\pi)\,/\,mm$	1.88, -2, 1.88	0, 0, 0	0, 0, 0
$n\,/\,elements$	3	3	3
$c_x\,/\,mm$	24	44	41
$c_y\,/\,mm$	24	45	17
Selection criteria			
$\Delta s_a\,/\,mm$	0	0	$2.75\ 10^{-3}$
$s'(0), s'(\pi), s'(2\pi)\,/\,mm$	0, 0, 0	0, 0, 0	0, 0, 0
$n\,/\,elements$	4	4	5
$c_x\,/\,mm$	24	41	38
$c_y\,/\,mm$	24	20	12

In Tab. 3.3.2 the best solutions for each considered criterion are depicted with gray color. Two solutions satisfied the most of the considered criteria, namely the noncircular gear mechanism in series with a scotch-yoke and the gear mechanism with geared sector and double symmetrical rack. Because the workspace along the translation direction is limited, the first design solution is chosen as the optimal design solution for the reel spool mechanism.

Fig. 3.3.20 shows the kinematic schema of the reel mechanism using the noncircular gear mechanism in series with a scotch-yoke.
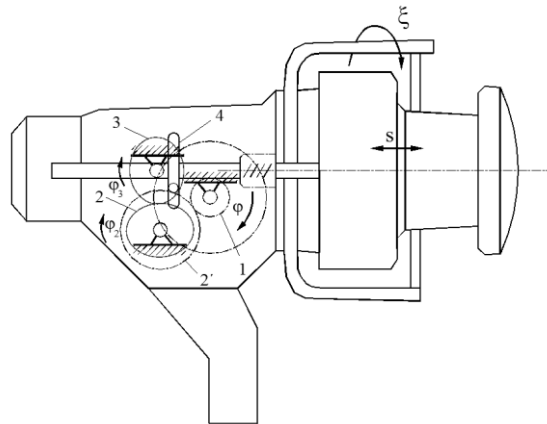
Fig. 3.3.20 Kinematic schema of the fishing reel with noncircular gear mechanism in series with a scotch-yoke

3.3.3.4. Model and prototype for the designed solution of the reel spool mechanisms

For the synthesized mechanism a scaled Plexiglas model shown in Fig. 3.3.21 was first manufactured.
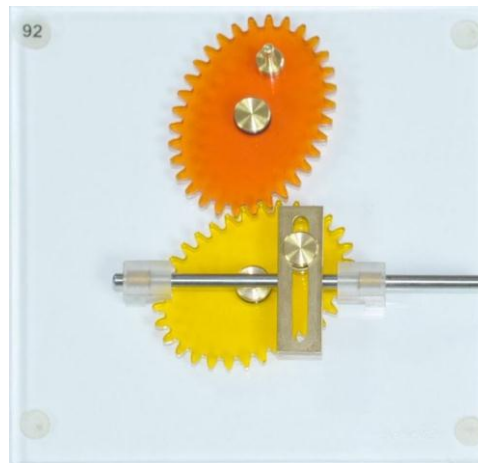
Fig. 3.3.21. A model of the noncircular gear mechanism in series with a scotch-yoke

The experimental transmission function of the manufactured model with the noncircular gear mechanism in series with a scotch-yoke was determined by using an optical measurement method. The experimental transmission function validates the theoretical results and it is given in the Fig. 3.3.22.
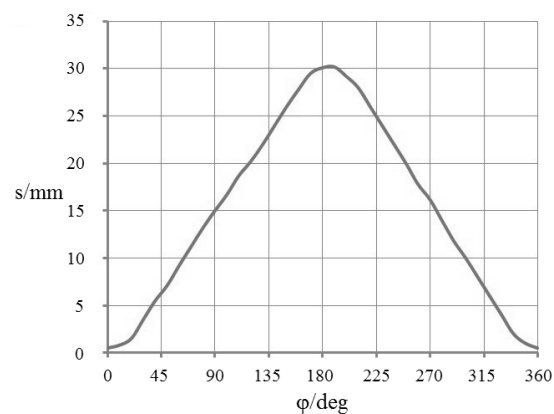
Fig. 3.3.22. Experimental transmission function of the manufactured mechanism model

The design schema of the novel reel spool mechanism prototype is shown in the Fig. 3.3.23.
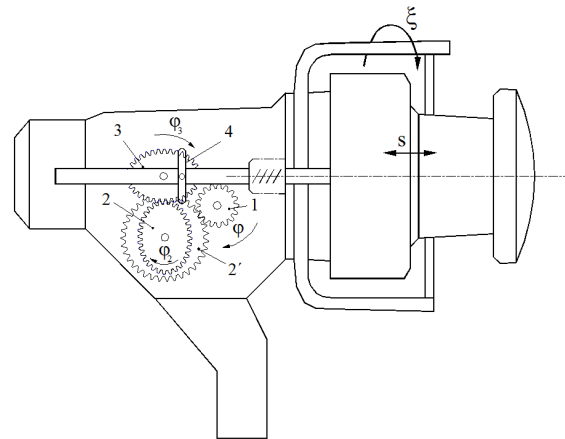
Fig. 3.3.23. Design of the fishing reel spool mechanism using noncircular gear mechanism
in series with a scotch-yoke

According with the design schema of the novel reel spool mechanism the prototype was manufactured. Fig. 3.3.24.a presents an overview of the reel and Fig. 3.3.24.b brings a close view of the mechanism. The noncircular gears were manufactured on a laser cutting CNC machine.

a)   b)
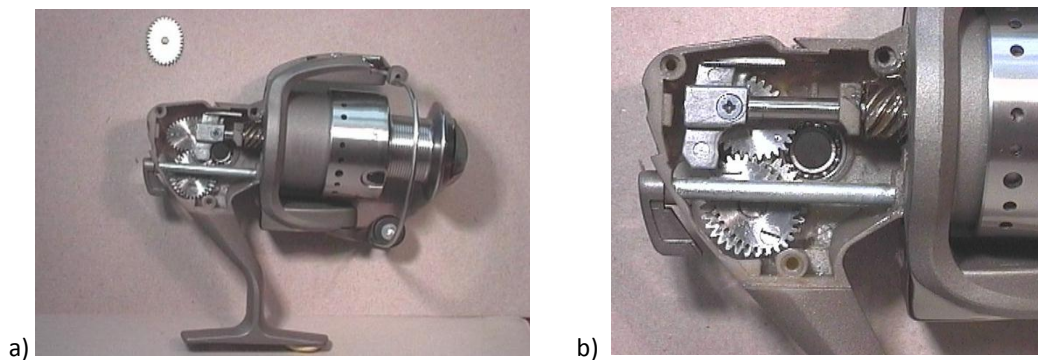
Fig. 3.3.25 Overview and detail of the prototype of the reel

3.3.4. Scientific contributions

Several mechanism solutions were considered for converting the unidirectional rotation of the crank into rectilinear alternate motion of the spool. The solutions were classified in basic and combined mechanism structures using an reduced number of elements.

The optimal mechanism solution for the reel spool mechanism avoids the jerk at the return points and is simple, because needs a reduced number of parts and requires a reduced size as the construction is compact. In addition, the chosen mechanism uses the same frame as by the previous reel spool mechanism and do not need to increase the costs for manufacturing a new frame.

The prototype of the reel with the mechanism described above was manufactured in the workroom of the Mechanisms Department at TU Dresden and the solution for the reel mechanism was patented [140]. The mechanism model with noncircular gear mechanism in series with a scotch-yoke was recorded and described in the DMG-Library.

The presented mechanism solutions can be used also for several other mechanical applications by uniform wrapping of cables on drum.

4. Scientific achievements regarding the analysis of compliant mechanisms

The scientific achievements in this chapter show the research of the compliant mechanisms, which use elastic connections, were focused on following opened or partial solved issues:
- structural analysis of the compliant mechanisms with elastic connections;
- simulation and analysis of a compliant mechanism with integrated piezo-actuators;

4.1. Analysis of the compliant mechanisms

4.1.1. State-of-art

The increasing number of compliant mechanisms industrial applications led to research on structural and design approaches of compliant mechanisms for required motion and force-deflection characteristics [102]. Using the Pseudo-Rigid-Body-Model (PRBM) two parallel mechanisms a bicycle derailleur and parallel-motion bicycle brakes [123] were developed by Mattson et al. The PRBM allows compliant mechanisms to be modeled and analyzed as rigid-body mechanisms and significantly reduces the analysis complexity.

Gao and Zhang in [188] compared the compliance between the multi-spring and finite-element model for multidimensional acceleration sensors based on fully decoupled compliant parallel mechanism. Analysis and design of an under-actuated compliant variable stroke mechanism by employing PRBM is studied by Tanık and Söylemez [198] for prescribed output loading and constant input torque. The dynamics of a four-bar crank-rocker mechanism, suitable as a flapping mechanism and consisting of two flexural hinges is analyzed by Khatait et al. in [142] and the peak driving torque is minimized by modifying the stiffness of the flexural hinges and the unstrained positions of the flexural hinges.

A novel finger mechanism with 1 active DoF and similar human grasping is proposed by Ceccarelli in [184] for an under-actuated operation, where the mechanism used spring elements within the structure. The application on-chip sensing of bi-stable mechanism stated the using of piezo-resistive properties of poly-silicon [134], which was made by detection of changes in position for variable resistance across the mechanism. A fully compliant bi-stable micro mechanism (FCBMs) was designed, fabricated and tested, with repeatable and detectable results. Cherry et al. in [159] were compared 2D and 3D finite element models for these FCBMs regarding the influence of the three-dimensional effects on the motion characteristics. A compliant miniature parallel manipulator made of super elastic nitinol pipe and actuated by shape memory alloy (SMA) wires and its force–displacement analysis was proposed by Sreekumar et al. in [182]. Hutchison et al. in [190] developed a class of carbon-nanotube composite materials to use the advantage of the precise high-aspect ratio shape of patterned vertically grown nanotube forests, rendered mechanically robust by chemical vapor infiltration and released by etching an underlying sacrificial layer. The development of a piezoelectric driven compliant-based micro-gripper mechanism capable of delivering high precision and fidelity manipulation of micro objects adopts Nashrul et al. in [180] a flexure based concept on its joints to address the inherent nonlinearities associated with the application of conventional rigid hinges. A combination PRBM and FEA was implemented to expedite the prototyping procedure which leads to the establishment of high performance mechanism.

Based on the analysis of a numeric model developed by Modler in [162] for the active textile reinforced compliant mechanisms (A-TCM), a compliant mechanism with elastic links with piezoelectric actuators integrated in the textile reinforced material was built [77] and [137]. A flaps mechanism as a transmission A-TCM was chosen in [177] and [138] as these linkages can be found in various domains of equipment, machine and automotive applications. The A-TCM building method with its high elastic potential based on the material offers, next to other advantages, a reduced part number and thus an assembly cost reduction, in particular the possibility to adjust on purpose the flaps system's opening behavior and its energy consumption [109] and [149].

The technical requirements of mechanical and mechatronic products are generally complex and impose well-defined movements to ensure a mechanical constraint. The development of mechanisms theory focused primarily on the use of rigid links in the structure of mechanisms (classical theory). Following the new developments in the field of smart compound materials with controlled elastic deformation and alongside the advance of nanotechnologies, the use of elastic deformable components belonging to elastic connections is more and more frequent.

4.1.2.   Aim of the theoretical research

The aim of the theoretical research was to develop an up-to-date structural analysis of the theory of mechanisms by using both rigid elements and elastic connections. In this regard, one should reconsider the definition of the kinematic joint, of the link and then, express the formula of mechanism's degree of freedom (mobility) within a new form of structural analysis of these mechanisms. In the case of A-CM, analytical calculations can only give rough approaches because the calculus models must include partial differential equations or equation systems, the initial and limit condition depending on the parts geometry. The second aim was analysis and simulation of some alternative kinematic models of A-CM with active prismatic joints and rotational joints, having concentrated torsion rigidity and the ability to predict the actual motion of compliant mechanisms with integrated piezo-ceramic actuators.

4.1.3.   Theoretical contributions

The main structural parameter of a kinematic chain or of a mechanism is the degree of freedom of the chain and the degree of freedom (mobility) of the mechanism (DoF), respectively. The analytical condition for constrained motion needs to have identity between the mobility and the number of the drives. The condition to have a constrain motion of the mechanisms was studied by many scientists beginning with Chebyches [1] and continuing with Grübler [2], [3], Kutzbach [4], Dobrovolski [5], Artobolevski [6], Manolescu [22], Waldron [19], Antonescu [26], Hervé [30], Gronowicz [33], Angeles and Gosselin [42], Huang [173], Yang et al [167], Zhang and Mu [199] and others. Gogu presented in [129], [130] an overview on the calculation of the mobility of the mechanisms with rigid bodies as elements.

4.1.3.1. Structural analysis of the compliant mechanisms

The classical theory of mechanisms considers the links/elements as rigid bodies. In regard with the strength characteristics, the rigid elements are considered theoretically non-deformable by tensile/compression, bending and torsion.

> *"The link is defined as a rigid mechanism element (component) carrying kinematic pairing elements [113], [249]."*

The links are connected through kinematic pairs and the closure of the kinematic pairs is a process of constraining two rigid bodies to form a kinematic pair by force (force closure), geometric shape (form closure) or flexible materials (material closure) [113], [249].

> *"The kinematic pair is defined as a mechanical model of the connection of two pairing elements having relative motion of a certain type and degree of freedom [113], [249]."*

The kinematic pairs are classified regarding the degree of freedom or the constrained motion in five classes. The class of the kinematic pair is given by the number of constrained movements in respect with the attached reference system.

> *"The degree of freedom of a kinematic pair is expressed as the number of independent coordinates needed to describe the relative positions of pairing elements [113], [249]."*

The connected links through kinematic pairs of different classes build a kinematic chain.

> *"The kinematic chain is defined as an assemblage of elements/ links and joints [113], [249]."*

The mechanism can be defined starting from the definition of the kinematic chain or according with its mechanical functions, as follows:

> *"Closed kinematic chain with one of its components (links) taken as a frame [113], [249]."*
>
> *"System of bodies designed to convert motions of, and forces on, one or several bodies into constrained motions of, and forces on, other bodies [113], [249]."*

The structural parameter of the kinematic chain and mechanism are defined in [113], [249] as:

> *"The degree of freedom of a kinematic chain or the degree of freedom (mobility) of a mechanism represents the number of independent coordinates needed to define the configuration of a kinematic chain or mechanism"*

The degree of freedom of a kinematic chain (Fig. 4.1.1) in respect with a reference system may be calculated according to [5], [6], [22] as:

$$L = 6n - \sum_{i=1}^{5} i \cdot c_i,$$
(4.1.1)

where: c_i is the number of kinematic pairs of class i, i = 1,2,...5;

   n − the number of links of the kinematic chain.
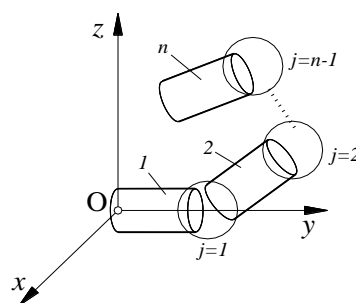
Fig. 4.1.1. Kinematic chain.

The relationship describing the degree of freedom (mobility) of mechanism is:

$$M = (6 - f) \cdot (n - 1) - \sum_{i=f+1}^{5} (i - f) \cdot c_i,$$
(4.1.2)

where: f represents the number of common restricted motions of the mechanism´s elements usually named "the family" [22], [26], [27].

For the planar mechanisms, with f = 3, the relationship (2) becomes:

$$M = 3 \cdot (n-1) - 2 \cdot c_5 - c_4 , \qquad\qquad (4.1.3)$$

where: c_5 the number of kinematic pairs of class V and

c_4 the number of kinematic pairs of class IV are.

The mechanical constrained motion is ensured according to the above mentioned condition if the relationship:

$$M = n_i \qquad\qquad (4.1.4)$$

is satisfied and n_i represents the number of drive elements with DoF=1.

The works [23] and [27] introduced the structural concept of connection. Connection means all the restrictions occurring in the relative movement between the elements in order to provide a constrained motion of the mechanism. The connections can be of kinematic/geometric type and of dynamic type. The kinematic/geometric connections are connections, which impose restrictions in terms of geometry and the dynamic connections in terms of forces equilibrium.

The definition of the connection [23], [27] is:

> *"Open kinematic chain interposed between two elements with known or imposed relative movement"*

The connections can be classified according to the number of their links and kinematic pairs (Fig. 4.1.2) in three types: connection of type A, which contains one kinematic pair, connection of type B, which contains one element and two kinematic pairs and connection of type C, which may have any structure.

Type of connection	Number of elements	Kinematic pairs		Kinematic schema of connection	Degree of freedom L_k	Notation
		Nr.	Class			
A	$n_k = 0$	1	$c_{5k}=1$		-2	$K_A(-2)$
			$c_{4k}=1$		-1	$K_A(-1)$
B	$n_k = 1$	2	$c_{5k}=2$		-1	$K_B(-1)$
			$c_{5k}=1$ $c_{4k}=1$		0	$K_B(0)$
C	$n_k = 2$	3	$c_{5k}=3$		0	$K_C(0)$
	any				L_k	$K_C(L_k)$

Fig. 4.1.2. Classification of connections

The up-to-date development of smart compound materials with controlled elastic deformation and their applications in mechanical structures requires the reconsidering of some definitions and at least the mobility relationship.

Generally, an element may contain one or more elastically deformable sections, called further on as elastic connections. Considering the definition of the dynamic connection the elastic connection may be defined as follows:

> *"The elastic connection is a dynamic/kinetostatic connection, which contains one or more elastically deformable sections materially closed with rigid sections of the element having a constrained relative motion"*

The elastic connection allows supplemental degrees of freedom. These degrees of freedom result from the elastic deformation corresponding to the bending and/or compression loading. These deformations generate a quasi-rotation and/or translation motion between the considered elements.

Fig. 4.1.3 presents a classification of elastic connections of type B, similarly with the kinematic connections. The classification takes into account only the kinematic pairs of class V. The other types of elastic connections are combinations of the kinematic and elastic connections of type B.

In order to up-date the definition of the mechanism, which contains elastic connections one must ensure preservation of the kinetostatic/dynamic conditions in a motion cycle. Therefore, the mechanism definition may be:

"System of rigid bodies with/without elastic sections designed to convert motions of, and forces on, one or several bodies into constrained motions of, and forces on, other bodies"

Type of elastic connection	Number of elements	Nr. of rigid sections	Nr. of elastic connection	Number of kinematic pairs	Kinematic schema of elastic connection	Supplemental degrees of freedom f_{elK}	Degree of freedom L	Notation
B	1	0	1	2		1	0	$K_{Bel}(0)$
		1	1			1	0	$K_{Bel}(0)$
		1	1			2	1	$K_{Bel}(1)$
		2	1			1	0	$K_{Bel}(0)$
		2	1			2	1	$K_{Bel}(1)$
		2	1			3	2	$K_{Bel}(2)$
		1	2			1	0	$K_{Bel}(0)$
		1	2			2	1	$K_{Bel}(1)$
		1	2			3	2	$K_{Bel}(2)$

Fig. 4.1.3. Classification of elastic connections of type B

The degree of freedom of a kinematic chain containing elastic connections results from the relationship:

$$L = 6 \cdot n + \sum_{k=1}^{m} f_{elK_k} - \sum_{i=1}^{5} i \cdot c_i ,$$ (4.1.5)

where: m the total number of elastic connections,

f_{elK} the number of the supplemental degrees of freedom of the connection k, are.

Using the same logics, the degree of freedom (mobility) of the spatial mechanism is:

$$M = 6 \cdot (n-1) + \sum_{k=1}^{m} f_{elK_k} - \sum_{i=1}^{5} i \cdot c_i ,$$ (4.1.6)

and for a planar mechanism the DoF is:

$$M = 3 \cdot (n-1) + \sum_{k=1}^{m} f_{elK_k} - 2 \cdot c_5 - c_4 \,. \tag{4.1.7}$$

As the mechanisms with elastic connection contain dynamic/kinetistatic connections, the constrained motion is ensured if the relationship:

$$n_i \leq M \leq n_i + n_d \tag{4.1.8}$$

is satisfied, n_d being the number of links in dynamic equilibrium and n_i represents the number of driving links.

4.1.3.2. Analysis of the active compliant mechanisms using equivalent models

The analysis of the active compliant mechanism A-CM is a sufficiently precise approach by using FEM models. However, the great numbers of design variables, including, besides all of the geometrical dimensions, the physical properties of the materials used, must be somehow known before the FEM modeling step in the A-CM developing process. In the case of A-CM, analytical calculations can only give rough approaches because the calculus models must include partial differential equations or equation systems, the initial and limit condition depending on the parts geometry (yet unknown). Or, the calculus model is simplified thoroughly, thus the results are not accurate enough.

The rigid and the passive compliant elements simulation was already studied with repeatable results and equivalent values for density, Young's modulus and Poisson's ratio, limit stresses and strains are reliably established. Thus, the challenge is the development of a model for the active element simulation, consisting of a passive base layer and an actuator layer (Figure 4).
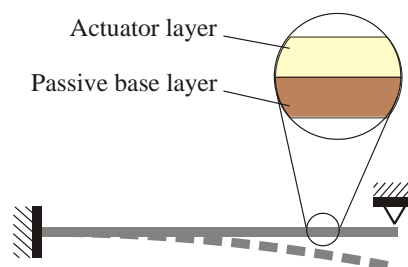
Fig. 4.1.4. The active and passive layers of the compliant bending piezo-actuator

Piezoelectric energy converters are characterized by great forces, response times of a few milliseconds and a positioning accuracy of a few nanometers, but only at more than 1-2 thousand Volt. The inverse piezoelectric effect used for actuation is defined analytical through the relationship (4.1.9), where the mechanical strain S depends on the mechanical load T and electric field strength E. If the tensor of mechanical parameters on the surface of a crystal is considered, the linear equation in vector form is, in Voigt's notation:

$$\{S\} = \left[s^E\right] \cdot \{T\} + \left[d^t\right] \cdot \{E\} \tag{4.1.9}$$

where:

   $[d^t]$ is the matrix for the reverse piezoelectric effect,

   ε^T - permitivity Matrix for T = 0,

   s^E - compliance matrix for E = 0.

For the equivalent model of A-CM the active compliant element will be considered as a mechanism composed of rigid elements, rotational and/or translational joints, both passive and active, and

torsion and translational springs. The simulated active element is composed of some simulation cells, serial connected. In the following, some types of simulation cells and models are shown: single layer passive and active cell/model and double layer active cell/model.

a) Model of the single layer passive compliant element

The single layer passive model is based on the flexible body/flexible link models already existing in the dynamical analysis procedures and software. These models approximate the mechanical behavior of flexible links by model cells j (see Fig. 4.1.5) composed of a rigid bar $A_{j-1}A_j$, with the length L_j:

$$L_j = \frac{l_2}{n}$$
(4.1.10)

where: l_2 is the length of the active element and

n is the cells number of the active element.
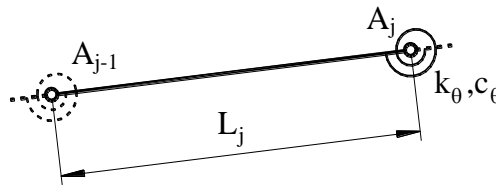
Fig. 4.1.5. The model of the passive single layer element

The cells are joined by the rotational joints A_j, and the equivalent torsion spring with the rigidity:

$$k_\theta = \frac{M_j}{\vartheta_j} = E_{eq} \cdot \frac{I_z}{L_j}$$
(4.1.11)

where:

M_j is the resulting moment;

ϑ_j the bending angle in the joint A_j;

E_{eq} equivalent Young's (elasticity modulus) for the two layer composite;

I_z the area moment of inertia of the two layer composite cross-section;

for the rectangular cross-section:

$$I_z = \frac{B \cdot H^3}{12}$$
(4.1.12)

with B the width and H the thickness of the compliant element.

The damping in the compliant element may be taken into account during simulation by introducing a concentrated damper in the revolute joint, with the damping coefficient:

$$c_\theta = D \cdot \frac{B \cdot H^3}{6} \cdot \sqrt{E \cdot \rho}$$
(4.1.13)

where: D is the damping ratio,

E the Young's modulus and

ρ the density of the compliant element's material.

b) Model of the single layer active compliant element

The single layer active model is similarly with the previous model by adding an actuation moment M_a in rotational joints A_j. The model of the single layer active element is shown in the Fig. 4.1.6.
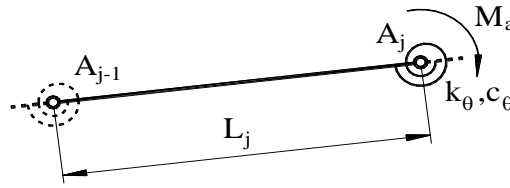
Fig. 4.1.6. The model of the active single layer element

The actuating moment M_a in the active joint A_j can be calculated knowing the actuating force F_a and the actuating layer thickness h_a :

$$M_a = -F_a \cdot h_a .$$
(4.1.14)

The actuating force can be calculated as follows:

$$F_a = -\frac{\Lambda}{\dfrac{h_1^2}{2 \cdot E_1 \cdot I_z} + \dfrac{1}{E_2 \cdot L_j \cdot b_2}} ,$$
(4.1.15)

with:

Λ is the actuating deformation,

E_1, E_2 Young's (elasticity) modulus of the base and active layers,

h_1, I_2, b_2 thickness of the base layer, length and width of the active layer.

The actuating deformation is computed with respect of the input voltage U :

$$\Lambda = d_{33} \cdot E = d_{33} \cdot \frac{U}{t_{IDE}} ,$$
(4.1.16)

with piezoelectric constant $d_{33} = 4,6 \cdot 10^2 \, \text{pC/N}$ and distance between electrodes $t_{IDE} = 0,5 \, \text{mm}$.
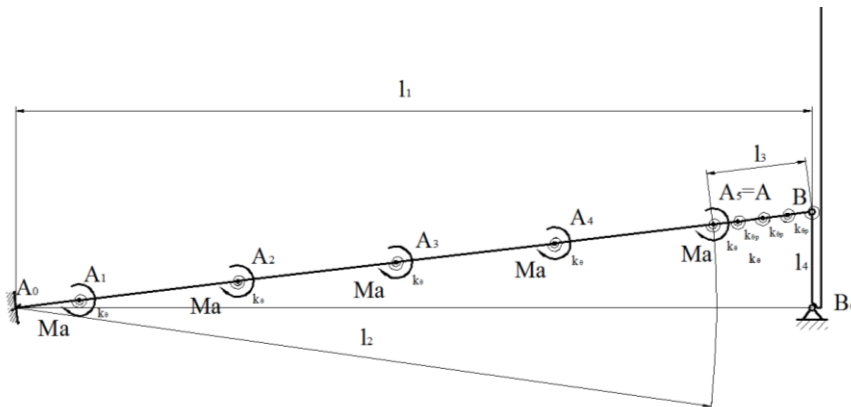
Fig. 4.1.7. The A-TCM with single layer active element used in a flaps mechanism

Using the single active layer elements in the Fig. 4.1.7, a model for the whole active thermoplastic compliant mechanism (A-TCM) in the structure of a flaps mechanism can be built.

c)   Model of the double layer active compliant cell with 1 DOF and 1 active prismatic joint

The model of the double layer active compliant cell with 1 DOF and 1 active prismatic joint consists of a RPRR four bar mechanism. The link $A_{s,j}A_{i,j}$ is the base of the cell model and represent the interface between the cells, the inferior link $A_{i,j}A_{i,j+1}$ represents the passive layer and the superior $A_{s,j}A_{s,j+1}A_{i,j}$ two elements with the active prismatic joint the actuator of the layer (Fig. 4.1.8). This kinematic cell moves only under the effect of the actuating constriction of the actuator layer $A_{s,j}A_{s,j+1}$, modifying its form from a rectangle to a quadrilateral with a right angle $A_{s,j}A_{s,j+1}A_{i,j}$.
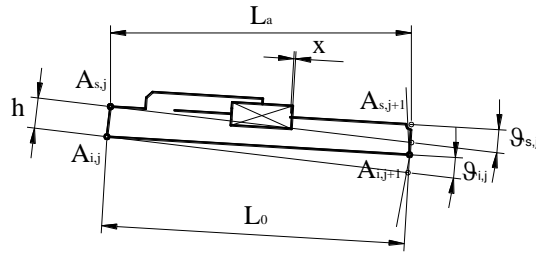
Fig. 4.1.8. Kinematical model of the double layer active compliant cell with 1 DoF and 1 active prismatic joint

The angles ϑ_i and ϑ_s made by the two equivalent inferior and superior layers with the cell base are different to 90° and can be determined as:

$$\vartheta_i = a\cos\left(\frac{2 \cdot L_0 \cdot x - x^2}{2 \cdot L_0 \cdot h}\right) , \tag{4.1.17}$$

$$\vartheta_s = a\cos\left(\frac{2 \cdot h^2 - 2 \cdot L_0 \cdot x + x^2}{2 \cdot h \cdot \sqrt{L_a^2 + h^2}}\right) - a\tan\left(\frac{h}{L_a}\right) , \tag{4.1.18}$$

where:

   L_0 is the initial cell length, equal to the passive layer length,

   x   the actuating constriction of the upper layer.

   L_a the actual length $L_a = L_0 - x$ of the upper layer,

   h   the cell height, or the equivalent thickness.

Defining the elements position and orientation in a reference system by the coordinates (x_{A0}, y_{A0}) and the initial angle φ_0 of the cell 0, the coordinates of all rotational joints can be analytically computed beginning with the element 1 and considering the actuating deflections angles ϑ_i and ϑ_s.

$$x_{As,i_{j+1}} = x_{As,i_j} + L_{a,0} \cdot \cos\varphi_{s,i_j}$$
$$y_{As,i_{j+1}} = y_{As,i_j} + L_{a,0} \cdot \sin\varphi_{s,i_j} \tag{4.1.19}$$

where φ_{s,i_j} the superior and inferior position angles of the modeling cell j, are also successively determined:

$$\varphi_{s,i_{j+1}} = \varphi_{s,i_j} - \vartheta_{s,i} + 90° . \tag{4.1.20}$$

   d)   Model of the double layer active compliant cell with 2 DOF and 1 active prismatic joint

In order to simulate compliant active elements, the cell must allow deformations under load and actuate the driving bending deformation. To fulfill this purpose, a cell with two DOF, one active prismatic joint and one joint with concentrated rotational rigidity were taken into account.

These cells may be linked together by free rotational joints, as their movement is fully determined by the actuating constriction, the external loads and the equivalent rigidity in the joint $A_{i,j}$ (Fig. 4.1.9.a) or in three joints $A_{i,j}$, $A_{i,j-1}$ and $A_{s,j-1}$ (Fig. 4.1.9.b). However, this rigidity has no direct physical meaning, as it tries to simulate the bending rigidity of two layers from different materials and the interface rigidity altogether.

a)   b)
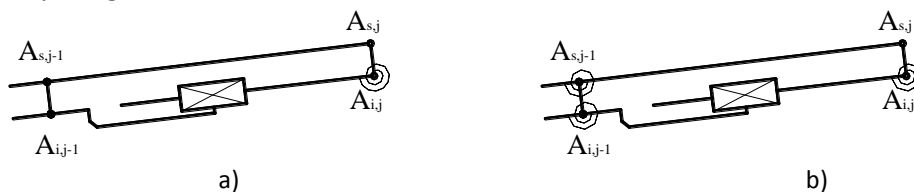
Fig. 4.1.9. Kinematical model cells with 2 DoF, 1 active prismatic joint and concentrated elastic stiffness in 1 and 3 joints, respectively

The cell's j deformation under actuation x and load is defined by the angles $\vartheta_{i,i}$, $\vartheta_{s,i}$ and $\vartheta_{H,i}$ (see Fig. 4.1.10), as all of the initially right angles are deformed. The values of these angles are obtained by solving the geometrical and kinetostatic equations system, taking into account the elastic moments M_e in the rotational joints:

$$M_{e_{s,i_j}} = k_{\theta_{s,i_j}} \cdot \vartheta_{s,i_j},$$ (4.1.21)

where $k_{\theta_{s,i}}$ are the rigidities of the equivalent torsion springs in the joints.
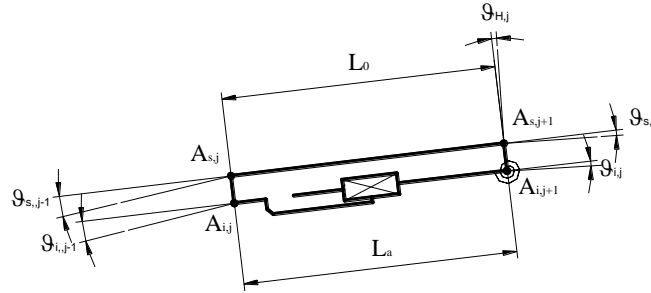
Fig. 4.1.10. Kinematical model cell with 2 DoF, one active prismatic joint and one concentrated elastic stiffness

The cell's geometry is defined by the equations:

$$L_0 \cdot \cos(\vartheta_s) - L_a \cos(\vartheta_i) = h \cdot \sin(\vartheta_i + \vartheta_H)$$ (4.1.22)

and

$$L_0 \cdot \sin(\vartheta_s) - L_a \sin(\vartheta_i) = h \cdot (1 - \cos(\vartheta_i + \vartheta_H)).$$ (4.1.23)

The deflection angles $\vartheta_{i,i}$, $\vartheta_{s,i}$ and $\vartheta_{H,i}$ can be computed from the static equilibrium equations for the elements $A_{s,j}A_{s,j+1}$, $A_{s,j+1}A_{i,j+1}$ and $A_{i,j}A_{i,j+1}$, when the loads $F_{i,j+1}$ $F_{s,j+1}$ in the joints $A_{i,j+1}$ and $A_{s,j+1}$, and their direction, imposed by the following cell j+1 are known.

In the Fig. 4.1.11 are presented the sketches with the equivalent force acting in the upper U, interface H and lower L elements, respectively. The upper passive layer Fig. 4.1.11.a is only axially loaded, i.e. its internal load $\overrightarrow{F_{s,j}}$ has the direction given by the angle $\vartheta_{s,i}$. Thus, the force equilibrium equation is:

$$\overrightarrow{F_{s,j}} + \overrightarrow{F_{s,j+1}} + \overrightarrow{F_{H,j}} = 0,$$ (4.1.24)

where: $\overrightarrow{F_{H,j}}$ is the interface element H transversal load.
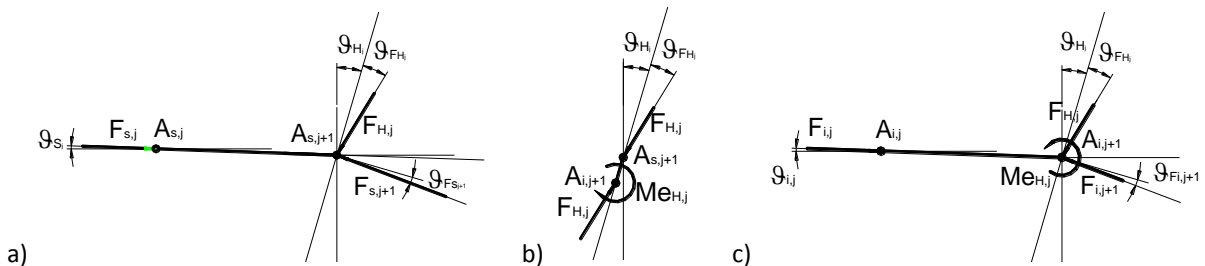
Fig. 4.1.11 Static equilibrium condition for the upper layer U (a), interface H (b) and lower L element (c)

For the interface element H, the moment equilibrium equation Fig. 4.1.11.b around it's insertion point $A_{i,j+1}$ on the I element (where the concentrated rigidity is applied) is:

$$Me_{H,j} = F_{H,j} \cdot h \cdot \cos\vartheta_{F_{H,j}},$$ (4.1.25)

$$Me_{H,j} = k_H \cdot \vartheta_{H,j}.$$ (4.1.26)

and k_H simulates the tangential rigidity of the interface.

For the lower layer element L, equivalent to the actuating layer at a given constriction, both force and moment equilibrium equations are necessary:

$$\vec{F_{i,j}} + \vec{F_{i,j+1}} + \vec{F_{H,j}} = 0 \, , \tag{4.1.27}$$

$$Me_{H,j} = F_{i,j} \cdot L_a \cdot \sin \vartheta_{F_{i,j}} \, . \tag{4.1.28}$$

The equation system can be numerically solved, and the cell's geometry and internal load can be found. In order to calculate the geometry of the whole actuator element, iterations must be performed, as the cells' geometries are not independent. The simulation steps should begin at the starting position (x=0) and follow the deformations as the actuating constriction advances. The deformations are dependent not only on the load and actuation, but also on the evolution of the A-TCM during the process. The 5-link linkage 4R1P is also in a singularity position, as the constriction of the $A_{i,j}A_{i,j+1}$ active equivalent layer may lead to upwards or downwards rotations. It will be always necessary to determine the static equilibrium first, and then to simulate the actuated movement.
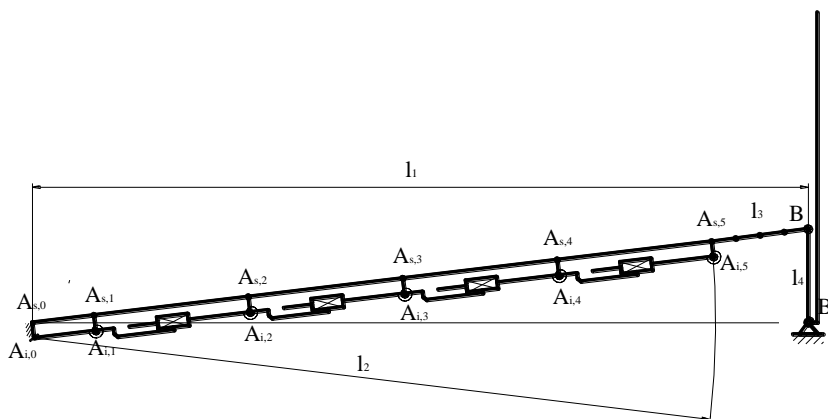
Fig. 4.1.12. Active element model with kinematical cells with 2 DoF 1 active prismatic joint and concentrated rigidities in the joints used in flaps mechanism

Fig. 4.1.12 shows the model for the A-TCM with kinematical cells having 2 DoF, 1 active prismatic joint and concentrated rigidities in the joints of flaps in differential design.

4.1.4.   Numerical examples
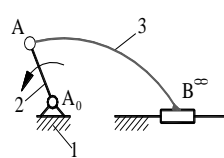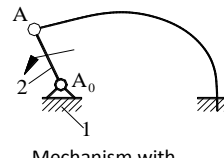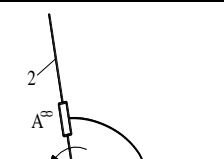
4.1.4.1. Structural analysis of compliant mechanism structures

For several mechanism structures was perform the structural analysis and shown in Tab. 4.1.1. For each structure was described the structure and computed of the degree of freedom (mobility) of structures containing elastic connections. The examples are derived from the classical linkages.

Tab. 4.1.1. Examples of mechanisms with elastic connections

Nr.	Kinematic schema		
1.	Four bar linkage with elastic connection	Number of the links and elastic connections		
		n=3	m = 1 with f_{elK} = 1	
		Number of kinematic pairs	Class V	Class IV
			c_5 =3	c_4 =0
		Degree of freedom (mobility) of the mechanism		
		$\mathbf{M = 3 \cdot (3-1) + 1 - 2 \cdot 3 - 0 = 1}$		
		Number of driving links	n_i = 1	n_d = 1
		Constrain motion condition		
		$1 \leq 1 \leq 1 + 1 = 2$ (fulfilled)		

Tab. 4.1.1. Examples of mechanisms with elastic connections (continuation)

2.	Slider crank with elastic connection	Number of the links and elastic connections		
		n=3	m = 1 with f_{elK} = 1	
		Number of kinematic pairs	Class V	Class IV
			c_5 =3	c_4 =0
		Degree of freedom (mobility) of the mechanism		
		$M = 3 \cdot (3-1) + 1 - 2 \cdot 3 - 0 = 1$		
		Number of driving links	n_i = 1	n_d = 1
		Constrain motion condition		
		$1 \le 1 \le 1 + 1 = 2$ (fulfilled)		
3.	Mechanism with elastic connection and 2 joints RR	Number of the links and elastic connections		
		n=2	m = 1 with f_{elK} = 2	
		Number of kinematic pairs	Class V	Class IV
			c_5 =2	c_4 =0
		Degree of freedom (mobility) of the mechanism		
		$M = 3 \cdot (2-1) + 2 - 2 \cdot 2 - 0 = 1$		
		Number of driving links	n_i = 1	n_d = 1
		Constrain motion condition		
		$1 \le 1 \le 1 + 1 = 2$ (fulfilled)		
4.	Mechanism with elastic connection and 2 joints RT	Number of the links and elastic connections		
		n=2	m = 1 with f_{elK} = 2	
		Number of kinematic pairs	Class V	Class IV
			c_5 =2	c_4 =0
		Degree of freedom (mobility) of the mechanism		
		$M = 3 \cdot (2-1) + 2 - 2 \cdot 2 - 0 = 1$		
		Number of driving links	n_i = 1	n_d = 1
		Constrain motion condition		
		$1 \le 1 \le 1 + 1 = 2$ (fulfilled)		

4.1.4.2. Simulation of A-TCM single layer active model of the flaps mechanism

The manufactured A-TCM contains a resilient drive element with two-layers: the base layer and the active layer. The base layer function is to enable a large non-linear elastic deformation of the flexible active element and a large strain without damage. In the example it was chosen the textile-reinforced thermoplastics. The active layer consists of piezo-actuators MFC-P1: M–8557–P1 offered by Smart Materials GmbH.

For the active element used for simulation the dimensions are given in Tab. 4.1.2 and the elasticity modules for the actuator element materials in Tab. 4.1.3.

Tab. 4.1.2. Geometrical and physical parameters fort the model construction

Parameter/ Element	Thickness h [mm]		Length l [mm]	Width b [mm]		Density ρ [kg/m³]	
1	0.53		3.5	75		1750	
2,3,4,5,8,9,10,11	h1	h2		b1	b2	ρ1	ρ2
	0.25	0.28	21.5	75	57	1750	4750
6,7,12	0.53		12.5	75		1750	

Tab. 4.1.3. Mechanical characteristics of materials and composite

Material/ Layer	Characteristic				
	Young's modulus	Poisson's ratio		Shear modulus	Density
	E1 [GPa]	υ.12 [-]	υ.21 [-]	G12 [GPa]	ρ [kg/m³]
CF/HT-EP-UD – base layer	111	0.29	0.022	4.5	1750
MFC active layer	30.336	0.3	0.16	5.515	4750

The flaps mechanism characteristic dimensions are shown in the Tab. 4.1.4.

Tab. 4.1.4. Construction parameters of the four-bar mechanism

Characteristic parameter	Value	Description
φ_1	0.119 rad / 6.8 º	Starting position angle of the active link
φ_{12}	-0.237 rad / -13.6 °	Rotation angle of the active link
ψ_1	$\pi/2$ rad / 90 °	Starting position angle of the driven link
ψ_{12}	$\pi/2$ rad / 90 °	Rotation angle of the driven link
l_1	250 mm	Frame lenght
l_2	211 mm	Active link lenght
l_3	40 mm	Coupler lenght
l_4	30 mm	Driven link lenght

a) Simulation of the A-TCM using ADAMS

On the basis of the kinematic schema of an A-TCM with single layer active element model a simulation model was constructed using the ADAMS Software (see Fig. 4.1.13). The active element is built of several single layer active elements, linked together by rotational joints, as shown in the Fig. 4.1.7 and Fig. 4.1.14.
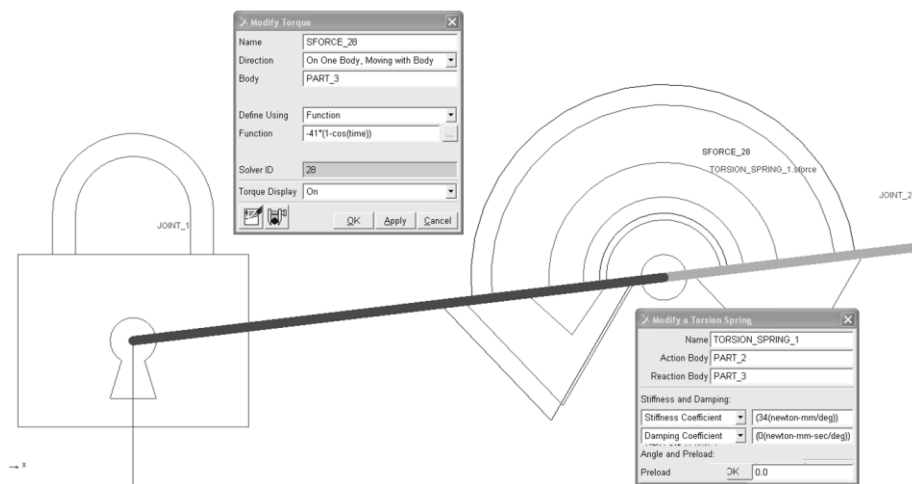
Fig. 4.1.13. The A-TCM single layer active cell model in ADAMS

In the joints (JOINT_2(3, 4, etc.)) are concentrated the bending rigidities of 34 N m/° (calculated with Eq. 3), as TORSION_SPRING_1(2, 3, etc.).sforce. The model cell is actuated by the moment SFORCE_28(29, 30, etc.), which increases from 0 to 82 N mm, as calculated with (4.1.14). The first active element cell is locked on the frame element (JOINT_1), and the other active elements are joined in series, a cell base to the tip of the previous cell, in order to compose the active element. This single layer active element is then connected to the rest of the A-TCM model, constructed under the specifications in Tab. 4.1.4 (Fig. 4.1.14).
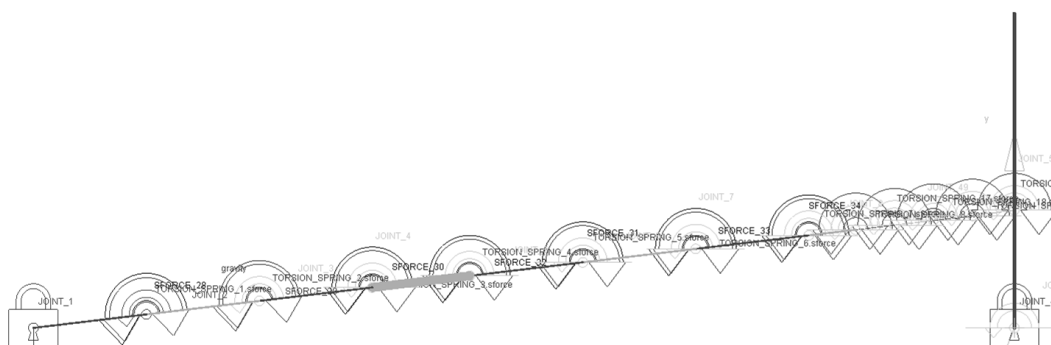
Fig. 4.1.14. The ADAMS A-TCM model with single layer active element

The simulation is then performed and the desired results may be obtained by plotting the variation of objects kinematical (position, velocity, etc) or dynamical (forces, moments) parameters or by insertion of sensors or other virtual measuring devices (e.g. angle measuring).

In Fig. 4.1.15.a the flaps opening angle and the actuating torque variation are presented. In the Fig. 4.1.15.b the transmission function of the equivalent mechanism is plotted, in order to asses the concordance with other simulation results.

a)

b)
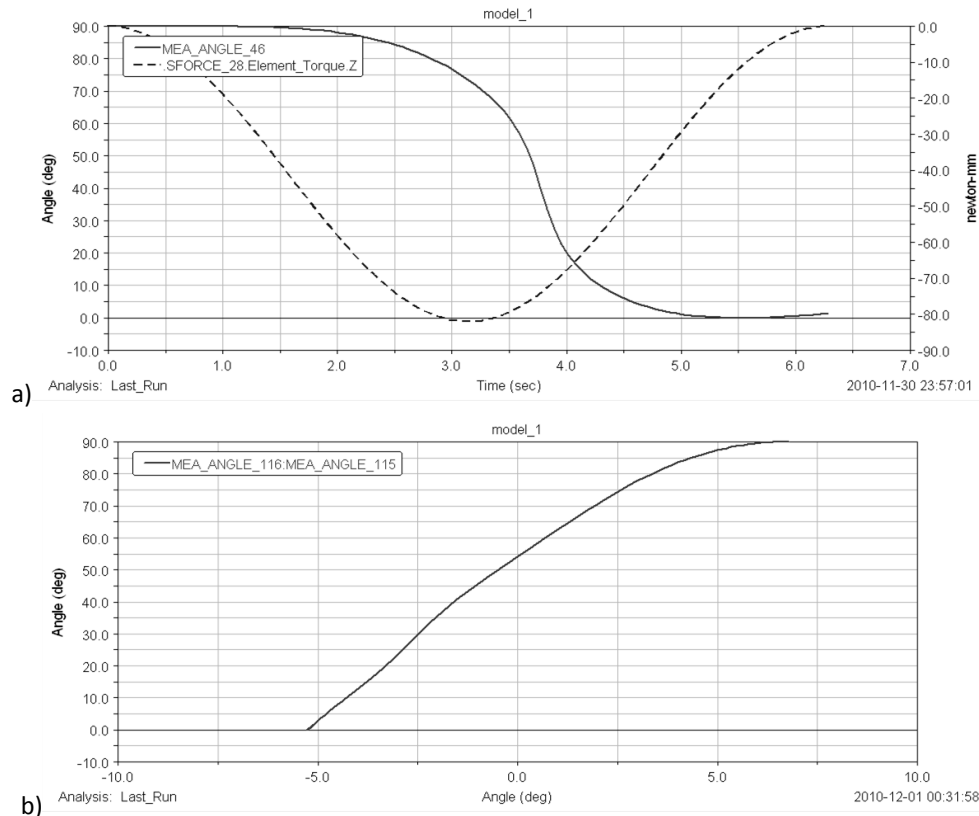
Fig. 4.1.15. ADAMS simulation results for opening angle for the A-TCM model with single layer active element

b) Simulation of the A-TCM using Matlab- Simulink

As a comparison, the same mechanism is modeled and analysed with the Matlab-Simulink software. The compliant active element is modeled as a subsystem (Fig. 4.1.16), composed of 8 active cells, simulating the integrated MFC/CFK active zones 2 and 4 passive cells simulating the zones 1 and 3.

The first Zone 1 is composed of a polyimid PI layer 0.048mm thick reinforced with a carbon fiber composite passive layer CFK with the thickness of 0.25mm. In the second actuator Zone 2, the carbon fiber composite layer is glued on a macro fiber composite actuator layer, 0.28 mm thick. The third reinforced Zone 3 has a much thicker 2.25 mm CFK layer.

 The cells (simulation elements) are linked together, the base of one cell on the tip of the previous. At both ends of the active element, conections are prepared to link it to the rest of the mechanism.

In Fig. 4.1.17 is shown the structure of a simulation cell as an element system. The system is composed of a rigid body (element), a custom joint and an actuator bloc. The element system is conected to two other elements or element systems, by the connection 1 (Base) to the previous and by the connection 2 (Tip) to the next Element.

The actuator bloc of the Element system consists of a sensor measuring the joint's rotation and an actuator imposing the rotation, under the effect of a bending moment resulting by adding the damping effect (Fig. 4.1.18).
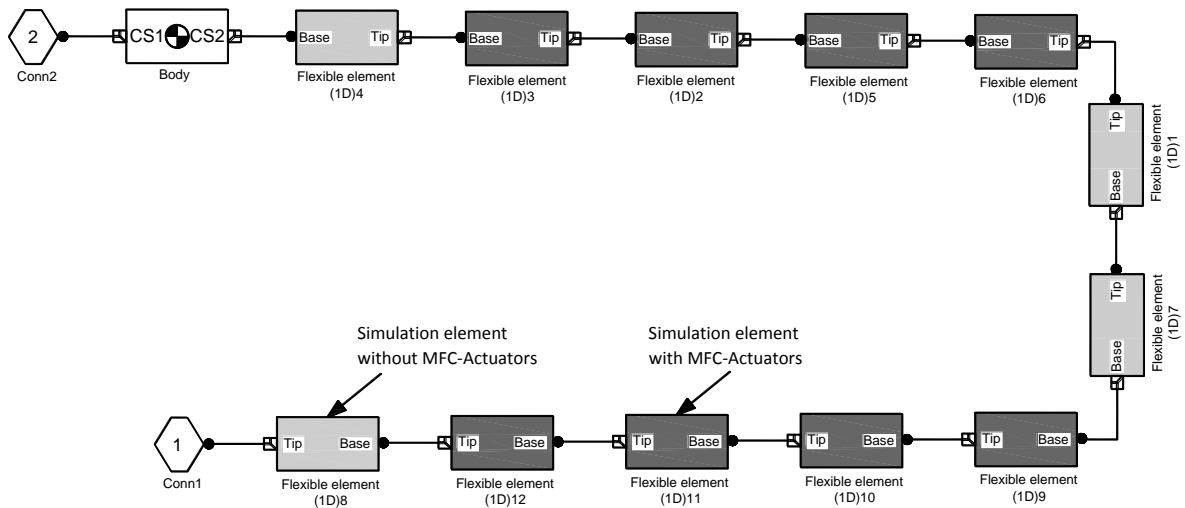
Fig. 4.1.16. Simulations model of the single layer active A-TCM
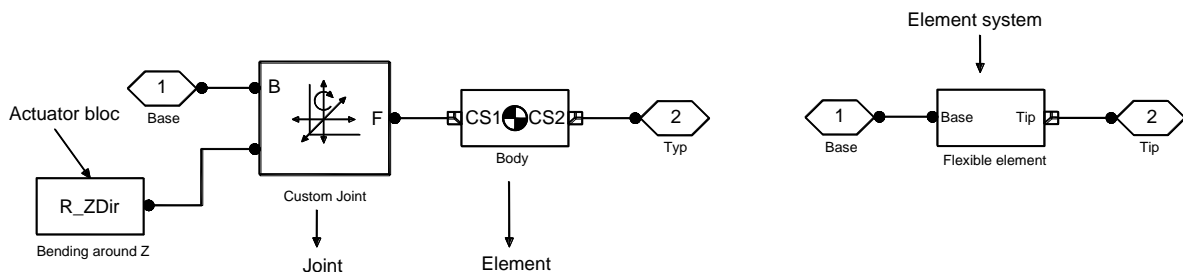
Fig. 4.1.17. Simulation cell as an Element system

In the active elements, the third parameter, input voltage, imposes an additional rotation of the element (Fig. 4.1.19).under the effect of a calculated function M(U):

$$M(U) = 2.3 \cdot 10^{-5} \cdot U \tag{4.1.29}$$
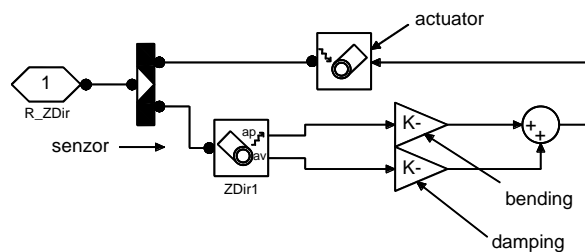
Fig. 4.1.18. Actuator bloc of the passive element
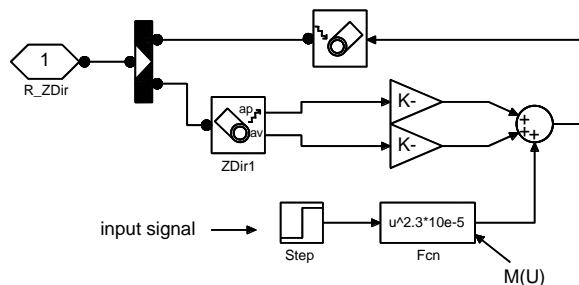
Fig. 4.1.19. Actuator bloc of the active element

In Fig. 4.1.20, the simulation results for a motion analysis of the 0.4 g flaps A-TCM are presented as motion sequences, for a maximal 1000 V (100%) step signal. The Fig. 4.1.21 shows the results obtained for the same mechanism actuated by a sine wave signal with the amplitude of 1380 V.

Opening angle 0º at 0 V	Opening angle 1.15º at 0 V under own weight	Opening angle 6.36º at 500 V (30%)
Opening angle 10.93º at 700 V (70 %)	Opening angle 18.38º900 V (90 %)	Opening angle 85.73º at 1000 V (100 %)
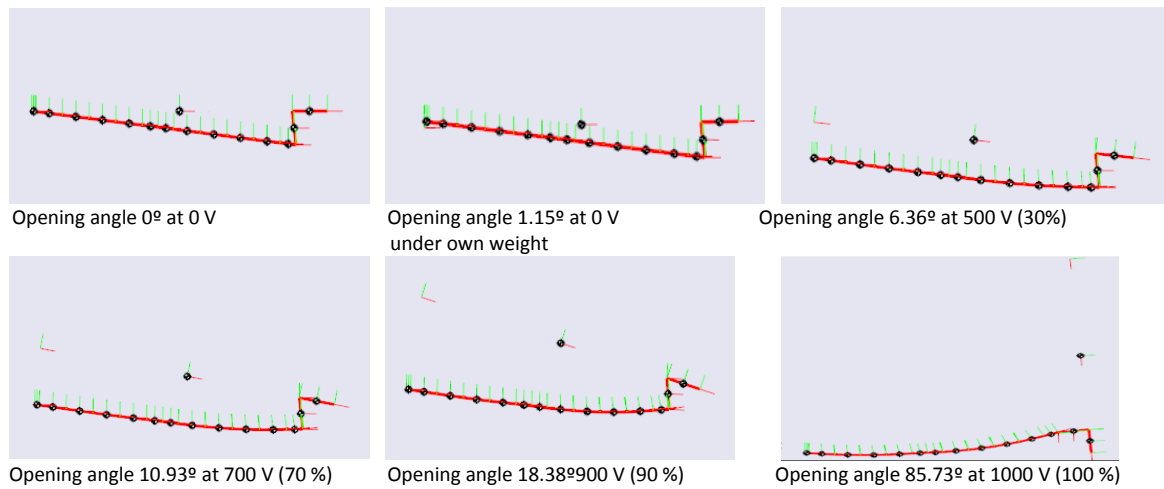
Fig. 4.1.20. Moving sequences of the Flaps A-TCM with the weight of 0.4 g, actuated with a step signal

Opening angle 0º at 0 V	Opening angle -1.15º at 0 V under own weight	Opening angle 5.25º at 500 V (36.23%)
Opening angle = 8.51º at 690 V (50%)	Opening angle 15.9º at 1000 V (72.46%)	Opening angle 86.38º at 1380 V (100%)
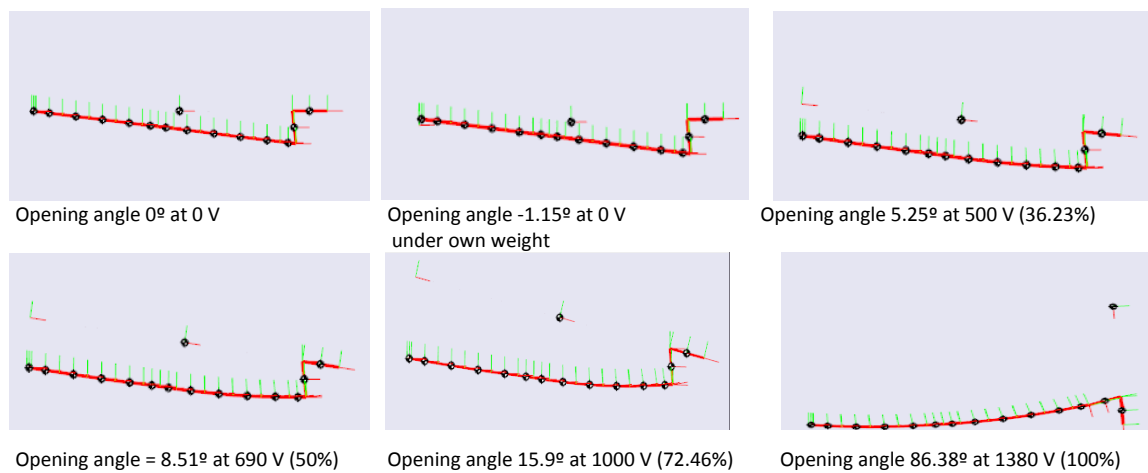
Fig. 4.1.21. Moving sequences of the Flaps A-TCM with the weight of 0.4 g, actuated with a sine signal

4.1.4.3. Simulation of A-TCM double layer active model of the flaps mechanism

The simulation model for the A-TCM flaps in differential design using double layer active cells with 1 DoF and 1 active prismatic joint is presented in the Fig. 4.1.23.a.
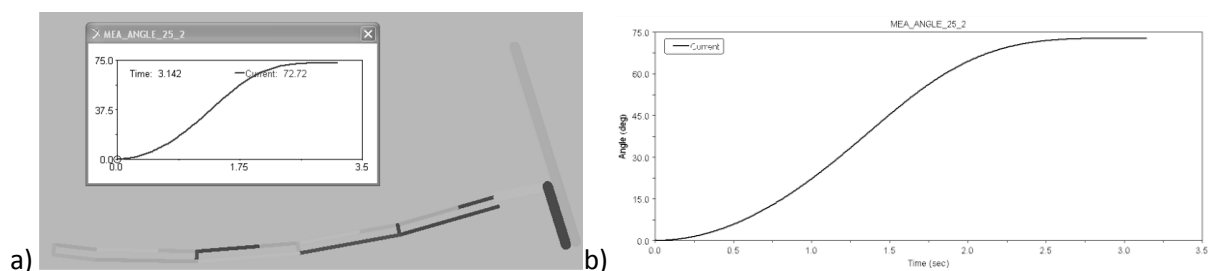
Fig. 4.1.22. Differential design A-TCM (a) simulation model with 1 DOF cells and 1 active prismatic joint (b) opening angle variation

The interface links are locked to the upper actuating link, in order to obtain the 1 DoF cell. The simulation results are presented in the Fig. 4.1.23.b. The final position and the flap's motion diagram obviously show a difference from the demonstrator movement. The mere 75° angle of deflection compared to the requested 90° (obtained by the demonstrator), show that the rigid model is not proper for this simulation case.

The model for a monolithic A-TCM with compliant coupler using double layer active cells with 2 DOF, 1 active prismatic joint and 1 concentrated rotational rigidity simulated by a torsion spring is presented in Fig. 4.1.23.

a)   b)
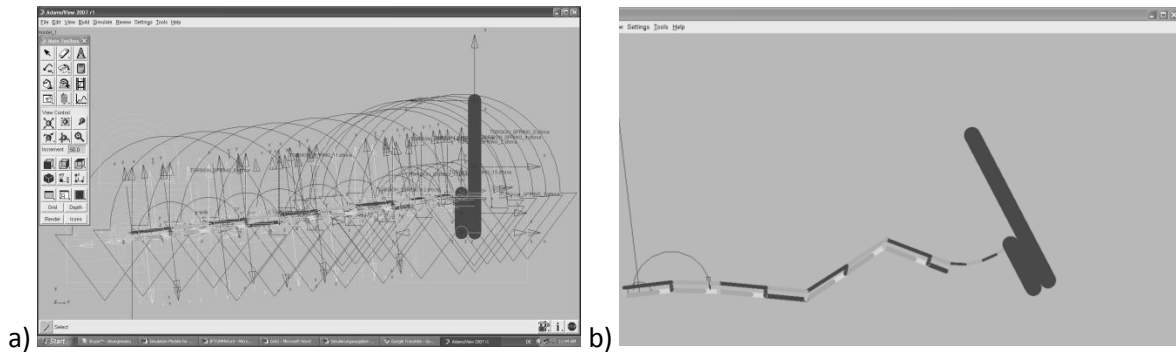
Fig. 4.1.22. Monolithic design A-TCM a) Simulation model with 2 DOF cells, 1 active prismatic joint and concentrated elastic stiffness in one joint; b) unstable movement due to insufficient rigidity of the model

The interface links are connected to the upper and lower layers by free rotational joints. Torsion springs are inserted in the joints between the interface and the lower layer. Their rigidity was arbitrarily given at 280 N mm/°, as they have no physical meaning, trying to add into account the elastic behavior of two material layers and the interface. Its proper value was intended to be obtained from simulation iterations. The compliant coupler is simulated by a series of links with rotational joints and 200 N mm/° rigidity torsion springs with a damping coefficient of 10 N mm s/°.

The reinforced middle section of the actuator element is simulated by two rigid layers connected to the interface by a 780 N mm/° torsion spring. Although this simulation model worked for the differential design, for the monolithic design it was a complete failure (see Fig. 4.1.22.b). The model buckled at the simulation beginning, due to its singularity position and improper rigidity. The variation of the equivalent rigidity had no or little effect on the simulation results.

The more complex model for the monolithic design with compliant coupler for the A-TCM flaps mechanism (Fig. 4.1.23) gives better results.

a)   b)

c)
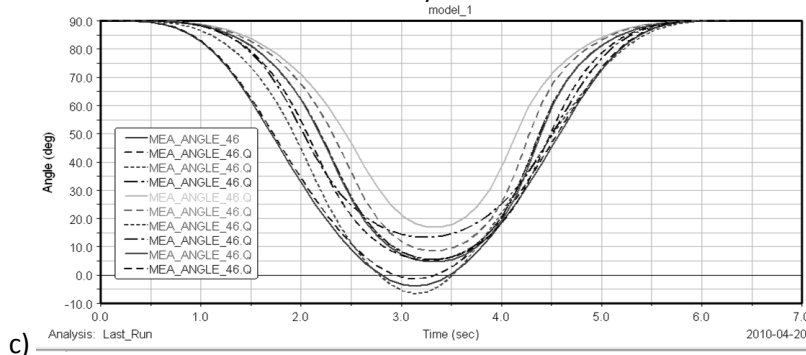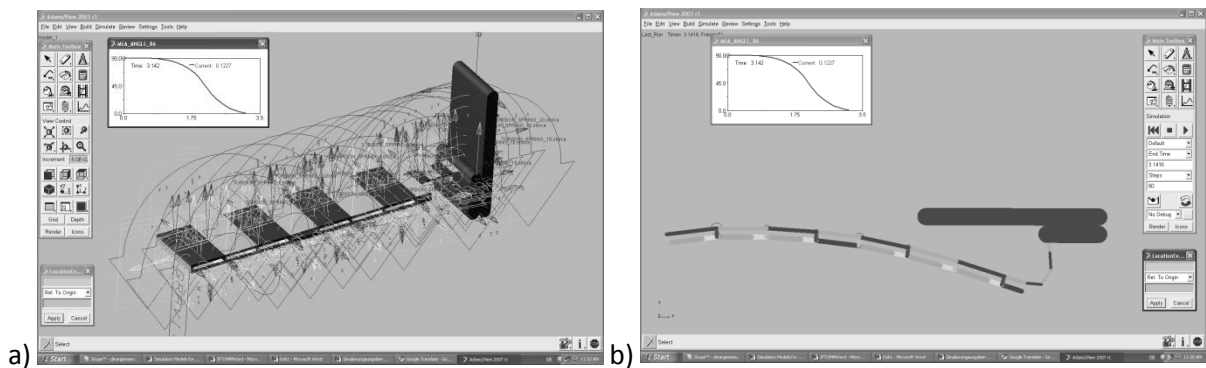
Fig. 4.1.23. Monolithic A-TCM design (a) simulation model, with 2 DOF cells, 1 active prismatic joint and 3 concentrated rigidities (b) (c) simulation results for the opening angle variation during actuation

The upper and the lower layers are provided with 370 N mm/° and 480 N mm/° torsion springs, respectively. These rigidities are determined according to the equation 6, with the values for the width and thickness and Young's modulus from the demonstrator, and the modeling cell's length of 30 mm. The interface rigidity simulating spring was added to the upper layer and set 5 N mm/°.

The simulation results are shown in Fig. 4.1.23.b. The value of the interface rigidity is obtained after a number of simulations, with the objective to achieve a 90° flaps angle. For 378.8 N mm/°, the model movement replicated with satisfactory precision the demonstrator's behavior.

Simulations performed using this models showed the important influence of all the physical and dimensional factors, including the damping in the equivalent joints.

4.1.5. Scientific contributions

The research proposes the redefinition of several basic terms in the mechanisms theory in order to include the elastic connections near the rigid elements. The elastic connection is redefined containing beside the rigid sections one or more elastic ones and proposes a classification of the elastic connections of type B similarly to the classification of the kinematic connections. Also, it was redefine the term of mechanism, implicitly the kinematic chain with elastic connections.

The computation of the degree of freedom of kinematic chains and the degree of freedom (mobility) of the mechanisms with elastic connections imposed the development of new formulae. For several mechanism structures with elastic connections, the structural analysis was exemplified.

The developed modeling concepts allow to asses in advance the behavior of A-TCM by multi-body dynamical simulation. This procedure may be performed in the initial design stage, as to obtain the initial dimensions for the mechanism. However, this step is followed by FEM simulations, in order to evaluate the strength of the structure and to refine the solution before the construction of the prototype. Thus, only with this continuous, synchronized approach, the high lightweight potential of active composite compliant mechanisms with integrated actuators can be fully exploited. The simulation models that take into account the piezoelectric effect are more reliable for the compliant active elements with high bending moment variation on their length. The double layer simulation model with 3DoF modeling cells with one active prismatic joint and torsion springs in the rotational joints gives the best results, as it has actuating and compliance properties and its parameters have physical meaning.

III. Academic and professional achievements

This section of the habiliation thesis mentions the main achievements of the candidate within the last 17 years after defending the PhD thesis in co-advisorship between University Politehnica Timişoara and Technical University Dresden, with the defende on 27th of February 1998 at TU Dresden and on 03 of June 1998 at PU Timişoara. From both universities I received the PhD diploma, the Romanian PhD diploma was confirmed by the Ministry of Education with the order 4090/03.07.1998. In September 1999 I was employed as Associate Professor at the University Politehnica Timisoara at the actual Department of Mechatronics.

I continued the teaching and research activities at the University Politehnica Timisoara. In the beginning, the teaching activities comprised "Mechanism Science" and "Programming and Using of Computers", continuing with teaching on "Intensive Therapy Biomedical Devices", "Prosthesis", "Advanced Robotics", "Special Structure of Robots" and "Service Robotics". The teaching classes were held in German and Romanian language. Beginning from 2011 I started to have concentrated classes at the TU Dresden about Mechanisms in Food Industry (presently, Mechanism Design).
In order to cover the course support I published several books addressed especially to the students, but also for specialists and researchers. In the following the title of the published books are listed:
1. Ioan Nicolae Văcărescu, Valeria Văcărescu, Erwin-Christian Lovasz, Marius Mateaş - Aparatură biomedicală (Biomedical Devices), Editura Mirton, 2001, ISBN 973-585-456-2 119.
2. Lovasz, Erwin-Chr. - Mechanismen in Verarbeitungsmaschinen (Mechanisms in Food Industry) – Studienbrief, TU Dresden Verlag, 2004.
3. Erwin-Chr. Lovasz, Cărăbaş, Iosif - Principii de sinteză a mecanismelor cu roţi dinţate şi came (Principles of the synthesis of the gears and cam mechanisms), Editura Politehnica, Timişoara, 2004, II Ed. 2006, ISBN 973-625-157-8.
4. Erwin-Chr. Lovasz - Getriebelehre II. Kurvengetriebe (Mechanisms II. Cam mechanisms), Editura Politehnica, 2008, ISBN 978-973-625-715-5.
5. Erwin-Chr. Lovasz - Mecanisme de tip centroidal (Centrode mechanisms), Editura Politehnica, 2009, ISBN 978-973-625-920-3.
6. Erwin-Chr. Lovasz, Corneliu Rădulescu - Robotică avansată (Advanced robotics), Editura Politehnica, 2013, ISBN 978-973-625-920-32011.

Beginning from 2011 I started to have concentrated classes at the TU Dresden, Germany about Mechanisms in Food Industry (now Mechanism Design). In 2000 during a teaching fellowship I taught in Hungarian language at the Szent István University in Gödölö, Hungary a course about Biomedical Devices. Last year in November I taught first time in English at the National Taiwan University of Science and Technology, Taipei, Taiwan the concentrated courses "Synthesis and Design of Cam Mechanisms".

The research activities were developed in parallel with the teaching activities in the same areas. The first research activities as project coordinator were in the field of mechanism science and biomechanical engineering. The grants were applied and successfully approved by the National Council of Scientific Research in Higher Education CNCSIS, in the call programs ANSTI and AT. These projects were continued with successfully approved projects for Excellence Centers CEEX, EU ICT-PSP FP7 as partner leader and CDI program of Romanian Space Agency as partner leader. In the following are shown the main projects developed under my coordination:

1. ANSTI Type T Gr 6153/2000, Code ANSTI 464, Studiul mecanismelor cu cuple cinematice de tip centroidal (Study of the mechanisms using centrode kinematic pairs), Lovasz E.-Chr. Project leader
2. CNCSIS Type AT 33501/2002 and 33550/2003, Proiectarea unui sistem asistat de calculator, destinat măsurării modificărilor antropometrice în urma efectuării de implanturi şi protezări (Designing a computer-aided system for measuring the changes in anthropometric after performing implants and prosthesis), Grant Tema 5 Cod 32, Lovasz E.-Chr. Project leader
3. Grant CEEX nr.88, 28.07.2006, Dezvoltarea şi implementarea unor sisteme performante de investigare şi recuperare a deformaţiilor de coloană vertebrală la populaţia de vârstă şcolară şi categorii profesionale cu activităţi sedentare (Development and implementation of advanced systems for investigation and recovery of spinal deformations in the school age population and professionals with sedentary activities), INBIRE, Lovasz E.-Chr. Project leader.
4. Project 250485/CIP-ICT-PSP-2009-3, Digital Mechanism and Gear Library goes Europeana, ThinkMOTION, Lovasz E.-Chr. UPT project parner leader.
5. Project CDI 113/19.11.2012, New Haptic Arm Exoskeletons for Robotics and Automation in Space, acronim EXORAS, Lovasz E.-Chr. UPT project partner leader.

In the same period I was involved in the University Politehnica research team of other 7 research projects nationally funded: CNFIS D 57/1998-2001, CNFIS C 148/1997-2001, CNCSIS A 33550/2003, CEEX I 03 21/2005-2007, PN II 72-197/2008, IDEI 1022/1998 and PNCDII 91-022/2007-2010. Also, I coordonated the developments and researches within the commisons no. 784/2007 with Takata Petri Romania SRL and BC 7/2010-2013 with ILK TU Dresden.

During my post-doctoral stages at TU Dresden I involved in 2 DFG research grants and 7 commisions with industrial applications:

1. DFG II D1 Go647/2-1/1999, Optimierung von Antriebssystemen in Verarbeitungsmaschinen durch Minimierung nichtlinear bewegter Massen. Lovasz E.-Chr. Project team member.
2. DFG II D1 Mo537/6-1, Mo537/5-2/2001-2003, Rechnergestützte Synthese von Räderkoppel-getrieben als Vorschaltgetriebe zur Erzeugung nichtlinearer Antriebsbewegungen. Lovasz E.-Chr. Project team member.
3. Commision, Audi AG, Ingolstadt, 2000, Optimierung der Höhensitzverstell-mechanismus für die Audi-Pkw. Lovasz E.-Chr. Project team member.
4. Commisíon, Spro BV, Vianen, 2002, Ersatz der S-Kurve durch ein neues kinematisches Prinzip. Lovasz E.-Chr. Project team member.
5. Commision, Hettich – ONI GmbH, Vlotho, 2002, Struktursynthese und Optimierung sechsgliedriger Koppelgetriebe für Scharnierbewegungen. Lovasz E.-Chr. Project team member.
6. Commisions 638, 654, 660, 674, Xenon Automatisierungs-technik GmbH, Dresden, 2002, Bestückungsautomat für Herstellung von Computerstecker, Lovasz E.-Chr. Project team member.

In 2005 I was employed for 5 mounths at TU Ilmenau in the DFG-Project, Digitale Mechanismen und Getriebe Bibliothek DMG-Lib and from 2008 to 2015 I contributed with researches in the DFG Collaborative Research Center SFB 639 Textile-reinforced composite components for function-integrating multi-material design in complex lightweight applications.

As a result of my reserch activity I registered in 2013 1 Trademark to OSIM, as follows:
1. A. Cipleu, A. Drăghici, G. Ciodaru, E.-Chr. Lovasz, Mecanism de direcţie cu camă plană (Steering mechanism with planar cam), RO 123472 B1, 2012

The publishing activity during this period as result of the research and development activities was very extensive, so I published 5 papers in ISI Journals, 11 papers in Scopus, Elsevier Science Direct

and Inspec indexed Journals, 24 papers indexed ISI Conference, 27 Scopus, IEEE and Springer indexed conferences and other 69 papers without indexing in different national and international conferences and IFToMM World Congresses. The ISI Journal indexed papers are the following:

1. Nemes D.I., Dragoi M., Poenaru D.V., Cretu O., Vermesan H., Prejbeanu R., Vermesan D., Popa D., Dragoi R., Suciu O., Surducan D., Nemes C., Lovasz E.-C. - Complex assessments and therapies of the secundary scoliosis in inflammatory rheumatic diseases, Arthritis and Rheumatism, 58 (2008) 736.
2. Modler K.-H., Lovasz E.-C., Bähr G., Neumann R., Perju D., Perner M., Margineanu D. - General method for the synthesis of geared linkages with non-circular gears, Mechanism and Machine Theory, 44(4) (2009) 726-738.
3. Lovasz E.-C., Modler K.-H., Neumann R., Gruescu C.M., Perju D., Ciupe V., Maniu I.: Novel design solutions for fishing reel mechanisms, Chinese Journal of Mechanical Engineering, 28(4) (2015) 726-736.
4. Hanke U., Lovasz E.-C., Zichner M., Modler N., Comsa A., Modler K.-H. - Synthesis of PR-/RP-chain-based compliant mechanisms – design of applications exploiting fibre reinforced material characteristics, Journal Mechanical Sciences, 6 (2015) 155-161.
5. Gruescu C. M., Garaiman A., Lovasz E.-C.: - Modeling of human spinal column and simulation of spinal deformities, Mechanika, 21(3) (2015) 214-219.

Begining from 2000 I was asked to review papers for Journals and Conferences. My first review was for the Mechanism and Machine Theory Juornal and continued with many other reviews for the same Journal (more than 15 reviews). Meanwhile, I reviewed many papers for the Journal Advanced Robotics Systems, ASME Journal Mechanism and Robotics, Journal of Mechanical Engineering Sciece, Robotics and Computer-Integrated Manufacturing, Textile Research Journal and recently for Arhive of Civil and Mechanical Engineering (more than 20 reviews). In 2015 I accepted to be Associate Editor by the Journal Advanced Robotics Systems. From 2009 I work as member of the scientific committtee of the University Journal "Bulletin of the Transilvania University of Brasov" and from 2013 as editorial office secretary for the International Journal "Robotica & Management".

In addition to the aformentioned I am involved in the national profesional organization ARoTMM (Romanian Association of Mechanism and Machine Science) associated to the International Federation of Mechanism and Machine Science IFToMM. I was elected in 2004 as member in the IFToMM Permanent Commision for Constitution and I worked in this Commision until 2011. My contribution in this international IFToMM PC recommended me to be elected in 2005 as scientifical secretary of the national organization ARoTMM and reelected for 3 other periods. In 2011 I was elected during the 13 IFToMM World Congress as chair of the Technical Committee Linkages and Mechanical Controls. I am currently in this position and I give my best to be very active in this professional organization, to promote the IFToMM activities as Conferences, Summer Schools and Tutorials and to develop briges between the enthusiastic scientist from countries all over the world. I gave scientifical support and advertised the national events of the countries affiliated to the professional organization IFToMM and I feel very enthusiastic to develop this activities.

Because my position in IFToMM I had the chance to organize as chair or as co-chair several international Conferences and to be editor of 5 books with the IFToMM Conference papers by Springer and Trans-Tech Publisher:

1. E.-Chr. Lovasz, B. Corves (Editors) - Mechanisms, Transmissions and Applications, Series: Mechanisms and Machine Science, Vol.3, Springer Verlag, 2011, ISBN 978-94-007-2726-7.
2. G. Gogu, I. Maniu, E.-Chr. Lovasz, J.-C. Fauroux, V. Ciupe (Editors) - Mechanisms, Mechanical Transmissions and Robotics, Series: Applied Mechanics and Materials, Trans Tech Publications, 2012, ISBN 978-3-03785-395-5.
3. V. Petuya, C. Pinto, E.-Chr. Lovasz (Editors) - New Advances in Mechanisms, Transmissions and Applications, Proceedings of the Second Conference MeTrApp 2013, Series: Mechanisms and Machine Science, Vol. 17, Springer Verlag, 2014, ISBN 978-94-007-7484-1.

4. E.-Chr. Lovasz, G. K. Ananthasuresh, B. Corves, V. Petuya (Editors) - Microactuators and Micromechanisms, Proceedings of MAMM 2014, Series: Mechanisms and Machine Science, Vol. 30, Springer Verlag, 2014, ISBN 978-3-319-15861-7.
5. B. Corves, E.-Chr. Lovasz, M. Hüsing (Editors) - Mechanisms, Transmissions and Applications, Proceedings of the Third MeTrApp Conference 2015, Series: Mechanisms and Machine Science, Vol.31, Springer Verlag, 2015, ISBN 978-3-319-17066-4.

I am involved also in other two profesional organizations: SRR Romanian Society of Robotics (up 2000) and VDI -Verein Deutscher Ingenieure (up 1996).

During the mentioned period I visited for scientifical purposes many universities from Europe, Asia and America: Technische Universität Dresden, Germany, Technical University of Liberec, Cech Republic, Technische Universität Chemnitz, Germany, University of Praga, Cech Republic, Gödöllöi Agrartudomanyi Egyetem, Hungary, University of Oulu, Finland, University of Nis, Serbia, University of Bonn, Germany, Technische Universität Braunschweig, Germany, Technische Universität Ilmenau, Germany, RHWT University Aachen, Germany, Technical University of Tianjin, China, University Franche-Comté LMARC Besancon, France, University of applied science Osnabrück, Germany, University of technology HAMK, Finland, University of Guanajuato, Mexic, Institut Français de Mécanique Avancée IFMA, France, University of Basque Country Bilbao, Spain, Tokyo Institute of Technology, Japan, Università degli Studi di Cassino e del Lazio Meridionale, Italy, University of Minho, Guimarães, National Taiwan University of Technology and Science, Taiwan, Izmir Institute of Technology, Turkey.

After the PhD presentation I received several post-doc and teaching fellowships in Germany, Hungary, Italy and Taiwan:
1999   Pro Renovanda Cultura Fellowship, Gödöllöi Agrartudomanyi Egyetem, (4 weeks)
2001-2002 Humboldt Research Fellowship, Roman Herzog Project, Technische Universität Dresden
up 2004   Erasmus Teaching Fellowships, Technische Universität Dresden, (anual 2-4 weeks)
2014   Teaching Fellowship, National Taiwan University of Technology and Science, (1 week)
2015   Erasmus Teaching Fellowships, University of Cassino, (1 week)

To the academic and professional career I added also a managerial activity through my election as Head of the Mechatronics Department of the University Politehnica Timisoara for 2 periods, from 2008 up today.

IV Career evolution and development plans

The mentioned scientific achievements in my research fields of mechanisms, robotics and mechatronics and other achievements in the field of biomechanical engineering will form the basis of the further career development plans. The mentioned research fields are important issues in many areas of the EU Framework Programme for Research and Innovation HORIZON 2020, because they focus on the product oriented research projects. My personal scientific achievements and topics were always oriented to improving and development of machines, equipment and devices.

The own career evolution and development plans will be shown in the following sections: key research directions, objectives, planned activities and financial and human resources.

A. Key research directions

The next researches will be oriented on several key directions and research areas:

1. Robotic and Mechatronics

- development of new parallel manipulators and improvement of the mechanical design and control of the new and existing structures. All the theoretical developments will be connected with industrial and service applications;
- development of the modular reconfigurable robots with high versatility, robustness and low costs. The robots should be developed for personal use, rescue in case of fire and disasters, space use, food industry, agriculture and should cover requirements of the society or industry.
- improvement and development of the arm and leg haptic exoskeletons for use in space applications, rehabilitation, teleoperation and others.

2. Mechanism science

- development of the analysis and synthesis methods for special mechanisms with minimum number of elements for specific industrial applications, mainly in the food and textile machines, automation of flexible manufacturing cells, sport and hobby equipment and others.
- development of synthesis and analysis methods for compliant mechanisms using textile reinforced composite materials with function integration and development of efficient simulation models by using of equivalent mechanism structure with higher degree of freedom, in order to implement the rigidity, damping and hysteresis characteristic of the materials.
- improvement of the classical mechanism structure regarding the minimum size, reduction of the energy consumption, force distribution, efficiency, wear, improving the dynamical behaviour.

3. Mechanics and Biomechanical Engineering

- developing of new flexible automated equipment and procedure for rehabilitation with quantitative evaluation of the cure progress for the leg, arm and spinal columns.
- development of the 3D body scanning facilities for reconstruction in the facial, breast and orthopaedic surgery in order to improve just in time the geometric and aesthetic parameters of the surgical act.

- researches for superposing of the 3D body surface scanned images with the computerised tomography or magnetic resonance scanning, in order to give more details about the medical investigation and to have an appropriate diagnosis.
- development and improvement of the upper and lower limb prosthesis and the hand prosthesis using new developments in the field of mechanics and automation.

B. Objectives

The pursued objectives in my career development will be classified in two major categories:

a)   short term goals

- developing the research group in field of Mechatronics and Robotics and starting the construction together with other PhD advisors of a new Doctoral Field of Mechatronics and Robotics inside of the Doctoral School of UPT – IOSUD;
- improving and development of the Mechatronics & Robotics Research Lab - MeRob, which I founded in one room of the Mechatronics Department in 2013 with more equipment and facilities. Actually, many bachelor and master students are involved in the Lab to prepare their bachelor thesis and master dissertation.
- using and extending the cooperation with the researchers and professors from both Romania and abroad for connecting the researches on the highest level. Actually, through my scientific connections with many top Universities in Europe and Asia, and from my position in the IFToMM I have already developed many common researches.
- participation in several consortiums for preparing proposals for EU HORIZONT 2020 projects and national research and structural grants.
- attracting as PhD students of the best students and developing the topic of the PhD study according with the running projects and grants. Also I intend to develop co-supervising with professors from abroad to replace the missing experimental facilities from the Lab.
- attracting of commissions and developing of projects with domestic and multinational companies from Timisoara and Romania.

b)   long term goals

- accreditation of the new Doctoral Field of Mechatronics and Robotics inside of the Doctoral School of UPT – IOSUD;
- accreditation and recognition of the Mechatronics & Robotics Research Lab –MeRob on national and international level, with high level research results;
- preparing of strategic project proposals for EU projects, bilateral country projects and national research grants.
- development of a network with professors and researchers from Romania and abroad to correlate and connect the research results on the highest level. Actually the IFToMM TC Linkages and Mechanical Control, which I chair, prepare an online easy-chair to review and award the best annual international PhD thesis in the Mechanism and Machine Science field;
- attracting of European and foreign PhD students for enriching and exchanging the research field knowledge. Developing of a worldwide network for supervising or co-supervising of PhD students in the expertise field of the PhD supervisors.
- founding of a research network with the researcher groups from the companies to orienting the PhD topic appropriate to the research and development interest of them.

C. Planed activities

In order to achieve the previous proposed objectives several activities should be developed:

- documentation and preparing the required conditions for developing and accreditation of the new Doctoral Field of Mechatronics and Robotics inside of the Doctoral School of UPT – IOSUD;
- documentation and preparing the required conditions for accreditation of the Mechatronics & Robotics Research Lab – MeRob on national and international level;
- continuously developing of the devices and equipment in the Lab and own development of the prototypes for the considered applications;
- founding of research rooms with the necessary infrastructure for the PhD and interested master students;
- permanent connection and research exchanges with the researchers and professors from both Romania and abroad for discussion and preparing of new research topics;
- maintaining of an important role and giving a great contribution to the professional association IFToMM, to be in touch with the new research areas in the field of Mechanism and Machine Science, Robotics, Mechatronics and Biomechanical engineering;
- preparing and sending of own or joint papers with the news research results to major Journals with topic in the related research field and the IFToMM supported conferences;
- contribution to reviewing papers in major Journals and Conferences;
- participation of PhD students at several Summer Schools to improve their knowledge;
- preparing and applying in several consortiums for proposals for EU HORIZONT 2020 projects, bilateral collaborations and national research or structural grants.
- developing of a multinational ERASMUS + project for exchange of the PhD students between the participant PhD advisors;
- developing of bilateral agreements or department/university agreements for exchanging of PhD, master and bachelor students, but also research and teaching staff.
- developing of commission agreements with domestic and multinational companies from Timisoara and Romania.
- publishing of new books improved with the newest research results and improving the quality of the teaching activity.

D. Financial, human and infrastructure resources

A very important issue to reach the previous objectives consists in the assuring the financing of the research activities and motivation of the research staff composed on one side of PhD and master students and on the other side of the research and teaching staff. The planned activities showed realistic proposals to cover through running projects or commissions, ERASMUS + program and university grants, the research activities of the PhD students. The human resources should include the own research and teaching staff with competences in the research area in the research activities. The research Lab infrastructure purchased during the previous and the next research projects and collaboration projects will constitute the research equipment and devices for developing the experimental research activities. For the research activities can be used several software programs, which are used also in the teaching activities (ProEng, Matlab-Simulink, AutoCAD, Solid Works, etc.). The missing experimental research facilities will be supplied by collaboration with Universities from abroad.

V References

1. P.A. Chebychev Théorie des mécanismes connus sous le nom de parallélogrammes, 2ème partie Mémoires Présentés à l'Académie Impériale des Sciences de Saint-Pétersbourg par divers savants, (1869).

2. M. Grübler, Allgemeine Eigenschaften der Zwangläufigen ebenen kinematischen Ketten, Part I, Zivilingenieur, 29 (1883) 167-200.

3. M. Grübler, Allgemeine Eigenschaften der Zwangläufigen ebenen kinematischen Ketten, Part II, In: Verein zur Beförderung des Gewerbefleisses. Verhandlungen, 64 (1885) 179-223.

4. K. Kutzbach, Mechanische Leitungsverzweigung, ihre Gesetze und Anwendungen, Maschinenbau, Betrieb., 8, (1929) 710-716.

5. V.V. Dobrovolski, Theory of Mechanisms, Moskow, (1951).

6. I.I. Artobolevskii, Theory of Mechanisms and Machines, Moskow, (1953).

7. K. Hain, Periodische Bandgetriebe, VDI-Zeitschrift 95(6) (1953) 192-196,

8. U. Olsson, Non-Circular Cylindrical Gears. Acta Polytechnica Mechanical Engineering Series, 135 2(10) (1953) 1-216.

9. K. Hain, Feder-Getriebe und Band-Getriebe für den Kraftausgleich, VDI-Zeitschrift 97(9) (1955) 278.

10. B. Dizioglu, Zur Dynamik des einfachen Bandgetriebes mit Anwendung auf die Synthese der Schlagmechanismen der Webstühle, VDI-Berichte 12 (1956) 55-62.

11. K. Hain, Einfache Bandgetriebe, Düsseldorf, VDI Verlag, 461 (1957) 40-55.

12. R. Beyer, T.P. Goodman, Beschleunigungsermittlung in Bandgetrieben und Zahnstangen - Kurbelgetrieben, Konstruktion 10(1) (1958) 10-16.

13. T.P. Bolotovskaia, I.A. Bolotovski s.a., Spravocinik po gheometrice skomurascetu evolventnih-zubciatihi cerviacinih peredaci, Gosudarstvenie naucino tehniceskoe izdatelistvo masino stroitelinoi literaturi, Moskva, (1963).

14. F. Freudenstein, E.J.F. Primrose, Geared five-bar motion. Trans. ASME, 85E, J.App.Mech. 30 (1963) 161-75.

15. S. A. 0leksa, D. Tesar, 1963, Multiply separated position design of the geared five-bar function generator. Trans. ASME, J. Eng. Ind., (1963) 298-305

16. F. Reuleaux, The kinematics of machinery. Dover, New York, (1963).

17. B. Roth, F. Freudenstein, Synthesis of path-generating mechanisms by numerical methods. Trans. ASME, J. Engng. Ind., 30 (1963) 298-305.

18. I.I. Artobolevski, Mechanism theory (Theory mehanizmov), Izdatelsvo Nauka, Moskva, (1965).

19. K.J. Waldron, The constrain analysis of mechanisms, J. of Mechanisms, 1(2) (1966) 101-114.

20. N.P. Chirinois, Gear Design and Application, McGraw-Hill, New York, (1967).

21. L.L. Leroux, Moulinet de peche a recuperation irreguliere, Brevet d'Invention P. V. nr. 123.967. Nr. 1.546.730, A01k, Bulletin Officiel de la Propriete Industrielle nr. 47, France, (1968).

22. I. Manolescu, For a united point of view in the study of the structural analysis of kinematic chains and mechanisms, Journal of Mechanisms, 3(3) (1968) 149-169.

23. F.V. Kovács, Contributii la elaborarea unei metode unitare de sinteza a mecanismelor (Contribution to the elaboration of a unitary method for mechanisms synthesis), Ph. D. Thesis, Polytechnic Institute "Traian Vuia" Timişoara, (1969).

24. W. Wunderlich, Contributions to the Geometry of Cam Mechanisms with Oscillating Followers, Journal Mechanisms, 6 (1971) 01-20.
25. N. Manolescu, F. Kovacs, A. Orănescu, Mechanisms and Machine Theory (Teoria mecanisme-lor şi a maşinilor), Ed. Didactică şi Pedagogică, Bucureşti, (1972).
26. P. Antonescu, Extending of structural formula of Dobrovolski to the complex mechanisms with apparent family, Proc. SYROM´73, 2 (1973) 1-10.
27. F.V. Kovács, D. Perju, G. Savii, Metode noi in sinteza mecanismelor (New methods in mechanisms' synthesis), Editura Facla, Timişoara, (1976).
28. M. Horani, Untersuchungen zur Analyse und Synthese zykloidengesteuerter Zweischläge, Dissertation, TU Dresden, (1977).
29. R. Neumann, Hochübersetzende Getriebe, Maschinenbautechnik, 26(7) (1977) 297-305.
30. J.M. Hervé, Analyse structurelle des mécanismes par groupe des déplacements, Mechanism and Machine Theory, 13(4) (1978) 437-450.
31. J. Volmer, Getriebetechnik, Koppelgetriebe. VEB Verlag Technik Berlin, 1. Auflage (1979).
32. I. G. Goryacheva, Contact Mechanics in Tribology, Kluwer Academic Publishers, Dordrecht, The Netherlands, (1980).
33. A. Gronowicz, Identifizierungsmethode der Zwanglaufbedingungen von kinematischen Ketten, Mechanism and Machine Theory, 16(2) (1981) 127-135.3.
34. V.R. Miller, Trip lever guide system, US 112912, 01 K 89/01, USA, (1981).
35. VDI 2727 Blatt2, Konstruktionskataloge; Lösung von Bewegungsaufgaben mit Getrieben; Erzeugung hin- und hergehender Schubbewegungen; Antrieb gleichsinnig drehend (Catalogues for machine design; Mechanisms for motion transfer. Converting unidirectional rotation into rectilinear alternate motion), Berlin, Beuth Verlag, (1981) (revised ed. 2015).
36. R. Neumann, Fünfgliedrige Räderkoppelgetriebe für große Schwingwinkel, Conference Dynamic und Getriebetechnik, TU Dresden, (1985).
37. R. Neumann, Fünfgliedrige Räderkoppel-Schrittgetriebe, Habilitation, TU Dresden, (1986).
38. K. Hain, Zweiräder-Punktrasstgetriebe, Ind. Anz. 11 (1987) 23.
39. R. Neumann, Fünfgliedrigen Räderkoppel-Schrittgetriebe, Aufbau, Synthese, Eigenschaften, Maschinenbautechnik, 36(10) (1987) 456-459.
40. D. Perju, Mechanisms with Variable Link Length, Proceedings of the VII IFToMM World Congress on TMM, Sevilla, Spain, 1 (1987) 107-110.
41. H. Rankers, Rückkehrender Koppelrädermechanismus mit Doppelschleife, Konstruktion, 39(9) (1987) 335-357.
42. J. Angeles, C. Gosselin, Determination du degre de liberte des chaines cinematique, Transactions of the Canadian Society for Mechanical Engineering, 12(4) (1988) 219-226.
43. J. Angeles, C. Lopez-Cajun, Optimal Synthesis of Cam Mechanism with Oscillating Flat-Face Followers, Mechanisms and Machine Theory, 23(1) (1988) 1-6.
44. D. Zlatanov, Generalized singularity analysis of mechanisms, PhD thesis, Department of Mechanical and Industrial Engineering, University of Toronto (1988).
45. H. Kazerooni, Design and Analysis of the Statically Balanced Direct-Drive Robot Manipulator, Robotics and Computer-Integrated Manufacturing, 6(4) (1989) 287-293.
46. F. Litvin, Theory of Gearing, NASA Publication, Washington DC, (1989).
47. G. Feng, Complete Shaking Force and Shaking Moment Balancing of 26 Types of Four-, Five- And Six-Bar Linkages with Prismatic Pairs, Mechanism and Machine Theory, 25(2) (1990) 183-192.
48. K. Luck, K.–H. Modler, Getriebetechnik: Analyse, Synthese, Optimierung. Springer, Berlin, (1990).
49. I.S. Kochev, General method for active balancing of combined shaking moment and torque fluctuations in planar linkages, Mechanism and Machine Theory 25 (1990) 679-687.
50. D. Perju, Mecanisme de mecanică fină (Mechanism for Precision Mechanics), vol. 1 and 2. Lito. UP Timişoara, Romania, (1990).

51. J. Angeles, C. Lopez-Cajun, Optimization of Cam. Mechanisms, Kluwer Academic Publishers, Dordrecht, (1991).

52. F. Freudenstein, C.K. Chen, Variable-ratio chain drives with noncircular sprockets and minimum Slack-theory and application, ASME, Journal of Mechanical Design 113 (1991) 253-262.

53. H. Hutten, Biomedizinische Technik, Springer, Graz, (1991).

54. G. Dittrich, Ellipsenrädergetriebe, Konstruktion, (1992).

55. T. Emura, A. Arakawa, A new steering mechanism using non circular gears, JSME International Journal, Series III, 35(4) (1992) 604–610.

56. K. Luck, K.-H. Modler, Burmester -Theory for Band-Mechanisms, In Mechanical Design and Synthesis, ASME, 46 (1992) 55-59.

57. D. A. Streit, E. Shin, Equilibrators for Planar Linkages, Transactions of the ASME, Journal of Mechanical Design, 115 (1993) 604-611.

58. W. Baumgartmer, D. Hamann, Fishing Reels with a Spool Receiving the Fishing Line, 5,350,131. A01k 89/015, USA, (1994).

59. T.H. Massie, J.K. Salisbury, The PHANTOM Haptic Interface: A Device for Probing Virtual Objects. Proc. of ASME Winter Annual Meeting, Symposium on Haptic Interfaces for Virtual Environment and Teleoperator Systems, Chicago IL, (1994) 1–6.

60. Z. Ye, M.R. Smith, Complete Balancing of Planar Linkages by an Equivalence Method, Mechanism and Machine Theory, 29(5) (1994) 701-712.

61. G. Leusch, Ein Beitrag zur Systematisierung und Maßsynthese ebener ungleichmäßig übersetzender Getriebe mit bereichsweise annähernd konstanter Übersetzung. Fortschritt-Berichte VDI: Reihe 1, Konstruktionstechnik, Maschinenelemente; 248 (1994).

62. F. Litvin, Applied theory of gearing: state of the art, ASME Journal of Mechanical Design, 117 (1995) 128–134.

63. K. Luck, K.-H. Modler, Getriebetechnik - Analyse, Synthese, Optimierung, Springer-Verlag, Berlin – Heidelberg, 2. Auflage, (1995).

64. J.J. Ryall, Fishing reel with improved spool disconnect, one-way lock and drag mechanisms, US5407144 A, USA, (1995).

65. S.L. Chang, C.B. Tsay, L.I. Wu, Mathematical model and undercutting analysis of elliptical gears generated by rack cutters, Mechanism and Machine Theory 31 (7) (1996) 879–890.

66. A B.-J. Hugnell, S. Björklund, S. Andersson, Simulation of the mild wear in a cam-follower contact with follower rotation, Wear, 199 (1996) 202-210.

67. G. Merziger, G. Mühlbach, D. Wille, T. Wirth, Formeln und Hilfen zur Höheren Mathematik, Binomi-Verlag, Springer, (1996).

68. K.C. Ludema, Friction, Wear, Lubrication, CRC Press, Inc. Florida, (1996).

69. D. Perju, I. Nicoara, E.-C. Lovasz, E. Creţu, Mecanism programator cu elemente de lungime variabila, Proc. of the 7-th national Symposium, MTM'96, Timisoara, (1996).

70. Q. Yu, H.P. Lee, Optimum Design of Cam Mechanisms with Flat-Face Followers, Mechanics Research Communication, 23(2) (1996) 181-187.

71. J. Zanon, Fishing Reel with Compensated Storage, 5,513,814. A01k 89/01, United States, (1996).

72. D. B. Dooner, Use of Noncircular Gears to Reduce Torque and Speed Fluctuations in Rotating Shafts, Journal of Mechanical Design 119 (1997) 299 – 306.

73. K.-H. Modler, E.-C. Lovasz, Viergliedrige Bandgetriebe als Übertragungsgetriebe. Proceedings of SYROM`97, Bucuresti, 1 (1997) 209-216.

74. D. Perju, V. Mesaros-Anghel, E.-C. Lovasz, On the kinematik analysis of the variable links length mechanisms, Proceedings of SYROM`97, Bucuresti, 1 (1997) 241-248.

75. C. Wadewitz, Ein Beitrag zur Analyse und Synthese von einfachen viergliedrigen Bandgetrieben, PhD Thesis, Dresden, (1997).

76. S.L. Chang, C.B. Tsay, Computerized tooth profile generation and undercut analysis of noncircular gears manufactured with shaper cutters, Journal of Mechanical Design, ASME Transactions 120 (1998) 92–99.

77. W.J. Elspass, M. Flemming, Aktive Funktionsbauweisen: Eine Einführung in die Struktronik, Springer-Verlag Berlin Heidelberg New York, (1998).

78. H. Dietl, R. Kaitan, R. Pawlik, P. Ferrara: C-Leg – Ein neues System zur Versorgung von Oberschenkelamputationen, Orthopädie-Technik, 3 (1998) 197-221.

79. T. Hasse, Auslegung ungleichförmiger Bewegungsgetriebe mit unrunden Zahnrädern und steuerbarem Antrieb unter Berücksichtigung der Bilanz der kinetischen Energie, VDI-Berichte, 1423 (1998) 171-192.

80. E.-C. Lovasz, Synthese der Übertragungsgetriebe mit Anwendungen in der Feinmechanik, PhD Thesis, Dresden/Timişoara (1998).

81. K.-H. Modler, C. Wadewitz, E.-C. Lovasz, Viergliedrige Bandgetriebe und ihre Anwendungen, VDI Verlag, 1423 (1998) 289-308.

82. P.A. Simionescu, A unified approach to the assembly condition of epicyclic gears, ASME Journal of Mechanical Design 120 (1998) 448–452.

83. T. Suga, O. Kameyama, R. Ogawa, M. Matsuura, H. Oka, Newly designed computer con-trolled knee-ankle-foot orthosis (Intelligent Orthosis), Prosthetics and Orthotics International, 22 (1998) 230-239.

84. S.H. Tong, D.C.H. Yang, Generation of noncircular pitch curves, ASME Journal of Mechanical Design 120 (1998) 337–341.

85. K. Wyrwa, R. Braune, Unrunde Zahnräder – Auslegung, Herstellung, Einsatzmöglichkeiten, VDI-Berichte, 1423 (1998) 107-130.

86. I. Doroftei, A. Preumont, Development of an autonomous micro walking robot with articulated body, Proc. of the 2nd International Conference on Climbing and Walking Robots, CLAWAR 99, Portsmounth, England, (1999) 497-507.

87. C. Duca, Basics in Cam Mechanisms Design (Bazele proiectării mecanismelor cu came), Ed. Gh. Asachi, Iasi, (1999).

88. U. Gnasa, K.-H. Modler, E.-R. Richter, Mechanismen zur Kraftübertragung bei hydraulisch angetriebenen Manipulatoren. 44. Internationales Kolloquium, TU Ilmenau, 20-23 September, (1999) (online).

89. F.E. Joutras, R.J. Hruska Jr., Exercise Apparatus and Technique. US005954621A. 5,954,621. A63B 21/021. (1999).

90. T. Laliberte, C. M. Gosselin, M. Jean, Static Balancing of 3-DOF Planar Parallel Mechanisms, IEEE/ASME Transactions on Mechatronics, 4(4) (1999) 363-377.

91. W. Long-Iong, W. Shiau-Huei, Y. Hong-Sen, Simplified graphical determination of disk-cam curvature, Mechanism and Machine Theory, 34 (1999) 1023-1036.

92. R. L. Williams, A. R. Joshi, Planar Parallel 3-RPR Manipulator, Proceedings of the 6-th Conference on Applied Mechanisms and Robotics, Cincinnati OH, (1999), 1–8.

93. J. Wang, C. M. Gosselin, Static Balancing of Spatial Three-Degree-of-Freedom Parallel Mechanisms, Mechanism and Machine Theory, 34(3) (1999) 437-452.

94. D.C.H. Yang, S.-H. Tong, J. Lin, Deviatione-Function based Pitch Curve Modification for Conjugate Pair Design, Journal of Mechanical Design, 2 (1999) 579–586.

95. G. Figliolini, C. Lanni, M. Ceccarelli, On kinematic synthesis of non-circular gears, International Journal of Gearing and Transmissions 3 (2000) 90–98.

96. T. Hasse, Unrundgetriebe mit deckungsgleichen unrunden Zahnrädern für typische Getriebeaufgaben, Konstruktion, 52 (11/12) (2000) 64–69.

97. K.-H. Modler, E.-C. Lovasz, Verstellmöglichkeiten in Bandgetriebe, Proceedings of MTM 2000, Timişoara, 1 (2000) 179-184.

98. T.A. Stolarski, Tribology in Machine Design, Butterworth-Heinemann, Oxford OX2, (2000).

99. H. von Wilmsdorff, H. Stinus, Biomechanik und Beurteilung des mikroprozessorgesteuerten Exoprothesenkniegelenkes C-Leg, Zeitschrift für Orthopädie und ihre Grenzgebiete, 138 (2000) 278-282.

100. U. Gnasa, Virtuelle Entwicklung von Gelenkarmmechanismen, Dissertation, TU Dresden (2001).

101. J.-C. Habumuremyi, I. Doroftei, Mechanical design and MANFIS control of a leg for a new deminig robot, Proceedings of the 4th International Conference on Climbing and Walking Robots, CLAWAR'2001, Karlsruhe, Germany, (2001) 457-464.

102. L.L. Howell, Compliant Mechanisms, New York Wiley & Sons, (2001).

103. D.H. Jeong, Vorrichtung zum Führen einer Hin- und Herbewegung einer Spule in einer Wickelrolle[P], DE 101 11 355 A1. B65 H54/28, Germany, (2001).

104. D.H. Nilsen, Drive mechanism for a fishing reel, US 6,254,020 B1. USA, (2001).

105. K. Wyrwa, Auslegung von Unrund-Zahnradpaaren, Unrund-Zahnriemengetrieben und Kurven-Rollensterngetrieben. Dissertation 2000, VDI-Fortschrittberichte, VDI Reihe 1 (347), Düsseldorf: VDI Verlag (2001).

106. B.W. Bair, Computerized tooth profile generation of elliptical gears manufactured by shaper cutters, Journal of Materials Processing Technology 122 (2002) 139-147.

107. I. Bonev, Geometric analysis of planar mechanisms, PhD thesis, Department de Genie Mecanique, Faculte des Sciences et de Genie, Universite Laval, Quebec (2002).

108. E. Colon, P. Hong, J.-C. Habumuremyi, I. Doroftei, Y. Baudoin, H. Sahli, D. Milojevic, J. Weemaels, An integrated robotic system for antipersonnel mines detection, J. of Control Engineering Practice, 10 (2002) 1283-1291.

109. W. Hufenbach, M. Gude, Analysis and optimisation of multi-stable composites under residual stresses, Composite Structures, 55 (2002) 319–327.

110. E.-C. Lovasz, K.-H. Modler, C. Hollman, Auslegung der Räderkoppelgetriebe mit linearem Antrieb. 47. Internationales Kolloquium, TU Ilmenau, 23-26 September, (2002) (online).

111. R.Q. Van der Linde, P. Lammertse, E. Frederiksen, B. Ruiter, The HapticMaster, a new high-performance haptic interface, Proceedings of Eurohaptics Conference, (2002) 1-5.

112. G.D. Caldwell, G.N. Tsagarakis, Development and Control of a 'Soft-Actuated' Exoskeleton for Use in Physiotherapy and Training, Autonomous Robots, 15(1) (2003) 21-33.

113. T.G. Ionescu Terminology for mechanisms and machine science, Mechanism and Machine Theory, 38 (2003).

114. P. Lindholm, S. Björklund, M. C. Cortes, Characterisation of wear on a cam follower system in a diesel engine, Wear, 254 (2003) 1199–1207.

115. R.E. Stiner, Reel Mechanism with Line Tension/Fish Weight Indicator, US 6,591,222 B2, USA, (2003).

116. Y.A. Yao, H.S. Yan, A new method for torque balancing of planar linkages using non-circular gears, Proceedings of the Institution of Mechanical Engineers Part C—Journal of Mechanical Engineering Science 217 (2003) 495–503.

117. K. Waldron, G.L. Kinzel, Kinematics, Dynamics and Design of Machinery, J. Wiley, (2003).

118. S. K. Agrawal, A. Fattah, Gravity-Balancing of Spatial Robotic Manipulators, Mechanism and Machine Theory, 39(12) (2004) 1331–1344.

119. Y. Bar-Cohen (ed.), Electroactive Polymer (EAP) Actuators as Artificial Muscles: Reality, Potential, and Challenges, SPIE PRESS. Bellingham, Washington USA, 765, (2004).

120. V. Hayward, O.R. Astley, M. Cruz-Hernandez, D. Grant, G. Robles-De-La-Torre, Haptic interfaces and devices, Sensor Review, 24(1) (2004) 16–29.

121. F. Litvin, Gear Geometry and Applied Theory, Cambridge University Press, (2004).

122. E.-C. Lovasz, I. Cărăbaş, Synthesis Principles of Gears and Cam Mechanisms (Principii de sinteză a mecanismelor cu roţi dinţate şi came), Ed. Politehnica Timişoara, (2004).

123. C.A. Mattson, L.L. Howell, S.P. Magleby, Development of Commercially Viable Compliant Mechanisms Using the Pseudo-Rigid-Body Model: Case Studies of Parallel Mechanisms, J. of Intelligent Material Systems and Structures, 15(3) (2004) 195-202.

124. K.-H. Modler, C. Hollmann, E.-C. Lovasz, D. Perju: Geared Linkages with Linear Displacement Actuator Used as Function Generating Mechanisms, Proc. of the 11-th IFToMM World Congress, Tian Jin, 01.04-05.04.2004, 1 (2005) 1254-1259.

125. Okuma Fishing Tackle CO. Ltd, Angelrolle, DE 202 20 624 U1, A01K 89/01, Germany, (2004).

126. D. Perju, K.-H. Modler, E.-C. Lovasz, V. Mesaros-Anghel, On the mechanisms´ synthesis of geometrical and static equilibrium conditions, Proc. of the 9-th international Symp. MTM'2004, Acta Technica Napocensis, Series: Applied Mathematics and Mechanics, 48(1) (2004) 155-161.

127. G. Bär, Skript zur Vorlesung „Ebene Kinematik", TU Dresden, Fak. MN, (2005).

128. G.A. Danieli, D. Mundo, New developments in variable radius gears using constant pressure angle teeth, Mechanism and Machine Theory, 40 (2) (2005) 203-217.

129. Gogu G.: Mobility of mechanisms: a critical review, Mechanism and Machine Theory 40 (2005) 1068-1097.

130. G. Gogu, Chebychev-Grübler-Kutzbach's criterion for mobility calculation of multi-loop mechanisms revisited via theory of linear transformations (Review), European Journal of Mechanics, A/Solids, 24(3) (2005) 427-441.

131. E.-C. Lovasz, D. Perju, I. Cărăbaş, E.S. Zăbavă, K.-H. Modler, On the synthesis of the cam mechanisms with tangential oscillating follower, Proceedings of the IX-th International Symposium SYROM´05, Ed. Printech, Bucharest, 2 (2005) 81-86.

132. E. Ottaviano, M. Ceccarelli, G.A. Danieli, D. Mundo, Analysis of non-circular gears and cam-follower systems as function generators, in: MUSME Conference, the International Symposium on Multibody Systems and Mechatronics, Uberlandia, Brasil, March 6–9, (2005).

133. G. Alici, B. Shirinzadeh, Optimum Dynamic Balancing of Planar Parallel Manipulators Based on Sensitivity Analysis, Mechanism and Machine Theory, 41(12) (2006) 1520–1532.

134. J.K. Anderson, L.L. Howell, J.W. Wittwer, T.W. McLain, Piezoresistive sensing of bistable micro mechanism state, J. of Micromechanics and Microengineering, 16 (2006) 943–950.

135. D. Chablat, P. Wenger, Self Motions of a Special 3-RPR Planar Parallel Robot, Advances in Robot Kinematics, Springer, (2006), 221 – 228.

136. L. Gramnaes, Combined active and passive leg prosthesis, Patent WO 2006112774, Göteborg, Swiss, 26.10 (2006)

137. W. Hufenbach, K.-H. Modler, O. Täger, N. Modler, O. Renner, Contribution to the development of active compliant lightweight mechanism structures, Proceedings of the 4th IFAC-Symposium on Mechatronic Systems, Heidelberg, 12.-14. September 2006. preprints on CD-ROM, (2006).

138. W. Hufenbach, K.-H. Modler, O. Täger, N. Modler, E.-C. Lovasz, Design and manufacturing of smart textile compliant hinges. Acta Technica Napocensis, 2 (2006) 831–836.

139. J.-P. Merlet, Parallel Robots, Kluwer Academic Publishers, (2006).

140. K.-H. Modler, Aandrijfmechanisme voor een spoel vissoer, en molen voor vissnoer, 1026487. A01 K89/1, Nederland, (2006).

141. D. Mundo, Geometric design of a planetary gear train with non-circular gears, Mechanism an Machine Theory, 41 (4) (2006) 456-472.

142. J.P. Khatait, S. Mukherjee, B. Seth, Compliant design for flapping mechanism: A minimum torque approach, Mechanism and Machine Theory, 41 (2006) 3–16.

143. N. Nayaka, P.A. Lakshminarayanan, M.K. Gajendra Babu, A.D. Dani, Predictions of cam follower wear in diesel engines, Wear, 260 (2006) 181–192.

144. D. Perju, K.-H. Modler, M. Mateaş, E.-C. Lovasz, On the compensatory mechanisms of the archimedean effect, Proc. of the 8-th International Conference COMEFIN-8", Acta Technica Napocensis, Series: Applied Mathematics and Mechanics, 49(3) (2006) 607-610.

145. H. Sert, A. Can, H. Arıkan, B. Selcuk, H. Toprak, Wear behavior of different surface treated cam spindles, Wear, 260 (2006) 1013–10.

146. Ch. Spiegelberg, S. Andersson, Simulation of friction and wear in the contact between the valve bridge and rocker arm pad in a cam mechanism, Wear, 261(1) (2006) 58–67.

147. H. Kr. Anand, R. Rastogi, G. C. Nandi, Techniques for Dynamic Damping Control in Above Knee Prosthesis, Proc. of the 13th National Conference on Mechanisms and Machines (NaCoMM07), Dec. 12-13, IISc, Bangalore, (2007) 289-295.

148. A. C. Fischer-Cripps, Introduction to Contact Mechanics, Springer, (2007).

149. W. Hufenbach, M. Gude, N. Modler, C. Kirvel, Novel function-integrated lightweight solutions based on thermoplastic composites and material-adapted piezoceramic actor modules, Advanced Materials and Technologies (AMT), 3-4 (2007) 254–260.

150. F.L. Litvin, I. Gonzalez-Perez, K. Yukishima, A. Fuentes, K. Hayasaka, Generation of planar and helical elliptical gears by application of rack-cutter, hob and shaper, Computer Methods in Applied Mechanics and Engineering, 196 (41-44) (2007) 4321-4336.

151. E.-C. Lovasz, K.-H. Modler, D. Perju, R. Neumann, D. Mărgineanu, M. Perner, Non-circular gear wheels in the geared-linkages mechanisms, The XII-th World Congress in Mechanism and Machine Science, Besancon, France, 3 (2007) 284-289.

152. D. Mundo, H.S. Yan, Kinematic optimization of ball-screw transmission mechanisms, Mechanism and Machine Theory, 42 (1) (2007) 34-47.

153. E. Ottaviano, D. Mundo, G.A. Danieli, M. Ceccarelli, Numerical and experimental analysis of non-circular gears and cam-follower systems as function generators, Mechanism and Machine Theory, 43(8) (2007) 996-1008.

154. V.K. Nguyen, P.D. Nguyen, Balancing Conditions of Spatial Mechanisms, Mechanism and Machine Theory, 42(9) (2007) 1141–1152.

155. P. Antonescu, O. Antonescu, A Unitary Method for Analytical Synthesis of Mechanisms with Rotary Disc-Cam, Proceedings of a 3rd International Conference on Manufacturing Engineering (ICMEN), Chalkidiki, Greece, 01-03 October, (2008), 599-609.

156. S. Briot, I. Bonev, D. Chablat, P. Wenger, A. Vigen, Self-Motions of General 3-RPR Planar Parallel Robots, International Journal of Robotics Research, SAGE Publications, 27(7) (2008) 855-866.

157. C. Baradat, V. Arakelian, S. Briot, S. Guegan, Design and Prototyping of a New Balancing Mechanism for Spatial Parallel Manipulators, Journal of Mechanical Design, 130(7) (2008).

158. R. Borjian, Design, Modeling, and Control of an Active Prosthetic Knee, PhD Thesis, Water-loo, Ontario, Canada, (2008).

159. B.B. Cherry, L.L. Howell, B.D. Jensen, Evaluating three-dimensional effects on the behavior of compliant bistable micromechanisms, J. of Micromechanics and Microengineering, 18(9) (2008) 095001.

160. E.C. Lovasz D. Perju, K-H. Modler, D.T. Mărgineanu, E.S. Zăbavă, Evaluation of Wear Susceptibility of a Cam Mechanism with tangential oscillating Follower, Buletinul ştiinţific al Univ. "Politehnica" din Timişoara, Seria Mecanică, Tom 53(67) fasc.S1 (2008) 27-30.

161. E.-C. Lovasz, K.-H. Modler, D. Perju, D. Mărgineanu, E.S. Zăbavă, On the relative sliding at the cam mechanisms with the tangential/flat follower, Proceedings of X–th International Congress on the Theory of Machines and Mechanisms, Liberec, Cehien, (2008) 371-376.

162. N. Modler, Nachgiebigkeitsmechanismen aus Textilverbunden mit integrierten aktorischen Elementen, Dissertation Technische Universität Dresden, (2008).

163. D. Mundo, G. Gatti, A graphical-analytical technique for the synthesis of noncircular gears in path-generating geared five-bar mechanisms, Trans. of the CSME/de SCGM, 32 (3-4) (2008) 487-495.

164. E. Pennestrì, R. Stefanelli, P.P. Valentini, L. Vita, Efficiency and wear in cam actuated robotized gearbox using virtual model. International Journal of Vehicle Design, 46(3) (2008) 347-366.

165. J. Perry, J. Rosen, Exoskeleton, US 2008/0009771 A1. A61B 5/103. (2008).

166. G. G. Scandaroli, G. Araújo Borges, A. Ferreira da Rocha, Assis de Oliveira Nascimento F., Adaptive Knee Joint Control for an Active Amputee Prosthesis, IEEE Latin American Robotic Symposium, (2008) 164-169.

167. D.-C. Yang, J. Xiong, X.-D. Yang, A simple method to calculate mobility with Jacobian, Mechanism and Machine Theory, 43 (2008) 1175-1185.

168. F. S. Cardona, F. E. Zayas, N. L. Jordi, Síntesis de leyes de desplazamiento en levas de anchura constante con palpador plano de traslación, IX Congreso Iberoamericano de Ingeniería Mecánica,. Las Palmas de Gran Canaria: (2009) 1519-1528.

169. J.E. Crawford, B.P. Gray, Fishing reel, WO2009099997 A2, USA, (2009).

170. D. Chablat, S. Staicu, Kinematics of A 3-PRP Planar Parallel Robot, U.P.B. Sci. Bull., Series D, 71(2) (2009) 3–15.

171. F.W. Flocker, Addressing cam wear and follower jump in single-dwell cam-follower systems with an adjustable modified trapezoidal acceleration cam profile, Journal of Engineering for Gas Turbines and Power, 131(3) (2009).

172. A. Golovin, A. Lafitsky, A. Simuskhin, Experimental and theoretical research of cams wearing of cams mechanism, Proceedings of EUCOMES 2008 - The 2nd European Conference on Mechanism Science, Cassino, (2009) 343-350.

173. Z. Huang, J.F Liu, D.X. Zeng, A general methodology for mobility analysis of mechanism based constraint screw theory, Science in China Serie E: Technological Sciences, 52(5) (2009) 1337-1347.

174. J. Kotlarski, R. de Nijs, H. Abdellatif, B. Heimann, New interval-based approach to determine the guaranteed singularity-free workspace of parallel robots, ICRA 2009 Proceedings. Kobe. Japan. IEEE International Conference on Robotics and Automation, (2009), 1256 - 1261.

175. J. Kotlarski, H. Abdellatif, T. Ortmaier, B. Heimann, Enlarging the useable workspace of planar parallel robots using mechanisms of variable geometry, Proceedings of ReMAR 2009. London, (2009) 63-72.

176. E.-C. Lovasz, K.-H. Modler, A. Drăghici, V. Văcărescu, Studies for a new prosthesis de-sign for the work capacity rehabilitation, The 20th International DAAAM Symposium "Intelligent Manufacturing & Automation: Theory, Practice & Education", 25-28th November 2009, Vienna, Austria, (2009) 1381-1382.

177. N. Modler, W. Hufenbach, K.-H. Modler, E.-C. Lovasz, D. Perju, D. Margineanu, A Design of Compliant Mechanisms with Integrated Actuators, - Proceedings of the 10th SYROM 2009, Springer, Series Mechanism and Machine Science, (2009) 655-664.

178. K.-H. Modler, E.-C. Lovasz, G. Bär, R. Neumann, D. Perju, M. Perner, D. Margineanu, General method for the synthesis of geared linkages with non-circular gears, Mechanism and Machine Theory, 44, (2009), 726-738.

179. D. Mundo, G. Gatti, D.B. Dooner, Optimized five-bar linkages and non-circular gears for exact path generation, Mechanism and Machine Theory 44 (4) (2009) 751-760.

180. M. Nashrul, M. Zubir, B. Shirinzadeh, Y. Tian, A new design of piezoelectric driven compliant-based microgripper for micromanipulation, Mechanism and Machine Theory, 44(12) (2009) 2248–2264.

181. D. Pisla, C. Daicoviciu, N. Plitea, A. Vidrean, B. Prodan, B. Gherman, D. Lese, Kinematics and design of two variants of a reconfigurable parallel robot, Proceedings of ReMAR. London (2009), 624-631.

182. M. Sreekumar, M. Singaperumal, A generalized analytical approach to the coupled effect of SMA actuation and elastic deflection, Smart Materials and Structures, 18 (2009) 115026.

183. F. E. Zayas, F. S. Cardona, N. L. Jordi, Analysis and synthesis of the displacement function of the follower in constant-breadth cam mechanisms, Mechanism and Machine Theory, 44 (2009) 1938-1949.

184. L.Ch. Wu, G. Carbone, M. Ceccarelli, Designing an underactuated mechanism for a 1 active DOF finger operation, Mechanism and Machine Theory, 44 (2009) 336–348.

185. B.R. Bancroft, Reel, A01K 89/01 20060101 AFI 20120314BHEP, USA, (2010).

186. B. Dariush, Exoskeleton Controller for a Human-Exoskeleton System, US 7,774,177 B2. G06F 17/10. (2010).

187. I. Farkhatdinov, J.-H. Ryu, A Preliminary Experimental Study on Haptic Teleoperation of Mobile Robot with Variable Force Feedback Gain, Proc. of IEEE Haptics Symp. 2010, Waltham, Boston, USA, (2010) 251-256.

188. Zh. Gao, D. Zhang, Design, analysis and fabrication of a multidimensional acceleration sensor based on fully decoupled compliant parallel mechanism, Sensors and Actuators, A 163 (2010) 418–427.

189. M. Z. Huang, L. L. Thebert, A study of workspace and singularity characteristics for design of 3-DOF planar parallel robots. The International Journal of Advanced Manufacturing Technology, 51(5-8) (2010) 789-797.

190. D.N. Hutchison, N.B. Morrill, Q. Aten, B.W. Turner, B.D. Jensen, L.L. Howell, R.R. Vanfleet, R.C. Davis, Carbon Nanotubes as a Framework for High-Aspect-Ratio MEMS Fabrication, J. of Microelectromechanical Systems, 19(1) (2010) 75 - 82.

191. P. Letier, Bras Exosquelette Haptique. Conception et Contrôle, PhD Thesis, (2010).

192. E.-C. Lovasz, D. Perju, I. Cărăbaş, K.-H. Modler, E. Zăbavă, Basic circle radius of the cam mechanism with flat oscillating follower, Bulletin of Politehnic Institut of Iaşi, Ed. Politehnicum, Iaşi, Tom LVI(LX) Fasc. 4A (2010) 255-262.

193. E.-C. Lovasz, D. Perju, C. Duca, K.-H. Modler, I. Cărăbaş, E.S. Zăbavă, Numerical Method for Determination of the Basic Circle Radius of the Cam Mechanism with flat oscillating follower. Scientific Bulletin of the „Politehnica" University of Timisoara, Transactions on Mechanics, 55(69)/1 (2010) 21-26.

194. E.-C. Lovasz, D. Perju, N. Dehelean, L.M. Dehelean, I. Maniu, C. Moldovan, Self-Balanced Conco-Balancer Manipulator with Band Mechanism, Solid State Phenomena, 166-167 (2010) 259-265.

195. L. Lu, C.H. Kim, S.H. Lee, J.H. Shin, S.-M. Kwon, A study on wear characteristic for oscillating disc cam mechanism using GA, IEEE International Conference on Mechatronics and Automation, ICMA 2010; Xi'an; China, (2010) 185-190.

196. V. Parlaktas, E. Soylemez, E. Tanik, On the synthesis of a geared four-bar mechanism, Mechanism and Machine Theory 45(8) (2010) 1142-1152.

197. I.A. Popescu, E.-C. Lovasz, V. Ciupe: Active Prosthesis for Lower Limb Amputated Above Knee, Robotica & Management International Journal, 15(1) (2010) 59-60.

198. E. Tanık, E. Söylemez, Analysis and design of a compliant variable stroke mechanism, Mechanism and Machine Theory, 45 (2010) 1385–1394.

199. Y.T. Zhang, D.J. Mu, A new concept and new theory of mobility calculation for multi-loop mechanisms, Science in China Technological Sciences, 53(6) (2010) 1598-1604.

200. F. Ebert, M. Berger, S. Heinrich, Ganzheitliche Systemsimulation komplexer Antriebssysteme mit nichtlinearer Charakteristik. Proc. of 9. Kolloquium Getriebetechnik, Chemnitz, 395-418, (2011).

201. J. Gancet, M. Ilzkovitz, G. Cheron, Y. Ivanenko, H. van der Kooij, F. van der Helm, F. Zanow, F. Thorsteinsson, MINDWALKER: A Brain Controlled Lower Limbs Exoskeleton for Rehabilitation. Potential Applications To Space, Proc. of ASTRA 2011. Noordwijk, Netherlands, (2011).

202. M. Z. Huang, Design of a Planar Parallel Robot for Optimal Workspace and Dexterity, Int J Advance Robotic Systems, 8(4) (2011) 176–183.

203. P. Letier, E. Motard, M. Ilzkovitz, A. Preumont, J.P. Verschueren, SAM: Portable Haptic Arm Exoskeleton Upgrade. Technologies and New Application Fields, Proc. of ASTRA 2011, Noordwijk, Netherlands, (2011).

204. V. Moise, M. Ene, I.A. Tabara, I. Dugăeşescu, Determination of the Minimum Size of the Disk Cam with translating Flat-Face Follower, Proceedings of 13th World Congress in Mechanism and Machine Science, Guanajuato, México, 19-25 June, (2011), A11_554.

205. C.E. Moldovan, Contribuţii la analiza şi sinteza mecanismelor având cuple cinematice de tip centroidal, PhD Thesis, Timişoara, (2011).

206. R.C. Soong, S.B. Chang, Synthesis of function-generation mechanisms using variable length driving links, Mechanism and Machine Theory, 46(11) (2011) 1696-1706.

207. K. Sugahara, Spinning Reel Fishing Line Guide Mechanism, 20110210197, AA01K8901FI, Japan, (2011).

208. W. Xinying, O. Guangyao, T. Di, The wear analysis for cam mechanism of diesel fuel injection pump based on multibody dynamics theories, Proceedings of 2011 International Conference on Electronic and Mechanical Engineering and Information Technology, EMEIT 2011, 3 (2011) 1278-1282.

209. R. Burdzik, P. Folega, B. Łazarz, Z. Stanik, J. Warczek, Attempt to assess operational wear of camshaft cams, Archives of Materials Science and Engineering, 57(2) (2012) 57-62.

210. M. Ceccarelli (ed.), Service robots and robotics, Design and Application, Engineering Science Reference, Hershey PA, (2012).

211. F.W. Flocker, A versatile acceleration-based cam profile for single-dwell applications requiring cam-follower clearance during dwell, Journal of Mechanical Design, Transactions of the ASME. 134(8) (2012).

212. P. Folega, R. Burdzik, Ł. Konieczny, Z. Stanik, J. Warczek, B. Łazarz, Impact of the cam and follower cooperation and of lubrication on the cam wear, Archives of Materials Science and Engineering, 58(2) (2012) 158-163.

213. A. Joubair, M. Slamani, I. A. Bonev, Kinematic calibration of a 3-DOF planar parallel robot, Industrial Robot: An International Journal, 39(4) (2012) 392 – 400.

214. J. Kotlarski, B. Heimann, T. Ortmaier, Influence of kinematic redundancy on the singularity-free workspace of parallel kinematic machines, Frontiers of Mechanical Engineering, 7(2) (2012) 120 – 134.

215. E.-C. Lovasz, D. Perju, K.-H. Modler, C.M. Gruescu, I. Maniu, E.-S. Zabava, Numerical Iterative Method for Computing the Base Circle Radius of Cam Mechanisms with Translating Flat-Face Follower, New Trends in Mechanism and Machine Science Theory and Applications in Engineering, Springer Publisher, Series: Mechanisms and Machine Science, 7 (2012) 237-244.

216. E.-C. Lovasz, D. Perju, C.M. Gruescu, K.-H. Modler, I. Carabas E.S. Zabava, Numerical Method for Determination of Base Circle Radius of Cam Mechanisms with Oscillating Flat-Face Folower, Advances in Mechanisms Design, Springer Publisher, Series: Mechanisms and Machine Science, 8 (2012) 143-149.

217. V. Patoglu, Exoskeleton, US 20120330198A1. A61H 1/02. (2012).

218. D. Perju, E.-C. Lovasz, K.-H. Modler, C.E. Moldovan I. Carabaş, Kinematic analysis of a belt mechanism with a circular eccentric output element, Proceedings of MMT and Robotics, Clermont-Ferrand, France, 162 (2012) 183-188.

219. A. Rama Krishna, G. Sowmya Bala, A.S.C.S. Sastry, B. Bhanu Prakash Sarma, G. Sai Alla, Design and Implementation of a Robotic Arm Based on Haptic Technology. J. of Engineering Research and Applications (IJERA), 2(3) (2012) 3098-3103.

220. W. Wei, N. Simaan, Design of Planar Parallel Robots With Preloaded Flexures for Guaranteed Backlash Prevention, Journal of Mechanisms Robotics, 2(1) (2012) 011012.

221. A. Comşa, Contribuţii privind automatizarea procesului de manipulare a cărţilor în biblioteci, PhD Thesis, Timişoara (2013).

222. U. Hanke, K.-H. Modler, A. Schmidtpott, S. Lin, Engineering aspects in solving guidance tasks with geared linkages, Mechanisms and Machine Science, 4th European Conference on Mechanism Science, EUCOMES 2012; Santander; Spain, 7 (2013) 209-216.

223. J. I. Ibarreche, O. Altuzarra, V. Petuya, A. Hernandez, C. Pinto, Structural Synthesis of the families of parallel manipulators with 3 degrees of freedom, Proceedings of 19th CSIM IFToMM Symposium. Springer, (2013) 35–42.

224. E.-C. Lovasz, V. Ciupe, K.-H. Modler, C.M. Gruescu, U. Hanke, I. Maniu, D. Mărgineanu, Experimental Design and Control Approach of an Active Knee Prosthesis with Geared Linkage, New Advances in Mechanisms, Transmissions and Applications, Springer Publisher, Series: Mechanisms and Machine Science, 17 (2013) 149-156.

225. D. Pisla, B. Gherman, C. Vaida, M. Suciu, N. Plitea, An active hybrid parallel robot for minimally invasive surgery, J. of Robotics and Computer-Integrated Manufacturing, 29 (4) (2013) 203-221.

226. D. Pisla, A. Szilaghyi, C. Vaida, N. Plitea, Kinematics and workspace modeling of a new hybrid robot used in minimally invasive surgery, J. of Robotics and Computer-Integrated Manufacturing 29(2) (2013) 463–474.

227. N. Plitea, D. Lese, D. Pisla, C. Vaida, Structural design and kinematics of a new parallel reconfigurable robot, Robotics and Computer-Integrated Manufacturing 29(1) (2013) 219–235.

228. B. Schena, Haptic Device Utilizing an Electroactive Polymer, US00RE44277E. G09G 5/00. (2013).

229. G. Yiyuan, W. Junfa, W. Guilian, L. Yaqin, Reliability design and wear extent determination of a cam mechanism, 2nd International Conference on Applied Mechanics, Materials and Manufacturing, ICAMMM 2012, Changsha, Applied Mechanics and Materials, 268(1) (2013) 1034-1038.

230. F. Buium, C. Duca, D. Leonchi, Problems regarding singularities analysis of a 0/3/3 parallel mechanism. Applied Mechanics and Materials 658, (2014) 569-574.

231. F. Buium, D. Leonchi, I. Doroftei, A Workspace Characterization of the 0/3/3R Parallel Mechanism, Applied Mechanics and Materials, 658, (2014) 563 – 568.

232. R. Burdzik, Ł. Konieczny, Z. Stanik, P. Folęga, A. Smalcerz, A. Lisiecki, Analysis of impact of chosen parameters on the wear of camshaft, Archives of Metallurgy and Materials, 59(3) (2014) 957-963.

233. F. Cabanettes, B-G. Rosén, Topography changes observation during running-in of rolling contacts, Wear, 315 (2014) 78–86.

234. K. Dong-Wook, K. Kyung-Woong, Effects of sliding velocity and ambient temperature on thefriction and wear of a boundary-lubricated, multi-layered DLC coating, Wear, 315 (2014) 95–102.

235. C. Duca, F. Buium, Transmission indices Adoption at 0/3/0 Structural Group, Applied Mechanics and Materials 658 (2014) 55–58.

236. C. Duca, F. Buium, Singularities Classification for Structural Groups of Dyad Type, Applied Mechanics and Materials 658 (2014) 47 – 54.

237. A. Hernandez, J. I. Ibarreche, V. Petuya, O. Altuzarra, Structural Synthesis of 3-DoF Spatial Fully Parallel Manipulators, International Journal of Advanced Robotic Systems, 11:101 (2014) 1–8.

238. J.S. Liu, S. Lin, Synthesis of rigid-body guidance mechanism with path and pose generation independently, Applied Mechanics and Materials, 6th International Conference on Mechanical and Electrical Technology, ICMET 2014; Bangkok; Thailand; 619 (2014) 115-120.

239. E.-C. Lovasz, D. Perju, K. -H. Modler, C. M. Gruescu, D. Mărgineanu, C. E. Moldovan, C. Pop, Path Generating Belt Mechanisms as Kinematic Chains for Mechatronic Applications, Proceedings of 5th EUCOMES, Guimarães, Portugal, New Trends in Mechanism and Machine Science, Series Mechanisms and Machine Science, 24 (2014) 111-119.

240. E.-C. Lovasz, D. Mărgineanu, V. Ciupe, I. Maniu, C.M. Gruescu, S.D. Stan, E.S. Zăbavă, Design and Control Solutions for Haptic Elbow Exoskeleton Module Used in Space Telerobotics, Proceedings of 2014 IFToMM Asian Conference on Mechanism and Machine Science, July 9–10, 2014, Tianjin, China, RM3-3, online.

241. M. Mateaş, E.-C. Lovasz, D. Mărgineanu, V. Ciupe, E.S. Zabava, I. Maniu, A. Diaconu: Control Characteristics of Haptic Exoskeleton Elbow Module Used in Space Robotised Applications, Applied Mechanics and Materials, Proceedings of the 6th International Conference on Advanced Concepts in Mechanical Engineering, Iasi, 658 (2014) 654-659.

242. E.-C. Lovasz, C. Pop, F. Pop, V. Dolga, Novel solution for leg motion with 5 link belt mechanism, International Journal of Advanced Mechanics and Engineering, 19 (2014) 699-708.

243. Y. Singh, V. Vinoth, M. Santhakumar, Dynamic Modelling and Control of a 3-DOF Planar Parallel Robotic (XYθZ Motion) Platfom, Procedia ICAMME 2014. Materials Science, 5 (2014) 1528–1539.

244. D. Mărgineanu, E.-C. Lovasz, V. Ciupe, M. Mateaş, E.S. Zabava, 3 DoF Haptic Exoskeleton for Space Telerobotic, Mechanisms, Transmissions and Applications, Proc. of 3rd Conference MeTrApp-2015, Series Mechanisms and Machine Science, Springer, 31 (2015) 279-287.

245. E.-C. Lovasz, S. Grigorescu, D. Margineanu, C.M. Gruescu, C. Pop, V. Ciupe, I. Maniu, Geared Linkages with Linear Actuation Used as Kinematic Chains of a Planar Parallel Manipulator, Proc. of 3rd MeTrApp Conference, Mechanisms, Transmissions and Applications, Series Mechanism and Machine Science, 31 (2015) 21-31.

246. E.-C. Lovasz, S. Grigorescu, D. Margineanu, C. Pop, Knitting Machine for Pretzels using Parallel Robots, Proc. of TrC-IFToMM Symposium on Theory of Machines and Mechanisms, Izmir, Turkey, June 14-17, (2015) (online).

247. E.-C. Lovasz, K.-H. Modler, R. Neumann, C.M. Gruescu, D. Perju, V. Ciupe, I. Maniu, Novel design solutions for fishing reel mechanisms, Chinese Journal of Mechanical Engineering, 28(4) (2015) 726-736.

248. E.-C. Lovasz, S. Grigorescu, D. Margineanu, C.M. Gruescu, C. Pop, I. Maniu, Kinematics of the planar parallel Manipulator using Geared Linkages with linear Actuation as kinematic Chains 3-R(RPRGR)RR, Proc. of 14th IFToMM World Congress Conference, October 25-30, 2015 (in press).

249. http://www.iftomm.org/index.php?option=com_content&view=article&id=101&Itemid=196 (last accessed 15.03.2013).

250. Information to: http://www.positech-solutions.com/products/concoBalanceMaster.pdf. (last accessed 18.02.2010).